

**FUNCTIONALIZED ORGANOBORON POLYMERS AND
SUPRAMOLECULAR STRUCTURES OF
PENTAFLUOROPHENYLCOPPER**

By Ami P. Doshi

A dissertation submitted to the
Graduate School-Newark
Rutgers, The State University of New Jersey
in partial fulfillment of the requirements
for the degree of
Doctor of Philosophy
Graduate Program in Chemistry
Written under the direction of
Professor Frieder Jäkle
and approved by

Newark, New Jersey

January, 2010

ABSTRACT OF THE THESIS

FUNCTIONALIZED ORGANOBORON POLYMERS AND SUPRAMOLECULAR STRUCTURES OF PENTAFLUOROPHENYLCOPPER

By Ami Doshi

Thesis Director: Professor Frieder Jäkle

This thesis is divided into four different parts. The first three chapters discuss the development of synthetic routes to new boron containing polymers for their potential use as supported borane reagents (Ch. 1.) and photoluminescent materials (Ch. 2. and Ch. 3.). The last chapter (Ch. 4.) discusses the formation of supramolecular structures of pentafluorophenylcopper upon complexation with pyridine nucleophiles and electron rich aromatic π -systems. The individual research projects are briefly summarized in the following.

Ch. 1. The functionalization of synthetic polymers with organoborane moieties has been extensively studied for applications as supported catalysts, sensors, stimuli responsive polymers, flame retardants, preceramic materials, and as intermediates for the preparation of other functional organic polymers. A polystyrene derivative in which the *para*-positions of the phenyl rings are selectively functionalized with BH_2 moieties (PS- BH_2)

has been prepared from poly(4-trimethylsilyl styrene). The polymer was successfully isolated in the form of its polymeric acid-base complexes PS-BH₂•D (D = ^tBuPy, PPh₂Me). The selective and nearly quantitative placement of the BH₂ functionalities was confirmed by multinuclear NMR spectroscopy and IR spectroscopy. Their thermal properties were studied by differential scanning calorimetry and thermogravimetric analysis.

Ch. 2. Boron containing water soluble polymers could find a variety of applications as polyelectrolytes, for anion recognition in aqueous media and in various biological fields. We have previously shown that polystyrene based side chain functionalized triarylborane polymers can be employed as sensors for the recognition of cyanide and fluoride in organic media. Here we have pursued the synthesis of polystyrene that bears Lewis acidic boron centers and dimethylamino-functionalized mesityl groups in the side chain. Attachment of these mesityl groups to the boron center has been realized by the use of boron-silicon exchange, followed by the replacement of the bromine on boron by suitable Grignard reagents. The polymers and model compounds show interesting photophysical properties and have the potential to be applied for anion sensing in aqueous media.

Ch. 3. Main chain organoboron conjugated polymers have been established as an important class of materials due to their unusual optoelectronic properties. This behavior arises as a result of overlap between the empty p-orbital on boron and the conjugated π -system. The hydroboration polymerization and in situ Grignard synthesis have been employed for the preparation of such polymers. Here we have synthesized boron-functionalized distyryl monomers, which can be polymerized via ADMET polymerization. All monomers and ADMET products were characterized by multinuclear

NMR spectroscopy. Moderate to high molecular weights in the range of 5,000-10,000 have been obtained. Photophysical data show that polymer emits in the blue-green region.

Ch. 4. Treatment of organocopper species with strongly coordinating ligands is known to lead to break-down of the aggregated structures. One such example is the 1:1 complex of pentafluorophenylcopper with pyridine. The monomeric pyridine adduct shows an intriguing supramolecular structure governed by cuprophilic interactions. This complex was also found to display strong blue luminescence in the solid state at room temperature. To further examine the structural and photophysical properties of this new class of complexes, the pentafluorophenylcopper tetramer was treated with different substituted pyridine ligands. The coordination of these ligands to copper was confirmed by ^1H , ^{19}F , ^{13}C NMR spectroscopy, x-ray crystallography and elemental analysis.

Treatment of pentafluorophenylcopper with π -bases such as bithiophene, naphthalene anthracene or pyrene lead to novel luminescent supramolecular structures that feature the intact organocopper aggregate as the building block. Formation of bis-adducts with two equivalents of arenes was realized and the formation of sandwich-like structures of the intact tetramer and the corresponding arene was observed via single crystal x-ray analyses. Interestingly, the 1:1 complexes form extended binary stacks in the solid state, where the intact tetramer alternates with the arene.

Dedicated to my Late Father

Mr. Pravinchandra O. Doshi

Acknowledgments

I wish to express my sincere thanks to my supervisor, advisor and mentor, Prof. Frieder Jäkle, for his helpful support, guidance and encouragement throughout my Ph.D. study. I would also like to thank him for always being helpful, understanding and patient through any ups and downs, both on a personal as well as the professional front.

I would like to thank my committee members, Prof. Elena Galoppini, Prof. Philip Huskey and Prof. Sergiu Gorun of NJIT at Newark, NJ, for spending their time reading and correcting my thesis, and for their helpful advice and encouragement.

I would like to thank Prof. Ralf Peetz and his student Arijit Sengupta (CUNY-Staten Island) for their collaboration, helpful discussions and all their help with synthesis and characterization of the boron containing ADMET polymers. I would specially like to thank Prof. Roger A. Lalancette for his help with solving and determination of structural parameters. I would also like to thank Dr. Lazaros Kakalis for helping me with NMR measurements. Thanks to Prof. Arnold L. Rheingold, of University of California, San Diego, and Dr. Krishnan Venkatasubbaiah of Rutgers University, Newark, for performing x-ray crystal structure determinations. I also thank all my professors who taught me throughout my graduate program. In addition, I would like to thank my colleagues and former group members for their help and support.

Finally, I am very grateful to my family and friends for giving me continuous support and encouragement. I would like to dedicate this thesis to my late father Mr. Pravinchandra O. Doshi, my mother Mrs. Sudha P. Doshi and my dearest husband Kshitij

Parab; whose support, patience, understanding and unconditional love gave me strength and enthusiasm to pursue my dreams and aspirations.

Disclaimer

The x-ray crystal determination for 4-MePy-CuC₆F₅ (18), 4-ClPy-CuC₆F₅ (20), (Bt)₂-CuC₆F₅ (28), (Pyr)₂-CuC₆F₅ (33) on pages 198, 200, 216, and 227 was carried out by Prof. Arnold L. Rheingold at University of California, San Diego.

The x-ray crystal determination for 2-MePy-CuC₆F₅ (19), 2-ClPy-CuC₆F₅ (21), and (Naph)-CuC₆F₅ (29) on pages 200, 201, and 218 was carried out by Dr. Krishnan Venkatasubbaiah at Rutgers University, Newark, NJ.

The ADMET polymerization of monomer (29), on page 159 was carried out by Arijit Sengupta at College of Staten Island, The City University of New York.

Table of Contents

Abstract of Thesis	ii
Dedication	v
Acknowledgements	vi
Disclaimer	viii
Table of Contents	ix
List of Figures	xvii
List of Schemes	xxi
List of Tables	xxiii
List of Charts	xxiv
Chapter 1. General Introduction.	1
1.1 Organoboron Polymers.	1
1.2 Synthesis of Boron Containing Polymers.	2
1.2.1 Direct Polymerization of Boron Monomers.	2
1.2.2 Polymer Modification Reactions.	8
1.2.2.1 Modification of Polyolefins.	8

1.2.2.2	From Mercuriated Polystyrene.	9
1.2.2.3	Side-chain Functionalized Organoboron Polymers via Si-B Exchange Reactions.	10
1.3	Applications of Boron Containing Polymers.	11
1.3.1	Applications in Organic Synthesis and Catalysis.	12
1.3.2	Applications as Sensor Materials.	12
1.3.3	Other Applications.	15
1.4	References and Notes.	16
Chapter 1A.	Boron Polymers as Supported Reagents.	22
1A.1	Polymers Supported Reagents.	22
1A.2	Synthesis of Supported Borane Reagents.	23
1A.3	Hydroboration Chemistry.	29
1A.4	Results and Discussion.	34
1A.4.1	Synthesis.	34
1A.4.2	Structural Characterization.	37
1A.4.2.1	Multinuclear NMR Spectroscopy.	37
1A.4.2.2	IR Spectroscopy.	39

1A.4.2.3	Molecular Weight Determination.	39
1A.4.2.4	Thermal Properties.	39
1A.5	Conclusions.	41
1A.6	Experimental Section.	42
1A.6.1	Materials and Instrumentation.	42
1A.6.2	Preparation of Polymers and Model Compounds.	44
1A.7	References and Notes.	48
Chapter 1B.	Amine Functionalized Organoboron Polymers.	53
1B.1	Introduction.	53
1B.2	Donor- π -Acceptor Type Organoboron Systems and Their Applications.	54
1B.3	Water Soluble Polymers.	67
1B.3.1	Conjugated Polyelectrolytes.	68
1B.4	Side-chain Functionalized Organoboron Polymers with Dimethylamino Functionalized Group as the Chromophore.	72
1B.4.1	Synthesis.	73
1B.4.1.1	Synthesis of Model Compounds.	74

1B.4.1.2	Synthesis of Polymers.	80
1B.4.2	Structural Characterization.	82
1B.4.2.1	Multinuclear NMR Spectroscopy.	82
1B.4.2.2	Molecular Weight Determination.	86
1B.4.2.3	Determination of the X-ray Structure of MB(MesNMe ₂) ₂ (43).	87
1B.4.2.4	Photophysical Properties in Solution.	89
1B.4.2.5	Solvatochromism.	93
1B.5	Borylated Polystyrenes as Anion Sensors.	98
1B.6	Conclusions.	105
1B.7	Experimental Section.	106
1B.7.1	Materials and Instrumentation.	106
1B.7.2	Synthesis and Data for Precursors and Model Compounds.	108
1B.7.3	Synthesis and Data for Polymers.	115
1B.8	References and Notes.	119
Chapter 1C.	Boron Functionalized Monomers for ADMET Polymerization.	125

1C.1 Conjugated Polymers.	125
1C.2 Main Chain Functionalized Organoboron Polymers.	127
1C.2.1 Hydroboration Polymerization.	128
1C.2.2 Organometallic Routes.	131
1C.3 ADMET Polymerization.	134
1C.3.1 Metathesis Catalysts and Monomers for ADMET.	136
1C.3.2 Polymers Synthesized via ADMET Polymerization.	139
1C.3.3 Inorganic Polymers Synthesized via ADMET Polymerization.	144
1C.3.4 Boron Containing Monomers.	150
1C.4 Results and Discussion.	152
1C.4.1 Synthesis of Monomers.	152
1C.4.2 Structural Characterization.	154
1C.4.2.1 Multinuclear NMR Spectroscopy.	154
1C.4.2.2 X-ray Structure Determination of (29) and (30).	155
1C.5 Acyclic Diene Metathesis Polymerization of (29-32).	159
1C.5.1 Molecular Weight Determination.	161

1C.5.2	NMR Spectroscopy.	162
1C.5.3	Thermal Properties.	163
1C.5.4	Photophysical Properties.	164
1C.6	Conclusions.	168
1C.7	Experimental Section.	169
1C.7.1	Materials and Instrumentation.	169
1C.7.2	Synthesis of Boron Monomers and Polymers.	170
1C.8	References and Notes.	173
Chapter 2.	Pentafluorophenylcopper: Complexation Behavior and	180
	Supramolecular Structures.	
2.1	Introduction.	180
2.2	Pentafluorophenylcopper.	184
2.2.1	Solid State Structure of (C ₆ F ₅ Cu) ₄ (8).	185
2.3	σ-Complexes of Organocopper Compounds.	186
2.3.1	σ-Complexes of Pentafluorophenylcopper.	188
2.4	Cuprophilicity.	191
2.5	Pentafluorophenylcopper(I) Pyridine Complexes.	194

2.5.1	Synthesis.	194
2.5.2	Structures in Solution.	195
2.5.3	Solid-State Structures of (18-21).	198
2.5.4	Supramolecular Structures.	203
2.6	π -Complexes of Organocopper Compounds.	206
2.6.1	π -Complexes of Pentafluorophenylcopper.	209
2.6.2	Solid State Structure of $(\text{C}_6\text{F}_5\text{Cu})_4(\text{toluene})_2$ (9).	210
2.7	Binary Stacks of Pentafluorophenylcopper with Arenes.	211
2.7.1	Synthesis of Complexes (27-33).	212
2.7.2	Solid State Structures of Complexes (27-31).	214
2.7.3	Solid State Structures of (32) and (33).	221
2.8	Conclusions.	227
2.9	Experimental Section.	228
2.9.1	Materials and Instrumentation.	228
2.9.2	Reaction of Pentafluorophenylcopper with Substituted Pyridine.	230
2.9.3	Reaction of Pentafluorophenylcopper with Organic π -	233

Systems.

2.10 References and Notes. 234

Appendix 243

List of Publications 314

Vita 316

List of Figures

Figure 1.1	Schematic Representation of Properties of Organoboron Compounds.	11
Figure 1A.1	Comparison of ^{11}B NMR Spectra.	38
Figure 1A.2	Comparison of ^{13}C NMR spectra; only the region from 120 to 150 ppm is shown and the quaternary carbon signals are not marked.	38
Figure 1A.3	Thermogravimetric analysis (TGA) plots of (51), (56) and (58) (20 °C/min, N_2).	41
Figure 1B.1	Schematic Presentation of a Donor- π -Acceptor System.	54
Figure 1B.2	Comparison of the ^{11}B NMR Shifts of (43) and (44).	83
Figure 1B.3	^{13}C NMR Overlay of (43) and (44) (a) Aromatic Region; (b) Aliphatic Region.	84
Figure 1B.4	^{13}C NMR Overlay of (50) and (51) (a) Aromatic Region; (b) Aliphatic Region.	85
Figure 1B.5	Gel Permeation Chromatography (refractive index detector) Traces of (44) and (51).	87

Figure 1B.6	Molecular Structure of (43).	88
Figure 1B.7	Comparison of (a) the Absorption Spectra and (b) the Emission Spectra of (43), (44), (47), (50), (51), (52) and (53) in CH ₂ Cl ₂ Solution.	91
Figure 1B.8	(a) Comparison of the Absorption and Emission Spectra of MB(MesNMe ₂) ₂ in different solvents. (b) Comparison of the Absorption and Emission Spectra of PSB(MesNMe ₂) ₂ in different solvents. (c) Comparison of the Absorption and Emission Spectra of MBMes(MesNMe ₂) in different solvents. (d) Comparison of the Absorption and Emission Spectra of PSBMes(MesNMe ₂) in different solvents. (e) Comparison of the Absorption and Emission Spectra of MBMesNMe ₂ (MesCH ₂ NMe ₂) ₂ in different solvents.	97
Figure 1B.9	Comparison of Photophysical Properties of Model Systems and Polymers upon Titration with 10 Equiv of Different Anions (Borane Source = $\sim 3.2 \times 10^{-5}$ M per repeat unit for polymers, Fluoride Source = $\sim 3.2 \times 10^{-4}$ M).	105
Figure 1C.1	Mechanism of ADMET Polymerization.	136
Figure 1C.2	Comparison of the ¹¹ B NMR shifts of (29) and (30).	154
Figure 1C.3	¹ H NMR Spectrum of (Styryl) ₂ BQ in CDCl ₃ .	155

Figure 1C.4	Molecular Structure of (29).	156
Figure 1C.5	Molecular Structure of (30).	158
Figure 1C.6	(a) ^1H NMR plot of (29); (b) ^1H NMR plot of (29p) in CDCl_3 .	163
Figure 1C.7	Thermogravimetric Analysis Plot of 29p (10 $^\circ\text{C}/\text{min}$ under N_2).	164
Figure 1C.8	Comparison of Absorption and Emission Spectra of (29), (30) and (32) in THF Solution.	166
Figure 1C.9	Comparison of Absorption and Emission Spectra of (29) and (29p) in THF Solution.	168
Figure 2.1	Plot of the Molecular Structure of (8).	186
Figure 2.2	(a) Synthesis of (12); (b) Extended Structure of (12) Along the Crystallographic c-Axis.	190
Figure 2.3	^{19}F NMR spectra of compounds (18-21) in CDCl_3 at 25 $^\circ\text{C}$.	196
Figure 2.4	Molecular Structure of (18).	198
Figure 2.5	Molecular Structure of (19).	200
Figure 2.6	Molecular Structure of (20).	200
Figure 2.7	Molecular Structure of (21).	201
Figure 2.8	Plots of the Extended Structures of (18-21).	205
Figure 2.9	Molecular Structure of (9).	211

Figure 2.10	Plot of the Molecular Structure of (27) and (31).	215
Figure 2.11	Plot of the Molecular Structure of (28).	216
Figure 2.12	Plot of the Polymeric Structure of (29).	218
Figure 2.13	Plot of the Polymeric Structure of (30).	220
Figure 2.14	(a) Plot of the Polymeric Structure of (32), (b) View of Puckered Cu ₄ C ₄ Core.	224
Figure 2.15	Plot of the Molecular Structure of (33), (b) View of Cu ₅ C ₄ Core.	227

List of Schemes

Scheme 1.1	Examples of Borane Modification of Polyolefins.	9
Scheme 1.2	Si-B Exchange Route for the Synthesis of Organoboron Containing Polymers.	11
Scheme 1A.1	Preparation of Polymer-Supported Organoboranes.	25
Scheme 1A.2	Preparation of Carborane Containing Polymer-Supported Reagents.	28
Scheme 1A.3	Preparation of Polymer-Supported 9-BBN.	28
Scheme 1A.4	Synthesis of Main Chain Chiral Organoboron Polymers.	33
Scheme 1A.5	Synthesis of Organoboron Complexes $\text{RBH}_2 \cdot \text{D}$.	36
Scheme 1B.1	General Strategy for the Synthesis of Triarylborane Compounds.	74
Scheme 1B.2	Synthesis of Dimethylamino Functionalized Triarylborane Compounds.	80
Scheme 1C.1	Example of Boron-Containing Conjugated Polymers via Hydroboration Polymerization.	129
Scheme 1C.2	Conjugated Boron-Containing Polymers (Mes = 2,4,6-trimethylphenyl; Trip = 2,4,6-triisopropylphenyl).	130

Scheme 1C.3	Hydroboration Polymerization of 9,10-dihydro-9,10-diboraanthracene with Aromatic Dialkynes.	131
Scheme 1C.4	ADMET Polymerization.	134
Scheme 1C.5	Example of Thiophene Containing Polymers Synthesized via ADMET.	144
Scheme 1C.6	Example of poly(silanylthienylethene) via ADMET.	146
Scheme 1C.7	Synthesis of Boronate Functionalized Polymers via ADMET.	151
Scheme 1C.8	Synthesis of Boron Containing Monomers.	153
Scheme 1C.9	ADMET Polymerization of (29).	160
Scheme 2.1	Synthesis of C ₆ F ₅ Cu.	184
Scheme 2.2	Proposed Structures Involved in the Complexation of Pentafluorophenylcopper.	189
Scheme 2.3	Preparation of Pentafluorophenylcopper(I) Pyridine Complexes.	195
Scheme 2.4	Schematic Representation of Different Types of π -Complexes.	214

List of Tables

Table 1B.1	¹¹ B NMR Shifts (ppm) and Halfwidths ($w_{1/2}$) (Hz) of Organoboron Polymers and Molecular Model Compounds.	83
Table 1B.2	Molecular Weight Data for the Polymers Obtained from GPC.	86
Table 1B.3	Comparison of Photophysical Properties of Polymers and Model Compounds.	92
Table 1B.4	Comparison of Photophysical Properties of Polymers and Model Compounds in Various Solvents.	94
Table 1C.1	Results for ADMET Polymerization of (29).	161
Table 1C.2	Comparison of Photophysical Properties of Monomers and Polymers.	165
Table 2.1	Comparison of ¹⁹ F and selected ¹³ C NMR data.	197
Table 2.2	Comparison of Selected Bond Lengths [Å], Distances [Å], and Angles [°].	202
Table 2.3	Comparison of Selected Bond Lengths [Å], Distances [Å], and Angles [°].	217

List of Charts

Chart 1.1	Examples of Boron-containing Monomers for Free Radical Polymerization.	3
Chart 1.2	Examples of Boron-Containing Monomers for Controlled Free Radical Polymerization.	5
Chart 1.3	Examples of Boron-Containing Monomers for Ziegler-Natta Polymerization.	6
Chart 1.4	Examples of Boron-Containing Monomers for Metathesis Polymerization.	7
Chart 1.5	Examples of Main Chain Organoboron Polymer Sensors for Anions.	13
Chart 1.6	Examples of Side Chain Functionalized Organoboron Polymer Sensors.	14
Chart 1A.1	Some Examples of Polymer-Supported Reagents.	24
Chart 1A.2	Examples of Oxazaborolidine based Supported Reagents.	27
Chart 1A.3	Examples of Alkyl Borane Reagents.	30
Chart 1A.4	Examples of Chiral Borane Reagents.	31

Chart 1A.5	Examples of Arylborane Reagents.	32
Chart 1B.1	Examples of Organoboron Donor-Acceptor Compounds.	56
Chart 1B.2	Examples of Thiophene Containing Donor-Acceptor Compounds.	57
Chart 1B.3	Examples of Thienyl-vinylene Containing Donor-Acceptor Compounds.	58
Chart 1B.4	Examples of Donor-Acceptor Systems from Wang and Co-workers.	59
Chart 1B.5	Examples of Sensors from Wang and Co-workers.	62
Chart 1B.6	Examples of Phosphorescent Fluoride Sensors.	63
Chart 1B.7	Some Sensors from Gabbaï and Co-workers.	64
Chart 1B.8	Examples of Cationic Trimesityl Boranes.	66
Chart 1B.9	Examples of Water Soluble Conjugated Polymers.	70
Chart 1B.10	Example of a Donor-Acceptor Conjugated Polyelectrolyte.	72
Chart 1C.1	Some Examples of Conjugated Polymers.	127
Chart 1C.2	Some Examples of Conjugated Polymers Synthesized by Organometallic and Condensation Routes.	134
Chart 1C.3	Selected Catalysts used for ADMET Polymerization (Cy =	139

cyclohexyl; Mes = mesityl).

Chart 1C.4	Some Examples of Functionalized Polymers Synthesized via ADMET.	141
Chart 1C.5	Some Examples of Poly(<i>para</i> -phenylenevinylene) (PPV) and Poly(fluorenylvinylene) (PFV) Type Monomers.	143
Chart 1C.6	Examples of Silicon Containing ADMET Polymers.	147
Chart 1C.7	Examples of Germanium, Tin and Phosphazene Containing Polymers Synthesized via ADMET.	148
Chart 1C.8	Examples of Ferrocene Containing Polymers Synthesized via ADMET.	149
Chart 1C.9	Molybdenum Containing Polymers Synthesized via ADMET.	150
Chart 1C.10	Examples of Triarylborane Compounds with Triisopropylphenyl Substituents.	157
Chart 2.1	Aggregation of Organocopper Compounds.	180
Chart 2.2	Examples of Tetrameric Arylcopper Compounds.	183
Chart 2.3	Examples of Arylcopper Compounds Stabilized by P and S Donor Ligands.	188
Chart 2.4	Examples of Pentafluorophenylzinc and Pentafluorophenylsilver.	191

Chart 2.5	Examples of Trimeric Copper(I) Complexes.	193
Chart 2.6	Examples of π -complexes.	208
Chart 2.7	Examples of Cu- π Complexes.	210
Chart 2.8	Pentafluorophenylcopper and Selected Arenes.	212

Chapter 1. General Introduction

1.1 Organoboron Polymers

Inorganic and organometallic polymers have attracted much attention in the field of materials chemistry. Incorporation of the organometallic moieties into polymers can lead to higher thermal stability and electrical conductivity.¹ For example, it has been shown that polystannane polymers show unusual electronic properties²⁻⁵ due to the σ -delocalized backbone, and incorporation of ferrocenes into the polymeric backbone or side chain can lead to interesting redox properties of the polymers.⁶ Of particular interest to us, is the incorporation of organoboranes into polymers because they can act as Lewis acids due to the empty p-orbital on the boron center.⁷ The functionalization of synthetic polymers with organoborane moieties has been widely studied for applications as supported reagents, immobilized catalysts, sensor materials, stimuli responsive polymers, components of lithium ion batteries, flame retardants, preceramic materials and as intermediates for the preparation of other functional organic polymers.⁸⁻¹⁰ Boron containing polymers also allow for facile and reversible formation of donor-acceptor bonding for functionalization of polymers.¹¹⁻¹³

1.2 Synthesis of Boron Containing Polymers

Organoboron polymers are generally prepared either via direct polymerization of boron containing monomers or via post-polymer modification reactions. Synthesis of soluble organoboron polymers with controlled architecture, high molecular weights, and varying degree of functionalization can be achieved via side-chain functionalization. Free radical polymerization, Ziegler-Natta polymerization and metathesis polymerization have been used to synthesize side-chain functionalized polymers. The incorporation of boron into the main chain of polymers has been mainly achieved via hydroboration polymerization, cross coupling reactions and electro-polymerization reactions.¹⁴

1.2.1 Direct Polymerization of Boron Monomers

Side chain functionalized polymers can be prepared from organoboron monomers using a variety of polymerization techniques including standard and controlled free radical polymerization due to their simple synthetic procedures and reasonable compatibility with the monomers. For example, heat induced, BPO, AIBN, or potassium persulfate initiated free radical polymerization¹⁵⁻¹⁸ has been applied to the homo- and copolymerization of olefins containing boronic acid (1)^{19, 20} and boronic ester groups (2). Monomers such as vinylborazines (3)²⁰⁻²⁴, vinylphenylborazines (4)^{25, 26} have also been successfully

polymerized. The synthesis of homo and copolymers from monomers containing the *closo*-[B₁₂H₁₂]²⁻ cage (5 and 6) has been recently reported by Shore and coworkers.²⁷

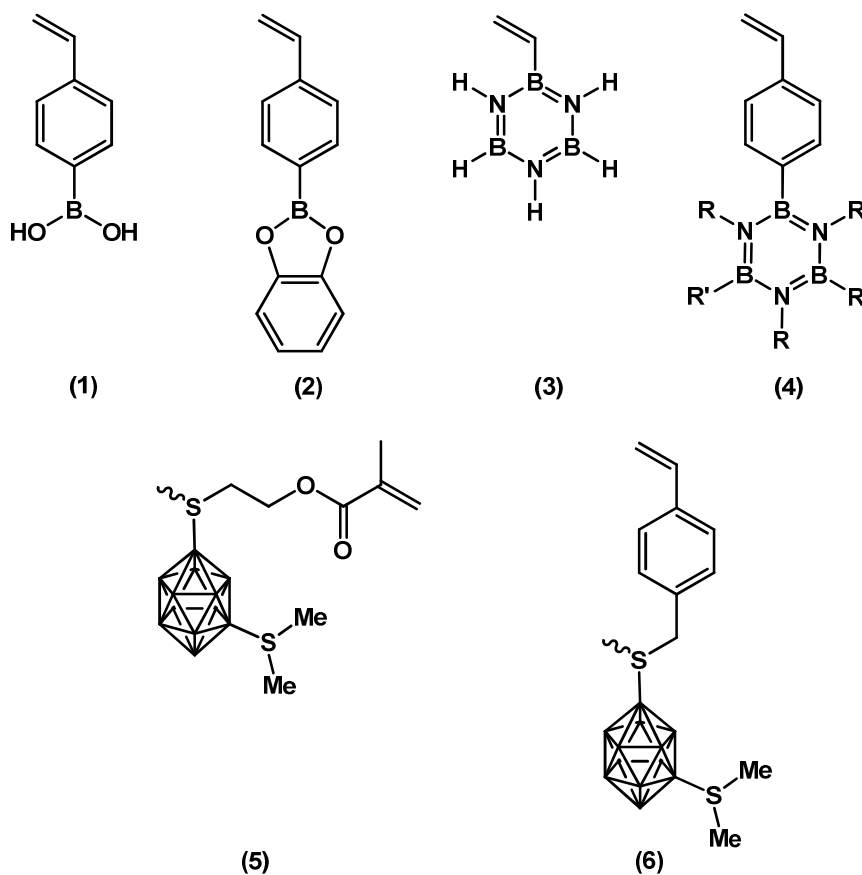


Chart 1.1 Examples of Boron-containing Monomers for Free Radical Polymerization.

Controlled free radical polymerization techniques have been utilized for the preparation of organoboron polymers with controlled architecture and high molecular weights with

functional end groups. Jäkle and coworkers have prepared the first example of a boron functionalized block copolymer using atom transfer free radical polymerization (ATRP)²⁸ of the organoboron monomer (7).²⁹ Sumerlin and coworkers have shown that it is not only possible to synthesize homopolymers of styrene boronic acid, acrylamidophenyl boronic acid (8) and ester via RAFT (Reversible Addition-Fragmentation Chain Transfer), but block copolymers of the above mentioned boronic acid/ester functionalized compounds with dimethylacrylamide can also be obtained.³⁰ Nitroxide-mediated Free Radical Polymerization (NMP) is another technique that has been used by Adronov and coworkers for the synthesis of carborane-containing dendronized polymers from the carborane-functionalized styrenic monomer (9).³¹ Well-defined polymers with high boron content and narrow molecular weight distributions were obtained.

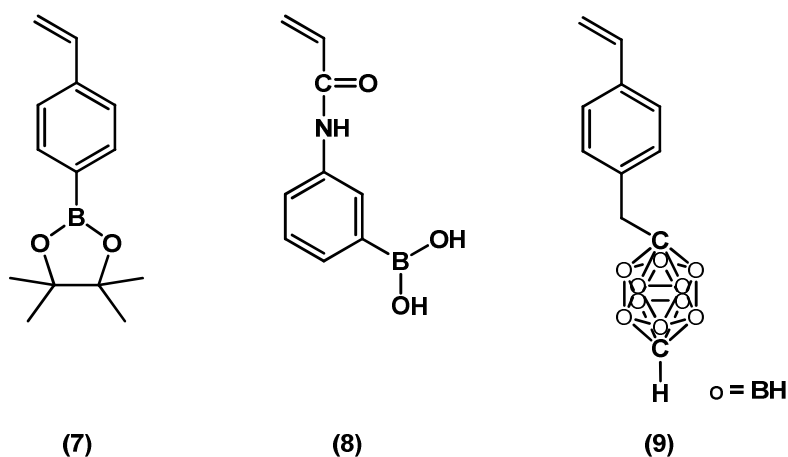


Chart 1.2 Examples of Boron-Containing Monomers for Controlled Free Radical Polymerization.

Ziegler-Natta polymerization has also been widely employed for the synthesis of boron containing polymers and is especially useful for the polymerization of more highly reactive and more strongly Lewis acidic organoboron species. Chung and coworkers have extensively studied the homo and random copolymerization of boron-functionalized monomers. For instance, boron functionalized α -olefin (10) was homo-polymerized with $\text{TiCl}_3/\text{Al}(\text{Et})_2\text{Cl}$ catalytic system to afford a 9-BBN functionalized polyolefin.³² Polymerization of the boron-functionalized styrene monomer (11) with the syndiospecific titanium catalyst $\text{Cp}^*\text{Ti}(\text{OMe})_3$ (Cp^* = pentamethylcyclopentadienyl) in the presence of methylaluminoxane (MAO) provided access to syndiotactic polymers.³³

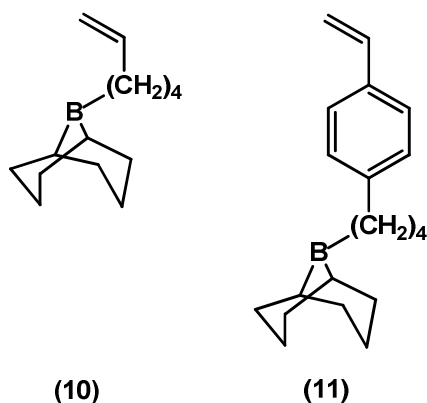


Chart 1.3 Examples of Boron-Containing Monomers for Ziegler-Natta Polymerization.

Metathesis polymerization is another methodology that has been employed for the synthesis of boron containing polymers from boron containing monomers. Chung and coworkers reported polymerizing *exo*-9-BBN functionalized norbornene (12) monomers using ring-opening metathesis polymerization (ROMP) with different tungsten carbene catalytic systems.³⁴ Polymerization of a series of enantiomerically pure organoboronate monomers in *exo*- as well as *endo*-forms (13) via ROMP was studied by Wagener.³⁵ GPC analysis of the boron-functionalized polymers indicated high molecular weights with dispersities in the range of 1.5-3.8. They have also studied ADMET of organoboronate monomers (14); however, cyclic by-products through ligand exchange reactions between boronate moieties and the catalyst prevented isolation and characterization of the polymers.³⁵ The synthesis of decaborane functionalized polymers through ROMP of

decaborane functionalized norbornene (15) and cyclooctene (16) was reported by Sneddon and coworkers.^{36, 37} The synthesis of a boron-containing monomer based on an oxonorbornene-functionalized *o*-carborane (17) and its subsequent ROMP to obtain low polydispersity and high-molecular weight carborane-based polymers was described by Coughlin and coworkers.³⁸ The formation of amphiphilic block copolymers was demonstrated via sequential monomer addition. ADMET polymerization will be described in detail in Chapter 1C.

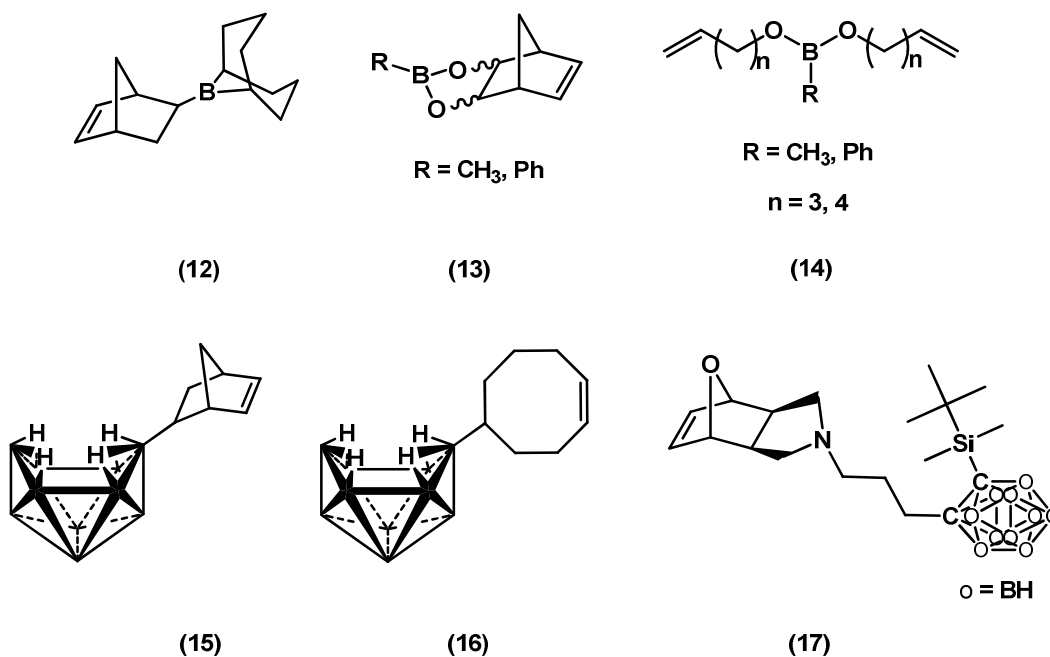


Chart 1.4 Examples of Boron-containing Monomers for Metathesis Polymerization.

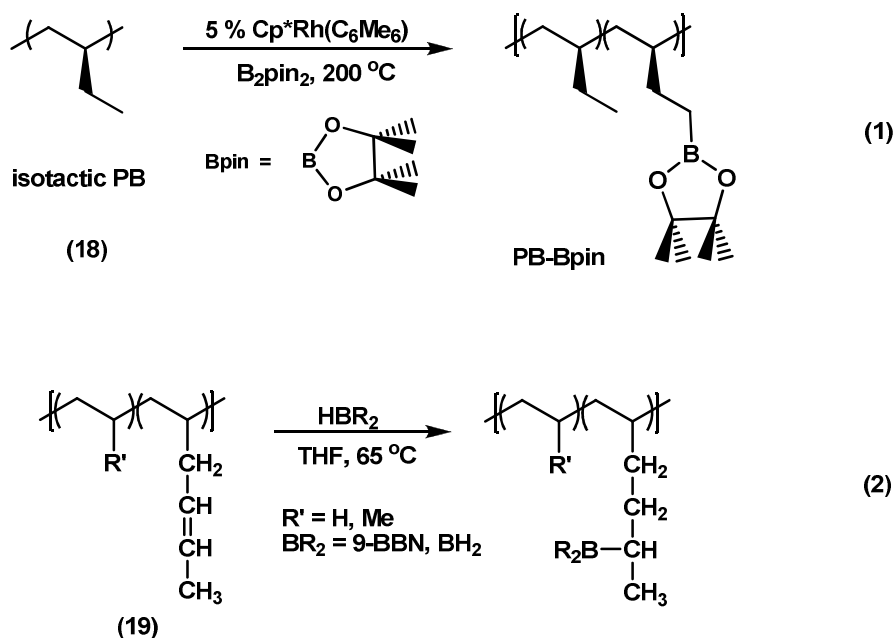
1.2.2 Polymer Modification Reactions

Post-polymerization modification represents an alternative to the direct polymerization of borylated monomers which allows us to avoid issues, like compatibility of the monomer with given polymerization techniques. In the past, polymer analogous procedures were mainly limited to polymer resins and generally resulted in relatively low degrees of functionalization and in the case of soluble polymers side-reactions that led to cross-linking were commonly observed.³⁹ Recent advances in this field have led to the successful application of hydroboration chemistry⁴⁰ and transition-metal catalyzed polymer modification reactions. Moreover, well-defined fully functionalized borylated polystyrene is readily accessible through facile silicon-boron exchange reactions.^{41, 42}

1.2.2.1 Modification of Polyolefins

Transition metal-catalyzed direct borylation of unfunctionalized polyolefins was reported by Bae and coworkers. As shown in Scheme 1.1, (1), isotactic polybutene (PBP) (18) was functionalized in the presence of $\text{Cp}^*\text{Rh}(\text{C}_6\text{Me}_6)$ and B_2pin_2 .⁴³ Alternatively, boron containing polymers can be prepared by hydroboration of unsaturated polyolefins. Chung and coworkers have extensively used unsaturated polyolefins such as poly(ethylene-co-1,4-hexadiene), poly(propylene-co-1,4-hexadiene) (19) and

poly(isobutylene-co-isoprene) (butyl rubber) for the preparation of boron-functionalized polymers via hydroboration with $\text{BH}_3 \cdot \text{THF}$ or 9-BBN-H (Scheme 1.1, (2)).^{44, 45}



Scheme 1.1 Examples of Borane Modification of Polyolefins.

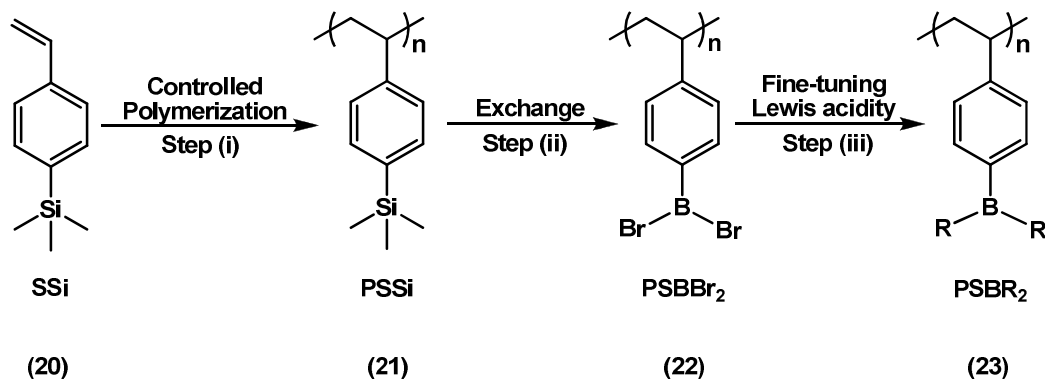
1.2.2.2 From Mercuriated Polystyrene

Studies by Paetzold showed that the direct borylation of polystyrene/divinylbenzene resin with haloborane Br_2BH occurs only under forcing conditions and is limited by relatively low selectivity.⁴⁶ Thorpe and coworkers treated linear and cross-linked polystyrene with mercuric(II) trifluoroacetate and subsequently reacted with different

boron hydrides including $\text{BH}_3\cdot\text{THF}$, $\text{BH}_3\cdot\text{SMe}_2$, $\text{BBr}_2\text{H}\cdot\text{SMe}_2$, $\text{BH}_2\text{Cl}\cdot\text{SMe}_2$, and HBcat (cat = catecholato).^{47, 48} Although high degrees of mercuriation were achieved, the functional yield for the borane treatment was moderate and cross-linking was apparent after hydrolysis to the respective boronic-acid functionalized polymers.

1.2.2.3 Side-chain Functionalized Organoboron Polymers via Si-B Exchange Reactions

Our group has developed a general strategy toward the synthesis of well-defined soluble organoboron polymers with controlled architecture, molecular weight and degree of functionalization.^{41, 42} Using this strategy, the boryl groups can selectively be attached to the side-chain of homo- and block copolymers, respectively, or alternatively placed at the polymer chain ends.^{29, 41, 49} This strategy involves the following steps (i) the quasi-living polymerization of the silylated functional monomer (20) via atom-transfer radical polymerization (ATRP) to obtain the silyl functionalized polymer, (21) (ii) exchange of the trimethylsilyl functional group with Lewis acidic boron centers (22) and (iii) fine-tuning of the Lewis acidity of the boron center by substituent exchange reactions (23) (Scheme 1.2).^{41, 42}



Scheme 1.2 Si-B Exchange Route for the Synthesis of Organoboron Containing Polymers.

1.3 Applications of Boron Containing Polymers

The Lewis-acidic boron has an empty p-orbital and can reach desired octet configuration either via π -overlap with suitable organic substituent or via formation of Lewis acid-base complexes.⁵⁰

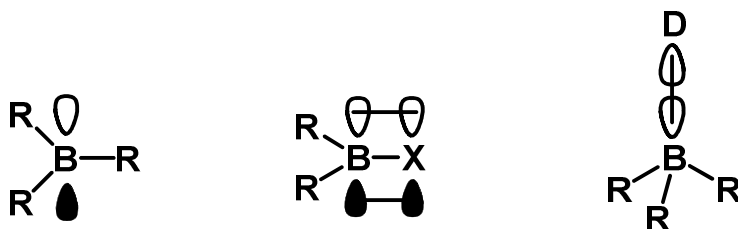


Figure 1.1 Schematic Representation of Properties of Organoboron Compounds.¹⁰

These interactions have been utilized in many applications of organoboron compounds. Interesting linear and non-linear optical properties result from the overlap of the empty p-orbital on boron with organic π -systems. Upon coordination of nucleophiles (D), the photophysical properties of organoboranes show significant changes which has been widely used in sensor applications.⁵¹ Donor-acceptor bonding between organoboranes and Lewis bases can be exploited for the reversible assembly of macrocycles and coordination polymers.⁵² Finally, the function of these organoboranes as catalysts and cocatalysts in organic synthesis is based on donor-acceptor interactions that lead to activation of organic substrates.^{12, 13, 53}

1.3.1 Applications in Organic Synthesis and Catalysis

Potential applications in synthetic chemistry include their use as supported catalysts and cocatalysts. Applications of organoboron polymers in organic synthesis and catalysis will be discussed in Chapter 1A.

1.3.2 Applications as Sensor Materials

Tricoordinate boron, with its vacant p-orbital, is a useful π -acceptor which can lead to significant delocalization when conjugated with an adjacent organic π -system. Both main chain and side chain organoboron polymers have been exploited as effective probes for

detection of anions. For example, Chujo and coworkers have studied the effect of fluoride binding to the main chain conjugated polymers (24), which were obtained through hydroboration of *p*-diethynylbenzene with MesBH₂ and TripBH₂, respectively.^{54, 55} A strong decrease in intensity and related blue shift of the absorption band at 377 nm was apparent upon addition of a fluoride source. A dramatic decrease in the fluorescence intensity was evident upon addition of 0.5 molar equivalents of fluoride at a concentration of 10⁻⁶ M in CHCl₃. The latter indicates significant signal amplification. Moreover, high selectivity for fluoride over other halides was confirmed.

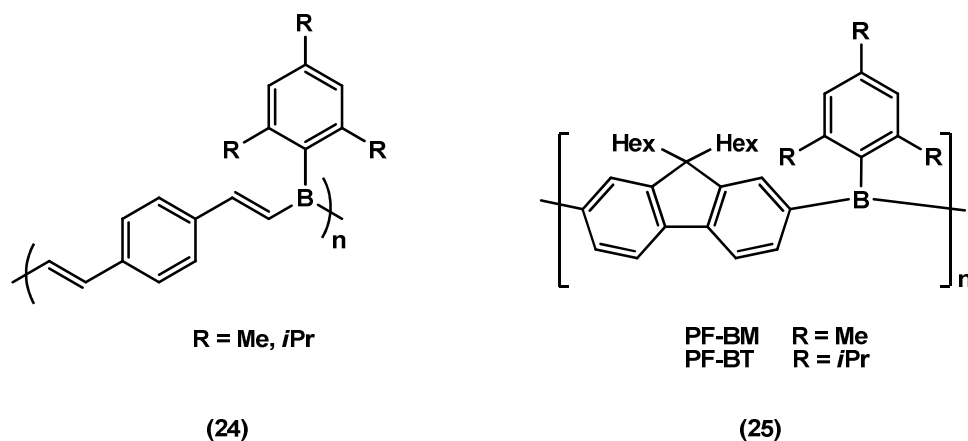


Chart 1.5 Examples of Main Chain Organoboron Polymer Sensors for Anions.

Jäkle and coworkers have investigated the binding of anions to the boron-modified polyfluorenes (25). Binding studies of fluorenylborane polymer PF-BT indicated that both

fluoride and cyanide effectively bind to the polymer, leading to distinct changes in the absorption and emission spectra. However, larger anions such as chloride and bromide did not bind effectively. Based on the spectral titration plots for fluoride and cyanide binding in THF, a two-step binding process was reported which was attributed to a charge-transfer structure with alternating electron-rich borate and electron-deficient borane moieties in the polymeric main chain.⁵⁶

Jäkle *et al.* have also reported polystyrene based side-chain functionalized organoboron polymers which employ substituted bithiophene units as the chromophores and mesityl groups as sterically protecting groups for boron (26).⁵⁷ These polymers have been shown to effectively detect fluoride and cyanide ions over other halide ions at millimolar concentrations. The strong binding to fluoride could easily be monitored by UV-vis and fluorescence spectroscopy.

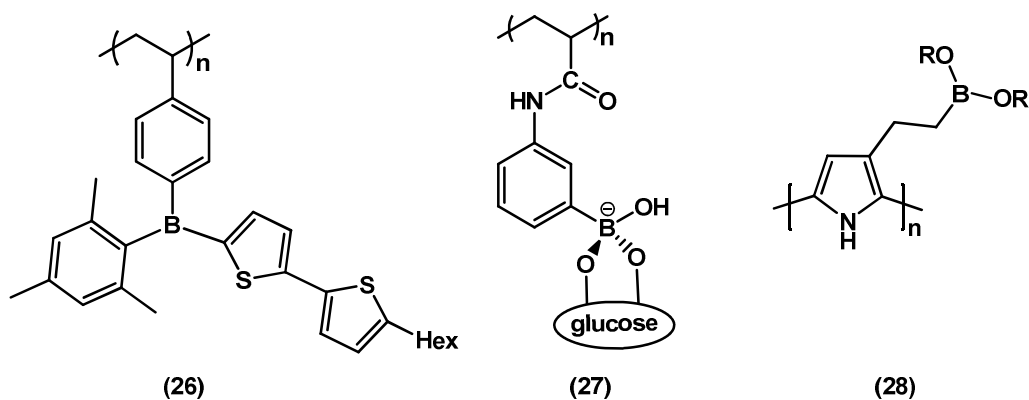


Chart 1.6 Examples of Side Chain Functionalized Organoboron Polymer Sensors.

Sumerlin and coworkers employed boronic acid functionalized poly(acryl amides) (27) as efficient sugar sensors and pH responsive materials.³⁰ The electrochemical synthesis of conjugated polymers that feature boronic acid or boronate moieties has been studied by Freund *et al.*, Fabre *et al.*, and He *et al.*⁵⁸ Boronic acid and boronate ester functionalized polypyrrole (28) and its use as a fluoride sensor was studied by cyclic voltammetry.^{59, 60}

1.3.3 Other Applications

Borates and boronic acids are well known to function as flame retardants. Flame-retardant properties of boron containing bisphenol-A resins have been reported by Gao and Liu.⁶¹ Thermal analysis of the resin revealed higher heat and oxidative resistance than for most common phenol-formaldehyde resins. Carborane-derived polymers have been used in the production of boron carbide ceramic fibers and matrices. Sneddon and coworkers reported blends of poly(norbornenyldecaborane) (PND) with commercially available silicon carbide preceramic polymers, such as poly(methylcarbosilane) (PMCS) or allylhydridopolycarbosilane (AHPCS) as excellent processable precursors to boron-carbide/silicon-carbide ceramic composite materials.⁶²

Conducting nanoparticles of poly(aniline boronic acid) with average diameter of 12-15 nm were synthesized via controlled electrochemical polymerization by Freund and coworkers. These nanoparticles were found to be extremely resistant to degradation at

extreme electrochemical potentials and hence may find applications as coatings or may be used for fabrication of nanoscale devices.⁶³

1.4 References and Notes

1. Archer, R. D., *Inorganic and organometallic polymers*; Wiley-VCH: New York, 2001; Abd-El-Aziz, A. S.; Carraher Jr., C. E.; Pittman Jr., C. U.; Sheats, J. E.; Zeldin, M. *Macromolecules Containing Metal and Metal-Like Elements, Volume I, A Half-Century of Metal- and Metalloid-Containing Polymers*; John Wiley & Sons: Hoboken, 2003; Manners, I. *Synthetic Metal-Containing Polymers*; Wiley-VCH, 2004; Abd-El-Aziz, A. S.; Manners, I.; Editors *Frontiers in Transition Metal-Containing Polymers*; Wiley-Interscience: Hoboken, NJ, 2007.
2. Sita, L. R. *Organometallics* **1992**, *11*, 1442-1444.
3. Sita, L. R. *Acc. Chem. Res.* **1994**, *27*, 191-197.
4. Imori, T.; Lu, V.; Cai, H.; Tilley, T. D. *J. Am. Chem. Soc.* **1995**, *117*, 9931-9940.
5. Yokoyama, Y.; Hayakawa, M.; Azemi, T.; Mochida, K. *J. Chem. Soc., Chem. Commun.* **1995**, 2275-2275.
6. Parab, K.; Jäkle, F. *Macromolecules* **2009**, *42*, 4002-4007.
7. Gabel, D. *Georg Thieme Verlag, Stuttgart, New York* 2005, *6*, pp. 1277.
8. Chujo, Y. *Macromol. Symp.* **1997**, *118*, 111-116.

9. Gabel, D. *Chapter 6.1.4.1 Boron-containing polymers. In Science of Synthesis: Houben-Weyl Methods of Molecular Transformations, D. Kaufmann, D.S. Matteson (Eds.), Georg Thieme Verlag, Stuttgart 1277* 2004.
10. Jäkle, F. *Coord. Chem. Rev.* **2006**, 250, 1107-1121.
11. Chen, E. Y.-X.; Marks, T. J. *Chem. Rev.* **2000**, 100 1391-1434.
12. Piers, W. E.; Irvine, G. J.; Williams., V. C. *Eur. J. Inorg. Chem.* **2000**, 2000, 2131-2142.
13. Yamamoto., E. H. *Lewis Acids in Organic Synthesis, Wiley/VCH, New York*, 2000.
14. Jäkle, F. J. *Inorg. Organomet. Polym. Mater.* **2005**, 15, 293-307.
15. Hoffmann, A. K.; Thomas, W. B. *J. Am. Chem. Soc.* **1959**, 81, 580-582.
16. Letsinger, R. L.; Hamilton, S. B. *J. Am. Chem. Soc.* **1959**, 81, 3009-3012
17. Lennarz, W. J.; Snyder, H. R. *J. Am. Chem. Soc.* **1960**, 82, 2169-2171.
18. Hartmann, M., Carlsohn, H., Rudolph, F. *Faserforschung und Textiltechnik* **1977**, 28, 59
19. Çimen, E. K.; Rzaev, Z. M. O.; Piskin, E. *J. Appl. Polym. Sci.* **2005**, 95, 573-582.
20. Pellon, J.; Deichert, W. G.; Thomas, W. M. *J. Polym. Sci.* **1961**, 55, 153-160.
21. Lynch, A. T.; Sneddon, L. G. *J. Am. Chem. Soc.* **1989**, 111, 6201-6209.

22. Su, K.; Remsen, E. E.; Thompson, H. M.; Sneddon, L. G. *Macromolecules* **1991**, *24*, 3760-3766.
23. Proux, Y.; Clement, R. *C. R. Chim.* **1968**, *266*, 890-892.
24. Proux, Y.; Clement, R. *Bull. Soc. Chim. Fr.* **1970**, 528-533.
25. Jackson, L. A., Allen, C. W. *J. Polym. Sci. A* **1992**, *30*, 577-581.
26. Jackson, L. A.; Allen, C. W. *Phosph. Sulf. Silicon* **1989**, *41*, 341.
27. Teshome, B. Y.; Xuenian, C.; Scott, S.; Jon, P.; Edward, A. M.; Sheldon, G. S. *Chem. Eur. J.* **2009**, *15*, 2190-2199.
28. Matyjaszewski, K.; Xia, J. H. *Chem. Rev.* **2001**, *101*, 2921-2990.
29. Qin, Y.; Sukul, V.; Pagakos, D.; Cui, C.; Jäkle, F. *Macromolecules* **2005**, *38*, 8987-8990.
30. Roy, D.; Cambre, J.; Sumerlin, B. *Chem. Commun.* **2008**, 2477-2479.
31. Benhabbour, S. R.; Parrott, M. C.; Gratton, S. E. A.; Adronov, A. *Macromolecules* **2007**, *40*, 5678-5688.
32. Ramakrishnan, S.; Berluche, E.; Chung, T. C. *Macromolecules* **1990**, *23*, 378-382.
33. Dong, J. Y.; Manias, E.; Chung, T. C. *Macromolecules* **2002**, *35*, 3439-3447.
34. Ramakrishnan, S.; Chung, T. C. *Macromolecules* **1989**, *22*, 3181-3183.
35. Wolfe, P. S.; Wagener, K. B. *Macromolecules* **1999**, *32*, 7961-7967.

36. Sneddon, L. G.; Pender, M. J.; Forsthoefel, K. M.; Kusari, U.; Wei, X. *J. Eur. Ceram. Soc.* **2005**, *25*, 91-97.
37. Matsumoto, A.; Kurata, T.; Shiino, D.; Kataoka, K. *Macromolecules* **2004**, *37*, 1502-1510.
38. Simon, Y. C.; Ohm, C.; Zimny, M. J.; Coughlin, E. B. *Macromolecules* **2007**, *40*, 5628-5630.
39. Caze, C.; Moualij, N. E.; Hodge, P.; Lock, C. J.; Ma, J. *J. Chem. Soc. Perkin Trans. I* **1995**, 345-349.
40. Chung, T. C.; Janvikul, W. *J. Organomet. Chem.* **1999**, *581*, 176-187.
41. Qin, Y.; Cheng, G.; Sundararaman, A.; Jäkle, F. *J. Am. Chem. Soc.* **2002**, *124*, 12672-12673.
42. Qin, Y.; Cheng, G.; Parab, K.; Achara, O.; Jäkle, F. *Macromolecules* **2004**, *37*, 7123-7131.
43. Bae, C.; Hartwig, J. F.; Boen Harris, N. K.; Long, R. O.; Anderson, K. S.; Hillmyer, M. A. *J. Am. Chem. Soc.* **2005**, *127*, 767-776.
44. Chung, T. C.; Rhubright., D. *J. Polym. Sci. A: Polym. Chem.* **1993**, *31*, 2759-2763.
45. Chung, T. C.; Lu, H. L.; Li., C. L. *Macromolecules* **1994**, *27*, 7533-7537.
46. Paetzold, P.; Hoffmann, J. *Chem. Ber.* **1980**, *113*, 3724-3733.

47. Bullen, N. P.; Hodge, P.; Thorpe., F. G. *J. Chem. Soc., Perkin Trans. 1*, **1981**, 1863-1867.
48. El-Assiery, S. A.; Dillingham, K. A.; Ponsonby, A.; G.Thorpe, F.; Wareham., R. *S. Eur. Polym. J.* **1993**, 29, 443-447.
49. Qin, Y.; Jäkle., F. *J. Inorg. Organomet. Polym. Mater.* **2007**, 17, 149-157.
50. Jäkle, F. "Boron: Organoboranes", Chapter in *Encyclopedia of Inorganic Chemistry*, Ed. B. King, Wiley, VCH 2005, pp 560-598.
51. Yamaguchi, S.; Akiyama, S.; Tamao., K. *J. Organomet. Chem.* **2002**, 652, 3-9.
52. Ma, K.; Scheibitz, M.; Scholz, S.; Wagner., M. *J. Organomet. Chem.* **2002**, 652, 11-19.
53. Chen, E. Y.-X.; Marks., T. J. *Chem. Rev* **2000**, 100, 1391-1434.
54. Matsumi, N.; Chujo, Y. *Polym. J.* **2008**, 40, 77-89.
55. Matsumi, N.; Naka, K.; Chujo, Y. *J. Am. Chem. Soc.* **1998**, 120, 5112-5113.
56. Li, H.; Jäkle, F. *Angew. Chem. Int. Ed.* **2009**, 48, 2313-2316.
57. Parab, K.; Venkatasubbaiah, K.; Jäkle, F. *J. Am. Chem. Soc.* **2006**, 128, 12879-12885.
58. Ma, Y.; Ali, S. R.; Wang, L.; Chiu, P. L.; Mendelsohn, R.; He, H. *J. Am. Chem. Soc.* **2006**, 128, 12064-12065.

- 59. Nicolas, M. F., B.; Marchand, G.; Simonet, J. *Eur. J. Org. Chem.* **2000**, 9, 1703-1710.
- 60. Nicolas, M., Fabre, B., Simonet, J. *J. Electroanal. Chem.* **2001**, 509, 73-79.
- 61. Gao, J., Liu, Y., Wang, F. *Eur. Polym. J.* **2001**, 37, 207-210
- 62. Guron, M. M.; Wei, X.; Welna, D.; Krogman, N.; Kim, M. J.; Allcock, H. R.; Sneddon, L. G. *Chem. Mater.* **2009**, 21, 1708-1715.
- 63. Deore, B. A.; Yu, I.; Woodmass, J.; Freund, M. S. *Macromol. Chem. Phys.* **2008**, 209, 1094-1105.

Chapter 1A. Boron Polymers as Supported Reagents

1A.1 Polymer Supported Reagents

In recent years there has been great interest in the functionalization of polymers, which allows for their use as catalysts or reagents in organic reactions. The interest in the field of solid phase catalysis with polymer supported reagents is being enhanced by the possibility of creating systems that combine unique properties of active moieties and those of high molecular weight polymer.¹ Insoluble polymers have been used frequently since they can easily be isolated by filtration and washed by passing solvent over them. Regeneration and reusability are some other important advantages of the polymeric reagents. The polymeric reagents often differ in reactivity from the low molecular weight counterparts due to the effects of the polymeric matrix.

The use of functional polymeric reagents depends on their physical properties (linear or cross-linked polymer) as well as chemical constitution. In the case of soluble polymeric reagents, such as polyethylene glycol (PEG) and linear polystyrene, the separation of the soluble polymer from its low molecular weight contaminants is difficult and hence the recovery of the polymer is not quantitative. The insolubility of crosslinked polymers provides for separation and hence simplified work-up procedures. Cross-linked styrene based polymers remain by far the most commonly used supports and the required

functional groups are introduced by the chemical modification of appropriate preformed polymers. This approach is the one used most extensively by organic chemists as one can start with commercially available polymer beads of suitable physical size and form, as well as with a known percentage of cross-linking. However, reaction conditions must be carefully chosen in order to avoid side-reactions because it is not possible to remove the polymer-bound impurities resulting from such reactions.

1A.2 Synthesis of Supported Borane Reagents

Many of the reactions which have been used to chemically modify polystyrenes involve electrophilic aromatic substitution, such as halogenation, sulphonation and Friedel-Crafts alkylations and acylation. Discussed in the following are boron-containing polymeric reagents.

Devaky and Rajasree have reported a polymer bound ethylenediamine borane reagent (29) for use as a reducing agent for the reduction of aldehydes. This polymeric reagent was synthesized from a Merrifield resin and 1,6-hexanediol diacrylate-cross-linked polystyrene resin (HDODA-PS).² The borane reagent was incorporated in the polymer by complexation with sodium borohydride. When the reducing agent was used in the competitive reduction of a 1:1 mixture of aldehyde and ketone, the aldehyde was selectively reduced to an alcohol. Polymer-supported sulfonamides (30) have been

prepared by treating polymeric sulfonyl chlorides with (*S*)-diphenylprolinol.³ They were investigated as catalyst supports for the reduction of ketones in the presence of borane-dimethyl sulfide complex. Itsuno and coworkers have reported the design of a highly enantioselective polymer-supported catalysts (31) that are derived from chiral oxazaborolidinone and feature different cross-linking structures for use in Diels-Alder reaction of methacrolein with cyclopentadiene.^{4, 5}

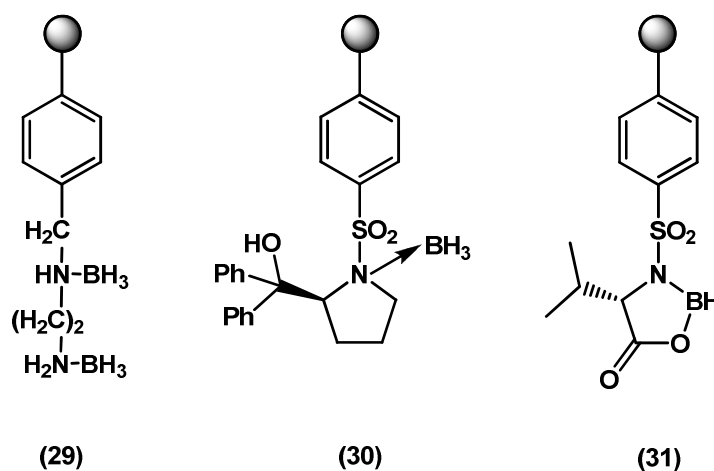
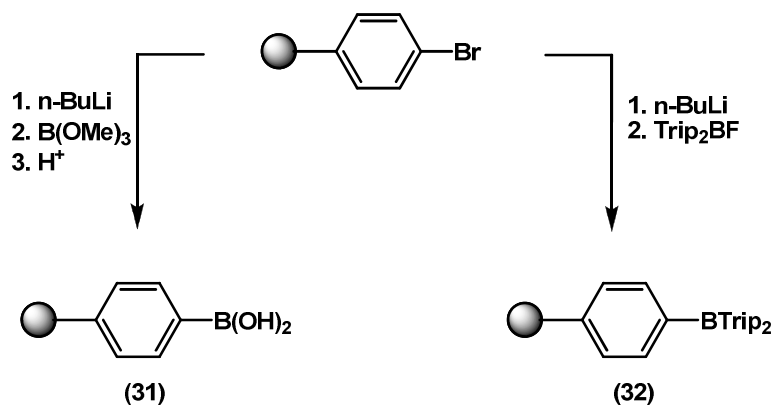


Chart 1A.1 Some Examples of Polymer-Supported Reagents.

To attach boron directly to the aromatic ring in PS, direct lithiation using excess *n*-BuLi can be applied, but only 25% functionality is realized and both the *meta* and *para* positions react. Upto 100% of the phenyl groups can be functionalized via Fréchet's three-step reaction sequence, which involves bromination and lithiation followed by

quenching with appropriate boranes.⁶ In this process, bromination was conducted with different catalysts including FeCl_3 , TiCl_3 and $\text{Ti}(\text{OAc})_3$ and was characterized via ^{13}C NMR spectroscopy. The lithiation step was done using excess $n\text{-BuLi}$ in the presence of TMEDA and was quantitative in aromatic solvents such as benzene. Treatment of lithiated polystyrene resins with an alkoxyborane followed by hydrolysis with HCl led to boronic acid functionalized resins (Scheme 1A.1).



Scheme 1A.1 Preparation of Polymer-Supported Organoboranes.

A high degree of functionalization with boronic acid or other functional groups can typically be achieved via this methodology. The resulting polystyrene boronic acid intermediate (31) can be further converted to diol complexes or transformed into chiral oxazaborolidines that serve as catalysts in organic reactions.⁷⁻¹⁰

A triarylborane functionalized resin (32) was prepared by Smith and coworkers through lithiation of brominated polystyrene resin with n-BuLi followed by addition of the bulky fluoroborane Trip_2BF (Trip = 2,4,6-triisopropylphenyl) in THF to give the resin with 66% functionality.¹¹ The resin was further converted to a lithium hydroborate resin with t-BuLi and used as highly diastereoselective and recoverable reagent in the reduction of methylated cyclohexanone derivatives. However, when this method was applied to soluble organoboron polymers, significant cross-linking was observed.

The polymer-bound (*S*)-diphenylprolinol based reducing agent (33) was established by Waldvogel and coworkers from boronic acid precursor (31) and used for enantioselective borane reduction of ketones in the presence of a borane source. The active species is formed upon complexation of BH_3 to the amine functionality of the oxazaborolidine moiety.¹² Caze and coworkers reported yet another oxazaborolidine catalyst⁸ (34), derived from cross linked polystyrene containing boronic acid groups (1*R*, 2*S*)-(–)-norephedrine for reduction of ketones. Caze *et al.* also synthesized poly(2-vinylthiophene) based oxazaborolidine containing supported reagent (35), which was used for the enantioselective reduction of prochiral ketones.¹⁰

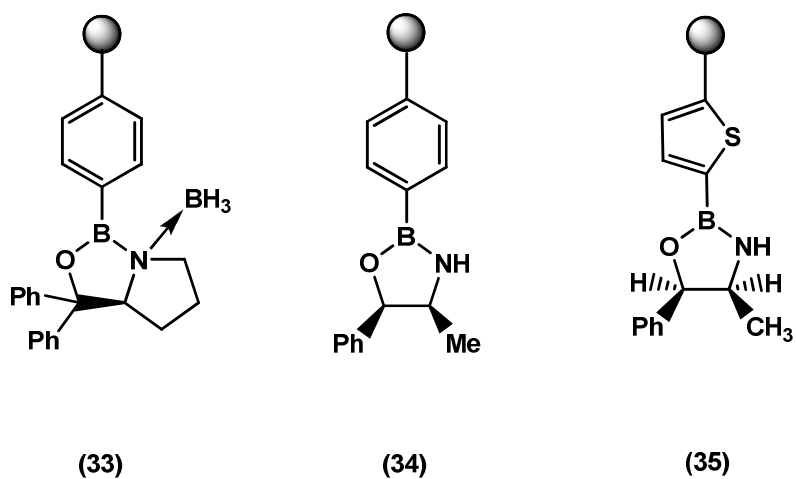
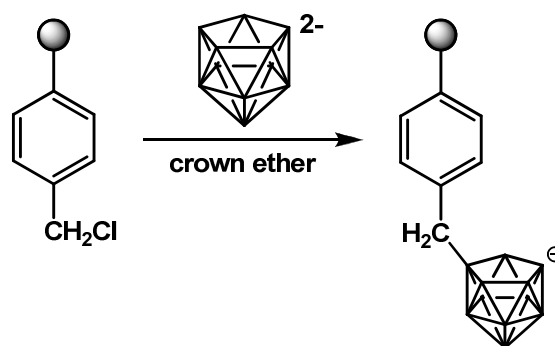


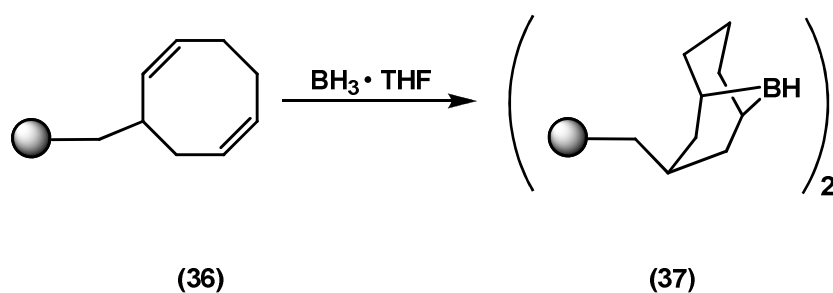
Chart 1A.2 Examples of Oxazaborolidine based Supported Reagents.

Some unusual boron functionalities, such as dianionic carborane cages were attached to polystyrene through a polymer modification route using crown ether as the catalyst.¹³ The resulting resins served as scaffold of supported catalysts by addition of different metal complexes to the carborane cages (Scheme 1A.2).



Scheme 1A.2 Preparation of Carborane Containing Polymer-Supported Reagents.

The preparation of polymer-supported 9-BBN from a high loading Merrifield resin has been reported by Ganesan *et al.* Immobilized cyclooctadiene (PS-COD) (36), was synthesized via reaction of Merrifield resin with deprotonated 1,5-cyclooctadiene.¹⁴ Hydroboration of this PS-COD with $\text{BH}_3 \cdot \text{THF}$ led to the supported organoborane resin (37) with a loading of 3.24 mmol/g which was used as supported reagent for alkene hydroboration-oxidation reactions.



Scheme 1A.3 Preparation of Polymer-Supported 9-BBN.

1A.3 Hydroboration Chemistry

The hydroboration reaction introduced by H. C. Brown is one of the most widely applied methods in the synthesis of organoboron compounds.¹⁵⁻¹⁷ Much of the early work in hydroboration was carried out using diborane. While hydroboration with $\text{BH}_3 \cdot \text{THF}$ and $\text{BH}_3 \cdot \text{SMe}_2$ is sufficient for simple substrates, the reagent shows poor regio- and diastereoselectivity for many other substrates. Where BH_3 has proven most useful is as a precursor to other, more selective reagents, partially substituted borane reagents, such as thexylborane¹⁸ (38), disiamylborane¹⁹ (39), dicyclohexylborane (40), and 9-borabicyclo[3.3.1]nonane (41) are finding an increasing role in these applications. For example, thexylborane (38) is a highly versatile reagent, valuable for the synthesis of unsymmetrical ketones. Disiamylborane (39) and dicyclohexylborane²⁰ (40) are highly hindered dialkylboranes and provide better regioselectivity than $\text{BH}_3 \cdot \text{THF}$ or $\text{BH}_3 \cdot \text{SMe}_2$ and are used for monohydroboration of less crowded alkenes. 9-BBN (41) is an exceptionally regioselective hydroborating reagent and also stable toward disproportionation and used widely for the selective reduction of organic functional groups.^{21, 22} Recently Snieckus and coworkers reported a new organoborane reagent, di(isopropylprenyl)borane ($i\text{PP}_2\text{BH}$)²³ (42), for hydroboration of both alkenes and alkynes.

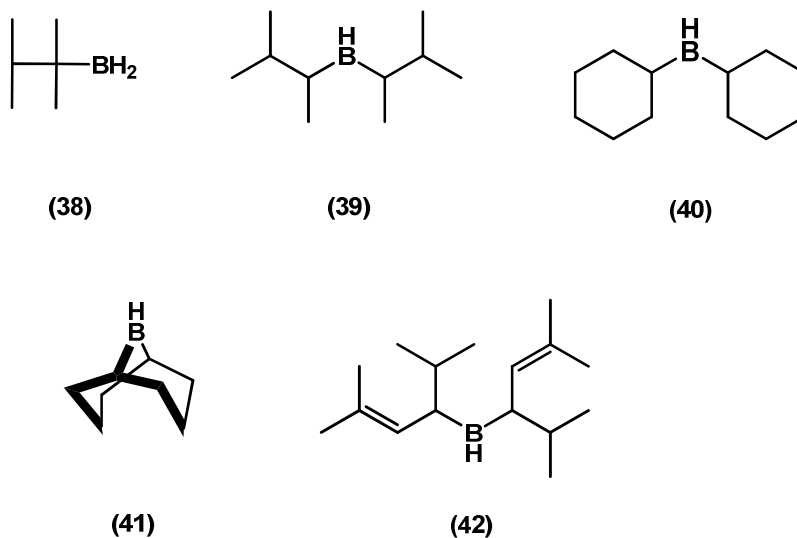


Chart 1A.3 Examples of Alkyl Borane Reagents.

Chiral organoboranes derived from optically active α -pinene (~92% ee), have been successfully used for asymmetric transformations, such as the hydroboration of prochiral olefins, reduction of prochiral ketones, asymmetric allyl- and crotylboration, asymmetric opening of *meso*-epoxides and asymmetric homologation. For instance, the versatile hydroborating reagent diisopinocampheylborane $\text{Ipc}_2\text{BH}^{24}$ (43), is readily available from the reaction of α -pinene with $\text{BH}_3 \cdot \text{SMe}_2$. It reacts with less sterically hindered *cis*-alkenes with 80-90% ee, in many cases. However hydroboration of *trans* and trisubstituted alkenes proceeds slowly and hence the degree of chiral induction is lowered to 14-22%. However, sterically less hindered monoisopinocampheylborane IpcBH_2 (44), reacts with aliphatic or phenyl substituted and *trans* and trisubstituted alkenes providing

enantiomeric purities in the range of 50 to 99%. Masamune's C_2 -symmetric borolane (45), is selective for all these substrates namely, cis, trans, and trisubstituted alkenes.²⁵ Soderquist and coworkers recently reported 10-substituted-9-borabicyclo[3.3.2]decanes (10-R-9-BBD-H, (46)) and their unique behavior in the asymmetric hydroboration of 1,1-disubstituted alkenes.²⁶

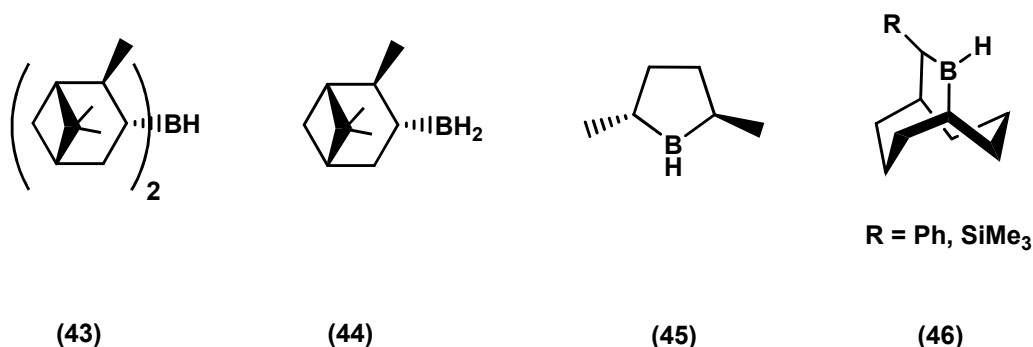


Chart 1A.4 Examples of Chiral Borane Reagents.

Arylboranes (ArBH_2 and Ar_2BH) have been used as alternatives to alkylboranes to counter retrohydroboration reactions. Diphenylborane, mesitylborane¹⁶ (47), dimesitylborane (48) and triisopropylphenylborane²⁷ (47) are examples of stable hydroboration reagents available. These arylborane reagents not only show better stability in solution but also exhibit very high regio and chemoselectivity in hydroboration reactions. Dimesitylborane (48) has proved to be an exceptionally selective reagent for

the hydroboration of alkynes. Perfluorinated diarylborane (C_6F_5)₂BH (49) synthesized by Piers and co-workers using the commercially available trispentafluorophenylborane ($\text{B}(\text{C}_6\text{F}_5)_3$) shows remarkable regio- and chemoselectivity as a hydroborating agent due to the electron-deficient nature of the boron and the formation of monomeric borane in solution.^{28, 29}

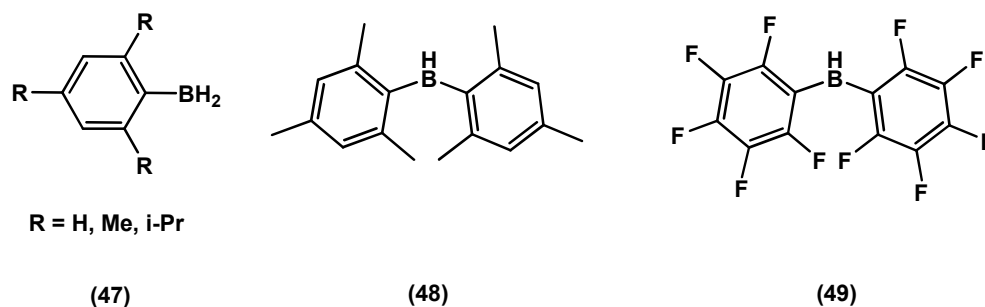
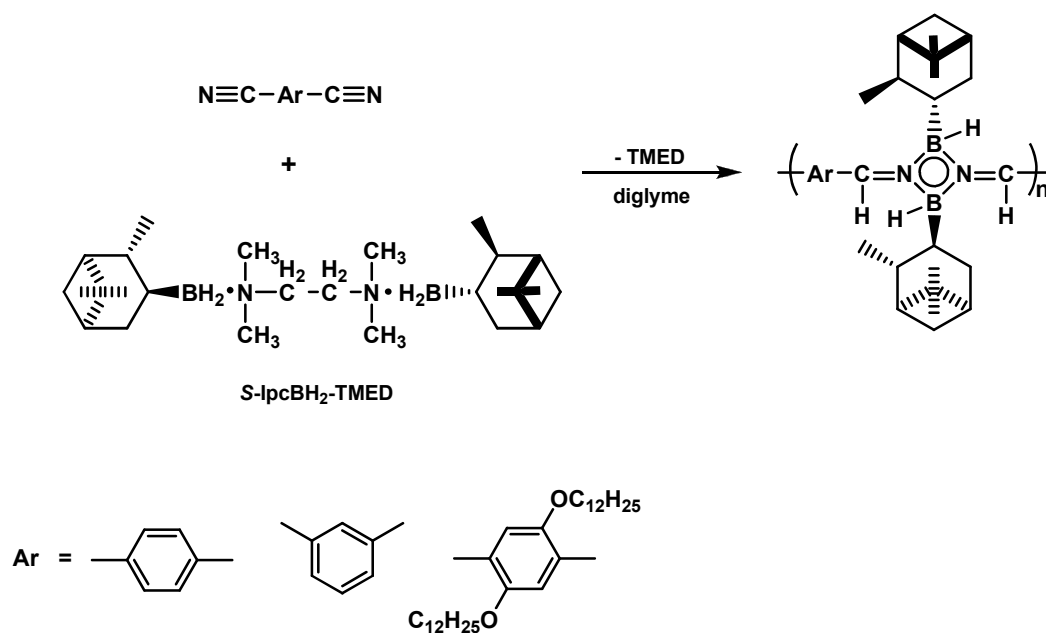


Chart 1A.5 Examples of Arylborane Reagents.

Hydroboration has also been successfully employed by Chujo and co-workers in their pioneering work on the incorporation of boron into the main chain of polymers through hydroboration polymerization reactions.³⁰⁻³⁴ The latter are among the most versatile and general methods for the preparation of organoboron polymers and, for example, provide facile access to electronically interesting conjugated organoboron polymers. Recently, Chujo *et al.* reported the synthesis of chiral luminescent organoboron polymers by hydroboration polymerization of a the chiral borane, monoisopinocampheylborane

(IpcBH₂), in the presence of *N,N,N',N'*-tetramethylethylenediamine with aromatic dicyanobenzene compounds (Scheme 1A.4). The polymers exhibited interesting photophysical properties and studies on specific rotation and circular dichroism (CD) confirmed the chirality of the resulting polymers.³⁵



Scheme 1A.4 Synthesis of Main Chain Chiral Organoboron Polymers.

We hypothesized that the versatility and exceptional selectivity of hydroboration could add significantly to the synthetic toolbox available to date for the preparation of functional materials derived from borylated polystyrene and therefore became interested

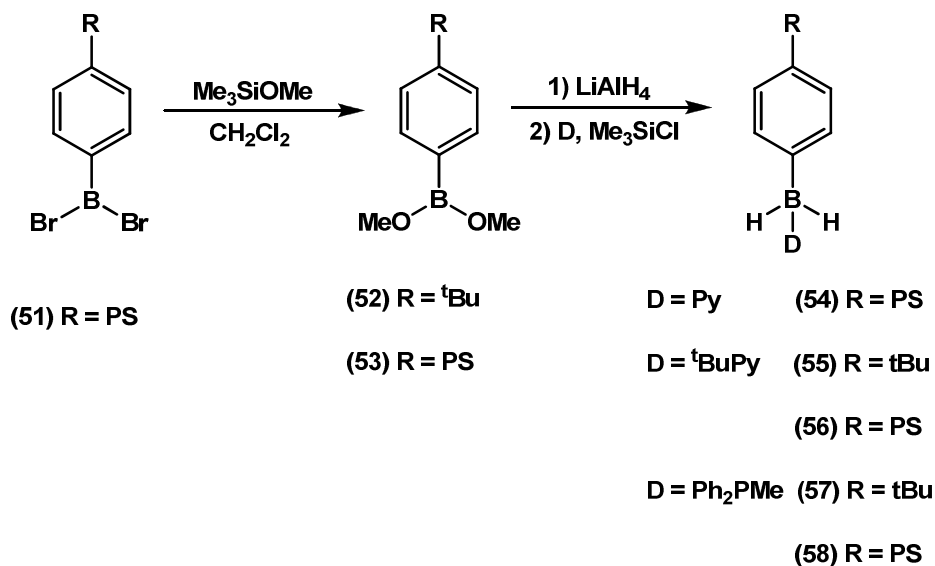
in the preparation of BH₂-functionalized polystyrene. We describe here the preparation of well-defined polymers containing BH₂ as pendant groups to polystyrene, which are complexed with pyridine, t-butylpyridine (^tBuPy), and PPh₂Me, respectively.

1A.4 Results and Discussion

1A.4.1 Synthesis

Poly(4-trimethylsilyl styrene) (50) of controlled molecular weight ($M_w = 35,000$ and $PDI = 1.11$) was prepared by polymerization of 4-trimethylsilyl styrene via atom transfer radical polymerization (ATRP) as described previously.^{36, 37} Treatment with a slight excess of BBr₃ in CH₂Cl₂ gave poly(4-dibromoboryl styrene) (PS-BBr₂) (51), which was reacted in situ with excess of Me₃SiOMe to give poly(4-dimethoxyboryl styrene) (PS-B(OMe)₂) (53). Me₃SiOMe was used rather than MeOH in order to prevent formation of the strong acid HBr, which possibly could lead to side reactions that even at a very small extent would be detrimental in the case polymer modification reactions. Conversion of PS-B(OMe)₂ to the boron hydride was performed in analogy to a method reported by Hawthorne *et al.*³⁸ for the preparation of C₆H₅BH₂•Py (Scheme 1A.5). Due to the different solubility characteristics of the polymer, THF was used instead of diethyl ether as the reaction medium. Slow addition of PS-B(OMe)₂ to a suspension of LiAlH₄ in THF at 0 °C led to formation of a white precipitate. Addition of pyridine, 4-*tert*-butylpyridine

(^tBuPy), and PPh₂Me, respectively, followed by addition of Me₃SiCl yielded the boron polymers PS-BH₂•Py (54), PS-BH₂•^tBuPy (56), and PS-BH₂•PPh₂Me (58). For comparison, the corresponding molecular model compounds ^tBuC₆H₄BH₂•D (D=Py, ^tBuPy (55), PPh₂Me (57)) were prepared using similar procedures. It is important to note that addition of the base is instrumental for the successful isolation of these arylborane polymers. In the absence of added base, complex mixtures were obtained for the model compounds and insoluble materials for the polymers. Presumably redistribution reactions of ArBH₂ to give Ar₂BH and Ar₃B take place, which ultimately leads to cross-linking of the polymers through boron bridges. The occurrence of redistribution reactions of this type was previously postulated to be responsible for cross-linking in reactions of mercuriated polymers with BH₃^{39, 40}, and has recently been exploited for the selective preparation of ferrocenylborane polymers [-FcB(Br)-]_n from in-situ generated Fc(BBrH)₂ (Fc = 1,1'-ferrocenediyl).⁴¹



Scheme 1A.5 Synthesis of Organoborane Complexes RBH₂ • D.

The pyridine-complexed polymer (54) showed very low solubility in common organic solvents such as CH₂Cl₂, THF, and toluene and was not further studied. The low solubility is likely related to strong interpolymer interactions between the relatively exposed pyridine π -systems. Indeed, complexation with ^tBuPy and PPh₂Me, respectively, led to highly soluble polymer complexes PS-BH₂•D ((56); D = ^tBuPy, (58); D = PPh₂Me). The observed solubility characteristics are in good agreement with our previous results on donor complexes of triarylboranes, where we found that complexation of pyridine to PS-BAr₂ (Ar = thienyl, C₆F₅) resulted in poorly soluble polymers, whereas use of ^tBuPy produced soluble colorless polymeric Lewis acid-base complexes.⁴²

1A.4.2 Structural Characterization

1A.4.2.1 Multinuclear NMR Spectroscopy

The polymers (56) and (58) and the corresponding molecular model compounds (55) and (57) were analyzed by multinuclear NMR and IR spectroscopy. The ^{11}B NMR shifts of -5.5 and -25.6 ppm for (56) and (58), respectively, are consistent with the formation of tetracoordinate boron polymers. Relative to the model compounds, no significant change of the chemical shift is observed, but a distinct signal broadening is evident especially for the $^t\text{BuPy}$ complex (Figure 1A.1). Coordination of the phosphine to boron was further confirmed by ^{31}P NMR, which showed two signals at 5.2 and 3.9 ppm, which are strongly downfield shifted in comparison to the free phosphine ($\delta = -26.7$ ppm). The observation of two separate resonances in comparison to only one doublet at 2.9 ppm for (57) is attributed to the effects of the atactic nature of the polymer backbone. In the ^1H NMR for (56) a broad signal for the BH_2 moiety is evident at ca. 3.4 ppm, while for (58), the polymer backbone resonances are overlapping with the BH_2 signal at ca. 2.4 ppm. The corresponding model compounds give rise to multiplets at similar chemical shifts of 3.45 and 2.36 ppm, respectively. The ^{13}C NMR spectra for the polymers also match very well with those of the model compounds and a representative comparison is provided in Figure 1A.2. Only the phenyl protons in *ortho*-position to boron significantly shift as expected upon incorporation into the polystyrene framework.

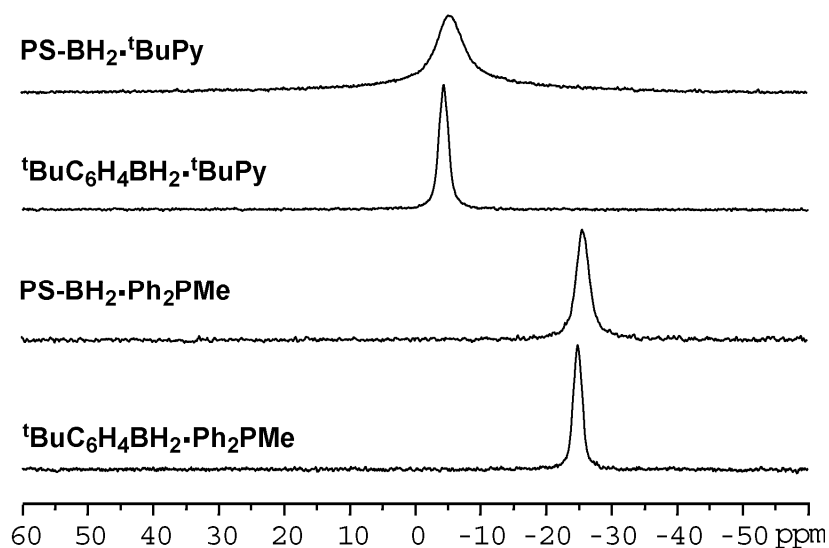


Figure 1A.1 Comparison of ^{11}B NMR Spectra.

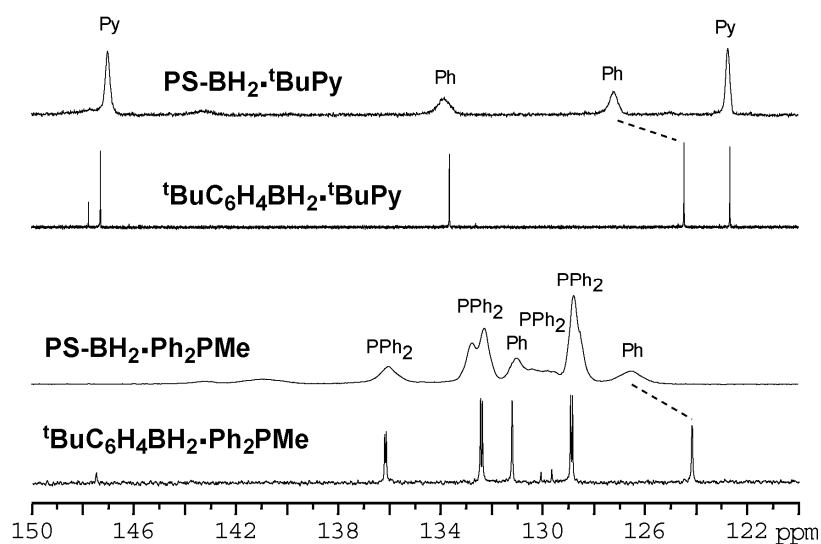


Figure 1A.2 Comparison of ^{13}C NMR spectra; only the region from 120 to 150 ppm is shown and the quaternary carbon signals are not marked.

1A.4.2.2 IR Spectroscopy

The infrared spectra of polymers (52) and (53) show strong absorptions at 2332 cm^{-1} and 2340 cm^{-1} , respectively, which are in a region typical of terminal B-H stretching modes.⁴³ The IR bands are similar to those for the molecular model compounds $^t\text{BuC}_6\text{H}_4\text{BH}_2\bullet^t\text{BuPy}$ (2327 cm^{-1}) and $^t\text{BuC}_6\text{H}_4\text{BH}_2\bullet\text{PPh}_2\text{Me}$ (2326 and 2360 cm^{-1}), thus further corroborating successful functionalization of the polymers with BH_2 moieties.

1A.4.2.3 Molecular Weight Determination

Molecular weight measurements for the polymers were attempted by gel permeation chromatography in THF. However, significant peak tailing was observed leading to unexpectedly low calculated molecular weight and to polydispersities that are considerably higher than the one of the starting polymer, PS-SiMe₃. The latter is attributed to partial decomplexation in THF and interaction of the BH_2 functional groups with the column material.

1A.4.2.4 Thermal Properties

The thermal characteristics of the polymers were examined by differential scanning calorimetry (DSC) and thermogravimetric analysis (TGA). PS-BH₂•PPh₂Me shows a

glass transition temperature (T_g) of 100 °C, which is in a similar range as that of unfunctionalized polystyrene. However, we were not able to observe a clear T_g in the case of PS-BH₂•^tBuPy, most likely due to gradual thermal degradation of the polymer as further indicated by thermogravimetric analysis (TGA). Multi-step decomposition processes were observed in the TGA plots of both polymers (Figure 1A.3). The phosphine complexed polymer (T_{dec} = 200 °C) shows slightly higher thermal stability than the polymer complex with *tert*-butylpyridine (T_{dec} = 145 °C). In comparison to silylated polystyrene (PS-SiMe₃) the onset of degradation is considerably lowered, indicating that initial decomplexation of the Lewis base plays a key role in the degradation processes. The air stability of the polymers was studied by NMR spectroscopy. No substantial degradation was observed in the solid state upon exposure to air over a period of three to four weeks for PS-BH₂•PPh₂Me, but additional sharp NMR signals corresponding to small molecule degradation products started to develop after ca. two weeks in solution. Polymer PS-BH₂•PPh₂Me shows comparatively higher stability than PS-BH₂•^tBuPy, possibly as a result of steric protection of the B-H functionalities with the bulkier phosphine.

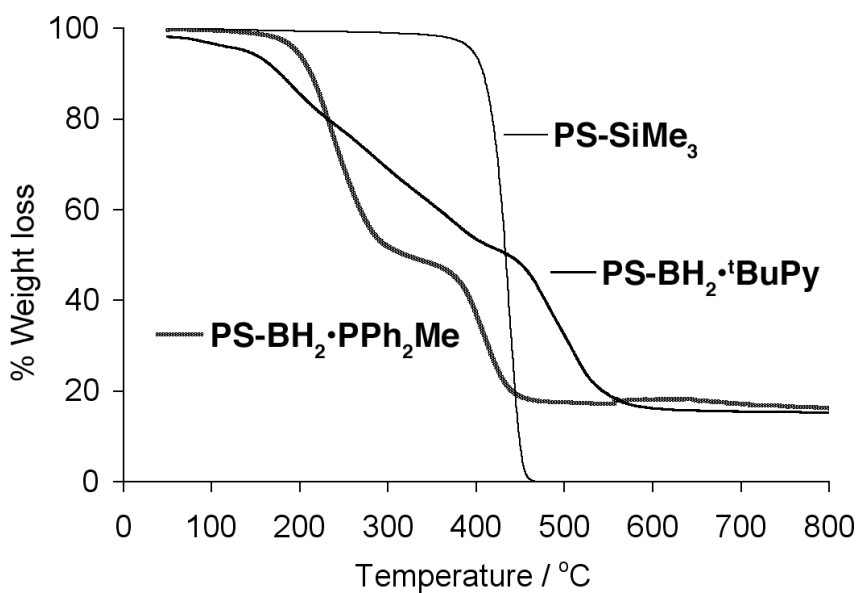


Figure 1A.3 Thermogravimetric analysis (TGA) plots of poly(4-trimethylsilyl styrene) (PS-SiMe₃), PS-BH₂·^tBuPy and PS-BH₂·PPh₂Me (20 °C/min, N₂).

1A.5 Conclusions

We have prepared a new organoborane polymer that is functionalized with BH₂ moieties, which are attached selectively to the para-position of the phenyl rings of a soluble polystyrene framework. For the successful isolation of the polymer, it is critical to prevent redistribution reactions of the ArBH₂ moieties through strong complexation with Lewis bases such as amines or phosphines.

1A.6 Experimental Section

1A.6.1 Materials and Instrumentation

LiAlH₄, pyridine, 4-*tert*-butylpyridine, PPh₂Me, Me₃SiOMe, and Me₃SiCl were purchased from Acros Organics and BBr₃ (99+%) from Aldrich. BBr₃ was further purified by vacuum distillation and pyridine, 4-*tert*-butylpyridine, methoxytrimethylsilane, and chlorotrimethylsilane were distilled from CaH₂ and degassed via several freeze-pump-thaw cycles. **Caution!** BBr₃ is toxic and highly corrosive and should be handled appropriately with great care. Fluorinated grease was used for ground glass joints in all reactions involving boron tribromide. Poly(4-trimethylsilyl styrene) (PS-SiMe₃) of $M_w = 35,000$ and $PDI = 1.11$ (GPC-RI) and ^tBuC₆H₄B(OMe)₂ were prepared as previously reported.^{36, 37} All reactions were carried out under inert atmosphere using Schlenk techniques or a glove box (Innovative Technologies). Ether solvents were distilled from Na/benzophenone and hydrocarbon and chlorinated solvents were purified using a solvent purification system (Innovative Technologies; alumina/copper columns for hydrocarbon solvents). The chlorinated solvents were subsequently distilled from CaH₂ and degassed via several freeze-pump-thaw cycles.

All 499.893 MHz ¹H, 125.7 MHz ¹³C, 160.4 MHz ¹¹B NMR and 499.895 MHz ³¹P NMR spectra were recorded at ambient temperature on a Varian INOVA spectrometer equipped with a boron-free 5 mm dual broadband gradient probe (Nalorac, Varian Inc.,

Martinez, CA). Solution ^1H and ^{13}C NMR spectra were referenced internally to solvent signals. ^{11}B NMR spectra were referenced externally to $\text{BF}_3 \cdot \text{Et}_2\text{O}$ ($\delta = 0$) and ^{31}P NMR spectra were referenced to D_3PO_4 in D_2O ($\delta = -0.26$). ^{11}B NMR spectra were acquired with boron-free quartz NMR tubes. IR spectra were recorded as KBr pellets using a Thermo Nicolet IR 200 Spectrophotometer. Mass spectral data were obtained in FAB mode with 2-nitrophenyloctyl ether (NPOE) as the matrix at Michigan State University Mass Spectrometry Facility which is supported, in part, by a grant (DRR-00480) from the Biotechnology Research Technology Program, National Center for Research Resources, National Institutes of Health. GPC analyses were performed in THF (1 mL/min) using a Waters Breeze system equipped with a 717plus autosampler, a 1525 binary HPLC pump, a 2487 dual λ absorbance detector, and a 2414 refractive index detector. A series of styragel columns (Polymer Laboratories; 5 μm Mix-D, 5 μm Mix-C, and 10 μm Mix-B), which were kept in a column heater at 35 $^\circ\text{C}$, were used for separation. The columns were calibrated with PS standards (Polymer Laboratories). DSC measurements were performed on a Perkin Elmer Differential Scanning Calorimeter Pyris 1 system with ca. 10 mg of polymer using the specified scan rate. Thermogravimetric analyses were performed under N_2 atmosphere using a Perkin Elmer Pyris 1 system with ca. 5 mg of polymer at a heating rate of 20 $^\circ\text{C}/\text{min}$ from 50 $^\circ\text{C}$ to 800 $^\circ\text{C}$.

1A.6.2 Preparation of Polymers and Model Compounds

Synthesis of ${}^t\text{BuC}_6\text{H}_4\text{BH}_2\cdot{}^t\text{BuPy}$ (55): A solution of ${}^t\text{BuC}_6\text{H}_4\text{B}(\text{OMe})_2$ (0.50 g, 2.5 mmol) in THF (10 mL) was transferred via cannula to a slurry of LiAlH_4 (0.15 g, 4.0 mmol) in 20 mL of THF at 0 °C. The resulting gray mixture was stirred at 0 °C for 1 h and then at room temperature for 2 h. 4-*tert*-Butylpyridine (0.45 mL, 3.0 mmol) was added and the resulting solution was stirred for 1 h. The reaction mixture was quenched with Me_3SiCl (5 mL) and stirred overnight. A solid precipitate (LiCl) formed which was removed by filtration using a fritted glass disk. The solvent was removed, the residue taken up in toluene and filtered once more. The filtrate was concentrated under high vacuum and the residue recrystallized from CH_2Cl_2 to give the product as colorless crystals (0.45 g, 64%). For ${}^t\text{BuC}_6\text{H}_4\text{BH}_2\cdot{}^t\text{BuPy}$: ${}^{11}\text{B}$ NMR (160.386 MHz, CDCl_3): $\delta = -4.3$ ($w_{1/2} = 260$ Hz); ${}^1\text{H}$ NMR (499.893 MHz, CDCl_3): $\delta = 8.55$ (d, 2H, $J = 7.0$ Hz, Py_o), 7.50, 7.25 (d, 2H, $J = 7.0$ Hz, m, 4H, Py_m , Ph), 3.45 (m, 2H, BH_2), 1.36, 1.30 ($2 \times$ s, $2 \times$ 9H, Py-CMe_3 , Ph-CMe_3). ${}^{13}\text{C}$ NMR (125.69 MHz, CDCl_3): $\delta = 164.9$ (Py_p), 147.8 (Ph_p), 147.3 (Py_o), 133.6 (Ph_o), 124.5 (Ph_m), 122.7 (Py_m), 35.7, 34.5 (Py-CMe_3 , Ph-CMe_3), 31.7, 30.5 (Py-CMe_3 , Ph-CMe_3), not observed (Ph_i). IR: ν (cm^{-1}) 2327, BH. FAB-MS (NPOE): m/z : 280 [$\text{M}^+ - \text{H}$] (100 %).

Synthesis of $\text{PS-BH}_2\cdot{}^t\text{BuPy}$ (56): A solution of BBr_3 (1.7 g, 6.8 mmol) in 10 mL of CH_2Cl_2 was added dropwise under stirring to PS-SiMe_3 (1.0 g; ca. 5.7 mmol SiMe_3

groups; $PDI = 1.11$) in 10 mL of CH_2Cl_2 . After completion of the addition the mixture was stirred for 24 h. Complete replacement of the silyl substituents for dibromoboryl groups was confirmed by ^1H NMR spectroscopy. The resulting solution of PS-BBr₂ was then treated with Me_3SiOMe (2.4 mL, 17 mmol) and stirred for 10 h. All volatile material was removed under high vacuum and the oily residue was redissolved in 20 mL THF. The solution of PS-B(OMe)₂ was transferred via cannula to a slurry of LiAlH_4 (0.32 g, 8.4 mmol) in 20 mL of THF at 0 °C. The resulting gray suspension was stirred at 0 °C for 1 h and then at room temperature for 20 h. 4-*tert*-Butylpyridine (1.25 mL, 8.5 mmol) was added; the resulting mixture was stirred for 24 h, and subsequently quenched with Me_3SiCl (10 mL). After stirring for 24 h, a solid precipitate (LiCl) formed, which was removed by filtration using a fritted glass disk. The filtrate was concentrated under high vacuum to ca. 5 mL and precipitated into a large volume of hexanes (ca. 250 mL). The precipitate was repeatedly taken up in a minimum amount of CH_2Cl_2 , filtered once more, and precipitated into hexanes. The product was dried at 50 °C under vacuum to give a white powder (0.77 g, 54 %). For PSBH₂•^tBuPy: ^{11}B NMR (160.386 MHz, CDCl_3): $\delta = -5.5$ ($w_{1/2} = 750$ Hz); ^1H NMR (499.893 MHz, CDCl_3): $\delta = 8.3$ (br, 2H, ^tBuPy_o), 7.3, 6.9, 6.4 (3 × br, 3 × 2H, Py_m, Ph_{o,m}), 3.4 (br, 2H, BH₂), 2.4-1.4 (br, 3H, polymer backbone), 1.2 (br, 9H, CMe₃). ^{13}C NMR (125.69 MHz, CDCl_3): $\delta = 164.5$ (br, Py_p), 147.0 (br, Py_o), 143.2 (br, Ph_i), 133.8 (br, Ph_o), 127.2 (br, Ph_m), 122.7 (br, Py_m), 40 (very br, polymer

backbone), 35.5 (br, CMe_3), 30.4 (br, CMe_3); IR: ν (cm^{-1}) 2332, BH. GPC-RI: $M_w = 19517$, PDI = 1.30. TGA (20 $^{\circ}\text{C}/\text{min}$; under N_2): 23 % weight loss between 145 $^{\circ}\text{C}$ and 303 $^{\circ}\text{C}$; 27% weight loss between 459 $^{\circ}\text{C}$ and 543 $^{\circ}\text{C}$.

Synthesis of $^t\text{BuC}_6\text{H}_4\text{BH}_2\cdot\text{PPh}_2\text{Me}$ (57): A solution of $^t\text{BuC}_6\text{H}_4\text{B}(\text{OMe})_2$ (0.50 g, 2.5 mmol) in THF (10 mL) was transferred via cannula to a slurry of LiAlH_4 (0.15 g, 4.0 mmol) in 20 mL of THF at 0 $^{\circ}\text{C}$. The resulting gray mixture was stirred at 0 $^{\circ}\text{C}$ for 1 h and then at room temperature for 3 h. PPh_2Me (0.57 mL, 3.1 mmol) was added and the resulting green solution was stirred for 6 h. The reaction mixture was quenched with Me_3SiCl (5 mL) and stirred overnight. A solid precipitate (LiCl) formed, which was removed by filtration using a fritted glass disk. The solvent was removed, the residue taken up in toluene and filtered once more. The filtrate was concentrated under high vacuum to ca. 1 mL and then precipitated into hexanes (ca. 20 mL). The solution was decanted and the product was isolated as a white solid (0.35 g, 40%). For $^t\text{BuC}_6\text{H}_4\text{BH}_2\cdot\text{PPh}_2\text{Me}$: ^{11}B NMR (160.386 MHz, CDCl_3): $\delta = -24.8$ ($w_{1/2} = 270$ Hz); ^1H NMR (499.893 MHz, CDCl_3): $\delta = 7.57$ (m, 4H, PPh_2), 7.49 (t, $^3J_{\text{HH}} = 7.5$ Hz, 2H, PPh_2), 7.42 (m, 4H, PPh_2), 7.17 (m, 2H, Ph_o), 7.17 (d, $^3J_{\text{HH}} = 8.0$ Hz, 2H, Ph_m), 2.36 (m, 2H, BH_2), 1.77 (d, $^2J_{\text{PH}} = 9.5$ Hz, 3H, PMe), 1.26 (s, 9H, CMe_3). ^{31}P NMR (499.895 MHz, CDCl_3): $\delta = 2.9$ (d, $J = 44$ Hz). ^{13}C NMR (125.698 MHz, CDCl_3): $\delta = 147.5$ (d, $^5J_{\text{PC}} = 4.5$ Hz, Ph_p), 141 (br, Ph_i), 136.2 (d, $^3J_{\text{PC}} = 7.5$ Hz, Ph_o), 132.5 (d, $^2J_{\text{PC}} = 8.4$ Hz, $o\text{-PPh}_2$),

131.3 (d, $^4J_{PC} = 2.2$ Hz, *p*-PPh₂), 129.9 (d, $^1J_{PC} = 53$ Hz, *i*-PPh₂), 129.0 (d, $^3J_{PC} = 9.9$ Hz, *m*-PPh₂), 124.2 (d, $^4J_{PC} = 3.0$ Hz, Ph_m), 34.4 (CMe₃), 31.7 (CMe₃), 9.6 (d, $^1J_{PC} = 39$ Hz, PMe). IR: ν (cm⁻¹) 2360, 2325, BH. FAB-MS: m/z : 345 [M⁺-H] (100 %).

Synthesis of PS-BH₂•PPh₂Me (58): A solution of BBr₃ (3.40 g, 13.6 mmol) in 10 mL of CH₂Cl₂ was added dropwise under stirring to PS-SiMe₃ (2.0 g; ca. 11.3 mmol SiMe₃ groups; *PDI* = 1.11) in 10 mL of CH₂Cl₂. After completion of the addition the mixture was stirred for 24 h. Complete replacement of the silyl substituents for dibromoboryl groups was confirmed by ¹H NMR spectroscopy. The resulting solution of PS-BBr₂ was then treated with Me₃SiOMe (4.9 mL, 36 mmol) and stirred for 9 h. All volatile material was removed under high vacuum and the oily residue was redissolved in 20 mL THF. The solution of PS-B(OMe)₂ was transferred via cannula at 0 °C to a slurry of LiAlH₄ (0.64 g, 17 mmol) in 20 mL THF. The resulting gray suspension was stirred at 0 °C for 1 h and then at room temperature for 20 h. PPh₂Me (3.2 mL, 17 mmol) was added, the resulting green mixture was stirred for 24 h, and subsequently quenched with Me₃SiCl (20 mL). Upon stirring for 24 h, a solid precipitate (LiCl) formed, which was removed by filtration using a fritted glass disk. The filtrate was concentrated under high vacuum to ca. 5 mL and precipitated into a large volume of hexanes (ca. 250 mL). The white precipitate was redissolved in toluene and filtered. After removal of toluene the residue was taken up in benzene (30 mL), the solution was filtered, and the product was freeze-dried. PS-

BH₂•PPh₂Me was isolated as a white solid (1.61 g, 45%). For PSBH₂•PPh₂Me: ¹¹B NMR (160.386 MHz, CDCl₃): δ = −25.6 (w_{1/2} = 420 Hz); ¹H NMR (499.893 MHz, CDCl₃): δ = 7.9-7.0 (br m, 10H, PPh₂), 6.9-6.5 (br m, 2H, Ph_o), 6.4-5.9 (br m, 2H, Ph_m), 2.4 (br, 2H, BH₂), 2.2-1.2 (nr, polymer backbone), 1.26 (br m, 3H, PMe). ³¹P{¹H} NMR (499.895 MHz, CDCl₃): δ = 5.2, 3.9. ¹³C NMR (125.69 MHz, CDCl₃): δ = 143.3, 141.1 (br, Ph_i and Ph_p) 136.0 (br, Ph_o), 132.7/132.3 (br, *o*-PPh₂), 131.2 (br, *p*-PPh₂), 131-130 (br, *i*-PPh₂), 128.8 (br, *m*-PPh₂), 126.5 (br, Ph_m), 50-38 (br, polymer backbone), 8.2/7.4 (br, PMe). IR: ν (cm^{−1}) 2340, BH. GPC-UV: M_w = 26280, PDI = 1.54. DSC (second heating curve; onset, 10 °C/min): T_g = 101 °C. TGA (20 °C/min; under N₂): 43 % weight loss between 201 °C and 277 °C; 26 % weight loss between 384 °C and 436 °C.

1A.7 References and Notes

1. Hodge, P. G.; Sherrington, D. C. *Polymer-Supported Reactions in Organic Synthesis*, Chichester ; New York : J. Wiley, 1980.
2. Rajasree, K.; Devaky, K. S. *J. Appl. Polym. Sci.* **2001**, 82, 593-600.
3. Hu, J-b.; Zhao, G.; Ding, Z-d. *Angew. Chem. Int.Ed.* **2001**, 40, 1109-1111.
4. Itsuno, S.; Kamahori, K.; Watanabe, K.; Koizumi, T.; Ito, K. *Tetrahedron: Asymmetry* **1994**, 5, 523-526.
5. Kamahori, K.; Ito, K.; Itsuno, S. *J. Org. Chem.* **1996**, 61, 8321-8324.

6. Farrall, M. J.; Fréchet, J. M. J. *J. Org. Chem.* **1976**, *41*, 3877-3882.
7. Giffels, G.; Beliczey, J.; Felder, M.; Kragl, U. *Tetrahedron: Asymmetry*, **1998**, *9*, 691-696.
8. Caze, C.; Moualij, N. E.; Hodge, P.; Lock, C. J.; Ma, J. *J. Chem. Soc. Perkin Trans. I* **1995**, 345-349.
9. Franot, C.; Stone, G. B.; Engeli, P.; Spöndlin, C.; Waldvogel, G. *Tetrahedron: Asymmetry*, **1995**, *6*, 2755-2766.
10. Caze, C.; Moualij, N. E.; Hodge, P.; Lock, C. J. *Polymer* **1995**, *36*, 621-629.
11. Smith, K.; El-Hiti, G. A.; Hou, D. J.; DeBoos, G. A. *J. Chem. Soc., Perkin Trans. I* **1999**, 2807-2812.
12. Itsuno, S. (*Wiley VCH, Weinheim, New York, Chichester, Brisbane, Singapore, Toronto*, 2000, *2*, pp. 945.
13. Sosinsky, B. A.; Kalb, W. C.; Grey, R. A.; Uski, V. A.; Hawthorne, M. F. *J. Am. Chem. Soc.* **1977**, *99*, 6768-6771.
14. Revell, J. D.; Dörner, B.; White, P. D.; Ganesan, A. *Org. Lett.* **2005**, *7*, 831-833.
15. Brown, H. C.; Singaram, B. *Acc. Chem. Res.* **1988**, *21*, 287-293.
16. Smith, K.; Pelter, A.; Jin, Z. *Angew. Chem. Int. Ed.* **1994**, *33*, 851-853.
17. Brown, H. C.; Ramachandran, P. V. A. Hassner (Ed.), *JAI Press, Greenwich* 147. 1995.

18. Negishi, E.; Brown, H. C. *Synthesis* **1974**, 77-89.
19. Brown, H. C.; Chandrasekharan, J. *J. Org. Chem.* **1985**, *50*, 518-520.
20. Zweifel, G.; Arzoumanian, H.; Whitney, C. C. *J. Am. Chem. Soc.* **1967**, *89*, 3652-3653.
21. Knights, E. F.; Brown, H. C. *J. Am. Chem. Soc.* **1968**, *90*, 5281-5283.
22. Brown, H. C.; Krishnamurthy, S.; Yoon, N. M. *J. Org. Chem.* **1976**, *41*, 1778-1791.
23. Kalinin, A. V.; Scherer, S.; Snieckus, V. *Angew. Chem. Int. Ed.* **2003**, *42*, 3399-3404.
24. Brown, H. C.; Zweifel, G. *J. Am. Chem. Soc.* **1961**, *83*, 486-487.
25. Masamune, S.; Kim, B. M.; Petersen, J. S.; Sato, T.; Veenstra, S. J.; Imai, T. *J. Am. Chem. Soc.* **1985**, *107*, 4549-4551.
26. Gonzalez, A. Z.; Roman, J. G.; Gonzalez, E.; Martinez, J.; Medina, J. R.; Matos, K.; Soderquist, J. A. *J. Am. Chem. Soc.* **2009**, *130*, 9218-9219.
27. Smith, K.; Pelter, A.; Jin, Z. *J. Chem. Soc., Perkin Trans. 1*, **1993**, 395-396.
28. Jäkle, F. "Boron: Organoboranes", Chapter in *Encyclopedia of Inorganic Chemistry*, Ed. B. King, Wiley, VCH 2005, pp 560-598.
29. Roesler, R.; Har, B. J. N.; Piers, W. E. *Organometallics* **2002**, *21*, 4300-4302.

30. Chujo, Y.; Tomita, I.; Hashiguchi, Y.; Tanigawa, H.; Ihara, E.; Saegusa, T. *Macromolecules* **1991**, *24*, 345-348.
31. Chujo, Y.; Tomita, I.; Hashiguchi, Y.; Saegusa, T. *Macromolecules* **1992**, *25*, 33-36.
32. Chujo, Y.; Takizawa, N.; Sakurai, T. *J. Chem. Soc., Chem. Commun.* **1994**, 227-228.
33. Chujo, Y.; Tomita, I.; Saegusa, T. *Macromolecules* **1994**, *27*, 6714-6717.
34. Miyata, M.; Chujo, Y. *Polym. J.* **2002**, *34*, 967-969.
35. Nagai, A.; Miyake, J.; Kokado, K.; Nagata, Y.; Chujo, Y. *Macromolecules* **2009**, *42*, 1560-1564.
36. Qin, Y.; Cheng, G.; Sundararaman, A.; Jäkle, F. *J. Am. Chem. Soc.* **2002**, *124*, 12672-12673.
37. Qin, Y.; Cheng, G.; Parab, K.; Achara, O.; Jäkle, F. *Macromolecules* **2004**, *37*, 7123-7131.
38. Hawthorne, M. F. *J. Am. Chem. Soc.* **1958**, *80*, 4291-4293.
39. Bullen, N. P.; Hodge, P.; Thorpe, F. G. *J. Chem. Soc., Perkin Trans. 1*, **1981**, 1863-1867.
40. El-Assiery, S. A.; Dillingham, K. A.; Ponsonby, A.; G.Thorpe, F.; Wareham., R. *S. Eur. Polym. J.* **1993**, *29*, 443-447.

41. Heilmann, J. B.; Scheibitz, M.; Qin, Y.; Sundararaman, A.; Jäkle, F.; Kretz, T.; Bolte, M.; Lerner, H.-W.; Holthausen, M. C.; Wagner, M. *Angew. Chem. Int. Ed.* **2006**, *45*, 920-925.
42. Qin, Y.; Jäkle, F. *J. Inorg. Organomet. Polym. Mater.* **2007**, *17*, 149-157.
43. Scheibitz, M.; Bats, J. W.; Bolte, M.; Lerner, H.-W.; Wagner, M. *Organometallics* **2004**, *23*, 940-942.

Chapter 1B. Amine-Functionalized Organoboron Polymers

1B.1 Introduction

Luminescent tri-coordinate organoboron compounds have recently attracted increasing attention as a new class of π -electron materials for optoelectronics.^{1, 2} One of the most important characteristics of tri-coordinated boron compounds is the presence of an empty p-orbital on boron making it electron poor which leads to strong π -electron acceptor interaction with a suitable donor.³ The electronic structure of these organoboron compounds can lead to significant delocalization when conjugated with an organic π -system. This p- π interaction can lead to interesting linear and non-linear optical (NLO) properties, such as single-photon excited fluorescence (SPEF)^{4, 5}, two-photon excited fluorescence (TPEF)^{6, 7}, molecular second harmonic generation (SHG)^{1, 8} and electroluminescence (EL).⁹⁻¹¹ However, the empty p-orbital is also readily accessible to nucleophiles, which can lead to either cleavage of the B-C bond or formation of a tetracoordinated boron species in which the extended conjugation is broken. Bulky substituents like mesityl (2,4,6-trimethylphenyl) or trip (2,4,6-triisopropylphenyl) are often used to improve the stability by steric protection of the boron center. Thus, both the

electronic and optical properties of borane-based π -conjugated molecules can be controlled by external stimuli, leading to the application to chemical sensors.¹

1B.2 Donor- π -Acceptor Type Organoboron Systems and Their Applications

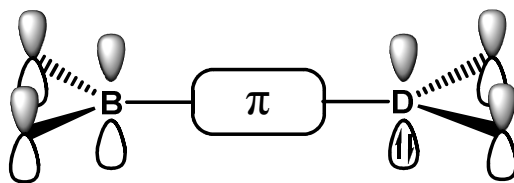


Figure 1B.1 Schematic Presentation of a Donor- π -Acceptor System.

These compounds often consists of donor- π -acceptor (D- π -A) dyads, in which the acceptor usually is a dimesitylboryl group which is separated from a donor group such as an amine, a phosphine, a ferrocene moiety, or other electron-rich groups through a π -conjugated bridge (Figure 1B.1). Insertion of electron-donor (D) and electron-acceptor (A) groups into the π -conjugated system allows an intense intramolecular charge transfer from the electron-rich moiety to the boron center. These push-pull systems have been shown to display interesting linear and nonlinear optical properties, including large hyperpolarizabilities and two-photon excited fluorescence (TPEF). These conjugated donor-acceptor triarylboron compounds typically involve non-coordinating aromatic linkers

such as phenyl, biphenyl, or thienyl.¹² In early work in this field, Marder and coworkers have synthesized various molecules (1-6) with conjugated alkene, alkyne, aryl linkers or related mixed systems and investigated their optical and NLO properties.^{4, 6} They reported large solvatochromic shifts with solvents of increasing polarity, which is indicative of highly polarized excited states relative to the ground states. Related compounds (7) and (8) were prepared by Lequan *et al.* and their second-order NLO properties were determined.¹³ Derivatives of (8) were subsequently incorporated as side chains in polyurethane matrices and their second harmonic response was determined after poling by the corona technique.

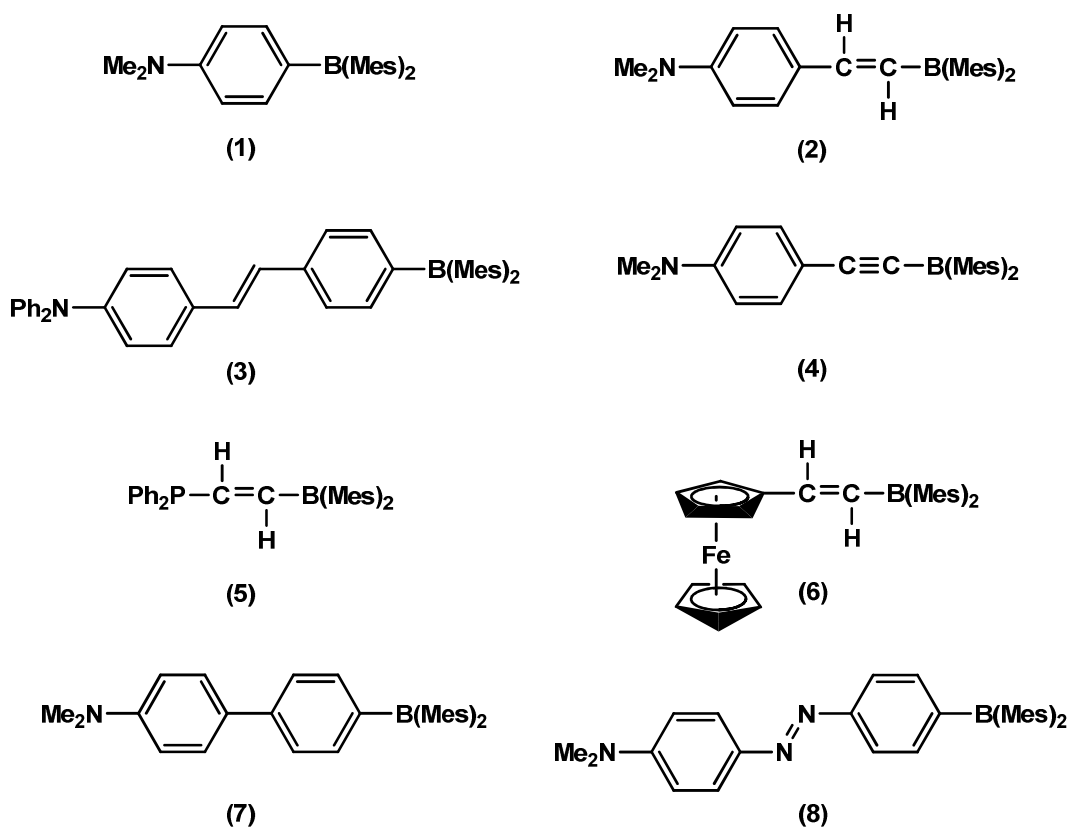


Chart 1B.1 Examples of Organoboron Donor-Acceptor Compounds.

Lequan *et al.* have investigated the NLO properties of donor-acceptor substituted oligothiophenes (9) using $\text{B}(\text{Mes})_2$ groups as the acceptor moiety, where an increasing delocalization of electrons from donor to acceptor was attributed to the reduced aromaticity and the greater planarity of oligothiophenes.¹⁴ On the other hand, Jäkle and coworkers have synthesized a donor- π -acceptor dyad that features a bis(pentafluorophenyl)boryl group as the acceptor moiety and a diphenylamino group as

the donor that is separated by a bithiophene bridge (10). The distinct bathochromic shift in both absorption and emission maxima compared to the non-fluorinated dyad was attributed to the smaller HOMO-LUMO gap due to the presence of strongly electron-withdrawing pentafluorophenyl groups.¹²

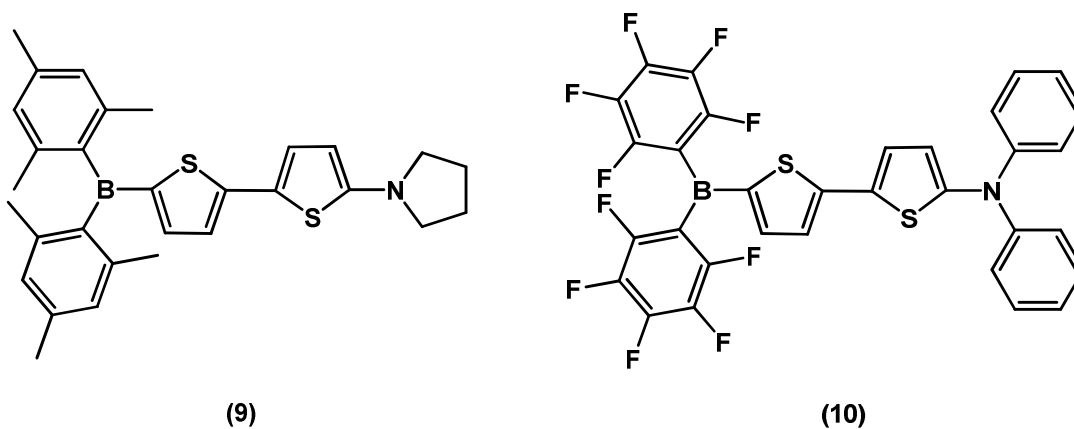
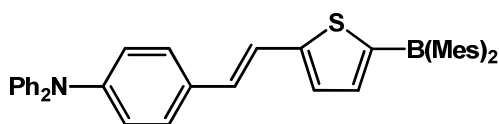
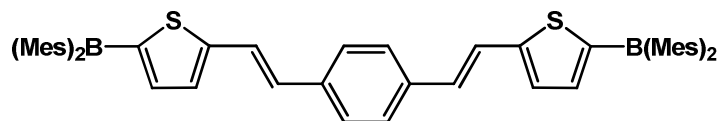


Chart 1B.2 Examples of Thiophene Containing Donor-Acceptor Compounds.

Huang and coworkers synthesized thienyl-vinylene type compounds (11-12) and studied their use as both single and two photon excited fluorescence sensors for fluoride ions. No change in emission intensity or shifts in emission maxima were observed in the presence of other halides or even acetate, perchlorate, nitrite and nitrate ions.¹⁵



(11)



(12)

Chart 1B.3 Examples of Thienyl-vinylene Containing Donor-Acceptor Compounds.

Wang *et al.* synthesized a series of linear donor- π -acceptor compounds (13-20) with different shape and conjugation type and investigated the absorption and emission properties. The study revealed that the most efficient charge transfer was present in the linear system due to the conjugative interaction.¹⁶ They also demonstrated that donor-acceptor triarylboranes are promising materials in anion sensing. For instance, compound (13) selectively binds fluoride ions.¹⁷ The intensity of the charge-transfer band ($\lambda_{\text{em}} = 475$ nm) in the absorption spectra decreases with a corresponding quenching of the fluorescence peak as fluoride ions binds to the boron center. Because of the quenching response, it can be described as a “switch-off” sensor for fluoride.

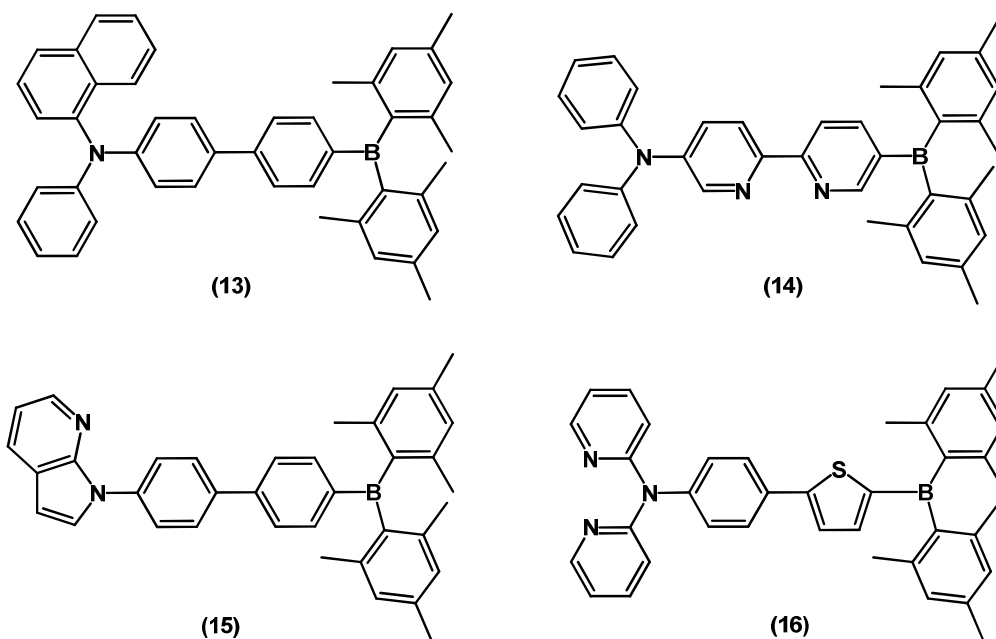


Chart 1B.4 Examples of Donor-Acceptor Systems from Wang and Co-workers.

Wang *et al.* have also reported the synthesis of a 2,2-bipyridine based donor-acceptor system (14).¹⁸ The chelating ability of 2,2-bipyridine promotes strong communication between boron and the metal center. Upon binding with fluoride, the emission spectra of compound (14) displays an unusual “turn-on” response that is independent of solvent or excitation energy, which was attributed to the presence of a low-energy π - π^* emission pathway originating from the donor-linker π system, made possible by the highly coplanar bipyridine bridge. Both the Cu(I) and Pt(II) complexes of (14) are luminescent in solution, displaying orange to red phosphorescence ($\lambda_{\text{em}} = 565$ nm). Interestingly, the

emission was switched from red-orange to blue-green when Pt(II) complexes were titrated with fluoride. The fluorescent “turn-on” response of free (14) was attributed to the blocking of the N→B/MLCT transition and activation of a π - π^* transition. This demonstrated that by incorporating an internal donor-acceptor system into the chelate ligand, phosphorescent “turn-on” sensors for fluoride may be achieved. Other chelating compounds (15) and (16) are very efficient blue emitters when attached to ions such as Zn(II), B(III), or Al(III). The thienyl linker in (16) was found to enhance the emission efficiency and lower the emission energy (465 nm, 100%) compared with the phenyl analogue (449 nm, 63%) due to improved donor-acceptor π -conjugation.¹⁹

Donor-acceptor molecules (17) and (18) possess a sterically demanding linker and the two chromophores adopt a nonconjugated conformation.^{20, 21} This rigid linker allows an electronic communication between these chromophores by a weak charge transfer through space. For instance, in solution, both (17) and (18) display a broad fluorescence peak at 507 nm in CH₂Cl₂ with low quantum efficiency and a strong dependence on solvent polarity, a characteristic of charge-transfer character as further confirmed by DFT calculations. In the presence of a fluoride source, the charge-transfer band in both compounds is quenched, with the appearance of a much brighter π - π^* emission band at 453 nm for (17) and 460 nm for (18). Thus, binding of fluoride to the boron center blocks the charge-transfer transition, leaving the lowest energy transition of the donor group as

the only source of emission and thus switches the emission color of the solution from green to blue. Similarly, compound (19) exhibits a through space charge-transfer emission in addition to the π - π^* transition as a shoulder band.²⁰ Like the non-conjugated system (17) and (18), compound (19) also acts as a “switch-on” sensor for fluoride, changing emission color from green to blue in the presence of F^- , with a large increase in emission intensity. Compound (20) is fluorescent in the solid state and solution at ambient temperature (405 nm, $\Phi = 12\%$). Addition of fluoride causes quenching of this peak with the appearance of a new, blue-shifted peak at 362 nm.²²

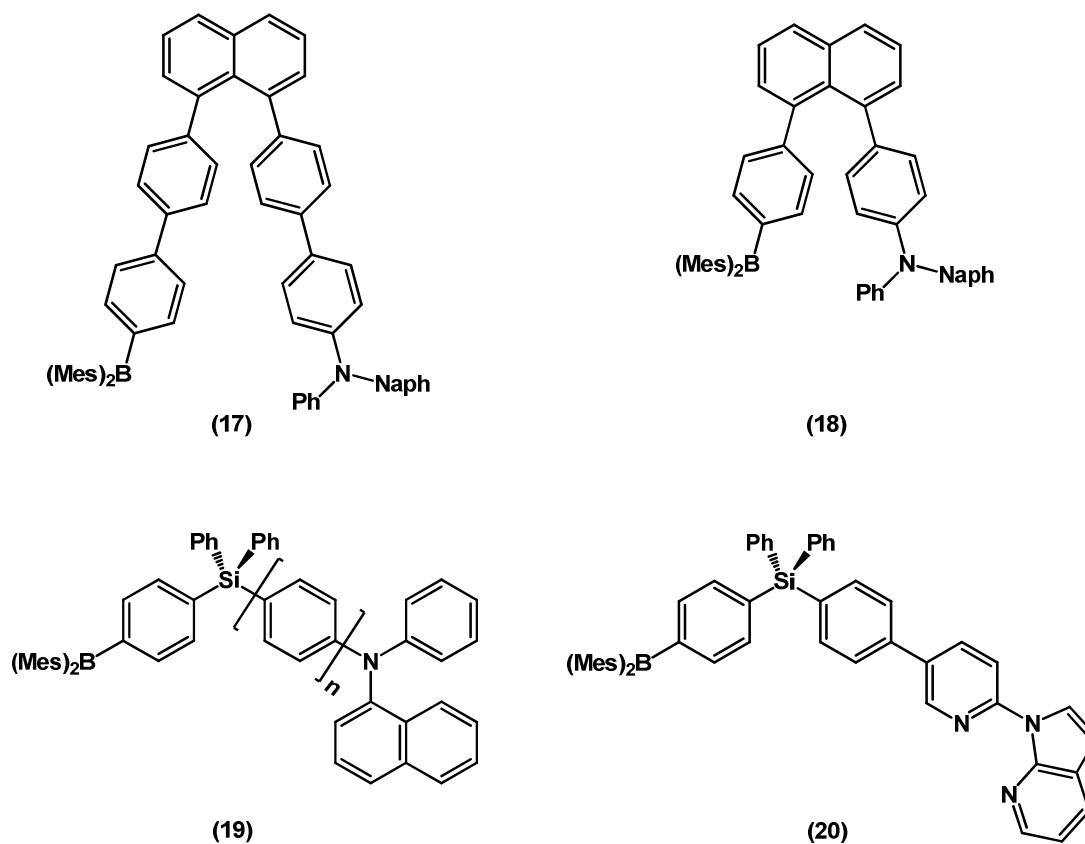


Chart 1B.5 Examples of Sensors from Wang and Co-workers.

A remarkable contribution to this area has been given by Gabbaï's group, which over the last few years, has reported many compounds (21-29).²³ The presence of the mercury atom in heteronuclear bidentate boranes (21-23) provides spin-orbit perturbation to the chromophore and gives rise to red emission due to phosphorescence of the dimesitylborylnaphthalenediyl moiety. They also observed high selectivity for fluoride in partial

aqueous medium (90/10 (v/v) THF/water mixture) and high binding constants, and these compounds can be used as phosphorescent fluoride sensors.²⁴⁻²⁶

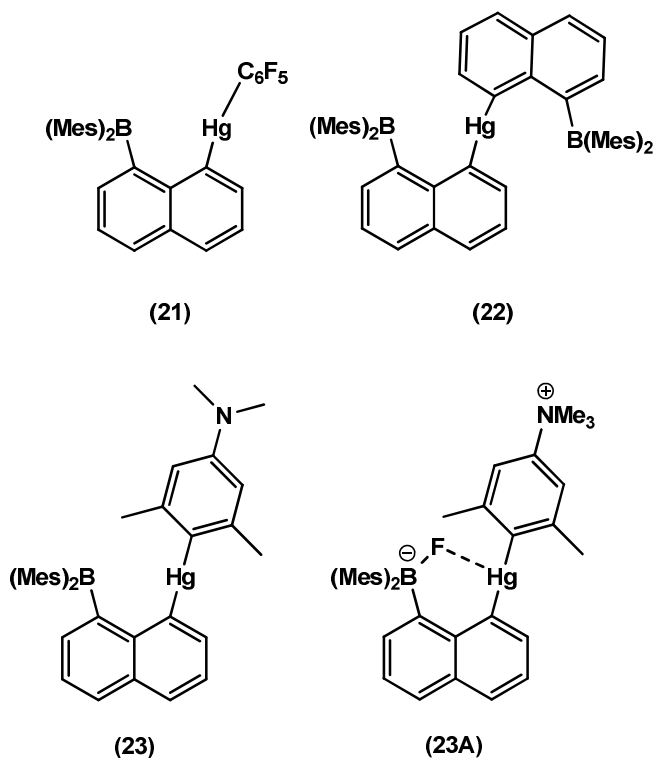


Chart 1B.6 Examples of Phosphorescent Fluoride Sensors.

In order to achieve fluoride binding in aqueous media, the Gabbaï group synthesized cationic boranes, whose anion affinity is enhanced by favorable Coulombic effects. First they synthesized cationic borane (24), which reacts with aqueous fluoride ions under biphasic conditions ($\text{H}_2\text{O}/\text{CHCl}_3$) to form the corresponding zwitterion (24A) which was

stabilized by a $\text{CH}\cdots\text{FB}$ hydrogen bond. Neutral boranes such as Mes_3B fail to capture fluoride under these biphasic conditions, attesting to the favorable influence of the ammonium group on the anion affinity of (24).^{27, 28}

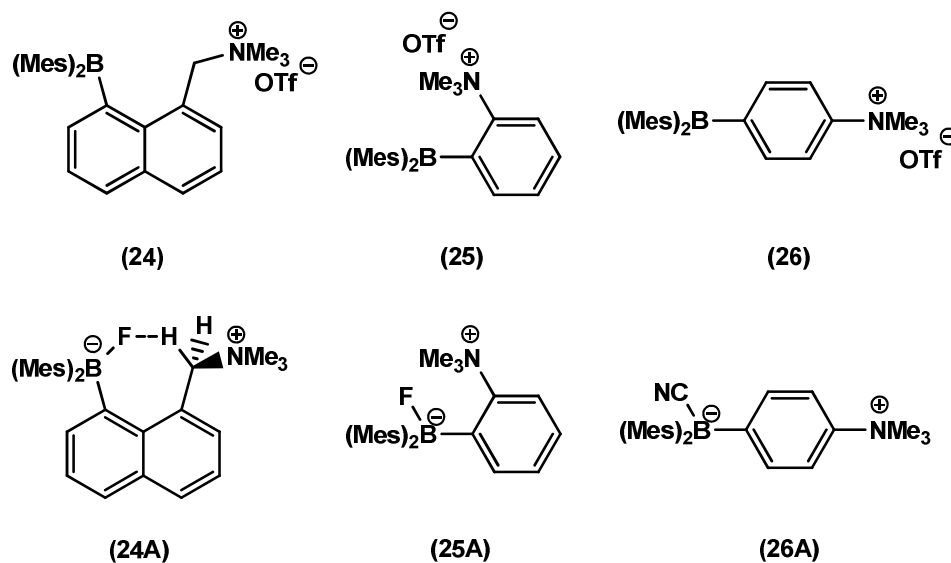


Chart 1B.7 Some Sensors from Gabbai and Co-workers.

Cations (25) and (26) were synthesized as their triflate salts by reaction of the known aminoborane precursors with MeOTf .²⁹ In CHCl_3 , both (25) and (26) react with fluoride and cyanide ions to the corresponding fluoroborate- or cyanoborate-ammonium zwitterions. However, in methanolic solution the binding process was reported to be selective. For example, *ortho*-substituted (25) only complexes fluoride ions to form

(25A) whereas *para*- substituted (26) complexes cyanide ions to form the corresponding (26A). In (25), the increased steric crowding of the boron center prevents coordination of the larger cyanide anion. The unusual cyanide binding properties of (26) were assigned to favorable Coulombic effects, which increase the Lewis acidity of the boron atom and strengthen the receptor-cyanide interaction. To verify whether Coulombic effects could be used to increase the anion affinity of chelating bifunctional boranes, the heteronuclear B-Hg compound (23) was converted into the corresponding ammonium triflate salt. Fluoride titration revealed a higher binding constant of $6.2 \times 10^4 \text{ M}^{-1}$ for (23A) as opposed to $1.3 \times 10^2 \text{ M}^{-1}$ for its neutral precursor (23). This was attributed to the lower energy of the vacant orbitals of the mercury atom, allowing them to mix more efficiently with the boron orbital and hence leads to an increase in the Lewis acidity of the mercury center and the anion affinity of the entire molecule.²⁶

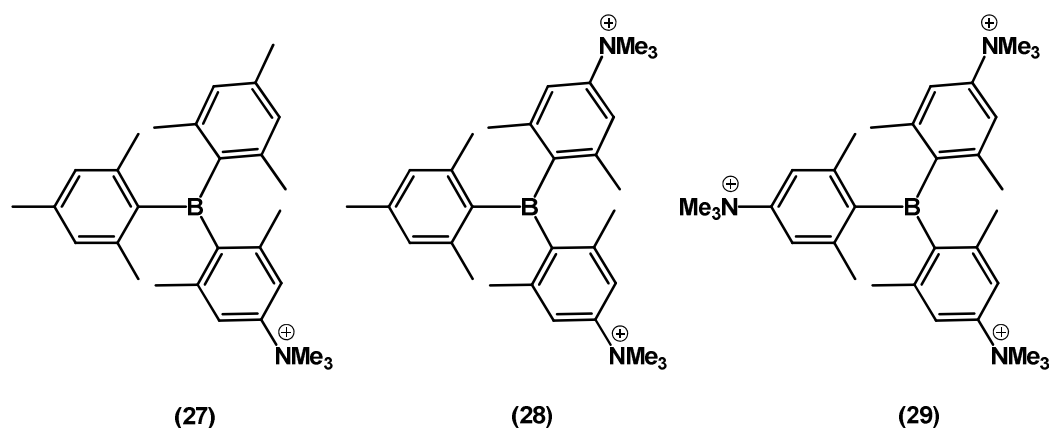


Chart 1B.8 Examples of Cationic Trimesityl Boranes.

Cationic analogues of trimesitylborane (Mes₃B) (27-29) were synthesized to further study the additive effects of multiple cationic groups on the electron deficiency and Lewis acidity of the boron center.³⁰ The cationic boranes in the form of their triflate salts were air- and moisture-stable due to the presence of the six *ortho*-methyl groups that sterically protect the boron center. To better assess the effect caused by the introduction of multiple cationic moieties, they decided to investigate the use of (28) and (29) for the complexation of small anions in water. The ¹H NMR spectra in the presence of KF and KCN showed that neither (28) nor (29) bind fluoride ions in pure water. The high hydration enthalpy of the fluoride anion and the steric protection of the boron center are most likely responsible for this lack of reactivity. The dication (28) also failed to react with cyanide under similar conditions. However, irreversible complexation of cyanide ion

was observed in the case of (29) and could be used for the development of water compatible chemosensors for the highly toxic cyanide anion. Thus they concluded that the electron deficiency and Lewis acidity of triarylboranes can be incrementally enhanced through peripheral decoration of the aryl ligands with cationic groups. This approach can also be used to increase the anion affinity and water solubility of the boranes.

1B.3 Water Soluble Polymers

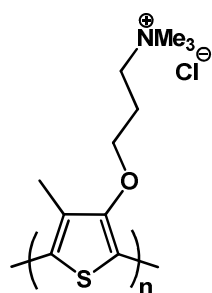
Water solubility in polymers is usually achieved by attaching polar functional groups such as carboxyl, anionic sulfonates or quaternary ammonium salts to the polymeric backbone. Water soluble conjugated polymers or conjugated polyelectrolytes (CPEs) find a variety of applications in various biological fields such as drug delivery and biosensors.^{31, 32} CPEs combine the properties and structural possibilities of conventional polyelectrolytes and conjugated polymers and offer unique potential in terms of both electrical and optical properties. For example, the π -conjugated backbone imparts strong optical absorption and fluorescence, conductivity and an amplified response to external stimuli due to the delocalized electronic structure. In addition, the polyelectrolyte functionality imparts water solubility, ionic conductivity, strong intra- and interchain interactions and interaction with ions in solution. Recent research has been focused on the synthesis and properties of conjugated polyelectrolytes, including those containing

poly(thiophene), poly(p-phenylene), poly(phenylenevinylene), poly(phenyleneethynylene) and poly(fluorene) backbones.

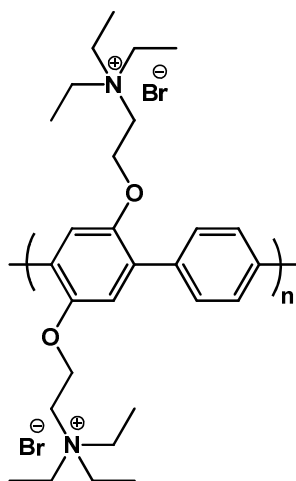
1B.3.1 Conjugated Polyelectrolytes

Recently, Shinkai and co-workers reported a cationic water-soluble poly(thiophene) (30) based sensor for adenosine triphosphate (ATP).³³ The presence of ATP causes a significant red shift in the absorption spectra changing the solution color from yellow to pink-red. These changes in the absorption spectra were attributed to the combination of electrostatic and hydrophobic interactions between the cationic polymer and anionic ATP. In 2000, Schanze and coworkers reported a fluorescence study of the polycation (31) which features side chains functionalized with tertiary amine groups.³⁴ The quaternization of the tertiary amine units was carried out with ethyl bromide and the resulting polyelectrolyte was used in solution and as thin films to demonstrate the amplified fluorescence-quenching effect. They also synthesized and studied the photophysical properties of the cationic CPE (32), which features a backbone consisting of alternating phenylene and thienylene units.³⁵ The green fluorescence of the cationic CPE (32) was efficiently quenched by anions such as $[\text{Fe}(\text{CN})_6]^{4-}$ and anthraquinone-2,7-disulfonate (AQS). Swager *et al.* synthesized polymer (33) by Sonogashira coupling.³⁶ A device was fabricated by the combination of layer-by-layer deposition of a pH-sensitive polyacrylate

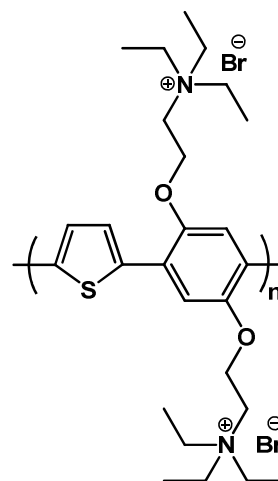
based dye and the cationic conjugated polymer in such a way that the polymer emission overlaps with the absorbance band of the dye, therefore encouraging FRET from the conjugated polymer to the dye. Fluorescence of the bilayer films was responsive to pH. For instance, when the conjugated polymer was excited at 420 nm, more than 90% of the polymer fluorescence was quenched at pH 11 due to efficient fluorescence resonance energy transfer (FRET) to the fluoresceinamine dye, which resulted in an intense red-shifted emission from the dye. However, at pH 6, the conjugated polymer fluorescence was strong and no fluoresceinamine emission was observed.



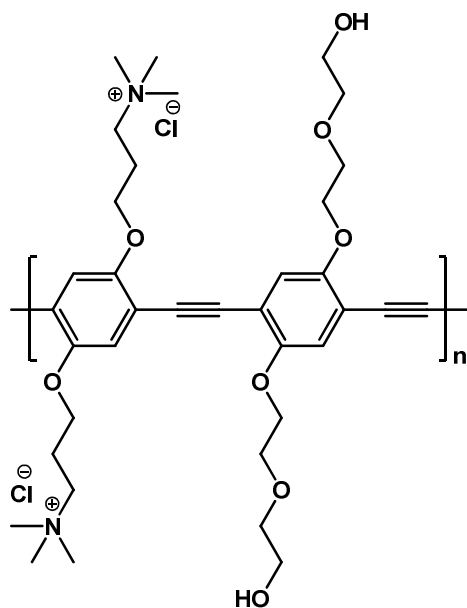
(30)



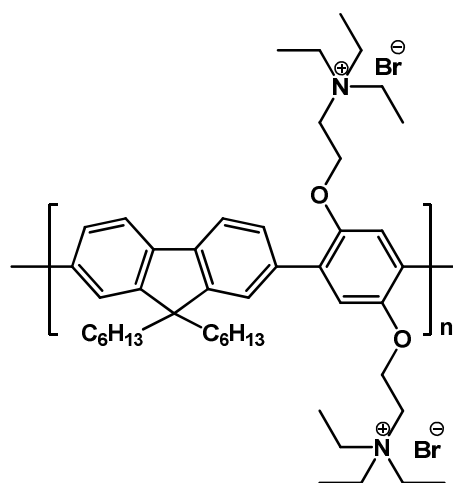
(31)



(32)



(33)



(34)

Chart 1B.9 Examples of Water Soluble Conjugated Polymers.

Polyfluorene based CPEs are another interesting class of materials that have recently gained considerable attention. For instance, Huang and co-workers introduced a cationic, water-soluble blue-emitting CPE with a backbone consisting of alternating fluorene and phenylene units (34), which was prepared through a post-polymerization modification approach.³⁷ The group of Bazan used various water soluble cationic conjugated polymers to detect specific DNA sequences via FRET to dye-labeled probe molecules. Their system (35) features an electrostatic attraction between the positively charged conjugated polymer and the polyanionic DNA which results in short distances between the conjugated polymer donor and the acceptor-labeled probe strand. The polymer displays a much higher water solubility due to the presence of more tetralkylammonium groups along the polymer chain and the oligo(ethyleneoxide) pendant groups on the phenylene units. In addition, the shorter propyl linkers on the fluorene units reduce the hydrophobic nature of the polymer.³⁸

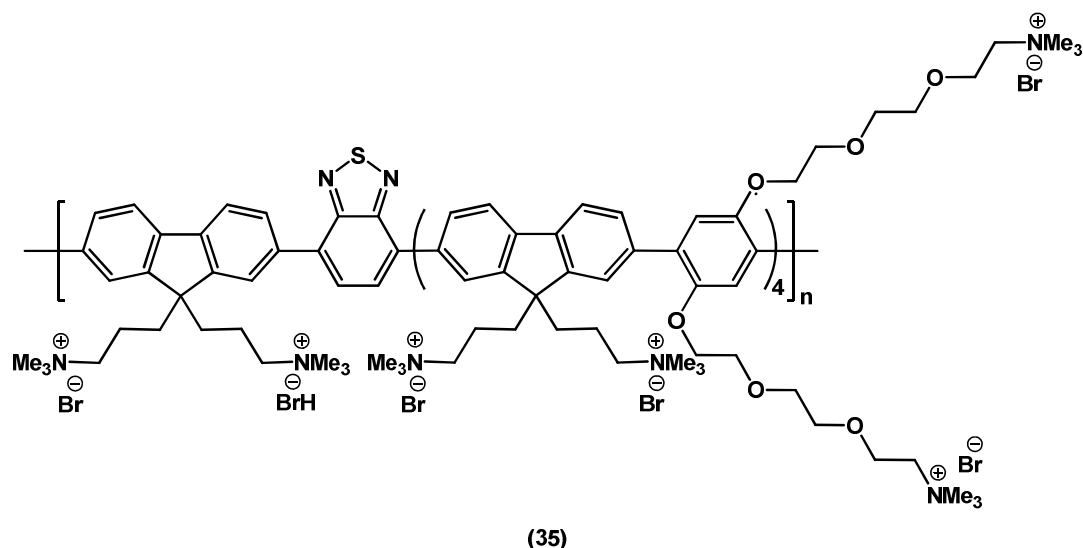


Chart 1B.10 Example of a Donor-Acceptor Conjugated Polyelectrolyte.

1B.4 Side-chain Functionalized Organoboron Polymers with a Dimethylamino Functionalized Group as the Chromophore

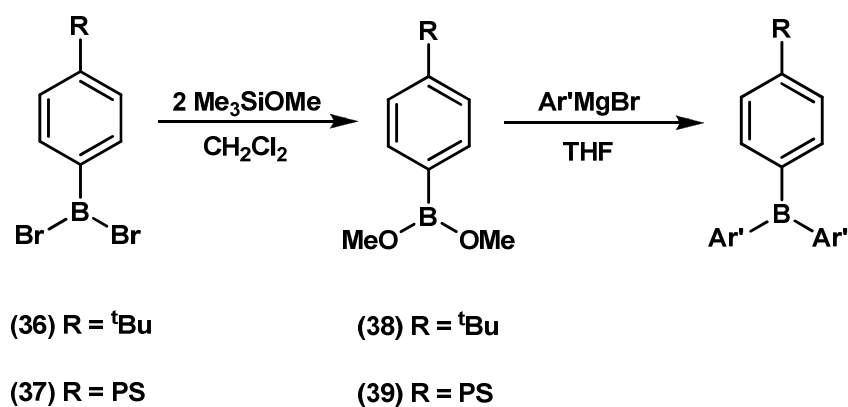
As discussed in Chapter 1, Section 1.2.2.3, the Jäkle group has developed a general strategy toward the synthesis of well-defined fully functionalized borylated polystyrene with controlled architecture, molecular weight and degree of functionalization. Using this strategy we can selectively and quantitatively replace the substituents on the boron center and hence organoboron polymers with varying properties can be easily synthesized. For instance, Parab *et al.* demonstrated that attachment of bithiophene moieties to the borylated polystyrene PS-BBr₂ leads to strongly luminescent materials that can be used as

chemosensors for the selective and highly efficient recognition of fluoride and cyanide.³⁹ From the literature it is known that the presence of multiple bulky groups like mesityl or 2,4,6-triisopropylphenyl (trip) is sufficient to sterically protect the boron center. Polymers containing only one mesityl group have been reported by Jäkle and coworkers to show decomposition products after approximately two weeks in solutions when exposed to air³⁹, whereas compounds with only one trip group are reported to be air stable.⁴⁰

The strategy of this project was to synthesize polystyrene based side chain functionalized polymers with quaternizable dimethylamino-functionalized mesityl groups as extended organic π -systems that can effectively overlap with the empty p-orbital on boron, while a second mesityl group serves to sterically protect the boron center or to change the solubility characteristics by quaternization.

1B.4.1 Synthesis

Recently, Parab *et al.* synthesized redox-active triarylborane polymers and studied their anion binding. Attachment of bulky substituents such as mesityl and triisopropylphenyl groups was achieved by reaction with the respective Grignard reagents.⁴¹ Using a similar synthetic methodology, we attempted the incorporation of dimethylamino-functionalized mesitylborane groups as the chromophores into the side-chain of polystyrene. The general synthetic strategy for both model systems and polymers is shown in Scheme 1B.1.



Scheme 1B.1 General Strategy for the Synthesis of Triarylborane Compounds.

1B.4.1.1 Synthesis of Model Compounds

For the synthesis of (43), dibromoborane compound (36) was treated with a slight excess (2.3 equiv.) of methoxytrimethylsilane in CH_2Cl_2 as the solvent (Scheme 1B.1). The reaction was allowed to proceed for 2 h at room temperature, after which all volatile components were removed under high vacuum. The intermediate (38) was then redissolved in THF and to this THF solution was added an excess of the Grignard reagent (41) dropwise. Upon addition of the Grignard, an immediate color change from colorless to yellow-green with a greenish yellow emission was observed. This solution was then heated in a Schlenk tube at 110 °C for a period of 15 d and monitored by ^{11}B NMR spectroscopy to confirm conversion of (38) to (43). While no color change was observed upon completion of the reaction, ^{11}B NMR spectrum of the crude product (43) revealed a

broad peak in the region of ~ 70 ppm, which is in the region typical of dimesityl boron containing compounds.⁴¹ ¹H NMR and GC-MS analysis of the crude product confirmed the presence of the desired product and in addition also showed the presence of free *N,N*,3,5-tetramethylaniline, which was removed by column chromatography using hexanes as an eluent. The latter results from hydrolysis of the excess Grignard reagent used.

For the synthesis of the unsymmetric compounds (50) and (52), the boronic ester (38) was first treated with one equivalent of mesityl Grignard reagent (40). The reaction mixture was stirred for ca. 20 h at ambient temperature. The selectivity and formation of the desired mono-substituted intermediate (48) was examined by ¹H and ¹¹B NMR spectroscopy. The ¹¹B NMR spectra showed the presence of a peak at 47 ppm for (48), which is distinctly downfield shifted in comparison to that at 30 ppm for (38). ¹H NMR confirmed the selective formation of (48) with trace amounts (less than 5 %) of free mesitylene as the only other product. A large excess of the Grignard reagents, (41) and (42) was added to ensure substitution of the second methoxy group by the desired aryl group with formation of compounds (50) and (52), respectively. The reaction was stirred at room temperature for 1 h and then heated to 110 °C in a Schlenk tube for a period of 20 days and monitored by NMR spectroscopy. Even upon reaction at 110 °C for a longer period of 1 month, the substitution did not occur completely as expected, which is

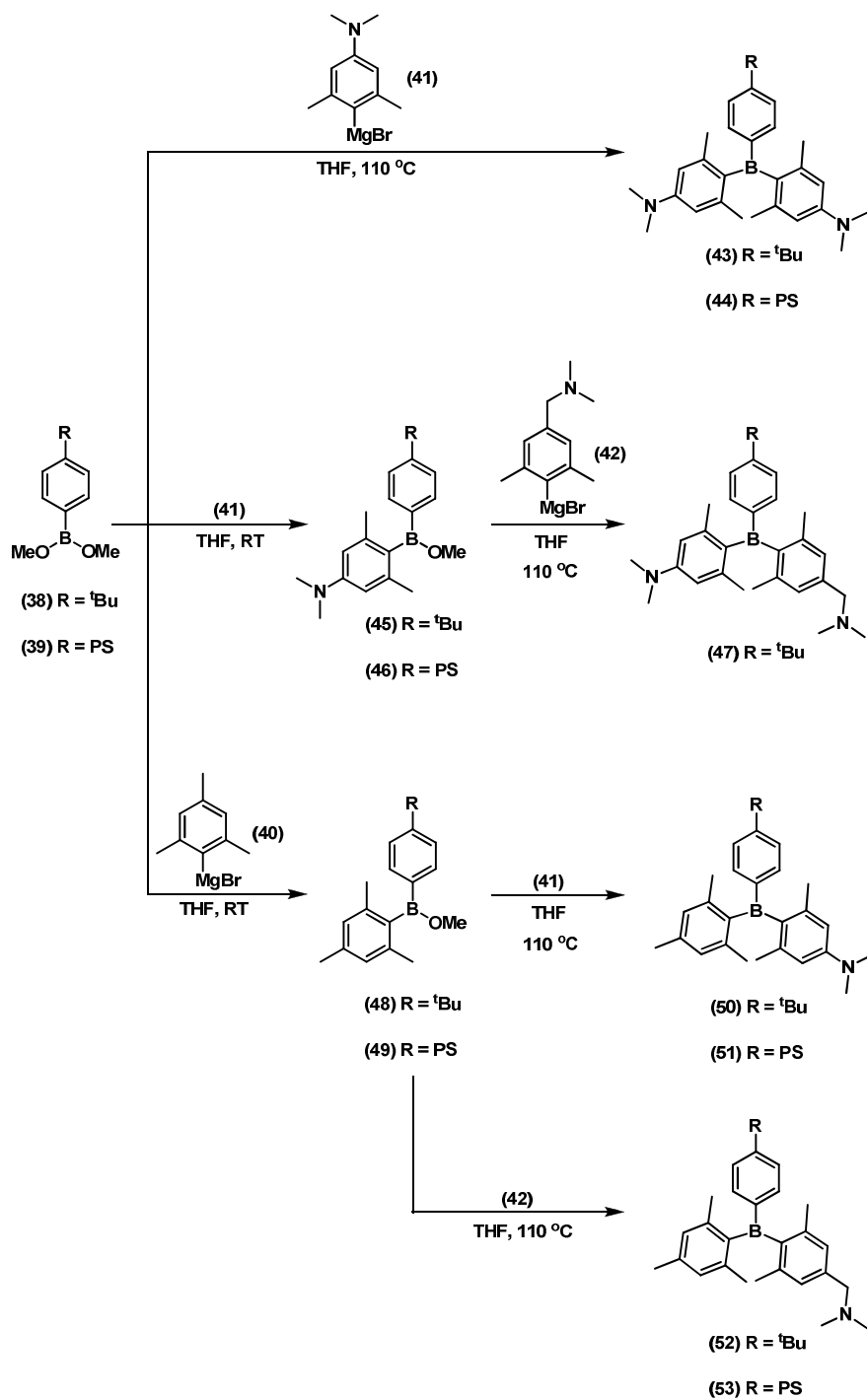
evidenced by the presence of an ^{11}B NMR peak at 47 ppm ($\sim 5\%$) in addition to the peak for the desired product at around 70 ppm ($\sim 95\%$). GC-MS analysis of the crude product (50) confirmed the presence of the desired product and in addition also showed the presence of free *N,N*,3,5-tetramethylaniline, trace amounts of symmetric compound (43) and unsymmetric compound (52). GC-MS analysis of crude (52) confirmed the presence of the desired product and showed the presence of free 1-(3,5-dimethylphenyl)-*N,N*-dimethylmethanamine along with compound (47) (around 3%). Formation of the symmetric compound $^t\text{BuPhB}(\text{Mes})_2$ was not observed in the case of (52). The crude compounds were purified by column chromatography using silica gel as the stationary phase and hexanes as the eluent to obtain (50) and (52) as solids in 45% and 36% yields, respectively. In addition to passing compound (43) through a silica gel column with hexanes it was further purified by recrystallization from hexanes and isolated as yellow colored solid in 25% yield.

A similar approach was used for the synthesis of (47). The intermediate (38) was treated with one equivalent of (41) and the reaction mixture was stirred for ca. 20 h at room temperature. The mono-substituted intermediate (45) was examined by ^1H and ^{11}B NMR spectroscopy. A single peak at around 47 ppm was observed in the ^{11}B NMR spectra. However, ^1H NMR of compound (45) showed the presence of trace amounts of free *N,N*,3,5-tetramethylaniline (less than 2%) in addition to the desired species (45). For

the second substitution, a large excess of (42) was added. The reaction was stirred at room temperature for 1 h and then heated to 110 °C in a Schlenk tube for a period of 30 days and monitored by NMR spectroscopy. The ^{11}B NMR spectrum of (47), showed the presence of two peaks; a peak at around 70 ppm (~ 95 %) corresponding to the desired product and an additional peak at 47 ppm (~ 5 %) which is tentatively attributed to the mono-methoxy substituted compound (45). This indicated incomplete installment of the aryl groups on to the boron center. Although a small percentage of starting material/intermediate was observed after 4 weeks of reaction time, the reaction was worked up by removal of the volatile components under high vacuum. GC-MS analysis of crude product (47) confirmed the presence of the desired product (~ 50 %) along with the symmetric bis-substituted compound $^t\text{BuPhB}(\text{MesCH}_2\text{NMe}_2)_2$ (~ 50 %). In addition it also showed the presence of free *N,N*,3,5-tetramethylaniline, 1-(3,5-dimethylphenyl)-*N,N*-dimethylmethanamine, and a small amount of (52). This indicates that the initial reaction of (38) with Grignard (40) may have been incomplete. The crude product was extracted with hexanes and isolated by column chromatography over silica gel using ether as the eluent.

High-resolution MALDI-TOF spectra of the isolated model compounds were acquired in positive ion mode using α -cyano-4-hydroxycinnamic acid as the matrix. They showed the molecular ion peaks with the expected isotope patterns, thus confirming the chemical

composition of these compounds. However, the presence of small amounts of bis-substituted compound (43) was also observed in the case of (47) and (50). ESI mass spectrum obtained for the compound (52) in acetonitrile, confirmed the presence of the desired product.



Scheme 1B.2 Synthesis of Dimethylamino Functionalized Triarylborane Compounds.**1B.4.1.2 Synthesis of Polymers**

For the synthesis of PSB(MesNMe₂)₂ (44), we used a similar approach as for the model compound (43), where both bromines of PS-BBr₂ were first replaced with methoxy groups and the intermediate, PSB(OMe)₂ (39), was then reacted with an excess of (41). The reaction was stirred at room temperature for 1 h and then heated to 110 °C in a Schlenk tube and was monitored by ¹¹B NMR spectroscopy. After 4 weeks, the ¹¹B NMR spectrum of (44) revealed a major peak at around 50 ppm (~ 95 %) with a minor peak at 40 ppm (~ 5 %) which suggests incomplete substitution on the boron centers i.e. one of the methoxy groups were still present on some of the boron centers in the polymer chain.

For the synthesis of (51) and (53), the bismethoxy intermediate (39) was treated with one equivalent of mesityl Grignard reagent (40). The reaction mixture was stirred for ca. 24 h at ambient temperature. The selectivity of formation of the desired mono-substituted intermediate (48) was examined by ¹H and ¹¹B NMR spectroscopy. The ¹¹B NMR spectra shows the presence of a distinctly downfield shifted peak at around 40 ppm for (49) in comparison to 30 ppm for (39). The attachment of a mesityl group on the boron center was also reflected in the ¹H NMR spectra. The protons in *meta*-position of the mesityl moiety can be clearly observed as a broad peak at 6.7 ppm. In addition, several sharp

peaks were observed which can be assigned to the free mesitylene. A large excess of the Grignard reagents, (41) and (42), respectively, was added to ensure substitution of the second methoxy group by the desired aryl group to obtain polymers (51) and (53). The reaction was stirred at room temperature for 1 h and then heated to 110 °C in a Schlenk tube for a period of 20 days and monitored by NMR spectroscopy. Even upon reaction at 110 °C for over a month, the substitution did not occur completely as expected, which is evidenced by the presence of an ^{11}B NMR peak at 40 ppm (~ 5 %) in addition to the peak for the desired product at around 55 ppm (~ 95 %).

All the polymers were isolated by silica gel column chromatography using THF as eluent to remove the magnesium salts followed by multiple precipitations into ethanol. Polymers (44) and (51) were isolated as bright yellow solids in ca. 25% yield, whereas polymer (53) was isolated as a colorless solid in ~50 % yield. All three polymers showed moderate to low solubility in common organic solvents like CH_2Cl_2 , THF and toluene. Detailed syntheses are described in the experimental section.

1B.4.2 Structural Characterization

1B.4.2.1 Multinuclear NMR Spectroscopy

The polymers and their respective molecular model compounds were fully characterized by ^1H , ^{13}C , and ^{11}B NMR spectroscopy (Table 1B.1). The presence of a broad signal at about 50-60 ppm in the ^{11}B NMR spectra is typical of triarylborane compounds. However, in comparison to the model compounds, which represent one repeating unit of the polymer chain, a significant upfield shift of the ^{11}B NMR resonance of about 10-15 ppm was observed (Figure 1B.2). The latter is tentatively attributed to additional shielding effects due to neighboring groups on the polymer chain and is consistent with prior observations for polymers with bithiophene as well as ferrocene containing pendant groups. In the case of the polymers, the presence of a small peak between 30-40 ppm is most likely due to incomplete substitution at the boron center after addition of the aryl Grignard reagents. This incomplete substitution may lead to hydrolysis which may form B-O-B cross-links; the amount of which could not be determined from ^1H and ^{11}B NMR spectroscopy.

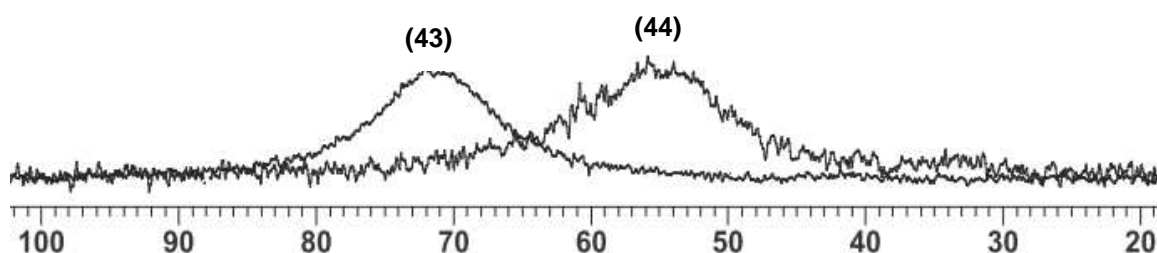


Figure 1B.2 Comparison of the ^{11}B NMR Shifts of (43) and (44).

Table 1B.1 ^{11}B NMR Shifts (ppm) and Halfwidths ($w_{1/2}$) (Hz) of Organoboron Polymers and Molecular Model Compounds.^[a]

Molecular Model	$\delta(^{11}\text{B}) / w_{1/2}$	Polymers	$\delta(^{11}\text{B}) / w_{1/2}$
(43)	72 / 1440	(44)	58 / 2040
(50)	71 / 1475	(51)	54 / 2005
(52)	73 / 1760	(53)	56 / 2080
(47)	72 / 1800		

[a] Data were obtained at RT in CDCl_3 (ca. 8×10^{-3} M).

The ^1H NMR spectra of all the polymers feature very broad overlapping signals in both the aromatic and aliphatic regions that are expected for an atactic polymer structure. Also, the ^{13}C NMR spectra correlate well with those of the molecular models and thus further confirm the structure of the polymers with borane moieties containing amino functionalized substituents (Figure 1B.3 and 1B.4).

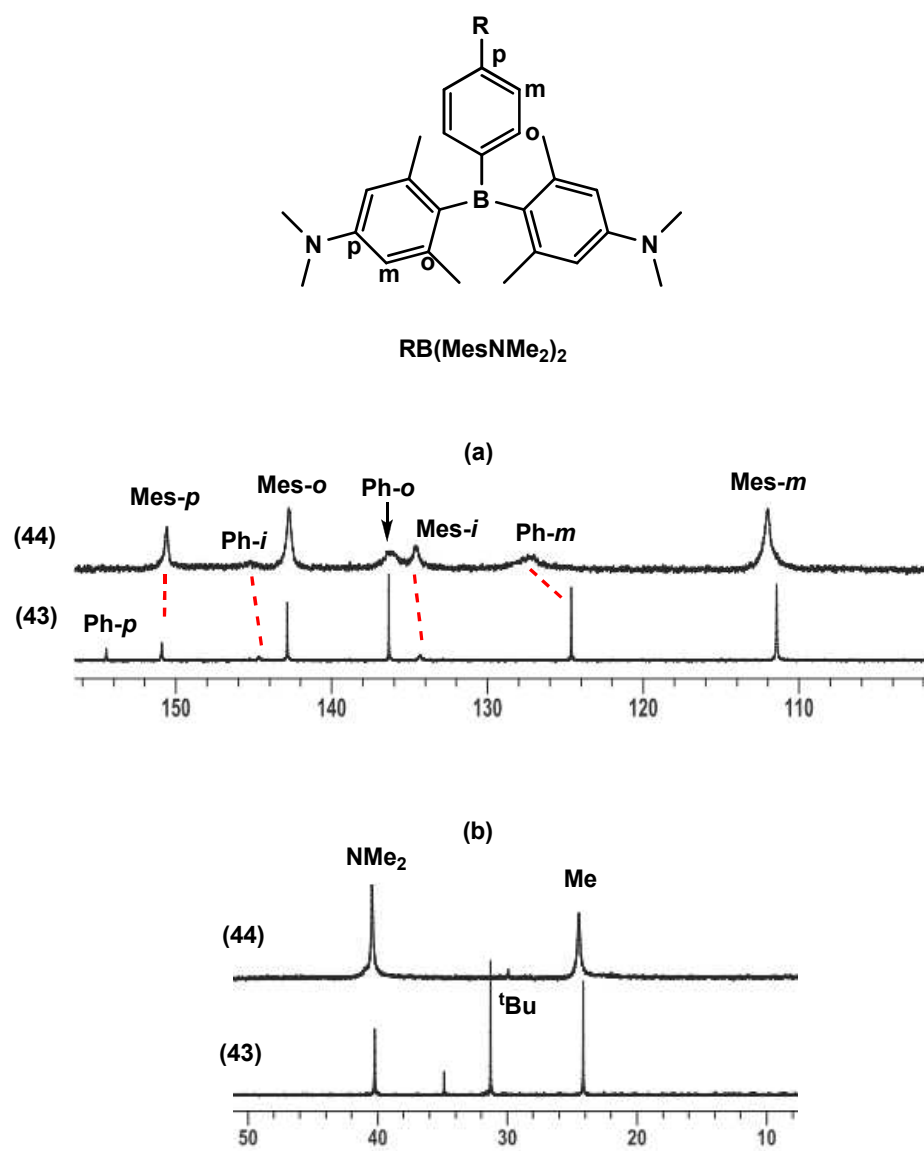
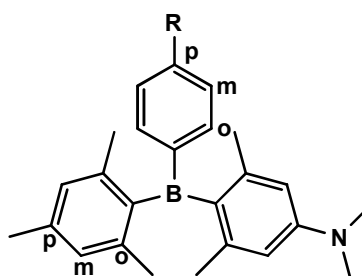
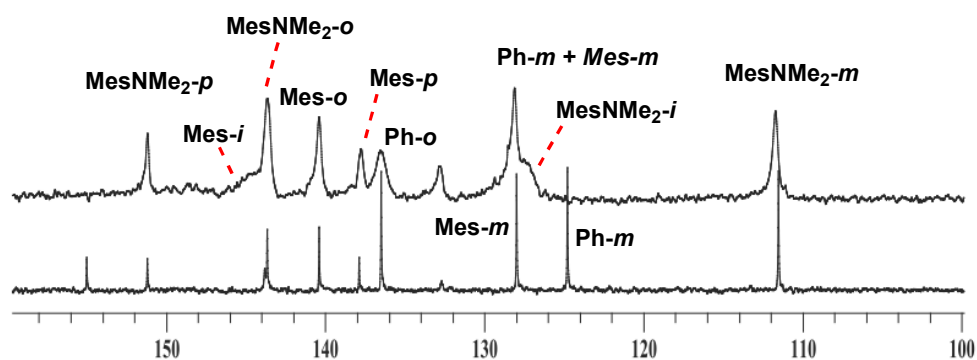


Figure 1B.3 ^{13}C NMR Overlay of (43) and (44) (a) Aromatic Region; (b) Aliphatic Region.



RB(Mes)(MesNMe₂)

(a)



(b)

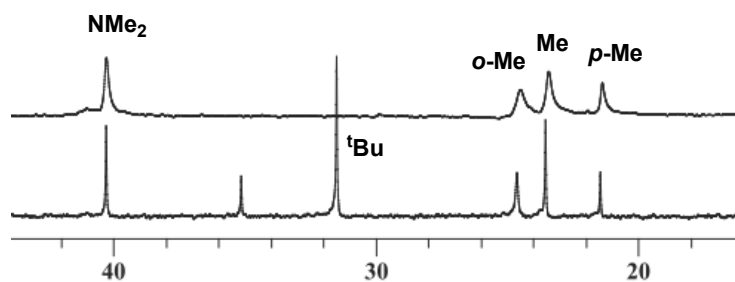


Figure 1B.4 ¹³C NMR Overlay of (50) and (51) (a) Aromatic Region; (b) Aliphatic Region.

1B.4.2.2 Molecular Weight Determination

The molecular weights of all the polymers were analyzed by gel permeation chromatography (GPC) in THF. Polymer (53) was studied in the presence of 5 wt % triethylamine in THF to minimize interactions of the amino groups with the column material. The molecular weights relative to polystyrene standards were found to be in the range expected on the basis of the MW of the poly(4-trimethylsilyl)styrene precursor. However, the band for (53) is strongly broadened (polydispersity (PDI) of 2.8), presumably due to interaction with the column material.

Table 1B.2 Molecular Weight Data for the Polymers Obtained from GPC.

Polymer	M _w	M _n	DP (M _n)	PDI
(36)	28860	26000	148	1.11
(44)	75590 / 30990	69550 (70%) / 27890 (30%)	170 / 68	1.08 / 1.11
(51)	114700 / 29240	87110 (60%) / 22360 (40%)	228 / 58	1.32 / 1.31
(53)	80930	28950	73	2.80

A high molecular weight shoulder was observed for (44) and (51) and a Gaussian fit suggested that the MW of this fraction is about double that of the main peak (Figure

1B.5). This bimodality may be due to incomplete substitution on the boron centers with aryl groups, which could potentially lead to the formation of B-O-B linkages giving rise to the higher molecular weight polymer. An alternative explanation may be that homo-coupling at the Br end groups may have occurred (radical coupling) to a small extent.

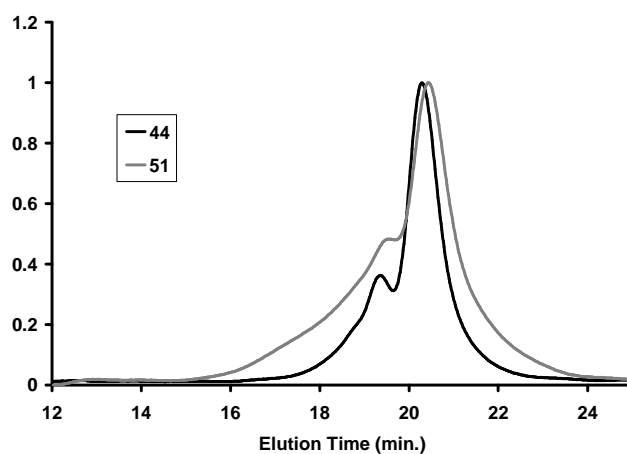


Figure 1B.5 Gel Permeation Chromatography (refractive index detector) Traces of (44) and (51).

1B.4.2.3 Determination of the X-ray Structure of $\text{MB}(\text{MesNMe}_2)_2$ (43)

The x-ray structure determination was performed on yellow-green single crystals of (43) obtained from hexanes at $-20\text{ }^\circ\text{C}$. (43) crystallizes in the orthorhombic space group $\text{Pna}2(1)$ and its structure is shown in Figure 1B.3. The Boron center adapts a trigonal

planar geometry as indicated by the sum of all bond angles which is equal to 359.9° . The $B(1)-C(3) = 1.576(3) \text{ \AA}$ and $B(1)-C(14) = 1.573(3) \text{ \AA}$ bond lengths in $MB(MesNMe_2)_2$ are similar to the $B(1)-C(8)$ bond length to the phenyl ring ($1.569(3) \text{ \AA}$) and almost identical to the $B-C(Mes)$ bonds in Mes_2BPh ($1.579(2) \text{ \AA}$).⁴² However, they are slightly longer than the $B-C(aryl)$ bond in $(p-Mes_2B-C_6H_4-NMe_2)$ ($1.545(2) \text{ \AA}$).⁷

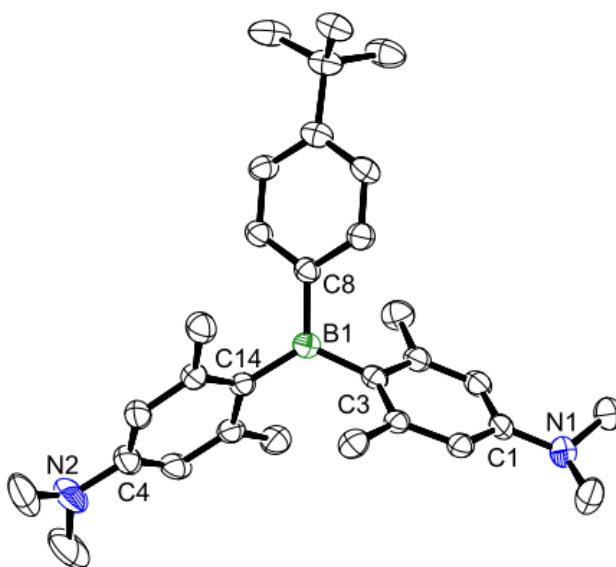


Figure 1B.6 Molecular Structure of (43) (ORTEP, 50% probability). Hydrogen Atoms are Omitted for Clarity. Selected Bond Lengths (\AA) and Angles ($^\circ$): $B1-C8 = 1.569(3)$, $B1-C3 = 1.576(3)$, $B1-C14 = 1.573(3)$, $C8-B1-C3 = 115.03(17)$, $C8-B1-C14 = 121.81(17)$, $C3-B1-C14 = 123.15(18)$.

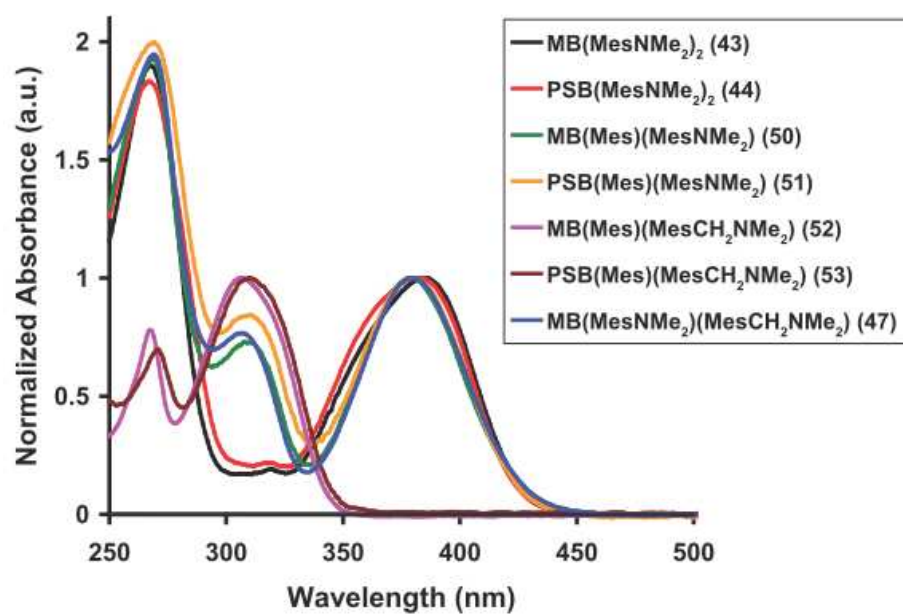
1B.4.2.4 Photophysical Properties in Solution

As shown in Figure 1B.7 and Table 1B.3, all four model compounds and polymers in CH_2Cl_2 solution exhibit several intense absorption bands in the UV-visible region. For instance, (43) and (44) absorb at $\lambda_{\text{abs}} = 381$ and 384 nm, respectively, and emit bright yellow-green light at $\lambda_{\text{em}} = 521$ and 501 nm. The absorption spectra of compounds (47), (50) and (51) in CH_2Cl_2 solution are quite similar. For all these compounds, the high energy absorption band at $\lambda < 280$ nm is assigned to a π - π^* transitions, while the low energy absorption band in the region of 350-400 nm can be attributed to a charge transfer transition between the amino group and the boron center.

In contrast, (52) and (53) show absorption bands at $\lambda_{\text{abs}} = 305$ and 307 nm, respectively, and do not show any charge transfer absorption in the 350-400 nm region, due to the presence of a methylene spacer that breaks the conjugation. The fluorescence spectra for (52) and (53) consist of a broad band at $\lambda_{\text{em}} = 405$ nm and 390 nm, respectively. Additionally, more intense low energy bands at approximately 509 nm for (52) and 485 nm for (53), respectively, were also observed. Since the compounds bear a very close resemblance to $^t\text{BuC}_6\text{H}_4\text{B}(\text{Mes})_2$, the high energy bands at 405 nm and 390 nm can be attributed to the desired products (52) and (53), respectively (the compound $^t\text{BuC}_6\text{H}_4\text{B}(\text{Mes})_2$, shows an emission at $\lambda_{\text{em}} = 387$ nm ($\lambda_{\text{exc}} = 310$ nm)); while the low

energy bands at 509 nm and 485 nm may be due to impurities such as a small amount of (50) or a similar conjugated species.

(a)



(b)

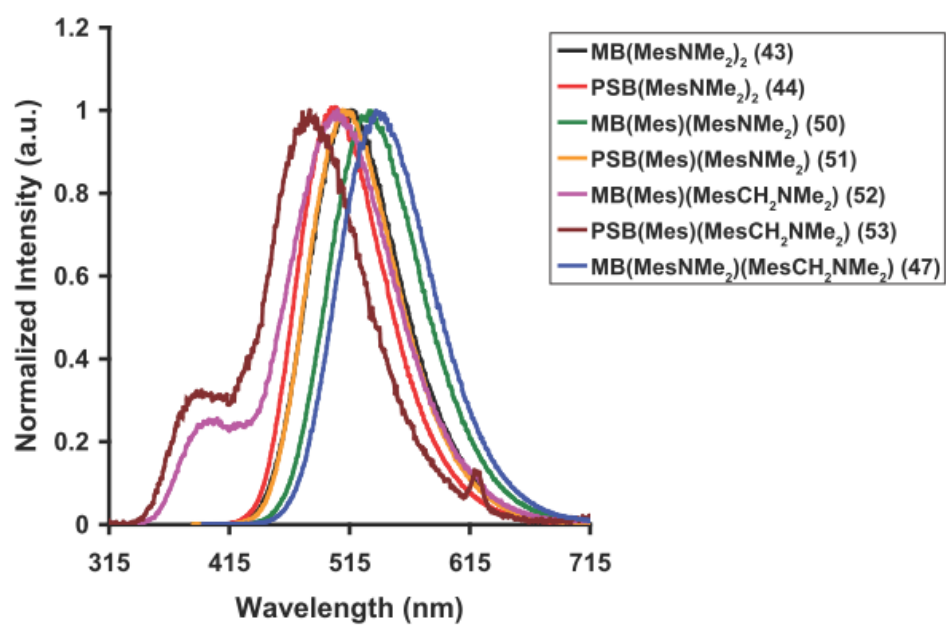


Figure 1B.7 Comparison of (a) the Absorption Spectra and (b) the Emission Spectra of (43), (44), (47), (50), (51), (52) and (53) in CH_2Cl_2 Solution.

Table 1B.3 Comparison of Photophysical Properties of Polymers and Model Compounds.

Polymer	(44)	(51)	(53)	
λ_{abs} (nm) ^a	381	380	310	
ϵ (L mol ⁻¹ cm ⁻¹)	21830	9330	14700	
λ_{em} (nm) ^{a,b}	501	508	390, 485	
Φ_{F} (%) ^c	9.0	10.3	3.9	
Model	(43)	(50)	(52)	(47)
λ_{abs} (nm) ^a	384	379	306	380
ϵ (L mol ⁻¹ cm ⁻¹)	23885	14950	17720	10630
λ_{em} (nm) ^{a,b}	521	534	403, 509	532
Φ_{F} (%) ^c	3.5	6.1	3.9	6.6

^a Data were acquired in CH₂Cl₂ solution (3.2 x 10⁻⁵ M of boron functional groups). ^b Excited at the absorption maxima. ^c Anthracene used as a standard.

The absorption and the emission data of the mixed model systems (47) and (50) are quite similar to one another. This similarity indicates that the presence of the dimethylamino functionalized mesityl group attached to the boron center leads to charge transfer and therefore dominates the absorption and emission characteristics.

1B.4.2.5 Solvatochromism

The fluorescence spectra of compounds (43), (44), (47), (50) and (51) display highly solvent-dependent emission, characteristic of donor-acceptor charge transfer. The emission energy for these compounds shifts to a lower energy with increasing solvent polarity, which is consistent with the presence of a highly polarized excited state.^{1, 6} The positions of the absorption bands for all the compounds are independent of solvents. In contrast to the absorption bands, the position of the emission band is solvent dependent.

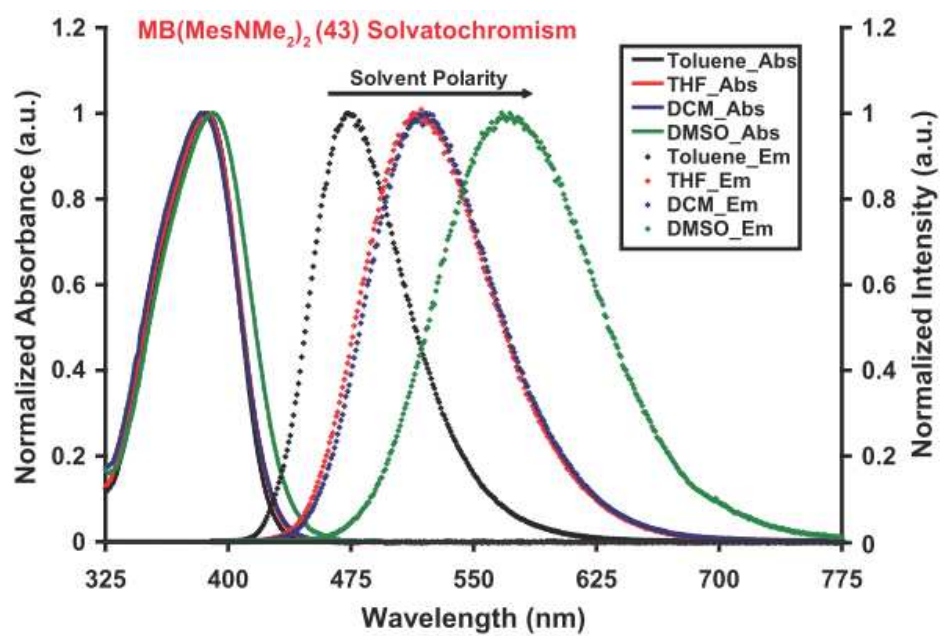
When the solvent is changed from toluene to THF or CH₂Cl₂ to DMF, the emission maximum of all the compounds shifts to a longer wavelength, as shown in Figure 1B.8. For example, in toluene solution, the emission λ_{max} of (43) is 475 nm, while in CH₂Cl₂ and DMF, the emission λ_{max} becomes 521 and 573 nm, respectively. The emission quantum efficiency of all the compounds decreases with increasing solvent polarity (Table 1B.4). This trend of the solvent-dependent emission energy and decrease in quantum efficiency is consistent with the behavior of three-coordinate boron compounds reported by Wang *et al.* and Marder *et al.*⁷ For instance, Marder and coworkers have reported tricoordinated (*p*-R-Phenyl)-dimesitylborane based donor- π -acceptor compounds. *p*-Mes₂B-C₆H₄-NMe₂ exhibits an emission at 368 nm in cyclohexane. A significant red shift was observed from 368 nm in cyclohexane to 465 nm in CHCl₃, and

506 nm in acetonitrile, whereas only a subtle solvent dependence is observed in the absorption maxima ($\lambda_{\text{max}} = 354$ nm in cyclohexane and 361 nm in THF).

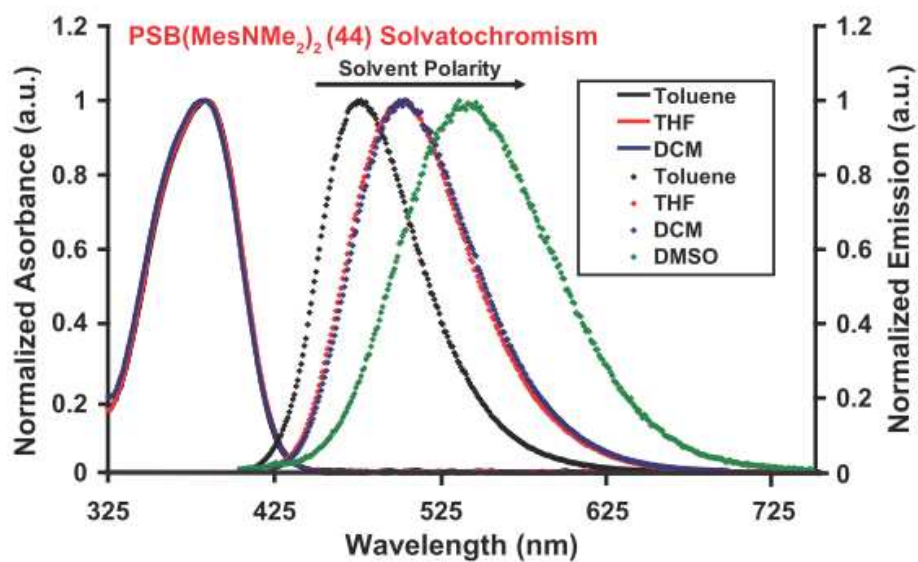
Table 1B.4 Comparison of Photophysical Properties of Polymers and Model Compounds in Various Solvents.

Compounds	Toluene	THF	DCM	DMSO
λ_{em} (nm) / Φ_{F} (%)				
MB(MesNMe ₂) ₂ (43)	473 / 20.0	516 / 12.3	521 / 3.6	573 / 4.8
PSB(MesNMe ₂) ₂ (44)	476 / 18.5	502 / 13.4	502 / 9.0	535 / 4.7
MB(Mes)(MesNMe ₂) (50)	484 / 13.2	530 / 7.2	534 / 6.1	590 / 3.3
PSB(Mes)(MesNMe ₂) (51)	485 / 16.0	516 / 9.2	508 / 10.3	536 / 7.1
MB(MesNMe ₂) (MesCH ₂ NMe ₂) (47)	489 / 24.0	532 / 14.1	532 / 6.6	592 / 7.0

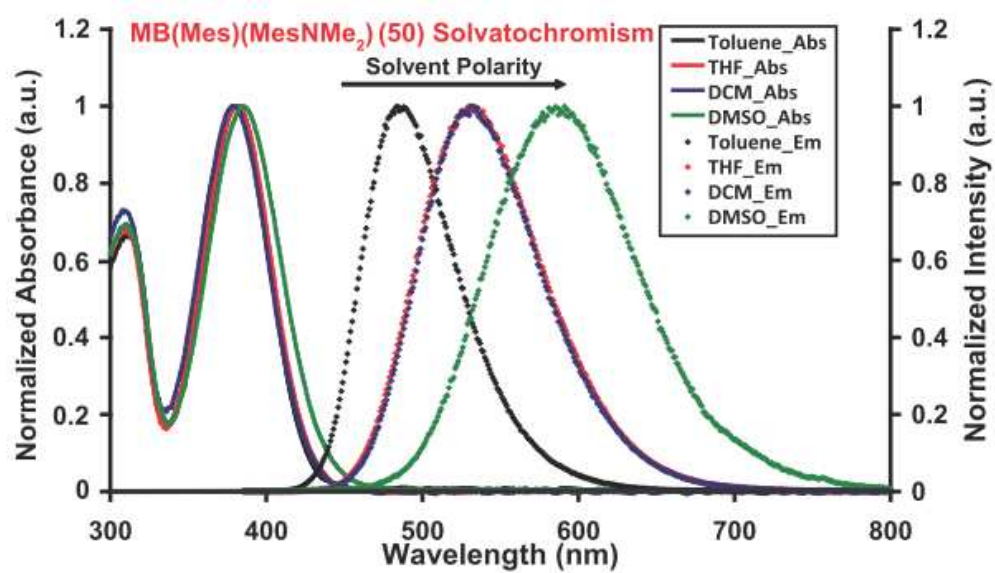
(a)



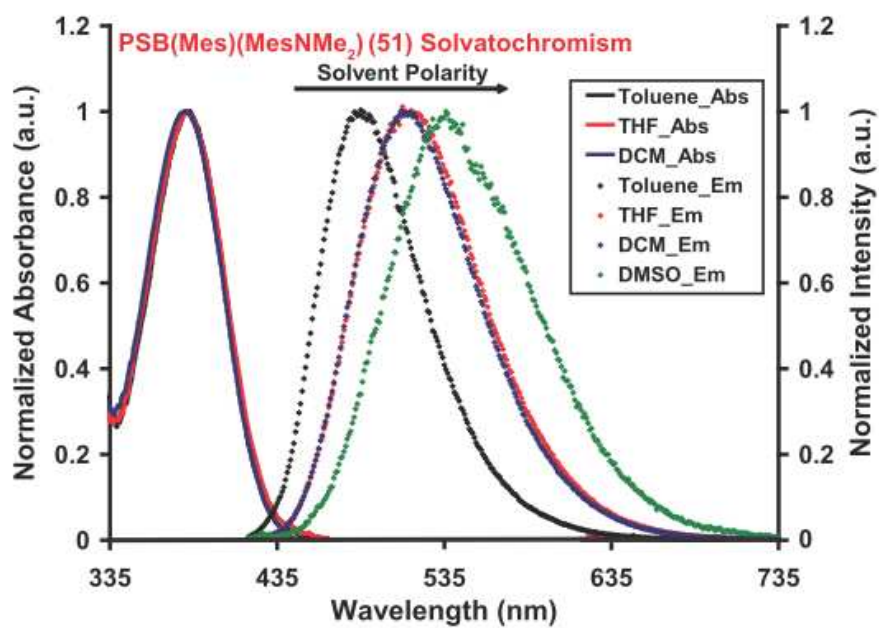
(b)



(c)



(d)



(e)

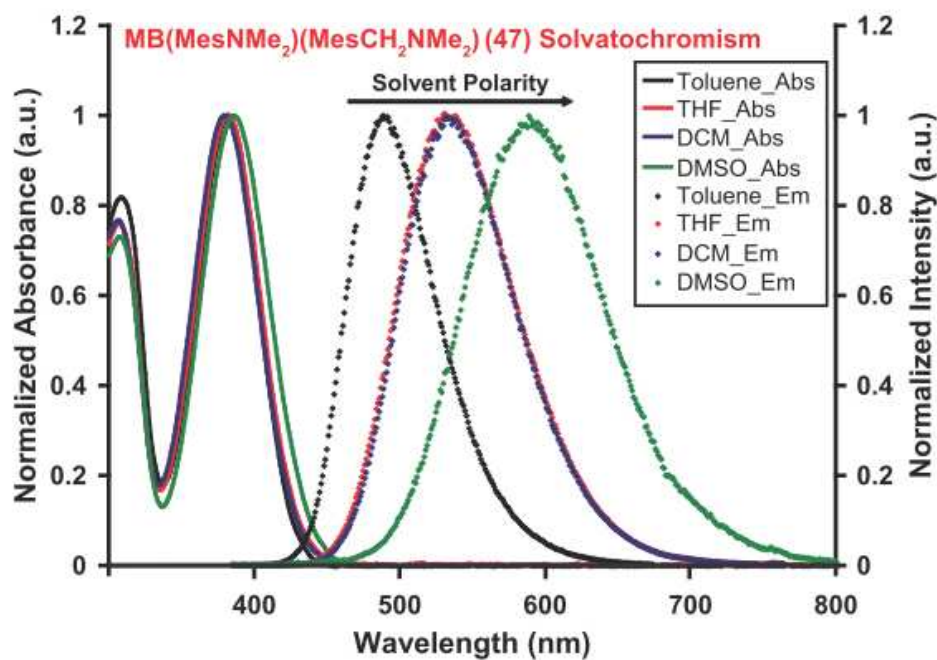


Figure 1B.8 (a) Comparison of the Absorption and Emission Spectra of MB(MesNMe₂)₂ (43) in different solvents. (b) Comparison of the Absorption and Emission Spectra of PSB(MesNMe₂)₂ (44) in different solvents. (c) Comparison of the Absorption and Emission Spectra of MB(Mes)(MesNMe₂) (50) in different solvents. (d) Comparison of the Absorption and Emission Spectra of PSB(Mes)(MesNMe₂) (51) in different solvents. (e) Comparison of the Absorption and Emission Spectra of MB(MesNMe₂)(MesCH₂NMe₂)₂ (47) in different solvents.

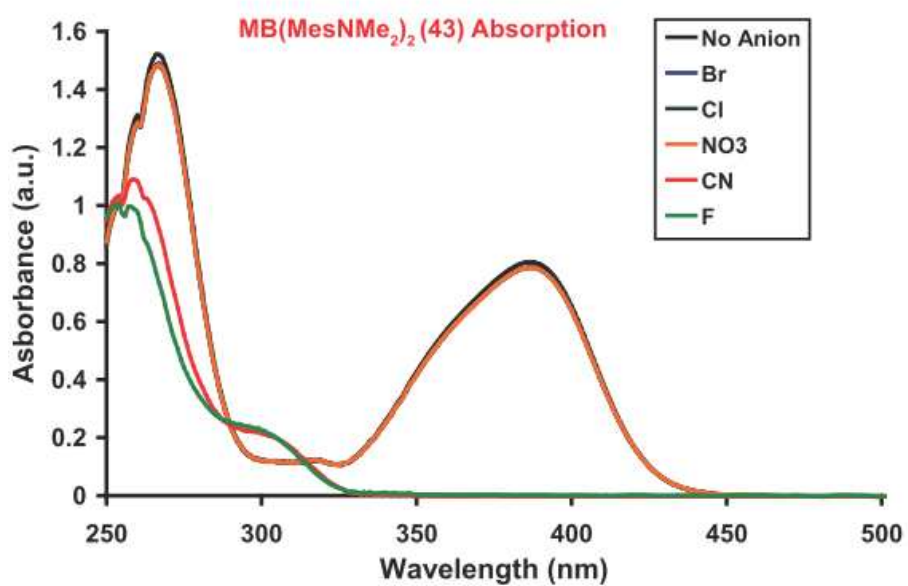
1B.5 Borylated Polystyrenes as Anion Sensors

To explore the potential use of both molecular models and polymers in anion recognition, we performed a comparative study in which a solution of each model and polymer was treated under identical conditions with a 10-fold excess of fluoride, chloride, bromide, nitrate, and cyanide, respectively. The photophysical response was monitored by UV-visible absorption and emission spectroscopy. From examination of the absorption and emission data, it is evident that fluoride and cyanide bind strongly to these boron compounds, while the other anions showed no significant response (Figure 1B.9). Gabbai and coworkers studied cyanide binding of compound (29) in H₂O at pH 7 by UV-vis spectroscopy. They observed that addition of cyanide to this solution results in progressive quenching of the absorbance at 307 nm indicating binding of the cyanide ion to the boron center. They also note that (29) is highly selective for cyanide and fails to bind F⁻, Cl⁻, Br⁻, I⁻, OAc⁻, NO₃⁻, H₂PO₄⁻ and HSO₄⁻.

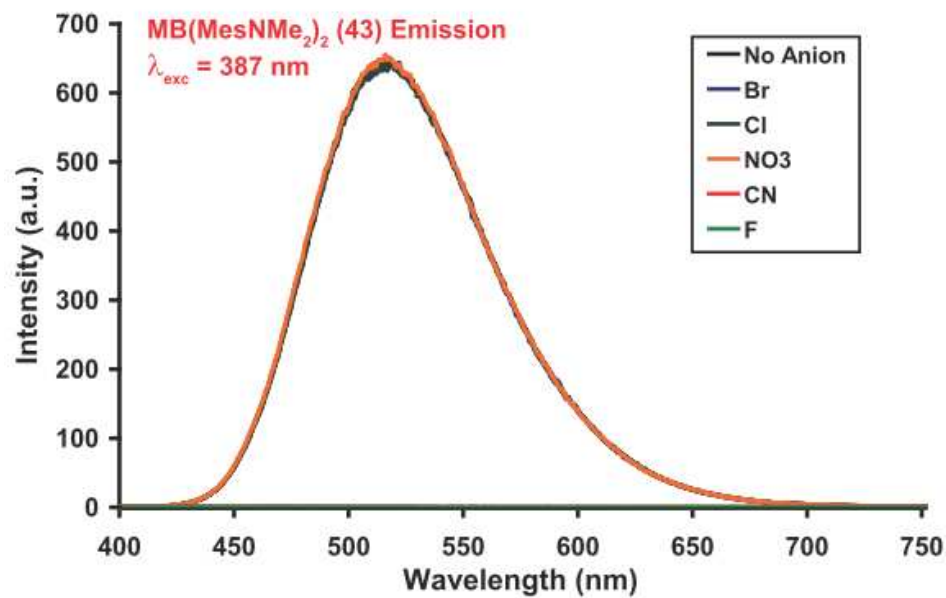
Upon addition of a large excess (~10 equiv.) fluoride and cyanide, the absorption spectra of all the polymers showed the development of a new band at around 300 nm, which is assigned to the complexed borane species. A less intense band at around 385 nm was also observed. The origin of this band is not clear but could be due to impurities in the polymer as also found by ¹¹B NMR spectroscopy. A similar trend is observed in the emission spectrum where a significant decrease in the emission intensity is observed upon

addition of large excess fluoride and cyanide and a slight blue shift of ~40 nm is observed. Again, an additional band was found at ca. 480 nm, which is likely due to the presence of uncomplexed organoborane sites of lower Lewis acidity (R_2B-OR').

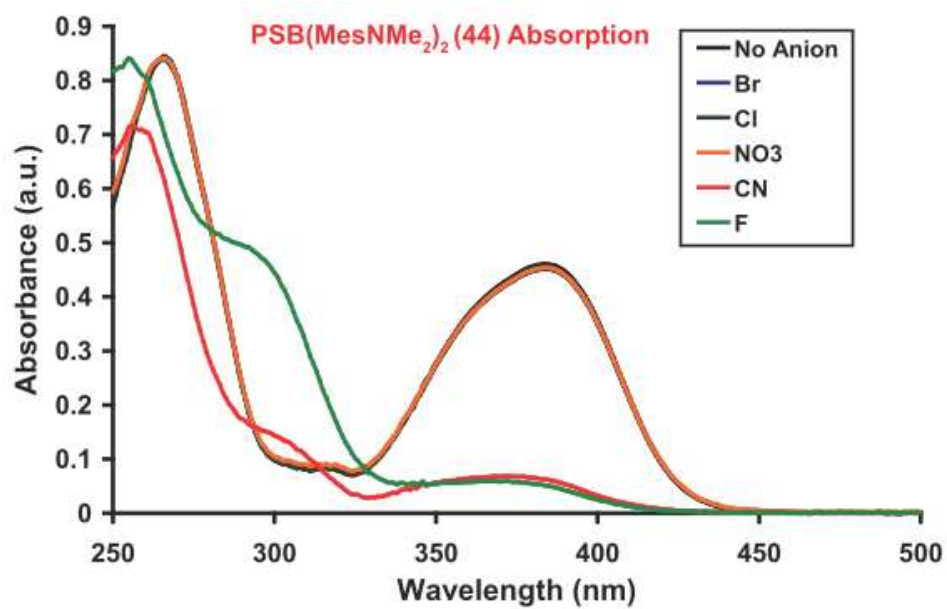
(a)



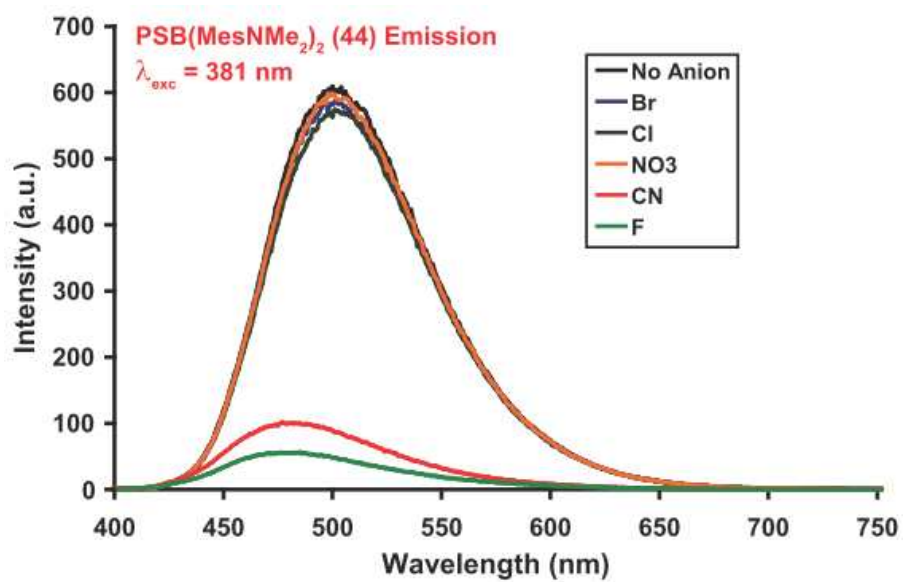
(b)



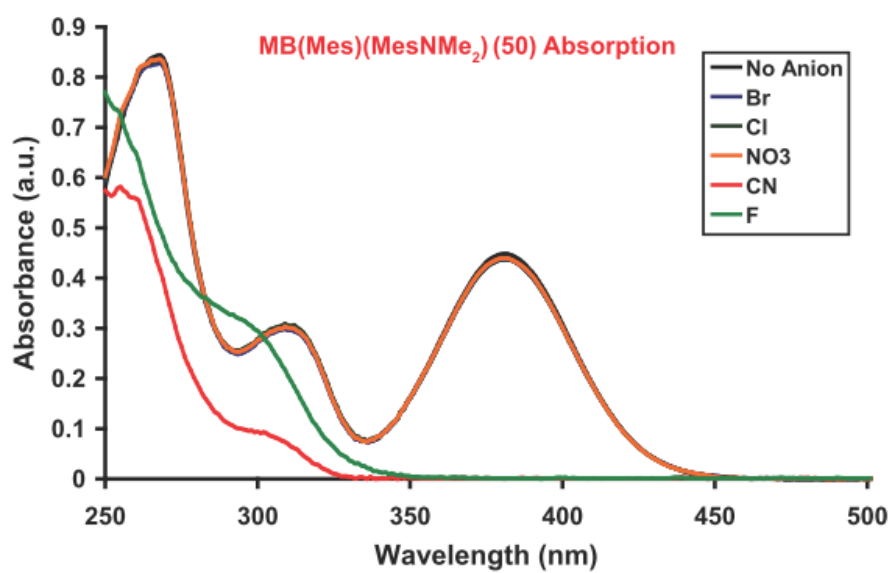
(c)



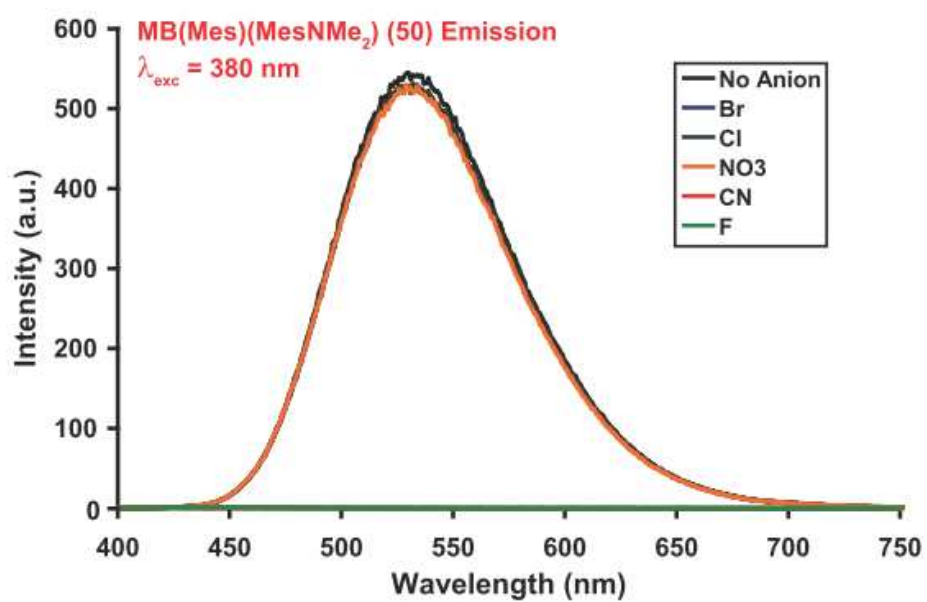
(d)



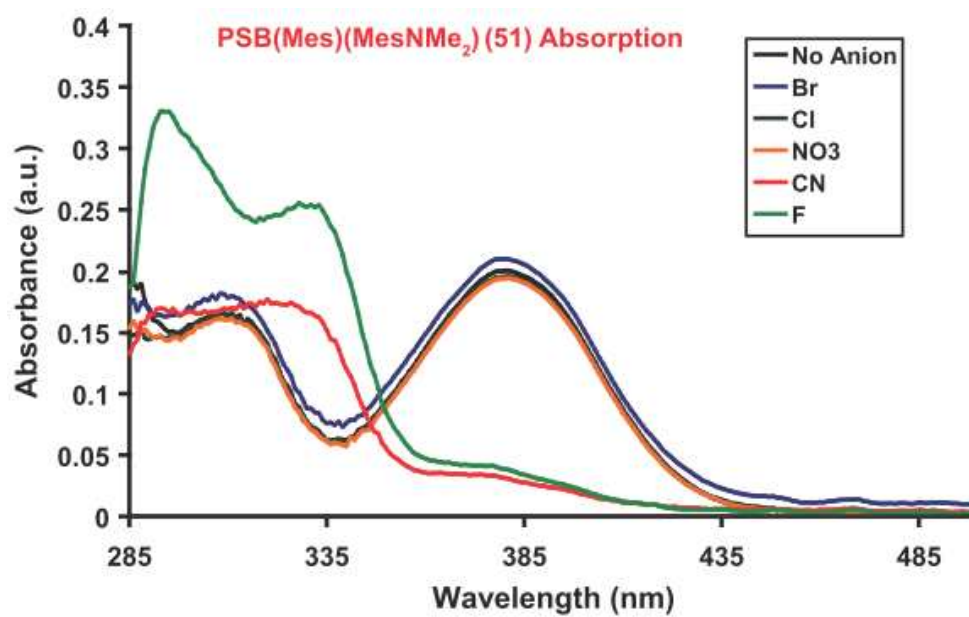
(e)



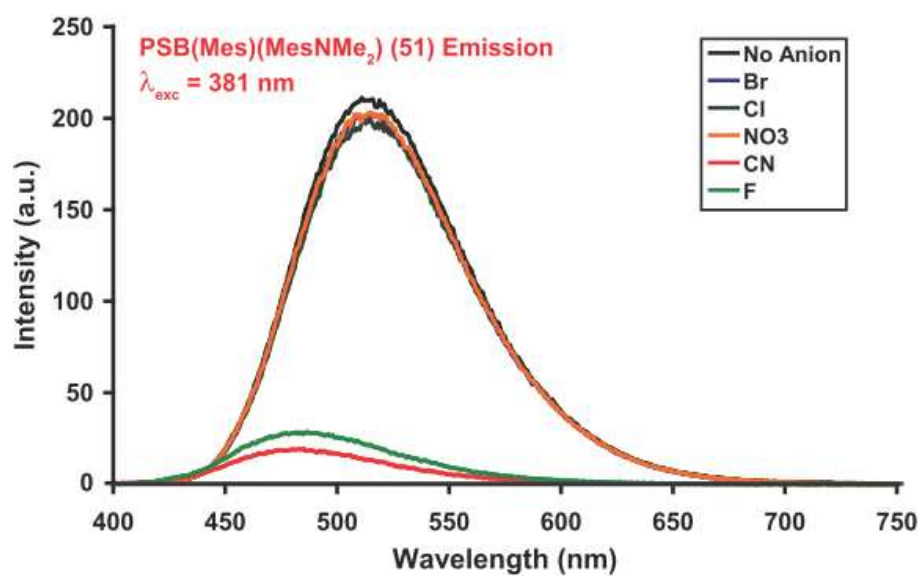
(f)



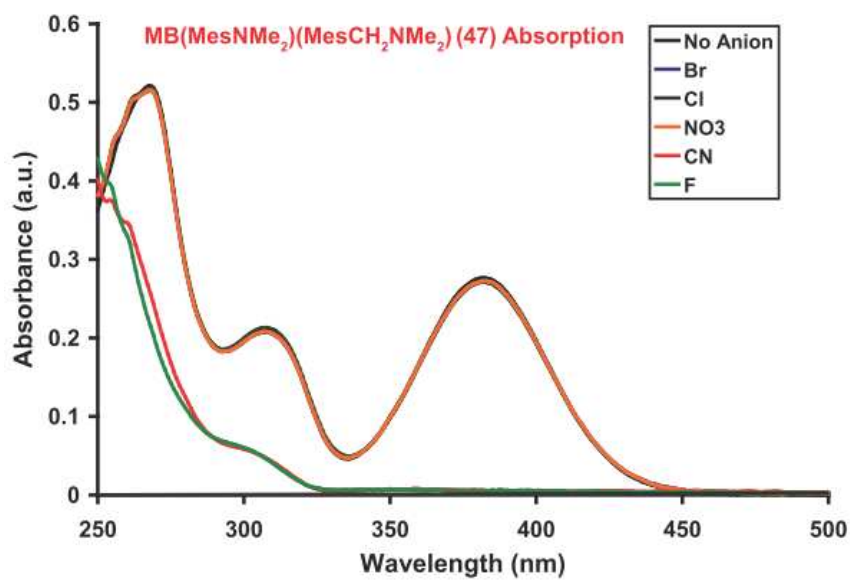
(g)



(h)



(i)



(j)

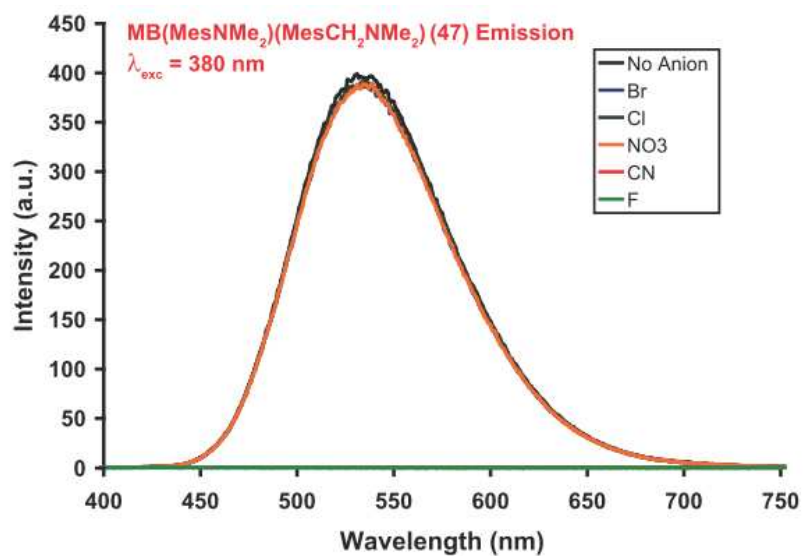


Figure 1B.9 Comparison of Photophysical Properties of Model Systems and Polymers upon Titration with ~10 Equiv of Different Anions (Borane Source = $\sim 3.2 \times 10^{-5}$ M per repeat unit for polymers, Fluoride Source = $\sim 3.2 \times 10^{-4}$ M).

1B.6 Conclusions

We have attempted the incorporation of dimethylamino-functionalized mesityl groups as chromophores into the side chain of polystyrene using Grignard reagents. However, aryl-transfer in the case of polymers and model systems was not very selective. All the polymers and model compounds with dimethylamino functionality display bright green luminescence depending on the substitution on the boron center. Anion binding studies indicate that the presence of these Lewis acidic boron moieties can be exploited for sensing of nucleophiles based on changes in the emission properties. Future work may involve further optimization of the post-polymerization modification methods to achieve higher degrees of functionalization and the quaternization of amino groups to achieve water solubility.

1B.7 Experimental Section

1B.7.1 Materials and Instrumentation

2,6-Dimethylaniline, 3,5-dimethylaniline, N-bromosuccinimide, sodium hydride, methyl iodide, anhydrous dimethylformamide, Me₃SiOMe (98%), *t*-BuLi (1.7 M in pentane), [Bu₄N]Cl, [Bu₄N]Br, [Bu₄N]CN, and Mg (turnings, 99.9%) were purchased from Acros. BBr₃ (99+%), [Bu₄N]NO₃, and [Bu₄N]F (1M in THF) from Aldrich. BBr₃ was further purified by vacuum distillation. **Caution!** *BBr₃ is toxic and highly corrosive and should be handled appropriately with great care.* Fluorinated grease was used for ground glass joints in all reactions involving boron tribromide. The compounds 4-bromo-3,5-dimethylbenzaldehyde⁴³ and (4-tert-butylphenyl)trimethylsilane⁴⁴ were synthesized according to literature procedures. 4-bromo-*N,N*,3,5-tetramethylaniline⁴⁵ and 1-(4-bromo-3,5-dimethylphenyl)-*N,N*-dimethylaminomethylbenzene was obtained by adaptation of a literature procedure for the synthesis of *N,N*-dimethylated tertiary amines.⁴⁶ Poly(4-trimethylsilylstyrene) (36) of $M_n = 26,450$; $M_w = 29,200$; $PDI = 1.10$ (GPC-RI) was prepared as previously reported.^{44, 47} All reactions were carried out under inert atmosphere using Schlenk techniques or a glove box (Innovative Technologies). Ether, hydrocarbon and chlorinated solvents were treated as described in Chapter 1A prior to use. All reactions and manipulations were carried out in a similar manner to that described in Chapter 1A. Detailed description of NMR abbreviations, elemental analyses,

GPC analysis, DSC and TGA analysis can be found in the experimental section of Chapter 1A.

Solution UV-visible measurements were performed in CH₂Cl₂ using a Varian Cary 500 scan UV-Vis-NIR spectrophotometer with a 1 cm quartz cuvette. The fluorescence data were measured on a Varian Cary Eclipse Fluorescence spectrophotometer with the same solutions as those used in the UV-visible measurements. Anthracene was used as the standard for determination of the quantum yields (Φ). Sample solutions were prepared using a microbalance (± 0.1 mg) and volumetric glassware. The quantum yield was calculated by plotting a graph of integrated fluorescence intensity vs. absorbance of at least four solutions with increasing concentration. The gradient of the graph is proportional to the quantum yield. The formula used to calculate the absolute quantum yield is $\Phi = \Phi_{\text{standard}} \times \text{Gradient compound} / \text{Gradient standard}$. X-ray diffraction intensities were collected on a Bruker SMART APEX CCD diffractometer at $T = 100(2)$ K using CuK α (1.54178 Å) radiations. SADABS⁴⁸ or numerical absorption correction was applied; the structure was solved using direct methods, completed by subsequent difference Fourier syntheses, and refined by full matrix least squares procedures on F^2 . All non-hydrogen atoms were refined with anisotropic displacement coefficients. The H atoms were placed at calculated positions and were refined as riding atoms. All software and source scattering factors are contained in the SHELXTL program package.⁴⁹ GC-MS

spectra were acquired on a Hewlett Packard HP 6890 Series GC system equipped with a series 5973 mass selective detector and a series 7683 injector. A temperature profile with a heating rate of 20 °C/min from 50 °C to 300 °C was used. MALDI-TOF and ESI data were obtained on an Apex-ultra 70 hybrid fourier transform mass spectrometer (FTMS) (Bruker Daltonics). α -Cyano-4-hydroxycinnamic acid were used as the matrices.

1B.7.2 Synthesis and Data for Precursors and Model Compounds

Synthesis of (42): To a solution of triethylamine (6.0 mL, 43.0 mmol) in ethanol (15.0 mL) were added dimethylamine hydrochloride (3.521 g, 43.0 mmol) and titanium(IV)isopropoxide (13.0mL, 43.0 mmol). The resultant suspension was poured into a flask containing 4-bromo-3,5-dimethylbenzaldehyde (4.33g, 20.3 mmol). After 24 hours of continuous stirring at 25°C, sodium borohydride (1.2g, 30 mmol) was added and the solution stirred for another 24 h. The reaction was then quenched with aqueous ammonia (2N, 200 mL), and the resulting inorganic precipitate was filtered and washed with CH₂Cl₂. The combined dichloromethane layers were dried over K₂CO₃ and concentrated in vacuo. The product (1-(4-bromo-3,5-dimethylphenyl)-*N,N*-dimethylmethanamine) was chromatographed on silica gel (hexane/triethylamine, 100:1) to yield a clear yellowish oil (3.71g, 75%); ¹H NMR (499.893 MHz, CDCl₃): δ = 7.02 (s, 2H, Ph_m, 3.31 (s, 2H, CH₂), 2.41 (s, 6H, CH₃), 2.24 (s, 6H, NMe₂); ¹³C NMR (125.69

MHz, CDCl₃): δ = 138.2 (Ph-*p*), 137.5 (Ph 2,6), 129.0 (Ph 3,5), 126.1 (Ph-*i*), 63.9 (CH₂) 45.6 (NMe₂), 23.9 (CH₃); GC-MS (*t* = 8.98 min): *m/z* (%): 241 [M⁺] (100). THF (20.0 mL) was added to magnesium turnings (0.31 g, 0.013 mmol). 1-(4-bromo-3,5-dimethylphenyl)-*N,N*-dimethylmethanamine (1.54 g, 0.0064 mmol) was then added and the resulting suspension stirred and activated using 1,2-dibromoethane. An exothermic reaction took place and the reaction mixture was stirred at ambient temperature. After 1 h, the cooled reaction mixture was stirred at 60 °C for 3 h. The reaction mixture was filtered and the filtrate was used directly.

Synthesis of (43): Me₃SiOMe (0.41 mL, 2.97 mmol) was added dropwise to a solution of ^tBuPhBBr₂ (0.36 g, 1.19 mmol) in CH₂Cl₂ (5 mL). The reaction mixture was stirred for 2 h. All volatile components were removed under high vacuum. The solid was taken up in THF (10 mL), and a solution of (41) (0.5 M in THF, 20.0 mL, 10 mmol) was added. The reaction mixture was stirred at room temperature for 30 min and then heated to 110 °C for 15 days. The solvent was removed under high vacuum to leave behind a yellow solid that was extracted with hexanes. Purification by repeated extraction with hexanes and crystallization from hexanes gave the product in the form of yellow-green crystals (0.130 g, 25 %). For (43): ¹¹B NMR (160.386 MHz, CDCl₃): δ = 72 ppm (*w*_{1/2} = 1440 Hz); ¹H NMR (499.893 MHz, CDCl₃): δ = 7.47 (d, ³J = 8.5 Hz, 2H, Ph_o), 7.33 (d, ³J = 8.5 Hz, 2H, Ph_m), 6.40 (s, 2H, MesNMe_{2m}), 2.98 (s, 6H, NMe₂), 2.00 (s, 6H, *o*-Me), 1.35 (s, 9H,

CMe_3); ^{13}C NMR (125.69 MHz, CDCl_3): δ = 154.5 (Ph_p), 150.9 (MesNMe_{2p}), 144.7 (Ph_i), 142.8 (Ph_o), 136.3 (MesNMe_{2o}), 134.3 (MesNMe_{2i}), 124.6 (Ph_m), 111.4 (MesNMe_{2m}), 40.3 (NMe_2), 35.0 (CMe_3), 31.4 (CMe_3), 24.4 (*o*-Me); UV-Vis (Toluene, 3.4×10^{-5} M): 387 nm (ϵ = 26,727); fluorescence (Toluene, 3.4×10^{-5} M): $\lambda_{\text{em,max}}$ = 473 nm, Φ = 0.12 (λ_{exc} = 387 nm); UV-Vis (THF, 3.4×10^{-5} M): λ_{max} = 264 nm (ϵ = 36,088), 387 nm (ϵ = 20,819); fluorescence (THF, 3.4×10^{-5} M): $\lambda_{\text{em,max}}$ = 516 nm, Φ = 0.12 (λ_{exc} = 387 nm); UV-Vis (CH_2Cl_2 , 3.2×10^{-5} M): λ_{max} = 268 nm (ϵ = 45,288), 384 nm (ϵ = 23,884); fluorescence (CH_2Cl_2 , 3.2×10^{-5} M): $\lambda_{\text{em,max}}$ = 521 nm, Φ = 0.036 (λ_{exc} = 384 nm); UV-Vis (DMSO, 3.5×10^{-5} M): λ_{max} = 269 nm (ϵ = 34,336), 391 nm (ϵ = 16,867); fluorescence (DMSO, 3.5×10^{-5} M): $\lambda_{\text{em,max}}$ = 573 nm, Φ = 0.048 (λ_{exc} = 391 nm); High resolution MALDI-TOF (positive mode, matrix: α -Cyano-4-hydroxycinnamic acid): m/z = 440.3362 (calcd for $\text{C}_{30}\text{H}_{34}\text{BN}_2$ 440.3363); elemental analysis: calculated C 81.80, H 9.38, N 6.36; found C 81.38, H 9.29, N 6.26.

Synthesis of (50): Me_3SiOMe (0.2 mL, 1.46 mmol) was added dropwise to a solution of $^t\text{BuPhBBr}_2$ (0.19 g, 0.63 mmol) in CH_2Cl_2 (5 mL). The reaction mixture was stirred for 2 h. All volatile components were removed under high vacuum. The solid was taken up in THF (10 mL), and a solution of (40) (0.5 M in THF, 1.3 mL, 0.65 mmol) was added. The reaction mixture was stirred at room temperature for 24 h. The solvent was removed under high vacuum to leave behind a colorless solid which was then extracted with

toluene to remove insoluble salts. For (48): ^{11}B NMR (160.386 MHz, CDCl_3): $\delta = 47$ ppm; ^1H NMR (499.893 MHz, CDCl_3): $\delta = 7.55$ (d, $^3J = 8.0$ Hz, 2H, Ph_o), 7.30 (d, $^3J = 8.0$ Hz, 2H, Ph_m), 6.81 (s, 2H, Mes_m), 3.68 (s, 3H, OCH_3), 2.28 (s, 3H, $p\text{-Me}$), 2.09 (s, 6H, $o\text{-Me}$), 1.26 (s, 9H, CMe_3). Without further purification, this colorless solid was dissolved in THF (5 mL), and a solution of (41) (3.91×10^{-4} moles/g in THF, 5.7 mL, 3.1 mmol) was added. The reaction mixture was stirred at room temperature for 1 h and then heated to 110 °C for 15 days. The solvent was removed under high vacuum to leave behind yellow solid and the residue was extracted with hexanes. The crude product was kept under high vacuum at 80 °C to remove volatile impurities such as *N,N*,3,5-tetramethylaniline to give pure product as a yellow-green crystalline material (0.115 g, 45%). For (50): ^{11}B NMR (160.386 MHz, CDCl_3): $\delta = 71$ ppm ($w_{1/2} = 1475.8$ Hz); ^1H NMR (499.893 MHz, CDCl_3): $\delta = 7.46$ (d, $^3J = 8.5$ Hz, 2H, Ph_o), 7.33 (d, $^3J = 8.5$ Hz, 2H, Ph_m), 6.81 (s, 2H, Mes_m), 6.40 (s, 2H, MesNMe_{2m}), 3.00 (s, 6H, NMe_2), 2.32 (s, 3H, $p\text{-Me}$), 2.04 (s, 6H, $o\text{-Me}$), 2.01 (s, 6H, $o\text{-MesNMe}_2$), 1.34 (s, 9H, CMe_3); ^{13}C NMR (125.69 MHz, CDCl_3): $\delta = 155.0$ (Ph_p), 151.2 (MesNMe_{2p}), 143.8, 143.7, 140.4, 137.9, 136.5, 127.9, 124.8, 111.5, 40.3 (NMe_2), 35.0 (CMe_3), 31.5 (CMe_3), 24.6 ($o\text{-Me}$), 23.5 ($o\text{-MesNMe}_2\text{-Me}$), 21.4 ($p\text{-Me}$); UV-Vis (Toluene, 3.2×10^{-5} M): $\lambda_{\text{max}} = 284$ nm ($\epsilon = 9,315$), 311 nm ($\epsilon = 9,191$), 381 nm ($\epsilon = 13,817$); fluorescence (Toluene, 3.2×10^{-5} M): $\lambda_{\text{em,max}} = 484$ nm, $\Phi = 0.13$ ($\lambda_{\text{exc}} = 381$ nm); UV-Vis (THF, 3.2×10^{-5} M): $\lambda_{\text{max}} = 268$ nm

($\epsilon = 26,109$), 309 nm ($\epsilon = 9,435$), 381 nm ($\epsilon = 13,858$); fluorescence (THF, 3.2×10^{-5} M): $\lambda_{\text{em,max}} = 530$ nm, $\Phi = 0.072$ ($\lambda_{\text{exc}} = 381$ nm); UV-Vis (CH_2Cl_2 , 3.1×10^{-5} M): $\lambda_{\text{max}} = 269$ nm ($\epsilon = 28,768$), 308 nm ($\epsilon = 10,896$), 379 nm ($\epsilon = 14,946$); fluorescence (CH_2Cl_2 , 3.1×10^{-5} M): $\lambda_{\text{em,max}} = 534$ nm, $\Phi = 0.061$ ($\lambda_{\text{exc}} = 379$ nm); UV-Vis (DMSO, 3.2×10^{-5} M): $\lambda_{\text{max}} = 269$ nm ($\epsilon = 24,732$), 310 nm ($\epsilon = 9,050$), 385 nm ($\epsilon = 13,048$); fluorescence (CH_2Cl_2 , 3.2×10^{-5} M): $\lambda_{\text{em,max}} = 590$ nm, $\Phi = 0.047$ ($\lambda_{\text{exc}} = 385$ nm); GC-MS ($t = 27.7$ min): m/z (%): 411 [M^+] (56), 262 [$\text{M}^+ - \text{MesNMe}_2$] (100); High resolution MALDI-TOF (positive mode, matrix: α -Cyano-4-hydroxycinnamic acid): $m/z = 411.3093$ (calcd for $\text{C}_{29}\text{H}_{38}\text{BN}$ 411.3097); elemental analysis: calculated C 84.66, H 9.31, N 3.40; found C 82.49, H 9.09, N 3.38.

Synthesis of (52): Me_3SiOMe (0.21 mL, 1.50 mmol) was added dropwise to a solution of $^t\text{BuPhBBR}_2$ (0.2 g, 0.65 mmol) in CH_2Cl_2 (5 mL). The reaction mixture was stirred for 2 h. All volatile components were removed under high vacuum. The solid was taken up in THF (10 mL), and a solution of (40) (0.5 M in THF, 1.34 mL, 0.67 mmol) was added. The reaction mixture was stirred at room temperature for 24 h. The solvent was removed under high vacuum to leave behind a colorless solid which was then extracted with toluene to remove insoluble salts. For (48): ^{11}B NMR (160.386 MHz, CDCl_3): $\delta = 47$ ppm; ^1H NMR (499.893 MHz, CDCl_3): $\delta = 7.55$ (d, $^3J = 8.0$ Hz, 2H, Ph_o), 7.30 (d, $^3J = 8.0$ Hz, 2H, Ph_m), 6.81 (s, 2H, Mes_m), 3.68 (s, 3H, OCH_3), 2.28 (s, 3H, $p\text{-Me}$), 2.09 (s,

6H, *o*-Me), 1.26 (s, 9H, CMe₃). Without further purification, this colorless solid was dissolved in THF (5 mL), and a solution of (42) (0.22 M in THF, 20.0 mL, 4.4 mmol) was added. The reaction mixture was stirred at room temperature for 1 h and then heated to 110 °C for 20 days. The solvent was removed under high vacuum to leave behind colorless solid and was extracted with hexanes. Purification by column chromatography using silica as the stationary phase and hexanes as the solvent gave the pure product as a white solid. (0.100 g, 36%). For (52): ¹¹B NMR (160.386 MHz, CDCl₃): δ = 73 ppm ($w_{1/2}$ = 1760 Hz); ¹H NMR (499.893 MHz, CDCl₃): δ = 7.47 (d, ³J = 8.0 Hz, 2H, Ph_o), 7.37 (d, ³J = 8.0 Hz, 2H, Ph_m), 6.94 (s, 2H, Mes_m), 6.83 (s, 2H, MesCH₂NMe_{2m}), 3.39 (s, 2H, CH₂), 2.32 (s, 3H, *p*-Me), 2.29 (s, 6H, NMe₂), 2.05 (s, 6H, *o*-Me), 2.03 (s, 6H, *o*-MesCH₂NMe₂), 1.34 (s, 9H, CMe₃); ¹³C NMR (125.69 MHz, CDCl₃): δ = 154.5 (Ph_p), 144.1 (MesCH₂NMe_{2i}), 142.5 (Mes_i), 141.8 (Ph_i), 141.1 (MesCH₂NMe_{2o}), 140.8 (Mes_o), 139.4 (MesCH₂NMe_{2p}), 138.6 (Mes_p), 136.9 (Ph_o), 128.3 (MesCH₂NMe_{2m}), 128.2 (Mes_m), 125.0 (Ph_m), 64.7 (CH₂), 45.8 (NMe₂), 35.2 (CMe₃), 31.4 (CMe₃), 23.7 (*o*-Me), 21.4 (*p*-Me); UV-Vis (CH₂Cl₂, 3.3 x 10⁻⁵ M): λ_{max} = 268 nm (ϵ = 13,766), 306 nm (ϵ = 17,717); fluorescence (CH₂Cl₂, 3.3 x 10⁻⁵ M): $\lambda_{\text{em,max}}$ = 509 nm, Φ = 0.039 (λ_{exc} = 306 nm); High resolution MALDI-TOF (positive mode, matrix: α -Cyano-4-hydroxycinnamic acid): m/z = 426.3334 [M⁺H] (calcd for C₃₀H₄₀BN 425.3254).

Synthesis of (47): Me₃SiOMe (0.26 mL, 1.89 mmol) was added dropwise to a solution of ^tBuPhBBr₂ (0.25 g, 0.82 mmol) in CH₂Cl₂ (5 mL). The reaction mixture was stirred for 2 h. All volatile components were removed under high vacuum. The solid was taken up in THF (10 mL), and a solution of (41) (0.27 M in THF, 3.1 mL, 0.82 mmol) was added. The reaction mixture was stirred at room temperature for 24 h. The solvent was removed under high vacuum to leave behind a colorless solid which was then extracted with toluene to remove insoluble salts. For (45): ¹¹B NMR (160.386 MHz, CDCl₃): δ = 48 ppm; ¹H NMR (499.893 MHz, CDCl₃): δ = 7.64 (d, ³J = 8.0 Hz, 2H, Ph_o), 7.35 (d, ³J = 8.0 Hz, 2H, Ph_m), 6.47 (s, 2H, MesNMe_{2m}), 3.75 (s, 3H, OCH₃), 2.29 (s, 6H, NMe₂), 2.16 (s, 6H, *o*-Me), 1.32 (s, 9H, CMe₃). Without further purification, this colorless solid was dissolved in THF (5 mL), and a solution of (42) (0.12 M in THF, 20.0 mL, 2.4 mmol) was added. The reaction mixture was stirred at room temperature for 1 h and then heated to 110 °C for 30 days. The solvent was removed under high vacuum to leave behind yellow solid and was extracted with hexanes. Purification by column chromatography using silica as the stationary phase and ether as the solvent gave the pure product as a white solid. (0.150 g, 40%). For (47): ¹¹B NMR (160.386 MHz, CDCl₃): δ = 72 ppm (*w*_{1/2} = 1800 Hz); ¹H NMR (499.893 MHz, CDCl₃): δ = 7.45 (d, ³J = 7.0 Hz, 2H, Ph_o), 7.34 (d, ³J = 7.0 Hz, 2H, Ph_m), 6.90 (s, 2H, MesCH₂NMe_{2m}), 6.39 (s, 2H, MesNMe_{2m}), 3.39 (s, 2H, CH₂), 2.99 (s, 6H, MesNMe₂), 2.29 (s, 6H, MesCH₂NMe₂), 2.05 (s, 12H, *o*-Me), 1.34

(s, 9H, CMe₃); ¹³C NMR (125.69 MHz, CDCl₃): δ = 155.1 (Ph_p), 151.2, 145.9 (Ph_i), 143.8 (MesNMe_{2o}), 143.6 (MesCH₂NMe_{2p}), 140.2 (MesCH₂NMe_{2o}), 138.5, 136.5 (Ph_o), 132.4, 127.9 (MesCH₂NMe_{2m}), 124.8 (Ph_m), 111.5 (MesNMe_{2m}), 64.7 (CH₂), 45.7 (MesCH₂NMe₂), 40.2 (MesNMe₂), 35.2 (CMe₃), 31.4 (CMe₃), 24.6 (*o*-MesNMe₂), 23.5 (*o*-MesCH₂NMe₂); UV-Vis (Toluene, 3.3 x 10⁻⁵ M): λ_{max} = 284 nm (ϵ = 8,272), 309 nm (ϵ = 7,696), 382 nm (ϵ = 9,363); fluorescence (Toluene, 3.3 x 10⁻⁵ M): $\lambda_{\text{em,max}}$ = 489 nm, Φ = 0.24 (λ_{exc} = 382 nm); UV-Vis (THF, 3.3 x 10⁻⁵ M): λ_{max} = 268 nm (ϵ = 15,787), 307 nm (ϵ = 6,363), 381 nm (ϵ = 8,363); fluorescence (THF, 3.3 x 10⁻⁵ M): $\lambda_{\text{em,max}}$ = 532 nm, Φ = 0.14 (λ_{exc} = 381 nm); UV-Vis (CH₂Cl₂, 3.2 x 10⁻⁵ M): λ_{max} = 269 nm (ϵ = 120,512), 307 nm (ϵ = 8,142), 380 nm (ϵ = 10629); fluorescence (CH₂Cl₂, 3.2 x 10⁻⁵ M): $\lambda_{\text{em,max}}$ = 532 nm, Φ = 0.066 (λ_{exc} = 380 nm); UV-Vis (DMSO, 3.3 x 10⁻⁵ M): λ_{max} = 269 nm (ϵ = 21,910), 307 nm (ϵ = 8,242), 386 nm (ϵ = 11303); fluorescence (DMSO, 3.3 x 10⁻⁵ M): $\lambda_{\text{em,max}}$ = 592 nm, Φ = 0.070 (λ_{exc} = 386 nm); High resolution MALDI-TOF (positive mode, matrix: α -Cyano-4-hydroxycinnamic acid): m/z = 454.3517 (calcd for C₃₁H₄₃BN₂ 454.3519).

1B.7.3 Synthesis and Data for Polymers

Synthesis of (44): A solution of BBr₃ (0.30 g, 1.05 mmol) in CH₂Cl₂ (10 mL) was added dropwise to a solution of (36) (0.15 g, ca. 0.87 mmol of Me₃Si groups) in CH₂Cl₂

(10 mL) and stirred for 24 h. Me₃SiOMe (0.42 mL, 3.03 mmol) was added neat, and the solution was stirred for another 24 h. All volatile components were removed under high vacuum. The remaining solid was taken up in THF (10 mL) and a solution of (41) (0.27 M in THF, 15.0 mL, 4.0 mmol) was added. The mixture was allowed to react for 1 h at RT and then refluxed for 4 weeks. The solution was concentrated to ca. 3 mL and precipitated into ethanol (350 mL). The product was purified by repeated precipitation from toluene into methanol (350 mL). The precipitate was dried under high vacuum to give a fine yellow-green powder (0.100 g, 28%). For (44): ¹¹B NMR (160.386 MHz, CDCl₃): δ = 58 ppm ($w_{1/2}$ = 2040 Hz); ¹H NMR (499.893 MHz, CDCl₃): δ = 7.2, 6.3 (aromatic H), 2.9 (br, 12H, MesNMe₂), 1.8 (br, 12H, *o*-MesNMe₂), the backbone protons are overlapping; ¹³C NMR (125.69 MHz, CDCl₃): δ = 150.7, 145.3, 142.8, 136.2, 134.5, 127.2, 111.6, 40.4 (MesNMe₂, polymer backbone), 24.5 (*o*-MesNMe₂); UV-Vis (Toluene, 3.4 x 10⁻⁵ M): λ_{max} = 284 nm (ϵ = 20,774), 384 nm (ϵ = 23,788); fluorescence (Toluene, 3.4 x 10⁻⁵ M): $\lambda_{\text{em,max}}$ = 476 nm, Φ = 0.12 (λ_{exc} = 384 nm); UV-Vis (THF, 3.2 x 10⁻⁵ M): 383 nm (ϵ = 14,177); fluorescence (THF, 3.2 x 10⁻⁵ M): $\lambda_{\text{em,max}}$ = 501 nm, Φ = 0.13 (λ_{exc} = 383 nm); UV-Vis (CH₂Cl₂, 3.3 x 10⁻⁵ M): λ_{max} = 267 nm (ϵ = 39,520), 381 nm (ϵ = 21,827); fluorescence (CH₂Cl₂, 3.3 x 10⁻⁵ M): $\lambda_{\text{em,max}}$ = 502 nm, Φ = 0.09 (λ_{exc} = 381 nm); UV-Vis (DMSO, 3.3 x 10⁻⁵ M): λ_{max} = 264 nm (ϵ = 26,508), 393 nm (ϵ =

3,343); fluorescence (CH_2Cl_2 , 3.3×10^{-5} M): $\lambda_{\text{em,max}} = 542$ nm, $\Phi = 0.03$ ($\lambda_{\text{exc}} = 393$ nm); elemental analysis: calculated C 81.94, H 8.60, N 6.83; found C 79.23, H 8.21, N 6.38.

Synthesis of (51): A solution of BBr_3 (0.43 g, 1.7 mmol) in CH_2Cl_2 (10 mL) was added dropwise to a solution of (36) (0.25 g, ca. 1.43 mmol of Me_3Si groups) in CH_2Cl_2 (10 mL) and stirred for 24 h. Me_3SiOMe (0.69 mL, 5.0 mmol) was added neat, and the solution was stirred for another 24 h. All volatile components were removed under high vacuum. The remaining solid was taken up in THF (10 mL) and a solution of (40) (0.5 M in THF, 2.90 mL, 1.45 mmol) was added. The mixture was allowed to react for 24 h at RT. THF was then removed under high vacuum and remaining white solid was taken up in toluene (10 mL). The toluene solution was stirred for 2 h. Insoluble salts were removed via filtration and solvent was removed under high vacuum. The solid was taken up in THF (10 mL) and a solution of (41) (0.27 M in THF, 20.0 mL, 5.5 mmol) was added. The mixture was allowed to react for 1 h at RT and then refluxed for 4 weeks. The solution was concentrated to ca. 3 mL and precipitated into methanol (350 mL). The product was purified by repeated precipitation from toluene into methanol (350 mL). The precipitate was dried under high vacuum to give a fine yellow-green powder (0.100 g, 18%). For (51): ^{11}B NMR (160.386 MHz, CDCl_3): $\delta = 54$ ppm ($w_{1/2} = 2005$ Hz); ^1H NMR (499.893 MHz, CDCl_3): $\delta = 7.1, 6.7, 6.3$ (aromatic H), 2.9, 2.2, 1.8, 1.6, the backbone protons are overlapping; ^{13}C NMR (125.69 MHz, CDCl_3): $\delta = 151.2, 143.6, 142.8, 140.4, 137.7$,

136.5, 129.3, 128.4, 128.0, 111.6, 40.2 (MesNMe₂, polymer backbone), 24.4 (*o*-MesNMe₂), 23.5 (*o*-Me), 21.4 (*p*-Me); UV-Vis (Toluene, 3.0 x 10⁻⁵ M): λ_{max} = 312 nm (ϵ = 4,754), 383 nm (ϵ = 5,976); fluorescence (Toluene, 3.0 x 10⁻⁵ M): $\lambda_{\text{em,max}}$ = 482 nm, Φ = 0.10 (λ_{exc} = 383 nm); UV-Vis (THF, 3.0 x 10⁻⁵ M): λ_{max} = 263 nm (ϵ = 13,563), 310 nm (ϵ = 6,000), 381 nm (ϵ = 7630); fluorescence (THF, 3.0 x 10⁻⁵ M): $\lambda_{\text{em,max}}$ = 516 nm, Φ = 0.09 (λ_{exc} = 381 nm); UV-Vis (CH₂Cl₂, 3.0 x 10⁻⁵ M): λ_{max} = 269 nm (ϵ = 18,730), 311 nm (ϵ = 7,830), 380 nm (ϵ = 9,300); fluorescence (CH₂Cl₂, 3.0 x 10⁻⁵ M): $\lambda_{\text{em,max}}$ = 509 nm, Φ = 0.10 (λ_{exc} = 380 nm); UV-Vis (DMSO, 3.1 x 10⁻⁵ M): λ_{max} = 272 nm (ϵ = 1,840), 317 nm (ϵ = 1,493), 401 nm (ϵ = 1,620); fluorescence (DMSO, 3.0 x 10⁻⁵ M): $\lambda_{\text{em,max}}$ = 535 nm, Φ = 0.04 (λ_{exc} = 401 nm); elemental analysis: calculated C 85.06, H 8.46, N 3.67; found C 81.16, H 8.11, N 3.65.

Synthesis of (53): A solution of BBr₃ (0.43 g, 0.86 mmol) in CH₂Cl₂ (10 mL) was added dropwise to a solution of (36) (0.13 g, ca. 0.71 mmol of Me₃Si groups) in CH₂Cl₂ (10 mL) and stirred for 24 h. Me₃SiOMe (0.35 mL, 2.5 mmol) was added neat, and the solution was stirred for another 24 h. All volatile components were removed under high vacuum. The remaining solid was taken up in THF (10 mL) and a solution of (40) (0.5 M in THF, 1.45 mL, 0.73 mmol) was added. The mixture was allowed to react for 24 h at RT. THF was then removed under high vacuum and remaining white solid was taken up in toluene (10 mL). The toluene solution was stirred for 2 h. Insoluble salts were removed

via filtration and solvent was removed under high vacuum. The solid was taken up in THF (10 mL) and a solution of (42) (0.22 M in THF, 25.0 mL, 5.5 mmol) was added. The mixture was allowed to react for 1 h at RT and then refluxed for 4 weeks. The solution was concentrated to ca. 3 mL and precipitated into methanol (350 mL). The product was purified by repeated precipitation from toluene into methanol (350 mL). The precipitate was dried under high vacuum to give a white powder (0.150 g, 53%). For (53): ^{11}B NMR (160.386 MHz, CDCl_3): $\delta = 56$ ppm ($w_{1/2} = 2080$ Hz); ^1H NMR (499.893 MHz, CDCl_3): $\delta = 7.1, 6.8, 6.7$ (aromatic H), 3.3, 2.2, 1.8, the backbone protons are overlapping; ^{13}C NMR (125.69 MHz, CDCl_3): $\delta = 143.8, 142.1, 140.7, 138.5, 136.6, 128.3, 64.6$ (CH_2), 45.7 (MesNMe_2), 41.2 (polymer backbone), 23.6 (*o*-Mes), 21.4 (*p*-Mes); UV-Vis (CH_2Cl_2 , 3.1×10^{-5} M): $\lambda_{\text{max}} = 271$ nm ($\epsilon = 10,267$), 310 nm ($\epsilon = 14,700$); fluorescence (CH_2Cl_2 , 3.1×10^{-5} M): $\lambda_{\text{em,max}} = 481$ nm, $\Phi = 0.040$ ($\lambda_{\text{exc}} = 310$ nm); elemental analysis: calculated C 85.06, H 8.67, N 3.54; found C 80.56, H 8.26, N 2.78.

1B.8 References and Notes

1. Entwistle, C. D.; Marder, T. B. *Angew. Chem. Int. Ed.* **2002**, *41*, 2927-2931.
2. Yamaguchi, S.; Wakamiya, A. *Pure Appl. Chem.* **2006**, *78*, 1413-1423.
3. Jäkle, F. "Boron: Organoboranes", Chapter in *Encyclopedia of Inorganic Chemistry*, Ed. B. King, Wiley, VCH 2005, pp 560-598.

4. Yuan, Z.; Collings, J. C.; Taylor, N. J.; Marder, T. B.; Jardin, C.; Halet, J.-F. *J. Solid State Chem.* **2000**, *154*, 5-12.
5. Doty, J. C.; Babb, B.; Grisdale, P. J.; M.Glogowski; Williams, J. L. R. *J. Organomet. Chem.* **1972**, *38*, 229-236.
6. Yuan, Z.; Taylor, N. J.; Marder, T. B.; Williams, I. D.; Kurtz, S. K.; Cheng, L.-T. *J. Chem. Soc., Chem. Commun.* **1990**, 1489-1492.
7. Zheng, Y.; Entwistle, C. D.; Collings, J. C.; Albesa-Jové, D.; Batsanov, A. S.; Howard, J. A. K.; Taylor, N. J.; Kaiser, H. M.; Kaufmann, D. E.; Poon, S.-Y.; Wong, W.-Y.; Jardin, C.; Fathallah, S.; Boucekkine, A.; Halet, J.-F.; Marder, T. B. *Chem. Eur. J.* **2006**, *12*, 2758-2771.
8. Lequan, M.; Lequan, R. M.; Chane-Ching, K.; Callier, A. C. *Adv. Mater. Opt. Electron.* **1992**, *1*, 243-247.
9. Noda, T.; Shirota, Y. *J. Am. Chem. Soc.* **1998**, *120*, 9714-9715.
10. Noda, H. O.; Shirota, Y. *Adv. Mater.* **1999**, *11*, 283-285.
11. Shirota, Y.; Kinoshita, M.; Noda, T.; Okumoto, K.; Ohara, T. *J. Am. Chem. Soc.* **2000**, *122*, 11021-11022.
12. Sundararaman, A.; Varughese, R.; Li, H.; Zakharov, L. N.; Rheingold, A. L.; Jäkle, F. *Organometallics* **2007**, *26*, 6126-6131.

13. Lequan, M.; Lequan, R. M.; Ching, K. C.; Barzoukas, M.; Fort, A.; Lahoucine, H.; Bravic, G.; Chasseau, D.; Gaultier, J. *J. Mater. Chem.* **1992**, *2*, 719-725.
14. Branger, C.; Lequan, M.; Lequan, R. M.; Barzoukas, M.; Fort, A. *J. Mater. Chem.* **1996**, *6*, 555-558.
15. Liu, Z.-Q.; Shi, M.; Li, F.-Y.; Fang, Q.; Chen, Z.-H.; Yi, T.; Huang, C.-H. *Org. Lett.* **2005**, *7*, 5481-5484.
16. Hudson, Z. M.; Wang, S. *Acc. Chem. Res.* **2009**, *42*, 1584-1596.
17. Jia, W. L.; Feng, X. D.; Bai, D. R.; Lu, Z. H.; Wang, S.; Vamvounis, G. *Chem. Mater.* **2004**, *17*, 164-170.
18. Sun, Y.; Wang, S. *Inorg. Chem.* **2009**, *48*, 3755-3767.
19. Jia, W.-L.; Bai, D.-R.; McCormick, T.; Liu, Q.-D.; Motala, M.; Wang, R.-Y.; Seward, C.; Tao, Y.; Wang, S. *Chem. Eur. J.* **2004**, *10*, 994-1006.
20. Dong-Ren, B.; Xiang-Yang, L.; Suning, W. *Chem. Eur. J.* **2007**, *13*, 5713-5723.
21. Liu, X. Y.; Bai, D. R.; Wang, S. *Angew. Chem. Int. Ed.* **2006**, *45*, 5475-5478.
22. Hudson, Z. M.; Zhao, S.-B.; Wang, R.-Y.; Wang, S. *Chem. Eur. J.* **2009**, *15*, 6131-6137.
23. Hudnall, T. W.; Chiu, C.-W.; Gabbai, F. P. *Acc. Chem. Res.* **2009**, *42*, 388-397.

24. Dorsey, C. L.; Jewula, P.; Hudnall, T. W.; Hoefelmeyer, J. D.; Taylor, T. J.; Honesty, N. R.; Chiu, C.-W.; Schulte, M.; Gabbaï, F. P. *Dalton Trans.* **2008**, 4442-4450.
25. Melaimi, M.; Gabbaï, F. P. *J. Am. Chem. Soc.* **2005**, *127*, 9680-9681.
26. Lee, M. H.; Gabbaï, F. P. *Inorg. Chem.* **2007**, *46*, 8132-8138.
27. Chiu, C.-W.; Gabbaï, F. P. *J. Am. Chem. Soc.* **2006**, *128*, 14248-14249.
28. Chiu, C.-W.; Gabbaï, F. P. *Dalton Trans.* **2008**, 814-817.
29. Hudnall, T. W.; Gabbaï, F. P. *J. Am. Chem. Soc.* **2007**, *129*, 11978-11986.
30. Chiu, C.-W.; Kim, Y.; Gabbaï, F. P. *J. Am. Chem. Soc.* **2008**, *131*, 60-61.
31. Heeger, P. S.; Heeger, A. J. *Proc. Natl. Acad. Sci. USA* **1999**, *96*, 12219-12221.
32. Zhu, Q.; Swager, T. M. *J. Am. Chem. Soc.* **1995**, *117*, 7017-7018.
33. Li, C.; Numata, M.; Takeuchi, M.; Shinkai, S. *Angew. Chem. Int. Ed.* **2005**, *44*, 6371-6374.
34. Harrison, B. S.; Ramey, M. B.; Reynolds, J. R.; Schanze, K. S. *J. Am. Chem. Soc.* **2000**, *122*, 8561-8562.
35. Ramey, M. B.; Hiller, J.-A.; Rubner, M. F.; Tan, C.; Schanze, K. S.; Reynolds, J. R. *Macromolecules* **2005**, *38*, 234-243.
36. McQuade, D. T.; Hegedus, A. H.; Swager, T. M. *J. Am. Chem. Soc.* **2000**, *122*, 12389-12390.

37. Huang, F.; Wu, H.; Wang, D.; Yang, W.; Cao, Y. *Chem. Mater.* **2004**, *16*, 708-716.
38. Chi, C.; Mikhailovsky, A.; Bazan, G. C. *J. Am. Chem. Soc.* **2007**, *129*, 11134-11145.
39. Parab, K.; Venkatasubbaiah, K.; Jäkle, F. *J. Am. Chem. Soc.* **2006**, *128*, 12879-12885.
40. Kim, S.; Song, K.-H.; Kang, S. O.; Ko, J. *Chem. Commun.* **2004**, 68-69.
41. Parab, K.; Jäkle, F. *Macromolecules* **2009**, *42*, 4002-4007.
42. Fiedler, J.; Zalis, S.; Klein, A.; Hornung, F.; Kaim, W. *Inorg. Chem.* **1996**, *35*, 3039-3043.
43. Matthias, B.; Wilfried, W.; Martin, J.; Wolfgang, R.; Claudia, M.; Irene, B.; Hans, H.; Schlüter, A. D. *Eur. J. Org. Chem.* **2001**, *2001*, 3819-3829.
44. Qin, Y.; Cheng, G.; Sundararaman, A.; Jäkle, F. *J. Am. Chem. Soc.* **2002**, *124*, 12672-12673.
45. Saitoh, T.; Yoshida, S.; Ichikawa, J. *J. Org. Chem.* **2006**, *71*, 6414-6419.
46. Bhattacharyya, S. *J. Org. Chem.* **1995**, *60*, 4928-4929.
47. Qin, Y.; Cheng, G.; Acharya, O.; Parab, K.; Jäkle, F. *Macromolecules* **2004**, *37*, 7123-7131.

48. Sheldrick, G. M. *SADABS, Version 2. Multi-Scan Absorption Correction Program, University of Göttingen, Germany, 2001.*
49. Sheldrick, G. M. *SHELXTL, Version 6.14, Bruker AXS Inc., Madison, WI, 2004.*

Chapter 1C. Boron Functionalized Monomers for ADMET Polymerization

1C.1 Conjugated Polymers

Organic π -conjugated polymers (Chart 1) are an intriguing class of compounds that have been intensively studied for almost 3 decades.¹⁻³ The extensive delocalization of π -electrons is well known to be responsible for the array of interesting characteristics that these polymers tend to exhibit. These properties include non-linear optical behavior⁴, electronic conductivity and mechanical strength. Polymers composed of aromatic and heteroaromatic ring structures have been particularly outstanding from a materials perspective and can be used in a variety of applications including organic light emitting devices, photovoltaics, organic field-effect transistors, and sensor materials.⁵

Polyacetylene has been extensively studied due to its simple structure. A twelve fold increase in conductivity was achieved upon oxidative doping of polyacetylene which was observed by Heeger and MacDiarmid. However, polyacetylene is not a good candidate for electronic and electro-optical applications due to its instability.^{6, 7} Poly(*para*-phenylene)'s (**PPP**) and poly(*para*-phenylenevinylene)'s (**PPV**) are other classes of conjugated polymers which consist of aromatic rings in the backbone of the polymer and delocalized

π -electron structure. Aliphatic and other solubilizing groups on the aryl rings have been employed to circumvent some of the solubility issues and synthetic difficulties. The stability of these polymers is much higher than that of polyacetylene and hence they have been commercially employed in opto-electronic devices.^{4, 7} Polyfluorenes have been exploited as organic photovoltaic materials, layers in Organic Light Emitting Devices (**OLED's**), and also for application in organic thin film transistors. Heterocyclic polymers like polythiophenes and polypyrroles have also been used as opto-electronic materials. The solubility of these heterocyclic compounds can be enhanced by substitution at 3 position. Polythiophenes show superior stability, synthetic flexibility and chemical processability. Substituted polythiophenes have been widely studied due to their interesting electronic properties in both doped and undoped states.⁷

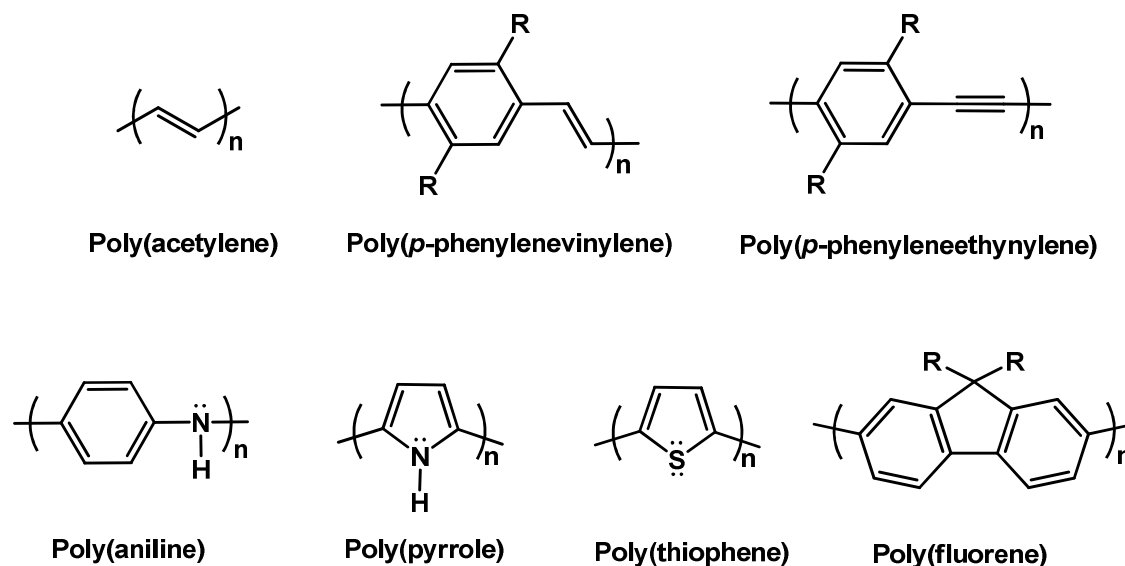


Chart 1C.1 Some Examples of Conjugated Polymers.

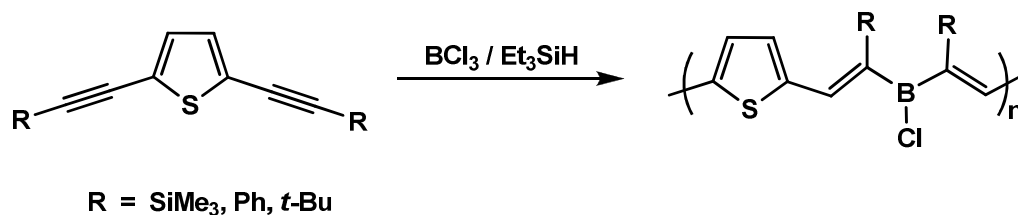
1C.2 Main Chain Functionalized Organoboron Polymers

Organoboron containing polymers can be classified as (i) main chain organoboron conjugated polymers in which the boron atom is attached into the backbone of the conjugated polymers and (ii) side chain organoboron polymers in which the boryl moiety is attached as a pendant group in the side chain. Since this project deals with attachment of the boron center in the backbone, main chain organoboron polymers; their synthesis, properties and applications will be discussed in detail herein. Main chain organoboron containing polymers often consist of an electron-deficient boron center alternating with

an organic π -system, which leads to extended delocalization.⁵ Main chain organoboron polymers can be synthesized via a variety of techniques. Hydroboration, haloboration and phenylboration polymerization techniques, introduced by Chujo, have become the most versatile synthetic methods for the incorporation of tri-coordinate boron into the main chain of polymers.^{8, 9} Organometallic condensation reactions with Grignard reagents^{10, 11}, organolithium species¹², and organotin precursors¹³ are also very attractive. These techniques will be briefly discussed in here.

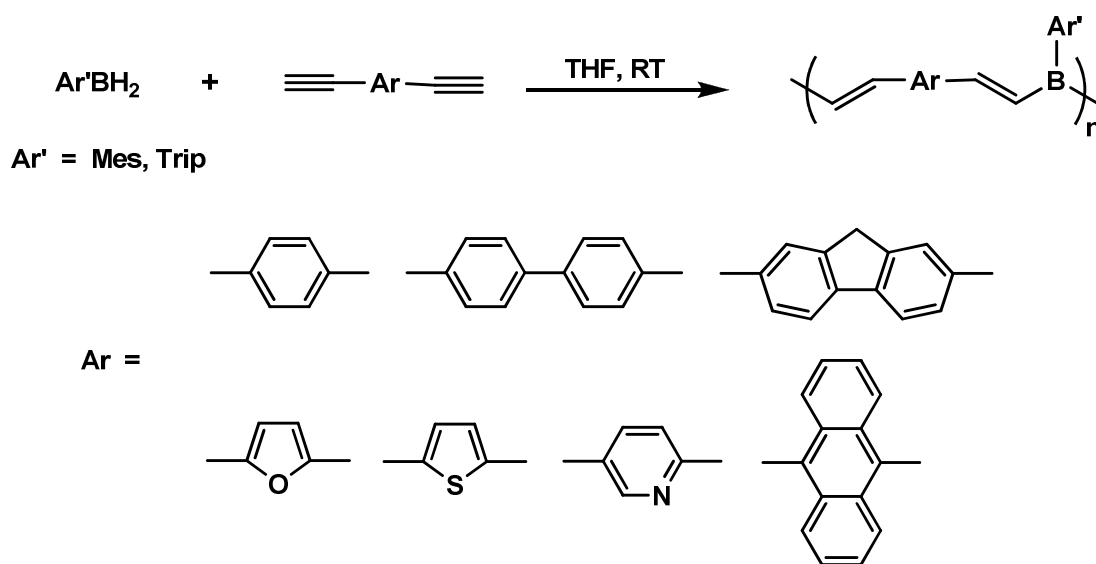
1C.2.1 Hydroboration Polymerization

Corriu *et al.* reported the synthesis of the first main-chain organoboron containing conjugated polymers via hydroboration polymerization of 2,5-diethynylthiophene derivatives using a mixture of borontrichloride with triethylsilane as a borane source (Scheme 1C.1). However, the polymers could not be characterized owing to their sensitivity to air and moisture.¹⁴



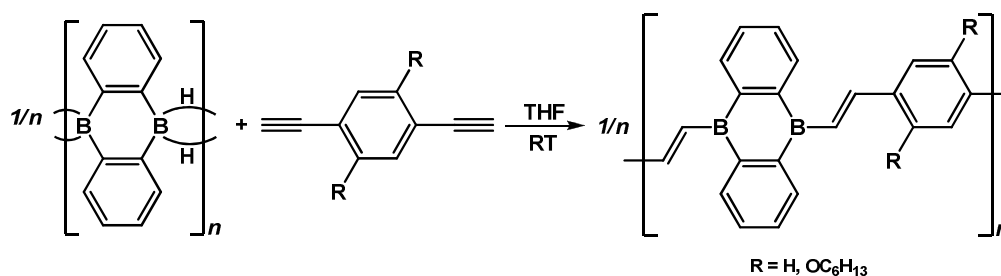
Scheme 1C.1 Example of Boron-Containing Conjugated Polymers via Hydroboration Polymerization.

Synthesis of the first air-stable polymer via hydroboration polymerization was reported by Chujo and co-workers.^{8,9} They reacted a variety of aromatic and heteroaromatic diynes with sterically hindered arylboranes ArBH_2 ($\text{Ar} = 2,4,6\text{-trimethylphenyl}$, $2,4,6\text{-triisopropylphenyl}$) to obtain polymeric materials that were claimed to show n-type properties (Scheme 1C.2). The bulky aryl groups on boron prevent attack of nucleophiles on boron and thus impart good environmental stability. Depending on the nature of the arenediyl bridge, these compounds exhibit strong green, blue, and even white photoluminescence. However, one aspect to note here is that both reactive hydrogen atoms are attached to the same boron atom. As a result, the first hydroboration event occurs under steric and electronic conditions that are significantly different to those of the second addition.



Scheme 1C.2 Conjugated Boron-Containing Polymers (Mes = 2,4,6-trimethylphenyl; Trip = 2,4,6-triisopropylphenyl).

To overcome this issue, Wagner and coworkers have prepared a ditopic 9,10-dihydro-9,10-diboraanthracene (Scheme 1C.3).¹⁵ This reagent shows an extended π -conjugated structure and forms a polymer in the solid-state via B-H-B bridges. The authors also reported hydroboration polymerization with aromatic dialkynes. The resulting polymer was obtained in 47% yield and showed green emission in toluene solution.

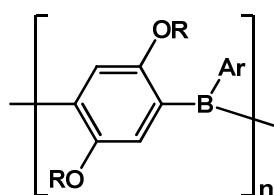


Scheme 1C.3 Hydroboration Polymerization of 9,10-dihydro-9,10-diboraanthracene with Aromatic Dialkynes.

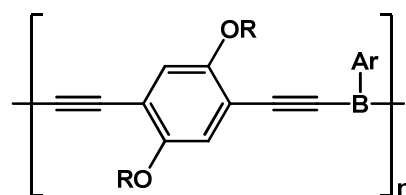
1C.2.2 Organometallic Routes

Other methodologies that have been used recently for incorporation of boron into the main chain involve the use of organometallic reagents. For instance, poly(*p*-phenyleneborane)s (1) were synthesized by polycondensation of aryldimethoxyborane and a bifunctional Grignard reagent.¹⁰ Polycondensation of bifunctional lithium acetylides and aryldimethoxyborane was used to obtain luminescent poly(ethynylene-*p*-phenylene-ethynylene-borane)s (2).¹⁶ Many other examples of polymers synthesized via these methods have been reported. For example, Jäkle *et al.* have recently been able to incorporate boron into the main chain of polythiophenes (3)¹¹ and polyfluorenes (4–5)¹⁷ using a facile tin-boron exchange reaction which affords polymers with molecular weight in the range of $M_n = 6,500$ to 10,000. Interestingly, the emission wavelength can be fine tuned by changing the substituents on the boron center. The polymers were found to bind

to pyridine as well as cyanide and may find applications as sensors for nucleophiles. Also, Lavigne and co-workers reported self-assembling conjugated boronate esters (6) synthesized via condensation reaction between 9,9-dihexylfluorene-2,7-diboronic acid and 1,2,4,5-tetra-hydroxybenzene.¹⁸ The resulting polymer was obtained in high yield (~90%) with $M_w \sim 25,000$ and emits in the blue region of the spectrum.

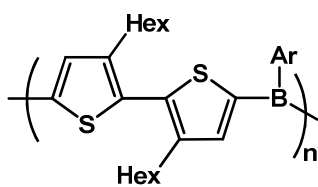


(1)

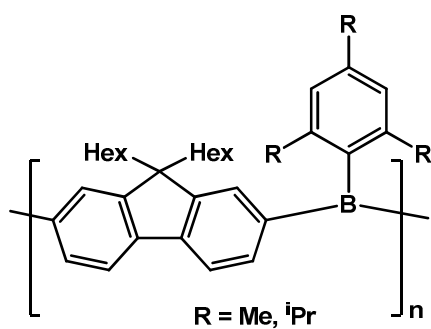
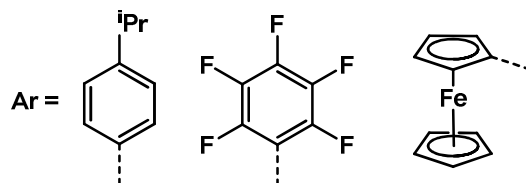


(2)

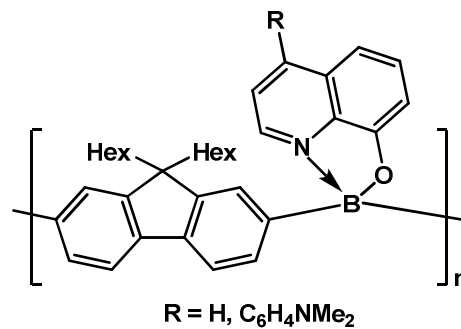
R = Me, C₈H₁₇, C₁₂H₂₅
Ar = Mes, Trip



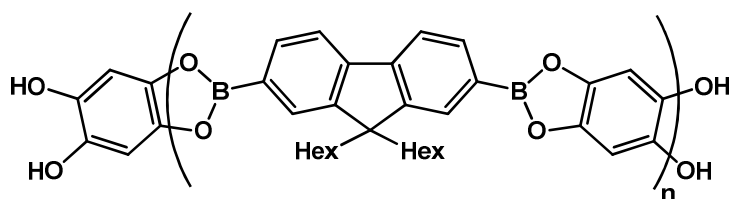
(3)



(4)



(5)

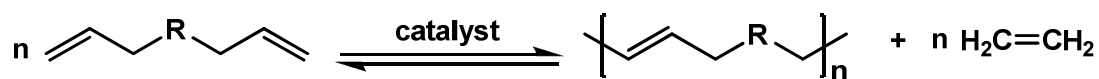


(6)

Chart 1C.2 Some Examples of Conjugated Polymers Synthesized by Organometallic and Condensation Routes.

1C.3 ADMET Polymerization

Acyclic diene metathesis polymerization (ADMET), is a step-growth condensation polymerization technique that has been employed to obtain non-conjugated (saturated) as well as conjugated (unsaturated) polymers (Scheme 1C.4). This reaction, like any condensation polymerization, is an equilibrium process, which proceeds in a stepwise manner to form dimer, trimer, tetramer, and so on to obtain a high molecular weight polymer. The size of the polymer increases continuously with time (conversion) at a relatively slow rate.



Scheme 1C.4 ADMET Polymerization.

This process is driven by the release of ethylene as a byproduct, which is the driving force of the reaction. The equilibrium of the ADMET polymerization is forced towards high polymer by performing bulk polymerizations under vacuum to remove ethylene.

Because ADMET is equilibrium-driven, addition of excess ethylene to a macromolecular chain will shift the reaction in the reverse direction leading to depolymerization. This procedure constitutes a possible method for recycling rubber and other unsaturated polymers. Quantitative conversion of monomer to polymer is standard in ADMET polymerization, as fewer or no side reactions occur other than a small amount of ring formation is common in all polycondensation chemistry.¹⁹

The mechanistic cycle of ADMET polymerization (Figure 1C.1) has been very well documented and is characterized by the presence of a metallacyclobutane ring as an intermediate. The catalytic cycle starts with formation of a π -complex (A) between an olefinic group of a diene and the electron deficient metal center, resulting in a metallacyclobutane ring (B). Productive cleavage leads to the formation of the metathesis active alkylidene complex (C), which initiates the polymerization cycle. The subsequent reaction produces another metallacyclobutane ring (D) which collapses to form an internal olefin within the growing polymer chain and generates catalytically active methylidene complex (E) followed by the coordination of another monomer. Productive cleavage of another metallacyclobutane ring (F) results in release of ethylene, and the cycle is repeated, growing polymer in a stepwise manner with every cycle.²⁰

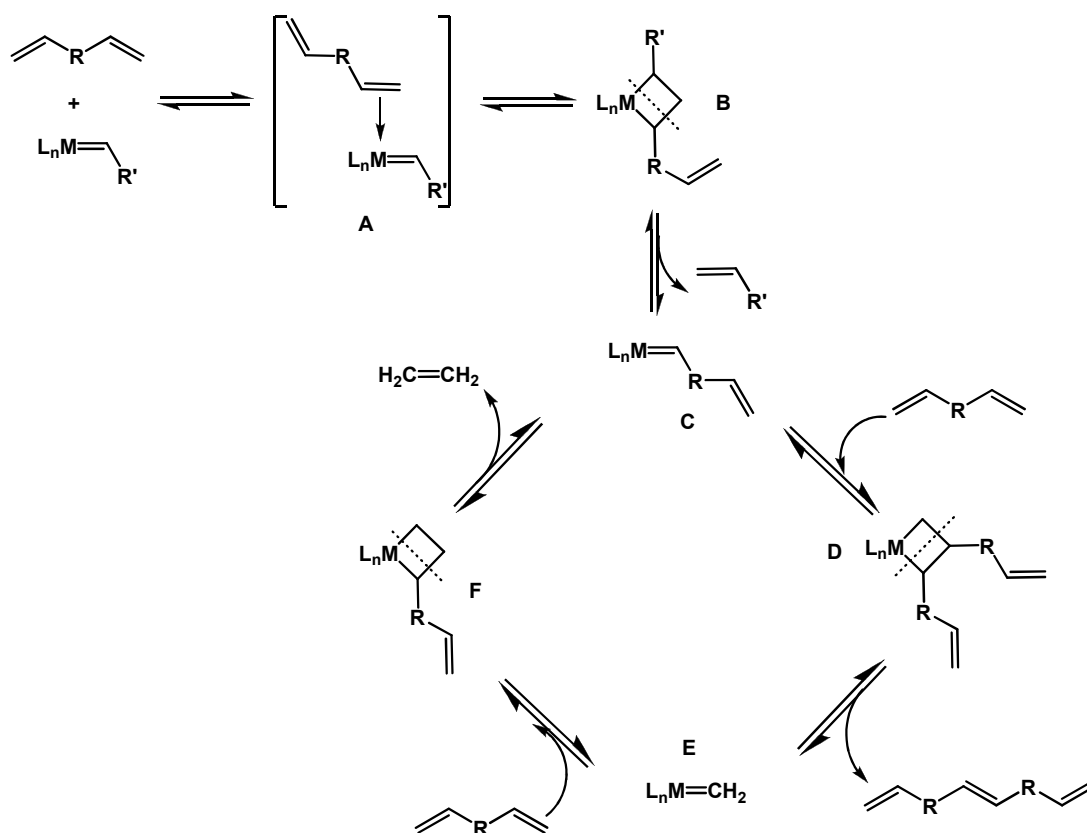


Figure 1C.1 Mechanism of ADMET Polymerization.

1C.3.1 Metathesis Catalysts and Monomers for ADMET

Early studies on the polymerization of 1,5-hexadiene and 1,9-decadiene were reported by Wagener and co-workers. They chose a classic catalytic system such as WCl₆/EtAlCl₂, which leads to cationic vinyl addition chemistry in addition to polycondensation chemistry.²¹ Fortunately, in the late 1980's, Schrock and co-workers successfully

prepared the first well-defined, Lewis acid free, single site catalyst. Only metathesis product was observed when studies were performed on styrene as a model substrate, which proved that the catalyst was effective in metathesizing a substrate that can readily undergo vinyl addition chemistry.²² Related molybdenum based catalysts (7) were most widely used as well-defined olefin metathesis catalysts.²³ These early transition metal-based complexes were highly sensitive to air and moisture, also relatively intolerant of many functional groups, such as alcohols, aldehydes, and carboxylic acids and hence their applicability was limited. The development of well-defined ruthenium-based catalysts by Grubbs in the early 1990's overcame many of the limitations of the Schrock-type catalysts. In 1995, Grubbs reported the synthesis of $\text{RuCl}_2(=\text{CHPh})(\text{PCy}_3)_2$ (first generation-Grubbs catalyst (8)), in high yield and purity.²⁴ This complex was stable but its activity was much lower compared to Schrock's molybdenum-based catalysts. A second generation-Grubbs catalyst was synthesized by replacing one of the phosphine ligands with a N-heterocyclic carbene ligand, commonly known as NHC.^{25, 26} The highly basic nature of NHC compared to phosphines and the presence of sterically hindered groups bound to the N-atoms, not only leads to a trans effect (i.e. facilitates elimination of the *trans*-phosphine ligand) but also facilitates the reductive elimination of the product from the metal center during catalysis. This second generation-Grubbs catalyst ((9), Grubbs II) showed higher activity, good functional group tolerance to aldehydes, alcohols

and acids, and allowed metathesis on tri- and tetra- substituted olefins.²⁷ The scope of Ru-catalyzed olefin metathesis was further developed by the introduction of Grubbs-type catalysts containing monodentate and/or chelating N-, O-, P- and Cl-donor ligands. Among them, styrenyl ether complexes (first and second generation Hoveyda-Grubbs catalysts (10) were the most widely used systems because of their high stability toward air and moisture. Grubbs-Hoveyda-Grela type catalyst (11) has also been employed in various types of metathesis reactions.^{28, 29} While the presence of a NO₂ group leads to a more active catalyst than both the second-generation Grubbs's catalyst and the phosphine-free Hoveyda's carbene, the reactivity is lower than that observed for a sterically activated Hoveyda-Grubbs catalyst.

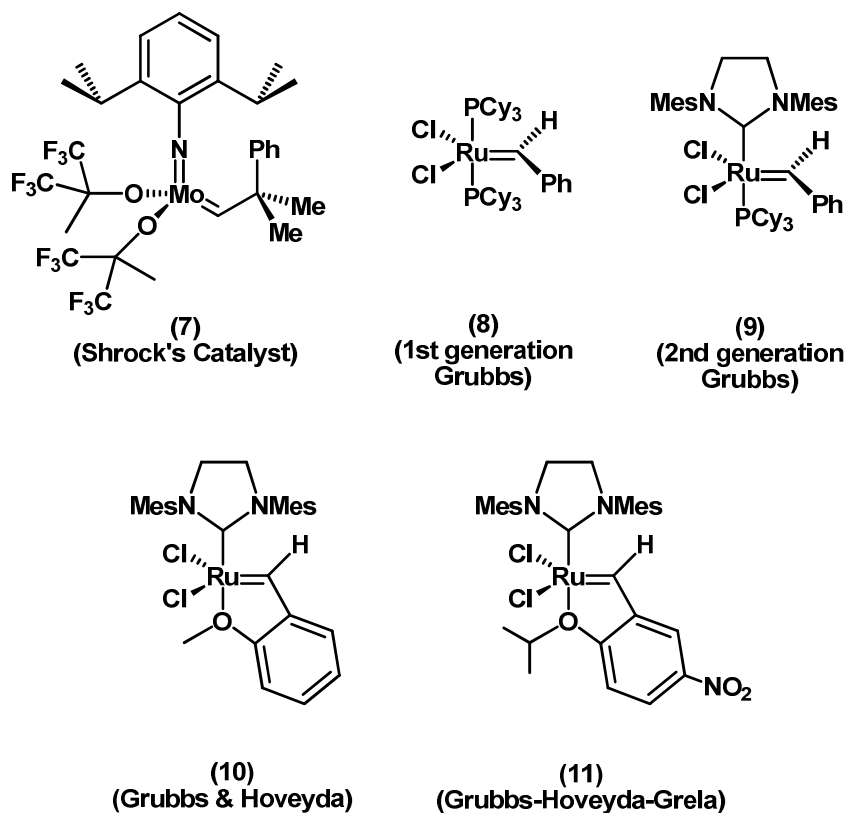


Chart 1C.3 Selected Catalysts used for ADMET Polymerization (Cy = cyclohexyl; Mes = mesityl).

1C.3.2 Polymers Synthesized via ADMET Polymerization

As discussed in section 1C.3, acyclic diene metathesis (ADMET) polymerization has become a highly versatile method for the synthesis of both saturated as well as unsaturated polymers. The onset of ADMET research began with the detailed study of

pure hydrocarbon dienes such as 1,5-hexadiene and 1,9-decadiene, that could be converted into their corresponding high molecular weight polymers. The “classical” catalysts such as $\text{WCl}_6/\text{EtAlCl}_2$ were used and the reaction was carried out under bulk conditions to maximize monomer concentration with a monomer to catalyst ratio of 1000:1. However, both cationic vinyl addition product in addition to polycondensation product was observed.^{21, 30} A high molecular weight polymer with a number average molecular weight of 50,000 with *PDI* of 2.0 was reported by Wagener and coworkers with Schrock’s tungsten alkylidene catalyst in the early 1990’s.³¹ In addition to these hydrocarbons, a wide variety of functionalized polyolefins (Chart 1C.4) containing both aliphatic and aromatic ethers, carbonates, esters, ketones, thioethers as well as amines have been synthesized and reported.³²⁻⁴⁰

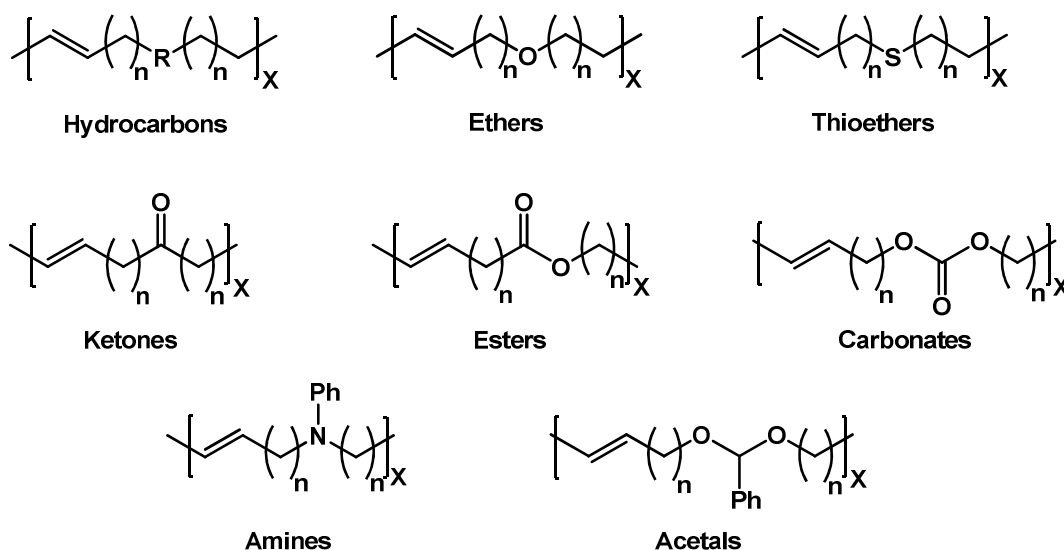


Chart 1C.4 Some Examples of Functionalized Polymers Synthesized via ADMET.

The first example of the synthesis of aliphatic conjugated polymers via ADMET polymerization was reported by Wagener and coworkers in the early 1990's. The author described the reactivity of 2,4-hexadiene and 2,4,6-octatriene, using Schrock's molybdenum catalyst.⁴¹ Under bulk reaction conditions, polyenes with similar lengths (approximately eight repeat units) were obtained for both monomers. Synthesis of aromatic conjugated polymers such as PPV via ADMET polymerization has since been reported by many researchers. For instance, Schrock and O'Dell utilized several molybdenum catalysts of the type $\text{Mo}(\text{CHCMe}_2\text{Ph})-(\text{NR})(\text{OR}')_2$ ($\text{R} = 2,6\text{-i-Pr}_2\text{C}_6\text{H}_3$, $2,6\text{-Me}_2\text{C}_6\text{H}_3$, $2\text{-i-PrC}_6\text{H}_4$, $2\text{-}t\text{-BuC}_6\text{H}_4$, $2\text{-CF}_3\text{C}_6\text{H}_4$, 1-adamantyl ; $\text{R}' = \text{CMe}_3$, $\text{CMe}_2(\text{CF}_3)$),

CMe(CF₃)₂, C(CF₃)₃) for polymerization of divinylbenzene.⁴² However, formation of only trans-dimer and tetramer was reported. Thorn-Csányi employed a Schrock-type olefin metathesis catalyst for the synthesis of PPV from the respective substituted divinylbenzenes. However, only short-chain oligomeric PPV species were formed.⁴³⁻⁴⁵ Nomura *et al.* used Grubbs-type catalysts to obtain extended chain PPV⁴⁶, but this method critically relies on the removal of ethylene by repeatedly cooling the reaction mixture to 30 °C every 60 min, followed by evacuation and reheating to the ADMET reaction temperature. On the other hand, Harper *et al.* reported the formation of PPV oligomers using Grubbs II catalyst.⁴⁷ Recently, Plenio and coworkers reported ADMET polymerization of alkyl and alkoxy substituted divinylbenzene and divinylfluorene using Grubbs II and Grubbs-Hoveyda-Grela-type catalysts.⁴⁸ Monomer (13) was converted into high molecular weight polymer of 100 kDa with $P_n = 330$. Oligomers with molecular weight of 1,500-4,000 were obtained in the case of monomer (14). This was attributed to the chelating nature of the monomer, whereas the molecular weights of polyfluorene (15) of $M_n = 75$ kDa was limited by poor solubility. Using similar methods, Nomura *et al.* synthesized end functionalized *all-trans*-polyfluorenevinylenes via ADMET polymerization.⁴⁹ The polymers were further functionalized with a polyethylene glycol moiety to achieve amphiphilic triblock copolymers.

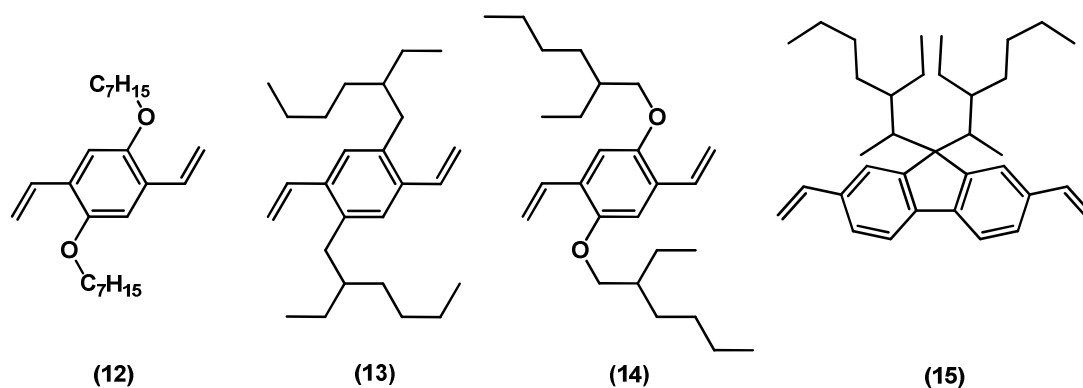
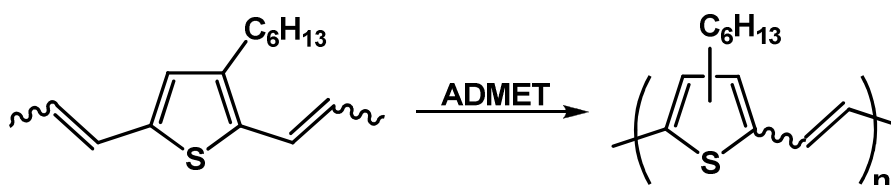


Chart 1C.5 Some Examples of Poly(*para*-phenylenevinylene) (PPV) and Poly(fluorenylvinylene) (PFV) Type Monomers.

Polythiophenylvinylenes (PTVs) have also been widely studied for their opto-electronic properties, rich synthetic flexibility, chemical processability, low band-gaps and high charge mobility. Due to these unique properties PTVs are among the most important classes of conjugated polymers with a wide range of applications such as conducting films, field-effect transistors and electrochromics.⁵⁰ PTVs can be synthesized in many different ways including ADMET polymerization (Scheme 5). For example, Qin *et al.* have successfully synthesized PTV type conjugated polymers using ruthenium-based Grubbs-type metathesis catalysts.⁵¹ High molecular weights of 10,000 were obtained by using 1,2,4-trichlorobenzene at elevated temperature under dynamic vacuum. Under these conditions, the resulting P3HTVs exhibited carboxaldehyde end groups, which was confirmed via MALDI-TOF analysis.



Scheme 1C.5 Example of Thiophene Containing Polymers Synthesized via ADMET.

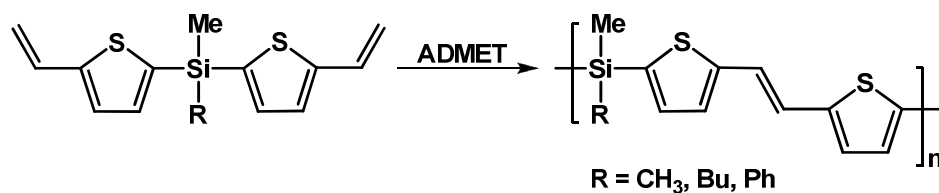
1C.3.3 Inorganic Polymers Synthesized via ADMET Polymerization

Incorporation of inorganic elements into polymers is usually accompanied by enhancement of polymeric properties such as thermal stability, flexibility, flame retardance, interesting electronic properties and biocompatibility. Inorganic and organometallic polymers can be used as precursors for ceramic materials, high strength fibers and magnetic materials. ADMET offers a versatile technique to produce main chain polymers with metals and main group elements that are difficult to obtain by other methods. A variety of organic/inorganic hybrid polymers, containing silanes, siloxanes, germanium, tin, and phosphazenes, have been made recently using ADMET polymerization and will be discussed in this section.

Silicon-carbon hybrid polymeric materials have gained a lot of attention due to their enhanced properties. For example, polycarbosilanes exhibit high thermal stability and can be used as ceramic precursors to silicon carbide.⁵² Polysiloxane with Si-O bond in the polymeric backbone show low glass transition temperatures and high hydrophobicity.

Incorporation of main group elements such as silicon, tin and germanium into polymers via ADMET was first shown by Wagener and coworkers when they synthesized polycarbosilanes in the early 90's. The first attempt to polymerize dimethyldivinylsilane did not proceed in the presence of the tungsten based Schrock's catalyst, which was attributed to the steric influence of the tetrasubstituted silicon atom adjacent to the double bond.³⁶ Similar results were obtained by Schrock *et al.*²³ in the attempted metathesis of vinyltrimethylsilane. The steric effect was further displayed via copolymerization of divinylsilane with 1,9-decadiene.⁵³ Further studies have shown that monomers with methylene spacers integrated between the silicon atom and the olefin were able to undergo metathesis polymerization. For example, polymer (16), was successfully synthesized with Schrock's tungsten alkylidene catalyst⁵³ and polycarbosiloxane (17)⁵³ was prepared using Schrock's molybdenum catalyst, which in turn demonstrated the compatibility of this catalyst with the siloxane functionality. Heteroatoms have also been successfully incorporated into conjugated polymers via ADMET. For instance, Bazan and coworkers have incorporated silicon into the main chain of PTVs. They synthesized a series of bis(vinylthienyl)silane monomers, which were converted into poly(silanyldithienylethene) with short repeat sequences using Schrock type initiators (Scheme 1C.6).⁵⁴ The sp^3 -hybridized silylene linkages allow for electronic delocalization

through the σ -bonds along with the π -conjugated segments, thus resulting in interesting photophysical properties.



Scheme1C.6 Example of poly(silanylthienylethene) via ADMET.

Silicon containing photoluminescent materials are known for their potential use in light-emitting diodes and as conducting polymers. One recent example comes from Peetz's research group, where they have demonstrated that silylene functionalized conjugated polymers (18) can be accessed via ADMET.⁵⁵ A red shift in the emission spectra of the products compared to the monomers showed the participation of silicon in the conjugation. In addition, photocurable and photoluminescent polycarbosilane (19) was reported by Interrante and coworkers.⁵⁶ The polymer films were thermally or photochemically cross-linked to yield thermally stable, blue-photoluminescent films.

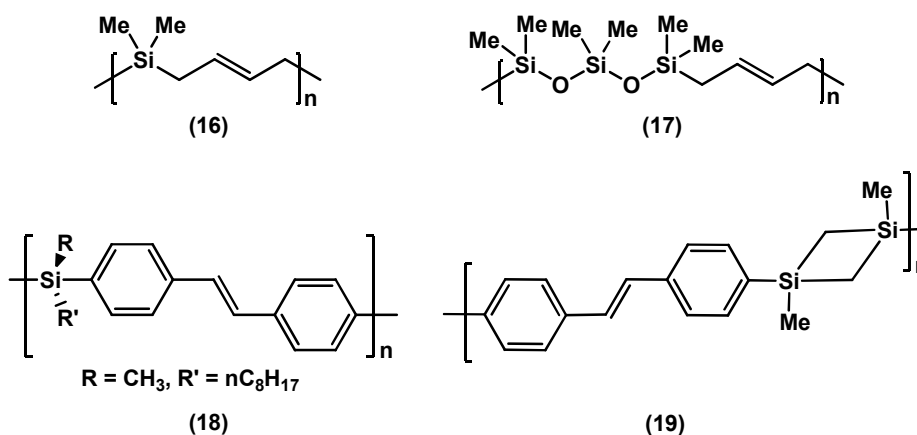


Chart 1C.6 Examples of Silicon Containing ADMET Polymers.

Polymers containing tin, germanium and phosphorous are further examples of inorganic polymers synthesized via ADMET polymerization. For example, germanium-based polymers could find applications in microlithography and as precursors for ceramics.⁵⁷ Inclusion of a small amount of phosphazene groups into an organic polymer can enhance its properties such as flame retardance, conductivity or biological compatibility. Allcock's research group has successfully prepared a series of substituted phosphazene containing polymers, with various pendant substituents on the phosphorus atoms, using Grubbs first and second generation catalysts. They reported molecular weights in the range of 10,000-40,000.⁵⁸

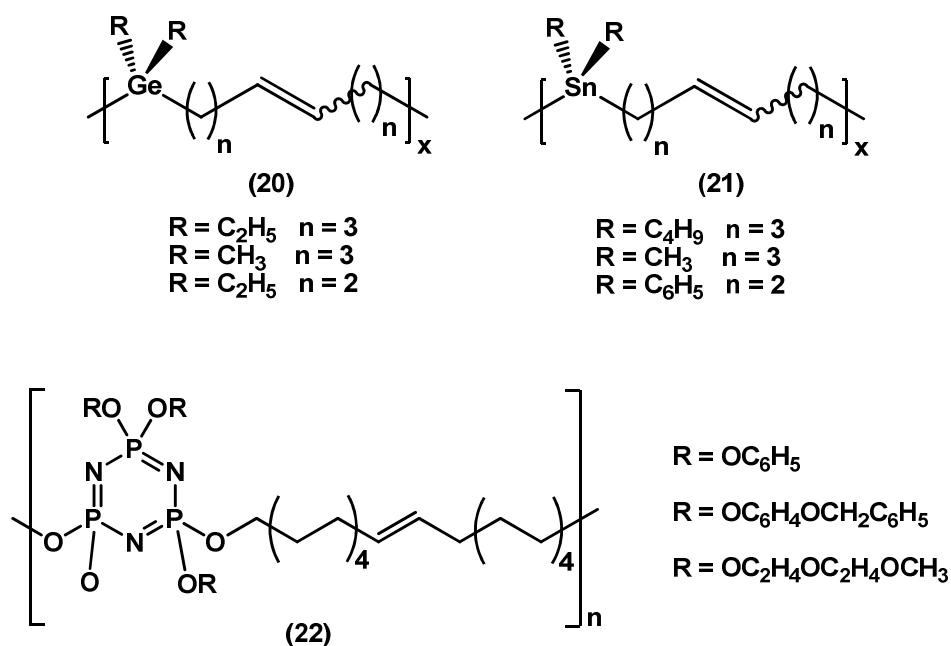


Chart 1C.7 Examples of Germanium, Tin and Phosphazene Containing Polymers

Synthesized via ADMET.

Transition metal containing polymers represent an interesting class of materials in which the presence of the metal can lead to unusual electronic, magnetic, and optical properties. The incorporation of transition metals into a polymer can lead to processable materials such as fibers, ceramic films and coatings in addition to significant enhancement of the electronic properties of the polymers themselves. Extensive studies have been done on ferrocene containing polymers, due to their excellent thermal and redox properties. In the early 1990's, Boncella and coworkers studied the ADMET

polymerization of 1,1'-divinylferrocene. They reported that the metathesis of 1,1'-divinylferrocene gave oligomers (23) with an average of four repeating units and a trans/cis ratio of 2:5. Formation of oligomers and the presence of cis-olefin groups were attributed to the poor solubility of the oligomers. Copolymerization with 1,9-decadiene (24) was performed to overcome the solubility issue.⁵⁹ Recently, researchers in Plenio's group incorporated ferrocene into polyvinylene type polymer (25) when using 1,1'-di(4-vinylphenyl)-3,3',4,4'-tetramethylferrocene as the monomer.⁴⁸ Conversely, homopolymer synthesis of 1,3-(diisopropenyl)ferrocene was unsuccessful due to solubility issues.

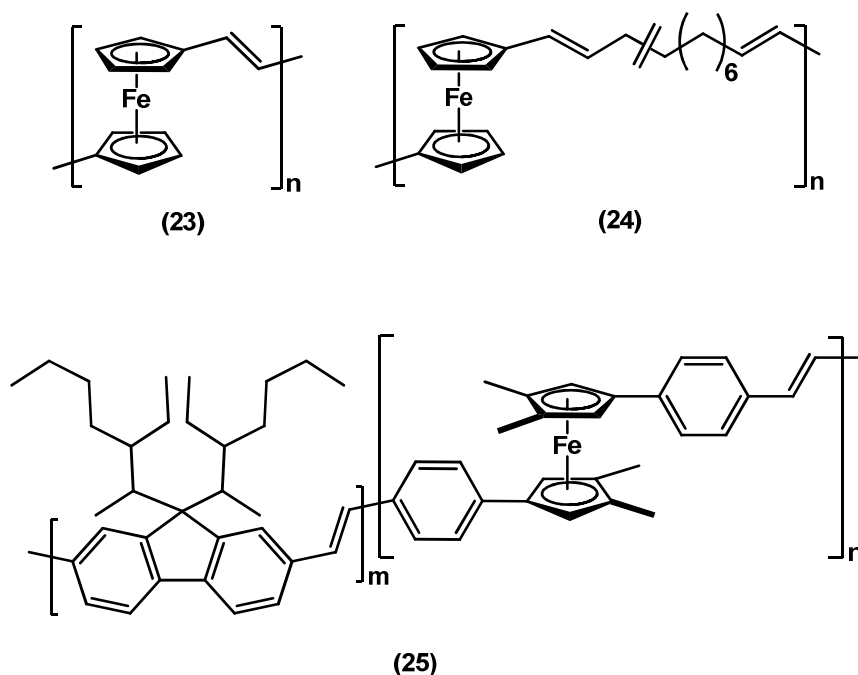


Chart 1C.8 Examples of Ferrocene Containing Polymers Synthesized via ADMET.

Other transition metals such as molybdenum have been embedded into polymeric backbones by Tyler *et al.*⁶⁰ They reported formation of oligomers with only $M_n = 2300$, owing to their lower solubility. Also, due to the presence of long flexible alkyl chains, ring closing metathesis products were observed under dilute conditions.

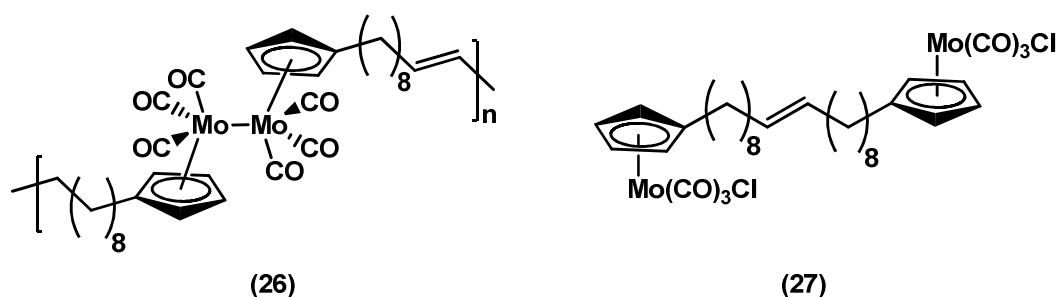


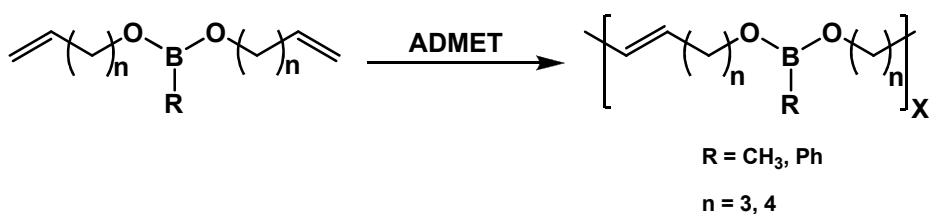
Chart 1C.9 Molybdenum Containing Polymers Synthesized via ADMET.

These polymers were shown to be photoreactive, i.e. upon irradiation with $\lambda > 520$ nm, the Mo-Mo bond was homolytically cleaved and the resulting Mo radicals were trapped by CCl₄. The formation of the corresponding metal halide product (27) was confirmed by IR spectroscopy and GPC analysis.

1C.3.4 Boron Containing Monomers

While a few examples of main group elements like Si, Sn, Ge containing ADMET monomers and polymers are known, the only example of a boron containing monomer is

that of an α, ω -boronate diene which was polymerized via ADMET by Wolfe and Wagener in the late 1990's.⁶¹ Although boronate monomers were metathesis active, ligand-exchange reactions among the boronate functional groups and ring formation in solution prevented isolation and characterization of the polymers. The presence of these scrambling processes was confirmed via NMR spectroscopy.



Scheme 1C.7 Synthesis of Boronate Functionalized Polymers via ADMET.

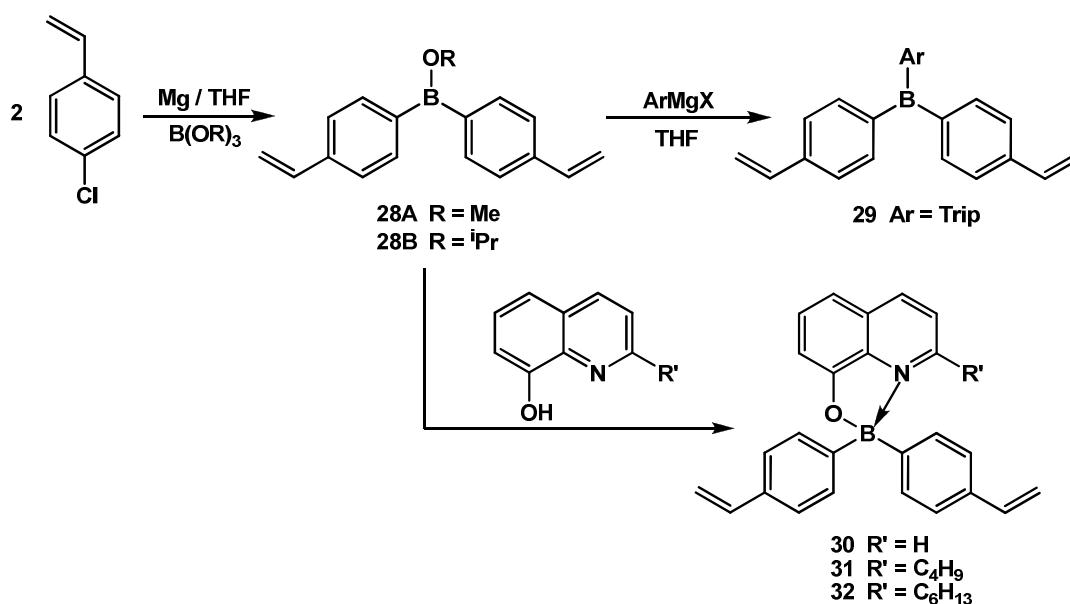
This part of the thesis describes work aimed at the synthesis of boron containing distyryl monomers and their subsequent polymerization using ADMET polymerization. Specifically, organoboron monomers that feature tricoordinate aryl borane and tetracoordinate organoboron quinolate functionalities were prepared. While conjugated triaryl boron polymers are promising candidates for anion sensing due to their inherent Lewis acidity; tetracoordinated organoboron quinolate polymers are expected to provide intense luminescence and may allow for tuning the emission properties by varying the substituents on the quinolate group. This substituent dependent emission has been

previously observed by our group in case of side-chain functionalized polystyrene with organoboron groups that have a quinolate moiety attached to the boron.⁶² To ensure good solubility of the quinolate polymers, we have successfully incorporated butyl and hexyl groups in 2-position of the quinoline ring. The synthesis of these boron containing monomers, their polymerization and their characterization will be discussed.

1C.4 Results and Discussion

1C.4.1 Synthesis of Monomers

The general strategy for the synthesis of all monomers is shown in Scheme 1C.8. Grignard metathesis reaction were utilized to synthesize these boron containing monomers.



Scheme 1C.8 Synthesis of Boron Containing Monomers.

The distyryl organoboron monomers (29-32) were prepared from 4-chlorostyrene. The reaction of styrene Grignard solution with half an equivalent of trialkyl borate in THF gives the alkoxyborane (28). Subsequent reaction with a slight excess of triisopropylphenyl Grignard solution at reflux temperature led to the formation of distyryl triisopropylphenylborane monomer (29) in 25% isolated yield. Three different 8-hydroxyquinoline ligands were also reacted with (28B) to obtain the tetracoordinate monomers (30-32). The monomers were purified by column chromatography using hexanes as the eluent and isolated by recrystallization from hexanes. All four monomers showed excellent solubility in common organic solvents like CH₂Cl₂, THF, and toluene.

1C.4.2 Structural Characterization

1C.4.2.1 Multinuclear NMR Spectroscopy

The monomers were fully characterized by ^1H , ^{13}C and ^{11}B NMR spectroscopy. In the case of (29), the presence of a broad ^{11}B NMR signal at ca. 70 ppm ($w_{1/2}$ ca. 1890) is typical of triarylborane species. All quinoline monomers (30-32) showed a relatively narrow signal at ca. 12 ppm ($w_{1/2}$ ca. 430 to 600 Hz) that is strongly upfield shifted relative to the broad signal of (27) at ca. 40 ppm ($w_{1/2}$ ca. 1800 Hz), consistent with tetra coordination at boron.

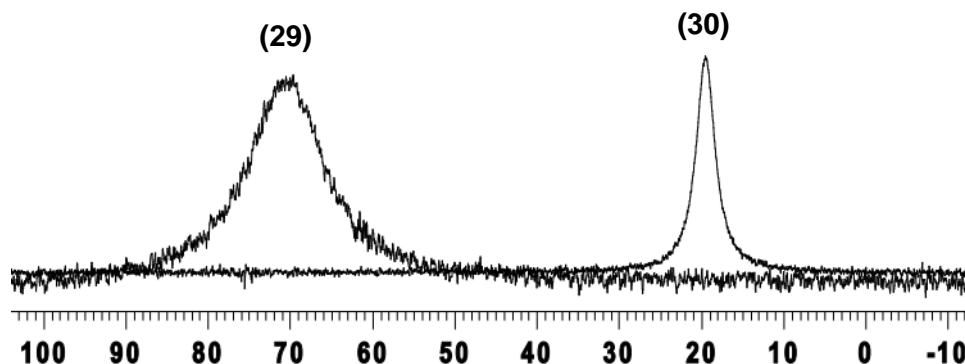


Figure 1C.2 Comparison of the ^{11}B NMR shifts of (29) and (30).

The ^1H NMR spectra showed the expected vinyl peak patterns. The vicinal protons $=\text{CH}_2$ exhibit two characteristic doublet resonance at around ~ 5.7 and ~ 5.1 ppm and the –

CH proton showed a double doublet at around 6.7 ppm. Integration of the ^1H NMR spectra of the monomers confirmed the 2:1 ratio expected for the styryl groups with respect to those of the aromatic protons of the triisopropylphenyl and quinolate groups, respectively. The ^1H NMR spectrum of $(\text{Styryl})_2\text{BQ}$ (30) is shown in Figure 1C.3.

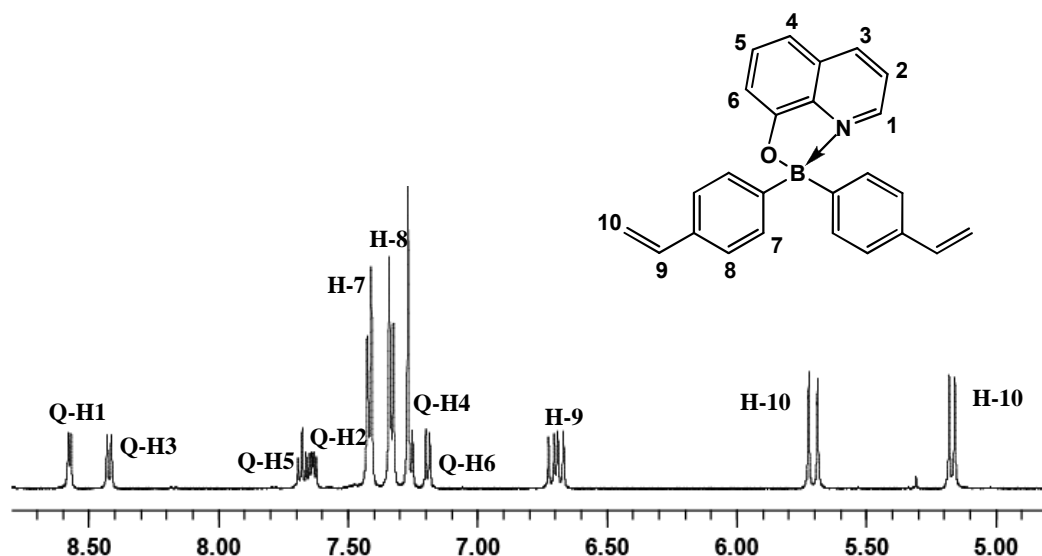


Figure 1C.3 ^1H NMR Spectrum of $(\text{Styryl})_2\text{BQ}$ in CDCl_3 .

1C.4.2.2 X-ray Structure Determination of (29) and (30)

The tri-coordinate nature of boron in monomer (29) was confirmed by an x-ray structure analysis which was performed on clear colorless plate like crystals obtained from hexanes at $-35\text{ }^\circ\text{C}$ (Figure 1C.4). The monomer crystallizes in the $\text{P2}_1/\text{c}$ space group

with a co-crystallized hexane molecule, but no short intermolecular contacts were observed. The boron center adapts a trigonal planar geometry as indicated by the sum of the $C_{\text{aryl}}\text{-B-}C_{\text{aryl}}$ angles ($\sum(C\text{-B-C}) = 360^\circ$). The dihedral angle θ formed between the boron trigonal plane and the plane containing the Trip ligand in (29) is 74° owing to large steric hindrance, indicates less p- π overlap compared to the two styryl ligands.

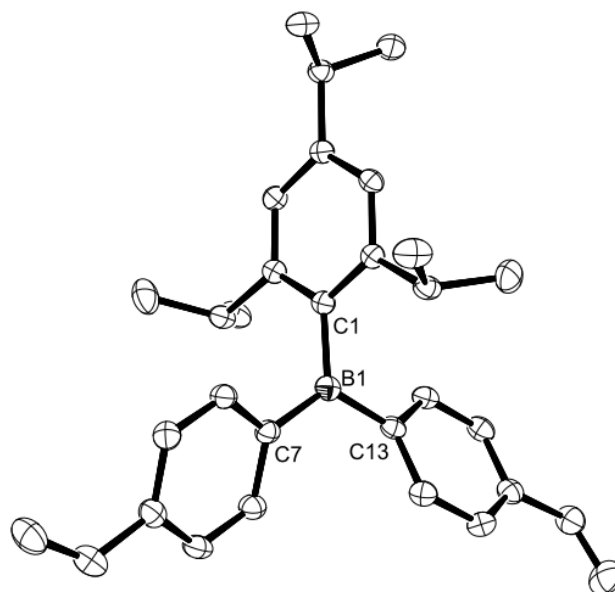
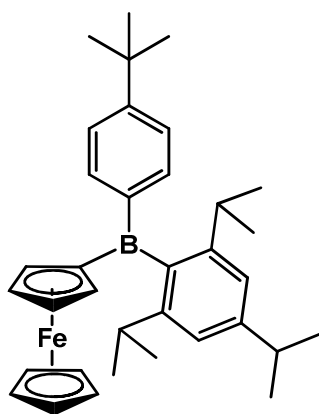
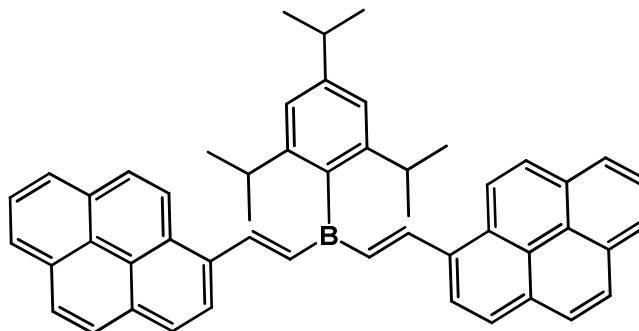


Figure 1C.4 Molecular Structure of (29) (ORTEP, 50% probability). Hydrogen Atoms and a Cocrystallized Hexane Molecule are Omitted for Clarity. Selected Bond Lengths (\AA) and Angles (deg): B1-C1 = 1.582(2), B1-C7 = 1.563(2), B1-C13 = 1.563(2), C1-B1-C7 = 120.66(10), C1-B1-C13 = 118.0(10), C7-B1-C13 = 121.24(10).

The B-C_{tip} bond length to the bulky triisopropylphenyl (Trip) group of 1.582(2) Å is slightly longer than the B-C_{styryl} bond lengths of 1.563(2) Å which is attributed to the steric effect. The bond length of the bulky triisopropylphenyl group is in a similar range as that of a related ferrocene substituted triisopropylborane ((33); B-C_{aryl} = 1.587(3) Å) reported by Parab *et al.*⁶³ and a pyrenylvinylene-substituted triarylborane ((34); B-C_{aryl} = 1.579(4) Å) reported by Chujo and co-workers⁶⁴ (Chart 1C.10).



(33)



(34)

Chart 1C.10 Examples of Triarylborane Compounds with Triisopropylphenyl Substituents.

Crystals of monomer (30) were grown by the slow evaporation of a solution in CDCl₃ at room temperature. As shown in Figure 1C.5, (30) has a tetrahedral geometry at boron,

typical of tetracoordinated boron compounds. The 8-hydroxyquinoline moiety is chelated to boron to form a five-membered chelate ring which is coplanar with the quinoline.

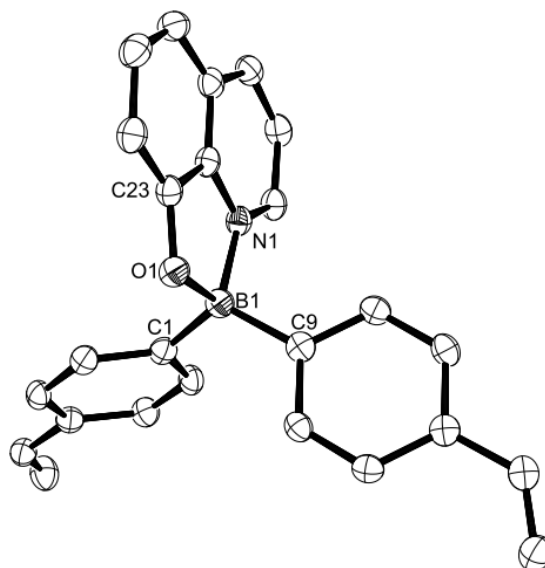


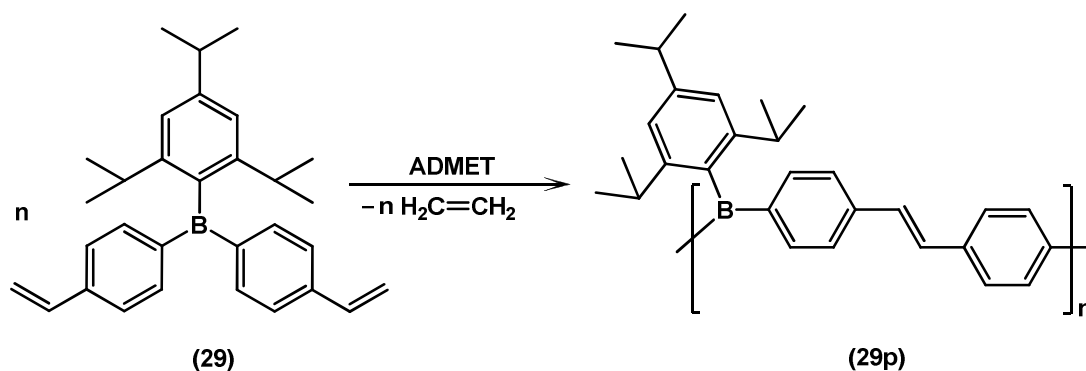
Figure 1C.5 Molecular Structure of (30) (ORTEP, 50% probability). Hydrogen Atoms are Omitted for Clarity. Selected Bond Lengths (Å) and Angles (deg): B1-C1 = 1.609(2), B1-C9 = 1.605(2), B1-N1 = 1.637(2), B1-O1 = 1.523(2), O(1)-B(1)-C(9) = 110.52(10), O(1)-B(1)-C(1) = 111.06(10), C(1)-B(1)-C(9) = 116.28(10), O(1)-B(1)-N(1) = 98.95(9), C(9)-B(1)-N(1) = 110.56(9), C(1)-B(1)-N(1) = 108.06(9).

The bond angle N-B-O of the complex is 98.95(9)°, which is comparable to other 8-hydroxyquinolato containing organoboron compounds reported by Wang and

coworkers.^{65, 66} Each boron center is further bound to two carbon atoms of the two styryl groups. The B1-C1 (1.609(2) Å, B1-C9 (1.605(2) Å), B1-N1(1.637(2) Å) and B1-O1 (1.523(2) Å) bond distances are also similar to those reported by Chujo *et al.* For instance, B(4-iodophenyl)₂Q, shows similar bond distances of B-C (1.598(8) Å) , B-N (1.629(6) Å) and B-O (1.524(7) Å).^{67, 68}

1C.5 Acyclic Diene Metathesis Polymerization of (29-32)

In a collaborative effort, ADMET polymerization was carried out by Arijit Sengupta in the Peetz group for all four monomers by using ruthenium-based Grubbs-Hoveyda second generation and Grubbs second generation alkylidene catalysts under typical ADMET conditions. Initial attempts to polymerize (30-32) were not successful due to lack of solubility of the resulting polymers and hence only polymerization of monomer (29) was further studied (Scheme 1C.9).



Scheme 1C.9 ADMET Polymerization of (29).

The results of ADMET polymerization of (29) are summarized in Table 1C.1. The second generation Grubb's catalyst [1,3-bis(2,4,6-trimethylphenyl)-2-imidazolidinylidene)dichloro(phenylmethylene)(tricyclohexylphosphine)ruthenium] did not produce any polymer, and only monomer was recovered (entry 1). ADMET polymerization using the Grubbs-Hoveyda second generation catalyst [(1,3-bis(2,4,6-trimethylphenyl)-2-imidazolidinylidene)dichloro(*o*-isopropoxyphenylmethylene)ruthenium] was conducted in toluene under dynamic vacuum (entry 2 and 3). The reaction temperature was lowered from 60 to 47 °C and kept for 16 h and 24 h, respectively. The resulting polymers were washed with toluene and isolated by filtration.

Table 1C.1 Results for ADMET Polymerization of (29).

Entry	Catalyst ^a (mol%)	Solvent	Time (h)	Temp (°C)	Yield (%)	M _n ^b	M _w ^b	PDI ^b
1	9 (3.5)	THF	16	60	No Reaction	–	–	–
2	10 (4.2)	Toluene	16	47	85%	5940	13520	2.27
3	10 (3.4)	Toluene	24	47	84%	17340 (55%)/ 4380 (45%)	20930 /5590	1.21 /1.28

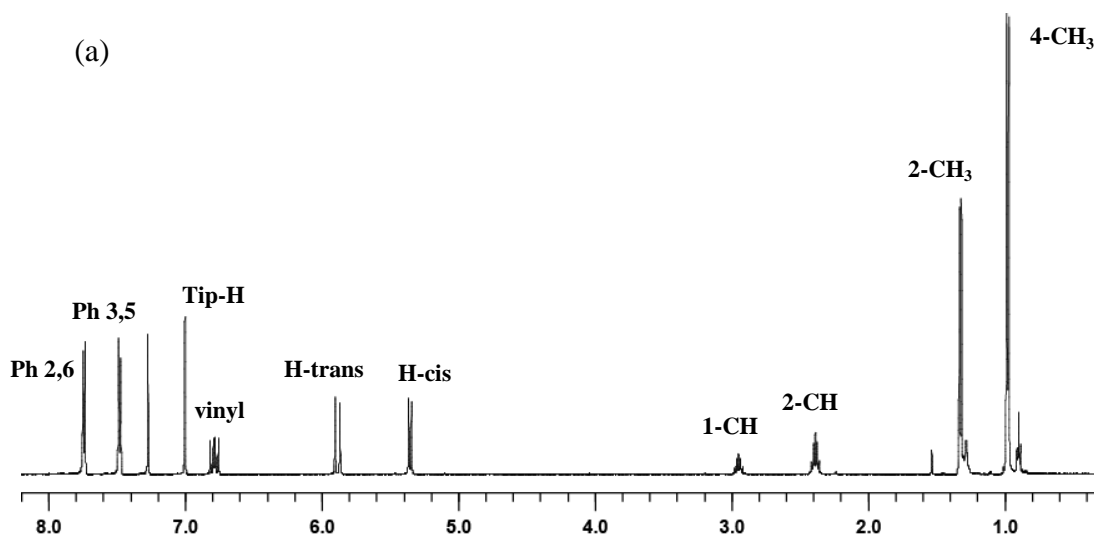
^aSee Chart 1C.3, ^bData acquired by GPC analysis in THF relative to polystyrene standards.

1C.5.1 Molecular Weight Determination

The molecular weight of the polymers was studied by GPC analysis in THF. For entry 2, the molecular weight relative to polystyrene standards was found to be $M_n = \sim 6000$ g mol⁻¹ with a polydispersity index (PDI) of 2.3, corresponding to an average degree of polymerization of $DP_n = 15$. An increase in molecular weight was observed by increasing the polymerization time from 16 h to 24 h. A polymer with higher molecular weight of $M_n = \sim 17000$ with PDI of 1.3, corresponding to an average degree of polymerization of $DP_n = 40$ was obtained.

1C.5.2 NMR Spectroscopy

The polymers obtained were further characterized by ^1H NMR spectroscopy as shown in Figure 1C.6. The ^1H NMR spectra of (29p) show a distinct change relative to that of monomer (29). The formation of product is marked by the appearance of a resonance at ~ 7.3 ppm, indicating the formation of a vinylene bond of the new trans-stilbene unit. The resonances from the terminal vinyl groups (~ 5.3 , 5.8 , and 6.7 ppm) in the monomer almost completely disappeared. The residual terminal vinylene peaks can be assigned to the polymer end groups.



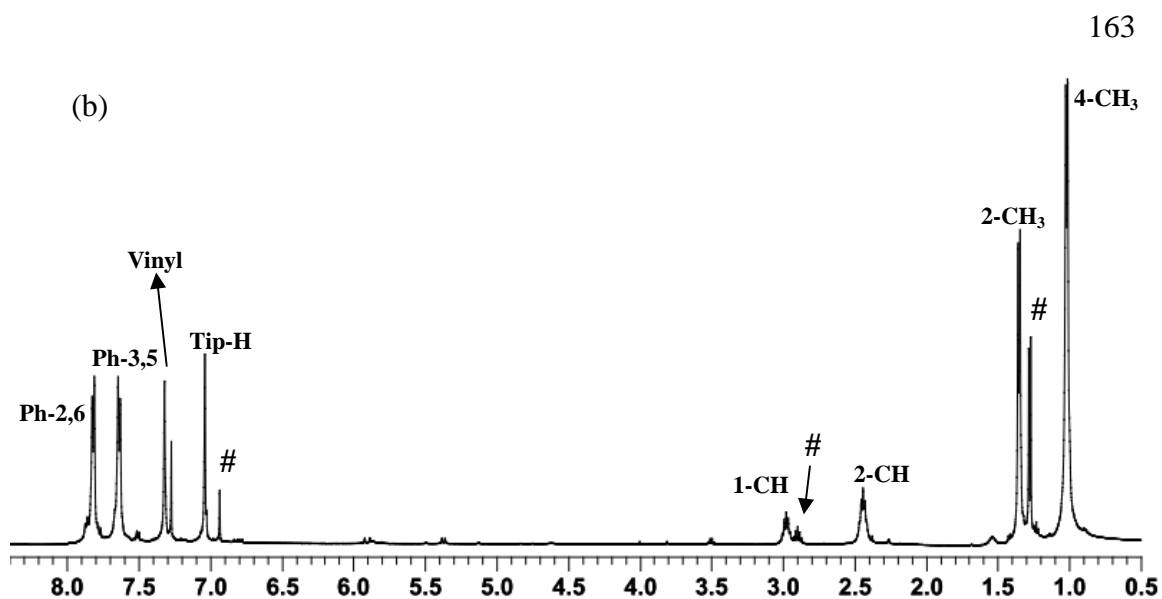


Figure 1C.6 (a) ^1H NMR plot of (29); (b) ^1H NMR plot of (29p) in CDCl_3 ; (# = 1,3,5-triisopropylbenzene).

1C.5.3 Thermal Properties

Thermogravimetric analysis was performed on (29p). The polymer showed good stability upto ca. 200 °C (4% weight loss). However it starts degrading rapidly above that temperature (Figure 1C.7).

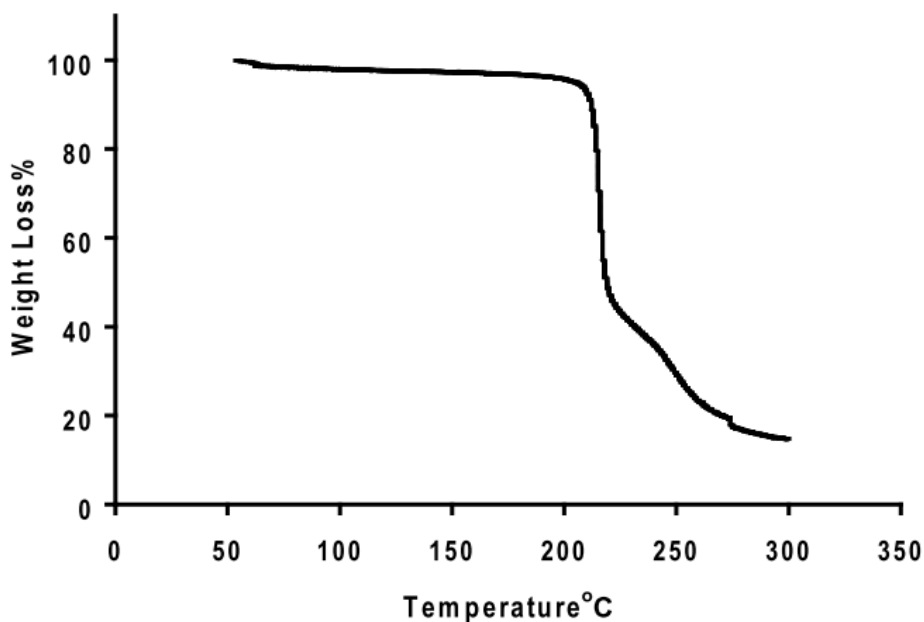


Figure 1C.7 Thermogravimetric Analysis Plot of 29p (10 °C/min under N₂).

1C.5.4 Photophysical Properties

The photophysical properties of monomers (29), (30), (32) and polymer (29p) were studied by UV-Visible and fluorescence spectroscopy. The data are summarized in Table 1C.2 and the absorption and emission spectra of this new series of organoboron monomers are displayed in Figure 1C.8.

Table 1C.2 Comparison of Photophysical Properties of Monomers and Polymers.

Compound	λ_{abs} (nm) ^a	ϵ (L mol ⁻¹ cm ⁻¹) ₁	λ_{em} (nm) ^{a,b}	Φ_{F} ^c (%)
29	324	51,360	423	0.9
29p	385, 405	44780, 46170 ^d	423, 446	5
30	395	3,190	505	21
32	386	3,380	498	23

^a Concentrations were $\sim 3.2 \times 10^{-5}$ M in THF. ^b Excited at the absorption maximum. ^c Anthracene used as a standard. ^d Per repeat unit.

In THF solution, monomer (29) shows an absorption maxima at $\lambda_{\text{abs}} = 324$ nm with $\epsilon = 51,360$ and blue emission at $\lambda_{\text{em}} = 423$ nm ($\lambda_{\text{exc}} = 324$ nm). Monomers (30) and (32) showed absorption peaks around 390 nm arising from the quinoline ligand and emit in the green region ($\lambda_{\text{em}} \sim 500$ nm), which correlates very well with the previously reported data for Ph₂BQ ($\lambda_{\text{max}} = 395$ nm; $\lambda_{\text{em}} = 504$ nm).⁶⁵ The quantum yield for (30) of 17% and (32) of 23% is in a similar range to (tBuPh)₂BQ, reported by Qin *et al.*¹³ A notably lower quantum yield of 0.9% was determined for (29).

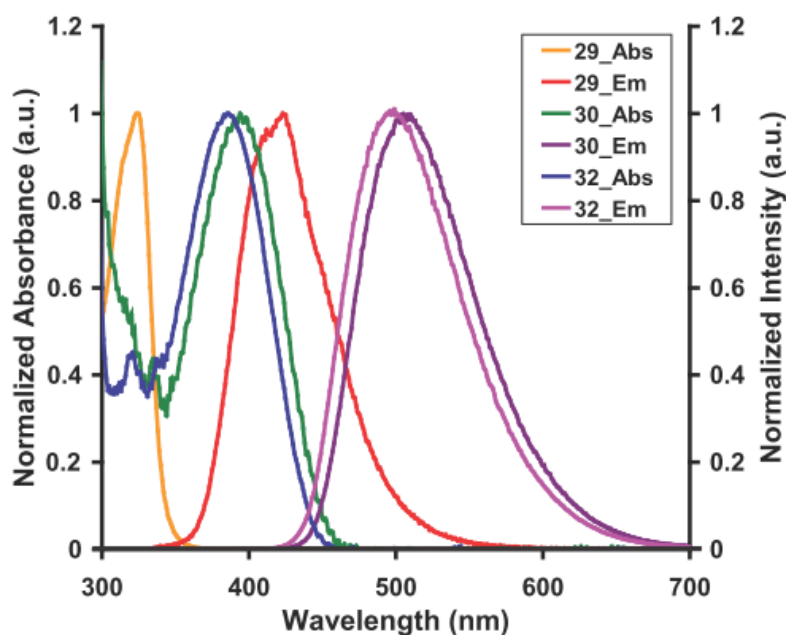


Figure 1C.8 Comparison of Absorption and Emission Spectra of (29), (30) and (32) in THF Solution.

A comparison between the boron polymer and the respective monomer is illustrated in Figure 1C.9. The absorption spectra of the polymer in THF show bands with fine vibronic structure and maxima at approximately 405 nm that are red-shifted by approximately 80 nm. This bathochromic shift is attributed to the extended conjugation through the boron moiety (p- π overlap) which results in the red shift of the absorption maximum for the polymer. The emission data for (29) is quite similar to that of the polymer with $\lambda_{\text{em max}} = 423$ nm, however the polymeric material shows a well-resolved structure with peaks at

423 and 448 nm, which can be assigned to 0-0 and 0-1 intrachain singlet transition with the 0-0 transition being the most intense. The perfectly mirrored absorption and emission bands and relatively small Stokes shift is indicating a highly rigid polymeric structure and has been observed for other rigid polymers.^{17, 69} The fluorescence quantum yield of the polymer (29p) is 5-fold higher than that observed for the monomer (29). This could potentially be due to the fact that the polymer backbone is quite rigid in nature. In addition, the steric hindrance of the Trip groups may prevent aggregation, thereby further reducing the probability of non-radiative decay. A similar enhancement of quantum efficiencies has been observed, for example, by Swager and co-workers upon incorporation of rigid pentyptycene moieties into polyphenylvinylenes.⁷⁰⁻⁷²

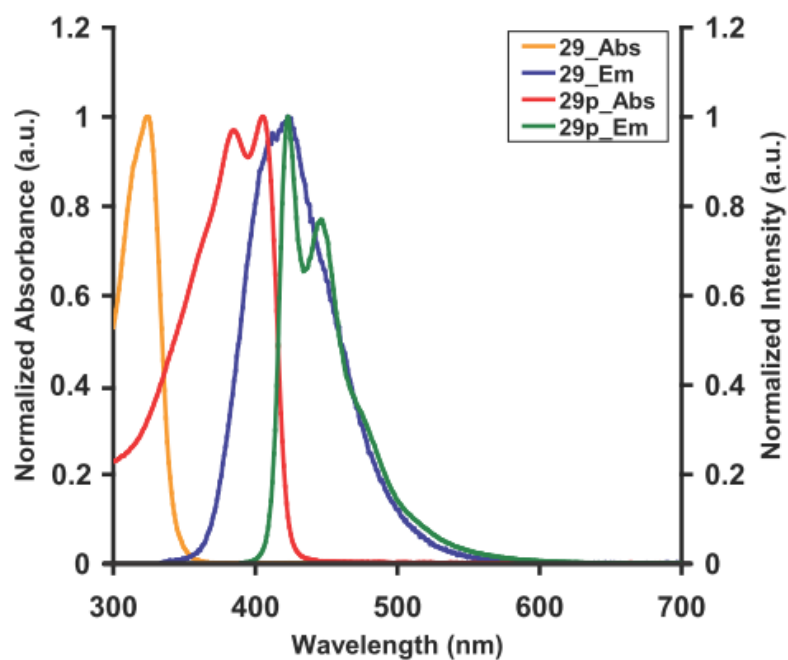


Figure 1C.9 Comparison of Absorption and Emission Spectra of (29) and (29p) in THF Solution.

1C.6 Conclusions

We have synthesized novel organoboron functionalized divinyl monomers, one of which was polymerized by ADMET polymerization using Grubbs-Hoveyda type ruthenium metathesis catalysts. The results from GPC analysis indicate that the polymer (29p) shows moderate molecular weight and polydispersity, typical of condensation polymerization. However, due to reduced solubility, polymers derived from monomers

(30-32) could not be isolated and characterized. Future work may involve further optimization of the polymerization of these monomers.

1C.7 Experimental Section

1C.7.1 Materials and Instrumentation

Mg (turnings), 8-hydroxyquinoline, 1,3,5-triisopropylbenzene, trimethyl borate, and triisopropyl borate were purchased from Acros. 4-chlorostyrene was purchased from Alfa Aesar. (2,4,6-triisopropylphenyl)magnesium bromide⁷³, 2-butylquinolin-8-ol and 2-hexylquinolin-8-ol⁷⁴ were prepared as previously reported.

All reactions and manipulations were carried out in a similar manner to that described in Chapter 1A. Ether, hydrocarbon and chlorinated solvents were treated as described in Chapter 1A. All reactions and manipulations were carried out in a similar manner to that described in Chapter 1A. Detailed description of NMR abbreviations, elemental analyses, GPC analysis and DSC can be found in the experimental section of Chapter 1A. UV-Vis, fluorescence measurements, quantum efficiency and x-ray data collection can be found in the experimental section of Chapter 1B. Thermogravimetric analysis (TGA) was performed under N₂ atmosphere using a Hi-Res TGA 2950 thermogravimetric analyzer from TA Instruments using a platinum pan with a heating rate of 10 °C/min from 50 °C to 300 °C.

1C.7.2 Synthesis of Boron Monomers and Polymers

Synthesis of 29: To a suspension of Mg (2.67 g, 0.11 mol) in 300 mL THF was added slowly 4-chlorostyrene (7.62 g, 0.055 mol) while maintaining the temperature below 60 °C. The reaction mixture was stirred at 60 °C for 2 h and allowed to cool to room temperature. The supernatant styrene-Grignard solution was then decanted to another flask using a cannula. Trimethylborate was then added slowly to the Grignard solution and the reaction was stirred for 3 h. Resulting borate solution was then added slowly to a solution of (2,4,6-triisopropylphenyl)magnesium bromide in THF and refluxed for 1.5 days. The crude product was extracted using hexanes and passed through silica gel column using hexanes as the eluent. The pure product was obtained via crystallization from hexanes as colorless crystals (2.5 g, 25 %). For **29**: ^{11}B NMR (160.380 MHz, CDCl_3): $\delta = 69.6$ ($w_{1/2} = 1890$); ^1H NMR (499.893 MHz, CDCl_3): $\delta = 7.75$ (d, $^3J = 7.5$ Hz, 4H, Ph-H2,6), 7.50 (d, $^3J = 7.5$ Hz, 4H, Ph-H3,5), 7.00 (s, 2H, Tip-H3,5), 6.80 (dd, $^3J = 18.0$ Hz, 2H, H9), 5.90 (d, $^3J = 18$ Hz, 2H, H10), 5.37 (d, $^3J = 12$ Hz, 2H, H11), 2.95 (sept, $^3J = \text{Hz}$, 1H), 2.40 (sept, $^3J = \text{Hz}$, 2H), 1.33 (d, $^3J = 7.0$ Hz, 6H), 0.98 (d, $^3J = 12.0$ Hz, 12H); ^{13}C (125.698 MHz, CDCl_3): $\delta = 149.07, 148.68, 142.44, 140.77, 140.76, 138.44, 138.38, 137.07, 125.68, 120.26, 115.73, 35.67, 34.44, 24.38$; UV-Vis (THF, 3.0×10^{-5} M): $\lambda_{\text{max}} = 324$ nm ($\epsilon = 51,360$); fluorescence (THF, 3.0×10^{-5} M): $\lambda_{\text{em,max}} = 423$ nm, $\Phi = 0.9$ ($\lambda_{\text{exc}} = 324$ nm); elemental analysis: calculated C 88.56, H 8.87; found C 88.32,

H 8.90. High resolution MALDI-TOF (negative mode, matrix: Benzo[a]pyrene): $m/z = 420.44$ (calcd for $^{12}\text{C}_{31}\text{H}_{37}^{11}\text{B}$ 420.44).

Synthesis of 30: A solution of borate 28B was prepared as described above (50.0 mmol, 300 mL THF). The resulting borate solution was then added slowly to 8-hydroxyquinoline in THF and stirred for 16 h. Insoluble salts were removed by filtration, the solvents were removed under vacuum and the crude product was re-dissolved in dichloromethane and passed through a silica gel column using hexanes as the eluent. The product as a yellow-green solid was obtained after solvent evaporation. (7.8 g, 86 %). For **30**: ^{11}B NMR (160.380 MHz, CDCl_3): $\delta = 11.3$ ($w_{1/2} = 430$); ^1H NMR (499.893 MHz, CDCl_3): $\delta = 8.58$ (d, $^3J = 5.0$ Hz, 1H, Q-H2), 8.43 (d, $^3J = 8.0$ Hz, Q-H4), 7.68 (pst, $^3J = 8.0$ Hz, 1H, Q-H6), 7.64 (dd, $^3J = 5.0$ Hz and 8.5 Hz, 1H, Q-H3), 7.42 (d, $^3J = 8.0$ Hz, 4H, Ph-H2,6), 7.34 (d, $^3J = 8.0$ Hz, 4H, Ph-H3,5), 7.25 (d, $^3J = 8.5$ Hz, 1H, Q-H5), 7.20 (d, $^3J = 7.5$ Hz, 1H, Q-H7), 6.70 (dd, $^3J = 11.0$ Hz, 18.0 Hz, 2H, H9), 5.67 (d, $^3J = 18.0$ Hz, 2H, H10), 5.18 (d, $^3J = 11.0$ Hz, 2H, H11); ^{13}C (125.698 MHz, CDCl_3): $\delta = 158.87, 147.0, 139.40, 138.97, 137.71, 137.42, 136.47, 133.09, 132.39, 128.61, 125.71, 122.95, 113.08, 112.48, 109.90$; UV-Vis (THF, 3.0×10^{-5} M): $\lambda_{\text{max}} = 395$ nm ($\epsilon = 3,190$); fluorescence (THF, 3.0×10^{-5} M): $\lambda_{\text{em,max}} = 504$ nm, $\Phi = 0.21$ ($\lambda_{\text{exc}} = 395$ nm).

Synthesis of 31: A solution of borate 28B was prepared as described above (11.0 mmol, 100 mL THF) and then added slowly to ^nBu -8-hydroxyquinoline in THF. The

reaction mixture was stirred for 20 h and insoluble salts were removed by filtration. Pure product was obtained via crystallization from hexanes as a yellow solid (0.13 g, 10 %).

For **31**: ^{11}B NMR (160.380 MHz, CDCl_3): $\delta = 11.7$ ($w_{1/2} = 610$), ^1H NMR (499.893 MHz, CDCl_3): $\delta = 8.35$ (d, $^3J = 8.0$ Hz, 1H, Q-H4), 7.58 (pst, $^3J = 8.0$ Hz, 1H, Q-H6), 7.45 (d, $^3J = 8.0$ Hz, 1H, Q-H3), 7.34 (dd, $^3J = 8.0$ Hz and 12.0 Hz, 8H, Ph-H2,6 and Ph-H3,5), 7.21 (d, $^3J = 8.5$ Hz, 1H, Q-H5), 7.09 (d, $^3J = 7.5$ Hz, 1H, Q-H7), 6.70 (dd, $^3J = 11.0$ Hz, 17.5 Hz, 2H, H9), 5.73 (d, $^3J = 17.5$ Hz, 2H, H10), 5.18 (d, $^3J = 11.0$ Hz, 2H, H11), 2.86 (m, 2H, Butyl), 1.01(br, m, 4H, Butyl), 0.65 (t, $^3J = 7.0$ Hz, 3H, Butyl); ^{13}C (125.698 MHz, CDCl_3): $\delta = 158.65, 157.80, 145.5, 139.31, 137.47, 137.43, 136.30, 133.54, 133.47, 131.63, 126.85, 125.55, 123.94, 112.93, 112.38, 109.75, 34.52, 31.40, 22.72, 13.71$.

Synthesis of 32: A solution of borate 28B was prepared as described above (29.0 mmol, 200 mL THF) and then added slowly to ^nHex -8-hydroxyquinoline (5.0 g, 0.022 mol) in 50 mL THF for 24 h. Complete conversion was confirmed via ^{11}B NMR spectroscopy and the mixture was then quenched with chlorotrimethylsilane (1.8 g, 0.017 mol) to remove any unreacted Grignard. Insoluble salts were removed by filtration. The pure product was obtained via crystallization from hexanes as a yellow solid (2.0 g, 32%).

For **32**: ^{11}B NMR (160.380 MHz, CDCl_3): $\delta = 11.7$ ($w_{1/2} = 610$); ^1H NMR (499.893 MHz, CDCl_3): $\delta = 8.35$ (d, $^3J = 8.5$ Hz, 1H, Q-H2), 7.58 (pst, $^3J = 8.5$ Hz, 1H, Q-H6),

7.45 (d, $^3J = 8.5$ Hz, 1H, Q-H3), 7.33 (dd, $^3J = 8.0$ Hz and 12.0 Hz, 8H, Ph-H2,6 and Ph-H3,5), 7.21 (d, $^3J = 8.5$ Hz, 1H, Q-H5), 7.09 (d, $^3J = 7.5$ Hz, 1H, Q-H7), 6.70 (dd, $^3J = 11.0$ Hz, 17.5 Hz, 2H, H9), 5.72 (d, $^3J = 17.5$ Hz, 2H, H10), 5.18 (d, $^3J = 11.0$ Hz, 2H, H11), 2.86 (t, $^3J = 7.0$ Hz, 2H, Hex), 1.11 (m, 2H, Hex), 0.99 (m, 6H, Hex), 0.78 (t, $^3J = 7.0$ Hz, 3H, Hex); ^{13}C (125.698 MHz, CDCl_3): $\delta = 158.74, 157.88, 145.6, 139.31, 137.54, 136.37, 133.51, 131.73, 126.91, 125.62, 123.95, 112.95, 112.38, 109.89, 34.84, 31.56, 29.51, 29.25, 22.57, 14.18$; UV-Vis (THF, 3.1×10^{-5} M): $\lambda_{\text{max}} = 258$ nm ($\epsilon = 58,160$), 386 nm ($\epsilon = 3,380$); fluorescence (THF, 3.1×10^{-5} M): $\lambda_{\text{em,max}} = 498$ nm, $\Phi = 0.23$ ($\lambda_{\text{exc}} = 386$ nm); elemental analysis: calculated C 83.59, H 7.24, N 3.14; found C 83.46, H 7.13, N 3.12.

1C.8 References and Notes

1. Kiess, H. E. *Conjugated Conducting Polymers*; 1992; Vol. 102.
2. Müllen, K.; Wegner, G., *Electronic Materials; the oligomer approach*. WILEY-VCH Verlag GmbH: Weinheim, 1998.
3. Nalwa, H. S. *Handbook of Conductive Materials and Polymers*; John Wiley and Sons: New York 1997.
4. McCullough, R. D.; Belot, J. A.; Rheingold, A. L.; Yap, G. P. A. *J. Am. Chem. Soc.* **1995**, *117*, 9913-9914.

5. Jäkle, F. *Coord. Chem. Rev.* **2006**, 250, 1107-1121.
6. Burroughes, J. H.; Friend, R. H. *The Semiconductor Device Physics of Polyacetylene. In Conjugated Polymers, Bredas, J. L.; Silbey, R., Eds. Kluwer Academic Publishers* 1991.
7. Allcock, H. R.; Lampe, F. W.; Mark, J. E. *Contemporary Polymer Chemistry. Third ed.; Pearson Education, Inc.: Upper Saddle River, NJ* 2003.
8. Matsumi, N.; Naka, K.; Chujo, Y. *J. Am. Chem. Soc.* **1998**, 120, 5112-5113.
9. Matsumi, N.; Chujo, Y. *Polym. J.* **2008**, 40, 77-89.
10. Matsumi, N.; Naka, K.; Chujo, Y. *J. Am. Chem. Soc.* **1998**, 120, 10776-10777.
11. Sundararaman, A.; Victor, M.; Varughese, R.; Jäkle, F. *J. Am. Chem. Soc.* **2005**, 127, 13748-13749.
12. Yamaguchi, S.; Akiyama, S.; Tamao, K. *J. Organomet. Chem.* **2002**, 652, 3-9.
13. Qin, Y.; Kiburu, I.; Shah, S.; Jäkle, F. *Org. Lett.* **2006**, 8, 5227-5230.
14. Corriu, R. J.-P.; Deforth, T.; Douglas, W. E.; Guerrero, G.; Deforth, T.; Siebert, W. S. *Chem. Commun.* **1998**, 963-964.
15. Lorbach, A.; Bolte, M.; Li, H.; Lerner, H-W.; Holthausen, M. C.; Jäkle, F.; Wagner, M. *Angew. Chem. Int. Ed.* **2009**, 48, 4584-4588.
16. Matsumi, N.; Umeyama, T.; Chujo, Y. *Polym. Bull.* **2000**, 44 431.
17. Li, H.; Jäkle, F. *Angew. Chem. Int. Ed.* **2009**, 48, 2313-2316.

18. Niu, W.; Smith, M. D.; Lavigne, J. J. *J. Am. Chem. Soc.* **2006**, *128*, 16466-16467.
19. Baughman, T. W.; Wagener, K. B. *Adv. Polym. Sci.* **2005**, *176*, 1-42.
20. Tindall, D.; Pawlow, J. H.; Wagener, K. B. *Recent Advances in ADMET Chemistry*, **1999**; Vol. 1.
21. Lindmark-Hamberg, M.; Wagener, K. B. *Macromolecules* **1987**, *20*, 2949-2951.
22. Schaverien, C. J.; Dewan, J. C.; Schrock, R. R. *J. Am. Chem. Soc.* **1986**, *108*, 2771-2773.
23. Schrock, R. R.; Depue, R. T.; J. Feldman, J.; Yap, K. B.; Yang, D. C.; Davis, W. M.; Park, L.; Dimare, M.; Schofield, M.; Anhaus, J.; Dewan, J. C.; Walborsky, E.; Evitt, C.; Betz, K. P. *Organometallics* **1990**, *9*, 2262-2275.
24. Schwab, P. F.; Marcia, B.; Ziller, J. W.; Grubbs, R. H. *Angew. Chem. Int. Ed. Engl.* **1995**, *34*, 2039-2041.
25. Scholl, M.; Ding, S.; Lee, C. W.; Grubbs, R. H. *Org. Lett.* **1999**, *1*, 953-956.
26. Scholl, M.; Trnka, T. M.; Morgan, J. P.; Grubbs, R. H. *Tetrahedron Lett.* **1990**, *40*, 2247-2250.
27. Trnka, T. M.; Grubbs, R. H. *Acc. Chem. Res.* **2001**, *34*, 18-29.
28. Michrowska, A.; Bujok, R.; Harutyunyan, S.; Sashuk, V.; Dolgonos, G.; Grela, K. *J. Am. Chem. Soc.* **2004**, *126*, 9318-9325.

29. Rix, D.; Caijo, F.; Laurent, I.; Gulajski, L.; Grela, K.; Mauduit, M. *Chem. Commun.* **2007**, 3771-3773.
30. Ivin, K. J.; Mol, I. C. *Olefin Metathesis and Metathesis Polymerization*, 2nd ed., Academic Press Inc., San Diego, **1997**.
31. Wagener, K. B.; Nel, J. G.; Konzelman, J.; Boncella, J. M. *Macromolecules* **1990**, *23*, 5155-5157
32. Wagener, K. B.; Patton, J. T. *Macromolecules* **2002**, *26*, 249-253.
33. Wagener, K. B.; Nel, J. G.; Konzelman, J.; Boncella, J. M. *Macromolecules* **2002**, *23*, 5155-5157.
34. Wagener, K. B.; Patton, J. T. *Macromolecules* **1993**, *26*, 249-253.
35. Wagener, K. B.; Brzezinska, K.; Anderson, J. D.; Younkin, T. R.; Steppe, K.; DeBoer, W. *Macromolecules* **1997**, *30*, 7363-7369.
36. Wagener, K. B.; Smith, D. W. *Macromolecules* **1991**, *24*, 6073-6078.
37. Wagener, K. B.; Boncella, J. M.; Nel, J. G. *Macromolecules* **2002**, *24*, 2649-2657.
38. Wagener, K. B.; Brzezinska, K. *Macromolecules* **1991**, *24*, 5273-5277.
39. Portmess, J. D.; Wagener, K. B. *J. Polym. Sci., Part A: Polym. Chem.* **1996**, *34*, 1353-1357.
40. Krystyna, R. B.; Regina, S.; Kenneth, B. W. *J. Polym. Sci., Part A: Polym. Chem.* **2000**, *38*, 1544-1550.

41. Tao, D.; Wagener, K. B. *Macromolecules* **1994**, 27, 1281-1283.
42. Fox, H. H.; Schrock, R. R.; O'Dell, R. *Organometallics* **1994**, 13, 635-639.
43. Thorn-Csányi, E.; Kraxner, P. *Macromol. Chem. Phys.* **1997**, 198, 3827-3843.
44. Peetz, R.; Strachota, A.; Thorn-Csányi, E. *Macromol. Chem. Phys.* **2003**, 204, 1439-1450.
45. Peetz, R. M.; Sinnwell, V.; Thorn-Csányi, E. *J. Mol. Catal. A: Chem.* **2006**, 254, 165-173.
46. Nomura, K.; Miyamoto, Y.; Morimoto, H.; Geerts, Y. *J. Polym. Sci.* **2005**, 6166.
47. Miller, C. G.; Harper, A. W. *Polym. Prep.* **2003**, 44, 816.
48. Weychardt, H.; Plenio, H. *Organometallics* **2008**, 27, 1479-1485.
49. Nomura, K.; Yamamoto, N.; Ito, R.; Fujiki, M.; Geerts, Y. *Macromolecules* **2008**, 41, 4245-4249.
50. Perepichka, I. F.; Perepichka, D. F.; Meng, H.; Wudl, F. *Adv. Mater.* **2005**, 17, 2281-2305.
51. Qin, Y.; Hillmyer, M. A. *Macromolecules* **2009**, 42, 6429-6432.
52. Zeldin, M.; Wynne, K. J.; Allcock, H. R. *Inorganic and Organometallic Polymers: macromolecules Containing Silicon, Phosphorus and Other Inorganic Elements*, American Chemical Society, Washington. 1988.
53. Smith, D. W.; Wagener, K. B. *Macromolecules* **1993**, 26, 1633-1642.

54. Miao, Y.-J.; Bazan, G. C. *Macromolecules* **1997**, *30*, 7414-7418.
55. Mukherjee, N.; Peetz, R. M. *Macromolecules* **2008**, *41*, 6677-6685.
56. Rathore, J. S.; Interrante, L. V. *Macromolecules* **2009**, *42*, 4614-4621.
57. Gómez, F. J.; Wagener, K. B. *J. Organomet. Chem.* **1999**, *592*, 271-277.
58. Allcock, H. R.; Kellam, E. C.; Hofmann, M. A. *Macromolecules* **2001**, *34*, 5140-5146.
59. Gamble, A. S.; Patton, J. T.; Boncella, J. M. *Makromol. Chem. Rapid Commun.* **1993**, *13*, 109-115.
60. Shultz, G. V.; Zakharov, L. N.; Tyler, D. R. *Macromolecules* **2008**, *41*, 5555-5558.
61. Wolfe, P. S.; Wagener, K. B. *Macromolecules* **1999**, *32*, 7961-7967.
62. Qin, Y.; Kiburu, I.; Shah, S.; Jäkle, F. *Macromolecules* **2006**, *39*, 9041-9048.
63. Parab, K.; Jäkle, F. *Macromolecules* **2009**, *42*, 4002-4007.
64. Nagata, Y.; Chujo, Y. *J. Organomet. Chem.* **2009**, *694*, 1723-1726.
65. Wu, Q.; Esteghamatian, M.; Hu, N.-X.; Popovic, Z.; Enright, G.; Tao, Y.; D'Iorio, M.; Wang, S. *Chem. Mater.* **2000**, *12*, 79-83.
66. Cui, Y.; Liu, Q.-D.; Bai, D.-R.; Jia, W.-L.; Tao, Y.; Wang, S. *Inorg. Chem.* **2005**, *44*, 601-609.
67. Nagata, Y.; Chujo, Y. *Macromolecules* **2007**, *40*, 6-8.

- 68. Nagata, Y.; Chujo, Y. *Macromolecules* **2008**, *41*, 2809-2813.
- 69. Dieter, N. *Macromol. Rapid. Commun.* **2001**, *22*, 1365-1385.
- 70. Yang, J. S.; Swager, T. M. *J. Am. Chem. Soc.* **1998**, *120*, 5321-5322.
- 71. Yang, J. S.; Swager, T. M. *J. Am. Chem. Soc.* **1998**, *120*, 11864-11873.
- 72. Kim, Y.; Zhu, Z.; Swager, T. M. *J. Am. Chem. Soc.* **2004**, *126*, 452-453.
- 73. Natalie, M. S.; Thomas, S.; Oleg, T.; Rhett, K. *Eur. J. Inorg. Chem.* **2004**, **2004**, 3297-3304.
- 74. Neumann, R.; Weber, E.; Moeckel, A.; Subklew, G. *J. Prakt. Chemie/Chemiker-Zeitung* **1998**, *340*, 613-622.

Chapter 2. Pentafluorophenylcopper: Complexation Behavior and Supramolecular Structures

2.1 Introduction

Organocopper compounds have emerged as one of the most important classes of organometallic compounds due to the rich structural diversity and applications as mild and selective reagents in organic synthesis.¹ They tend to form a variety of different aggregates both in the solid state as well as in solution. So far, a number of well-defined homoleptic arylcopper species $[\text{ArCu}]_n$ with varying degree of aggregation ($n = 2-8$) have been isolated and structurally characterized.²⁻⁴ Aggregation typically occurs through bridging of two or more copper centers with an organic moiety. The degree of aggregation depends on a number of factors including steric and electronic effects and the presence of external donor ligands.¹

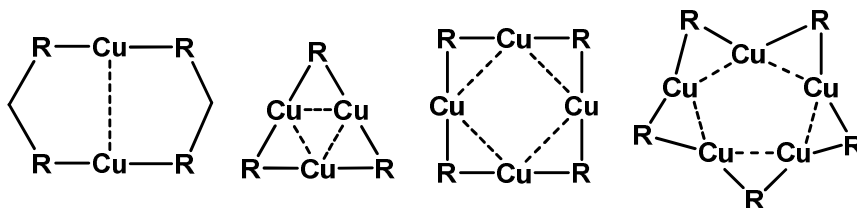


Chart 2.1 Aggregation of Organocopper Compounds.

For example, unsubstituted phenylcopper adopts a polymeric structure and hence is insoluble in common organic solvents, while the presence of substituents in the *ortho*-position of the aromatic ring leads to well-defined soluble oligomers as a result of steric bulk.³ In contrast, 2,4,6-triisopropylphenylcopper features a tetrameric square-planar aggregate due to the presence of sterically demanding isopropyl groups in the *ortho*-positions of the phenyl ring.⁵ Pioneering work done by van Koten and coworkers has shown that smaller arylcopper aggregates can be stabilized by the intramolecular coordination with chelating amino or alkoxy groups in the *ortho*-position of the aromatic ring.⁶ For example, (dimethylaminomethyl)phenylcopper (1) forms a stable tetramer due to the chelating nature of the (dimethylamino)methyl moiety present in the *ortho*-position. Stabilization via π -arene interaction has also been encountered for arylcopper species. This motif is present in the dimeric structure of (2,6-dimesitylphenyl)copper and the related trimer (2,6-diphenylphenyl)copper reported by Niemeyer *et al.*⁷

Floriani and coworkers reported the synthesis of mesitylcopper by Grignard metathesis. Recrystallization of the product from toluene yielded a pentameric structure in the solid state.⁸ Later they reported that pentameric mesitylcopper undergoes a ring contraction with tetrahydrothiophene (THT) to the corresponding tetrameric complex (2), which features two THT molecules coordinated to two of the copper atoms.⁹ Later Håkansson and coworkers reported structural changes of this compound upon varying the

recrystallization solvent.¹⁰ They isolated tetrameric mesitylcopper from THF/ether mixture solvent and characterized the complex by single-crystal x-ray diffraction. Interestingly, cocrystallized THF molecules do not show any interaction with the copper centers and the crystal packing pattern displayed channels that are formed from the positioning of the tetramers and are filled with four THF molecules for every tetramer. On prolonged standing at $-20\text{ }^{\circ}\text{C}$ in THF/ether, the pentameric phase of mesitylcopper was completely transformed into the tetrameric phase. They also performed a refinement of the pentameric mesitylcopper phase obtained by crystallization from toluene and were able to locate one toluene molecule for every pentamer in the crystal lattice. From the cryoscopic molecular weight determinations, an equilibrium between a tetramer and pentamer in both ethereal and aromatic solutions was proposed.¹⁰

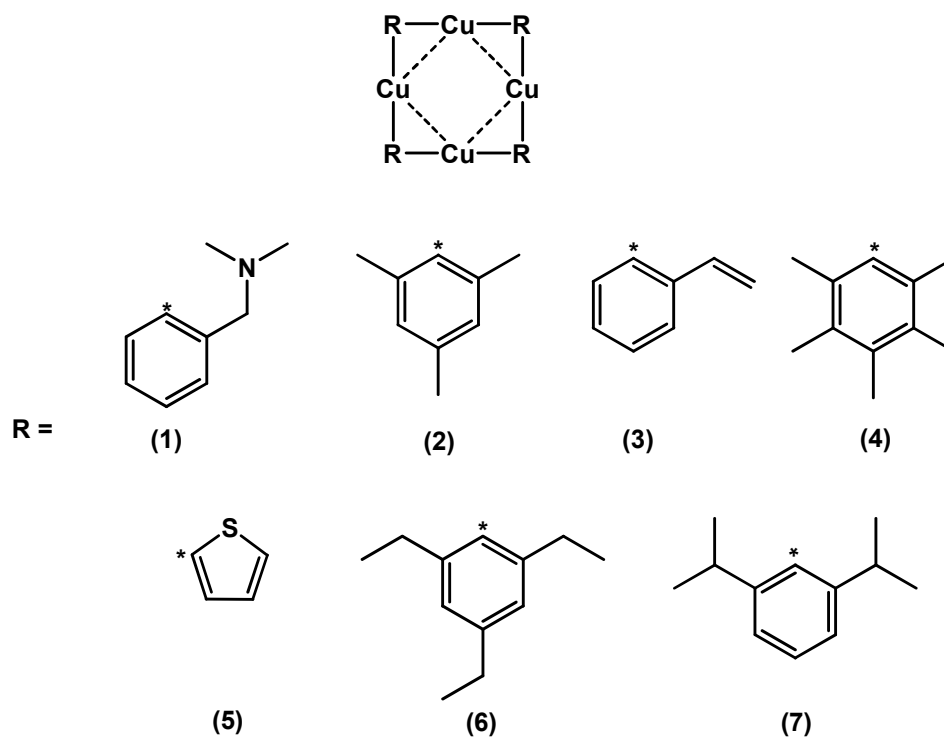


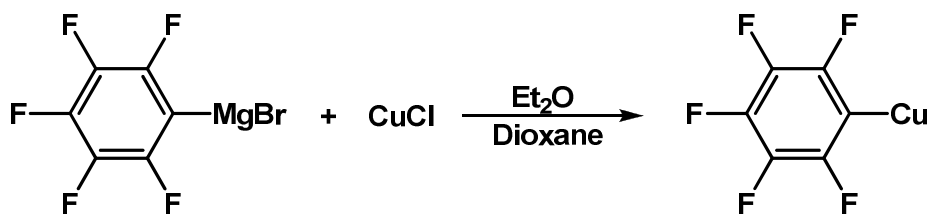
Chart 2.2 Examples of Tetrameric Arylcopper Compounds.

Interestingly, Håkansson and coworkers studied various other homoleptic aryl copper such as (*o*-vinylphenyl)copper¹¹ (3), pentamethylphenylcopper¹² (4), thienylcopper¹³ (5) and 2,4,6-triethylphenylcopper (6).¹⁴ These copper complexes exist as tetramers in the solid state where the aryl ligands are usually situated perpendicular to a puckered or square planar Cu_4 core. This leads to the formation of eight-membered rings composed of alternating copper(I) and C_{ipso} carbon atoms. Similarly, 2,6-diisopropylphenylcopper (7)¹⁵ was synthesized by Boéré and coworkers. The x-ray structure analysis of (7) revealed a

tetramer with trapezoidal copper plane with copper atoms bridged along each Cu–Cu contact by an approximately perpendicular aryl group. The *ispo*-carbon atoms are not coplanar with the copper atoms and are displaced to different sides of the copper plane in an alternating manner.

2.2 Pentafluorophenylcopper

Studies on the synthesis of pentafluorophenylcopper (8) were reported by Cairncross and Sheppard^{16, 17}, DePasquale and Tamborski¹⁸, and Gilman *et al.*¹⁹ The Grignard reagent $\text{C}_6\text{F}_5\text{MgX}$ or the organolithium species $\text{C}_6\text{F}_5\text{Li}$ were reacted with copper halides CuX ($\text{X} = \text{Cl}, \text{Br}, \text{I}$) (Scheme 2.1).²⁰⁻²³ However, the Grignard metathesis route was generally preferred over lithiation due to the thermal lability of $\text{C}_6\text{F}_5\text{Li}$ species and to avoid cuprate formation.



Scheme 2.1 Synthesis of $\text{C}_6\text{F}_5\text{Cu}$.

Pure pentafluorophenylcopper can be obtained by recrystallization from a mixture of 1,2-dichloroethane and cyclohexane (ca. 1:1) as colorless crystals, which were found to contain half a molecule of 1,2-dichloroethane per $(\text{C}_6\text{F}_5\text{Cu})_4$ unit.²⁴ Recrystallization from toluene yields the toluene adduct $(\text{C}_6\text{F}_5\text{Cu})_4(\text{toluene})_2$ (9) as a white crystalline solid.^{17, 24} The base-free complex can be obtained by removal of toluene at elevated temperature. The structure of (9) will be discussed in detail in section 2.6.2.

2.2.1 Solid State Structure of $(\text{C}_6\text{F}_5\text{Cu})_4$ (8)

The structure of the homoleptic tetrameric complex (8) is shown in Figure 2.1 and is similar to that of other homoleptic tetramers previously discussed.²⁴ An aggregation number $n = 4$ was also confirmed by cryoscopy, vapor pressure osmometry and EI-mass spectroscopy.¹⁷ The copper atoms show a distorted square-planar arrangement where the pentafluorophenyl substituents stand orthogonally to the Cu_4 plane but are dislocated from the Cu_4 plane which leads to slight puckering of the Cu_4C_4 ring. The four $\text{Cu}\cdots\text{Cu}$ distances between adjacent copper atoms range from 2.4286(3)–2.4534(3) Å and diagonal distances are 3.307 and 3.584 Å. All $\text{Cu}\cdots\text{C}$ distances in (8) are within a range from 1.962(2) to 2.007(2) Å, as expected for a symmetrical bridging situation of the pentafluorophenyl groups.²⁴

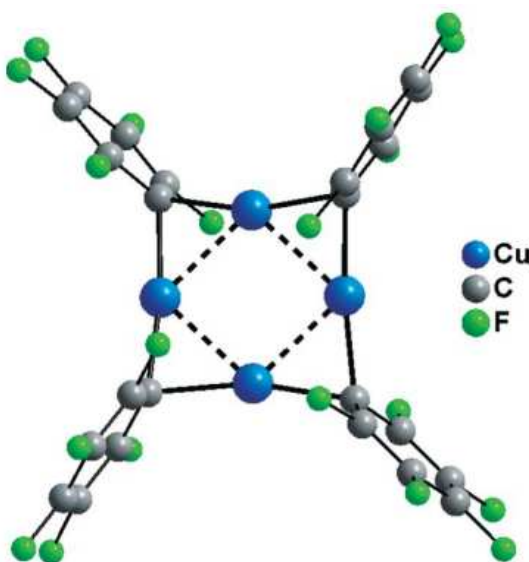


Figure 2.1 Plot of the Molecular Structure of (8); *Dalton Trans.*, 2007, 2851-2858; Reproduced with Permission of the Royal Society of Chemistry.

It is interesting to point out that (8) forms an extended structure with channels along the crystallographic *b*-axis. These channels are filled with cocrystallized solvent molecules (1,2-dichloroethane), which do not show any significant interactions with the organocopper tetramers.

2.3 σ -Complexes of Organocopper Compounds

It is also well-known that treatment of organocopper species with strongly coordinating solvents or external ligands can lead to breakdown of the aggregated structure. Smaller

organocopper aggregates can, for example, be obtained by using N, P or S compounds as donors. For instance, polymeric phenylcopper has been isolated as the dimethylsulfide solvate and has a square-planar tetranuclear copper(I) core.²⁵ However, it is difficult to predict whether monomeric species or partially aggregated complexes will be formed. Surprisingly, only few non-aggregated species (RCu-L_n) with either bulky groups and/or chelating ligands have been isolated and structurally characterized. Monomeric phenylcopper (10) was reported by Gambarotta *et al.*²⁶ They used the tridentate tripod-like ligand 1,1,1-tris[(diphenyl- phosphino)methyl]ethane (triphos) to provide appropriate coordination around the copper center. Power and coworkers have structurally characterized mononuclear and dinuclear organocopper compounds of formula $[\text{CuR}\cdot\text{Solvate}]_1 \text{ or } 2$ using dimethylsulfide.²⁷ Due to the presence of sterically demanding ortho substituents on the aryl ligand of both mononuclear $[\text{Me}_2\text{SCu}(\text{C}_6\text{H}_2\text{-}2,4,6\text{-}t\text{-Bu}_3)]$ (11) and dinuclear complex $[(\text{Me}_2\text{S})_2\text{Cu}(\text{C}_6\text{H}_2\text{-}2,4,6\text{-Ph}_3)_2]$, formation of higher aggregates was highly unlikely.

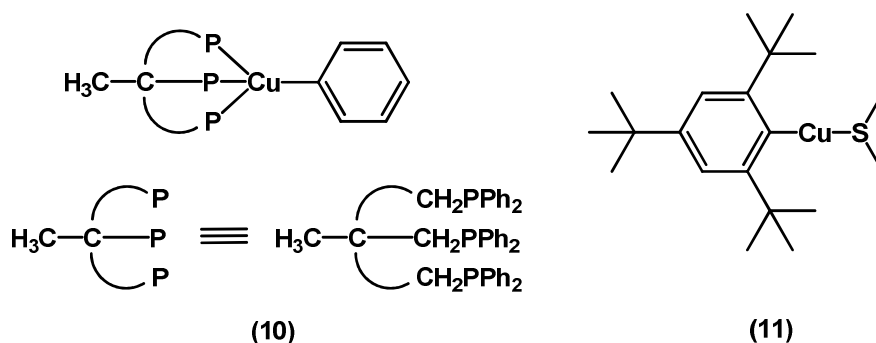
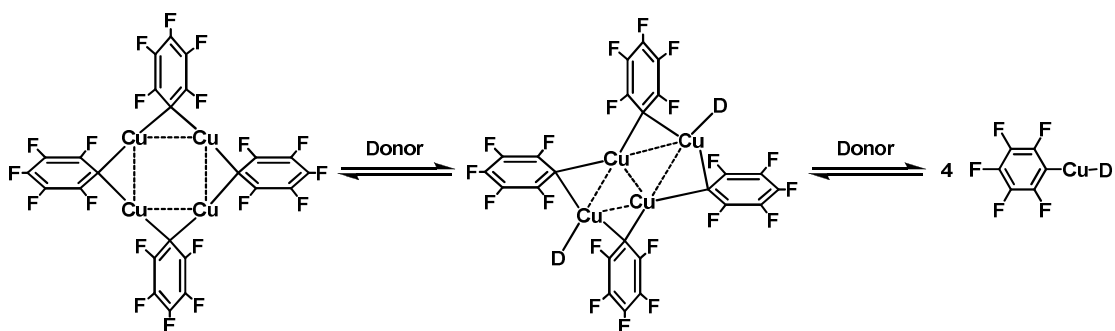


Chart 2.3 Examples of Arylcopper Compounds Stabilized by P and S Donor Ligands.

2.3.1 σ -Complexes of Pentafluorophenylcopper

The pronounced ability of pentafluorophenylcopper to form complexes with σ -donor ligands has been recognized by Cairncross and Sheppard. They reported that dioxane, quinoline, tributylamine as well as tetraethylammonium cyanide coordinate to the $(\text{C}_6\text{F}_5\text{Cu})_4$ tetramer.²⁸ However, no crystallographic evidence was reported for these complexes and no further studies on their properties were performed.

Jäkle and co-workers have recently reported that ^{19}F and ^{13}C NMR spectroscopy can be used to study the structural properties of pentafluorophenylcopper in solution. They have shown that the difference between the ^{19}F NMR chemical shifts for the *para* and *meta* fluorine atoms, $\Delta\delta_{m,p}$, a downfield shift of C_{ipso} , and an increase in the coupling constant of the *ipso*-carbon atom with fluorine, $^2J(^{13}\text{C}_{ipso}, ^{19}\text{F})$, in donor solvents are indicative of changes in the coordination environment of the copper centers (Scheme 2.2).²⁹



Scheme 2.2 Proposed Structures Involved in the Complexation of Pentafluorophenylcopper.

They demonstrated that, in the presence of excess donor, such as acetonitrile, DMSO or pyridine, the organocopper aggregate breaks down to form monomeric complexes. They further investigated the binding of pyridine to the pentafluorophenyl copper tetramer and examined the structure of the adduct by x-ray crystallography. Monomeric organocopper complex $\text{C}_6\text{F}_5\text{Cu}(\text{Py})$ (12) was synthesized by treatment of tetrameric pentafluorophenyl copper with an equimolar amount of pyridine (Figure 2.2 (a)). The solid state structure of the pyridine complex revealed a nearly linear coordination geometry with ($\text{C}-\text{Cu}-\text{N} = 178.54(6)^\circ$). The pentafluorophenyl groups and the pyridine rings are perfectly coplanar and the entire molecule resides on a crystallographic mirror plane (Figure 2.2 (b)).

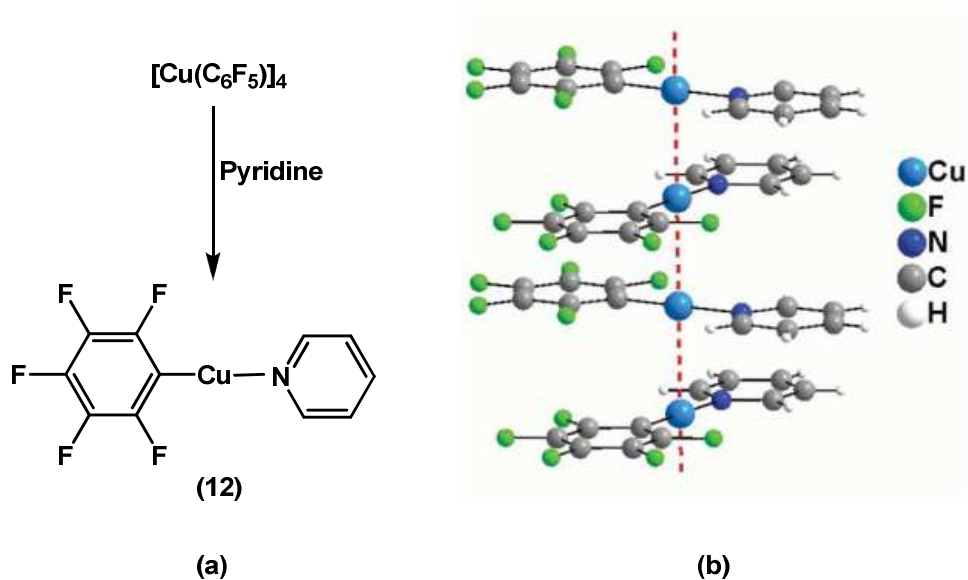


Figure 2.2 (a) Synthesis of (12); (b) Extended Structure of (12) Along the Crystallographic c-Axis; *Dalton Trans.*, 2007, 2851-2858; Reproduced with Permission of the Royal Society of Chemistry.

The extended structure of (12) shows that the ligands in adjacent RCuL units adopt a staggered conformation and hence do not undergo any π -stacking interactions. However, intriguingly, the copper atoms are arranged in one-dimensional chains with $\text{Cu}\cdots\text{Cu}$ distances of $2.8924(3) \text{ \AA}$, which are among the shortest reported for unsupported $\text{Cu(I)}\cdots\text{Cu(I)}$ contacts.²⁹ In contrast, the supramolecular structures of complexes of $\text{Zn}(\text{C}_6\text{F}_5)_2$ (13) are dominated by π -stacking interactions.³⁰ Pentafluorophenylsilver was isolated as a 1:1 adduct with EtCN. The crystal structure of $\text{AgC}_6\text{F}_5\cdot\text{EtCN}$ shows the

presence of both $[\text{Ag}(\text{C}_6\text{F}_5)_2]^-$ (14) and $[\text{Ag}(\text{EtCN})_2(\text{C}_6\text{F}_5)_2]^-$ (15) units in the crystal lattice with an infinite Ag-Ag chain (Ag-Ag 2.82 Å).³¹

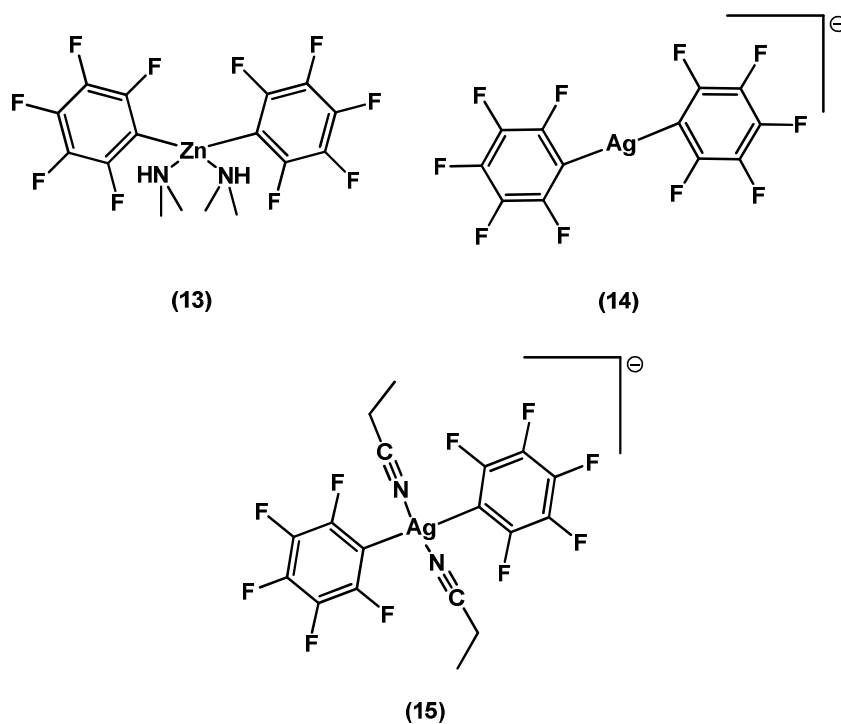


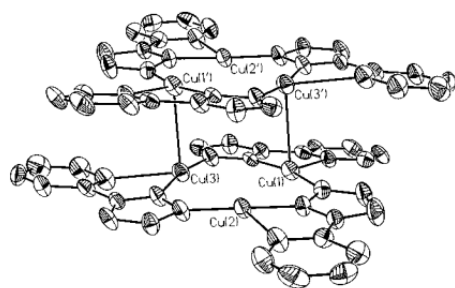
Chart 2.4 Examples of Pentafluorophenylzinc and Pentafluorophenylsilver.

2.4 Cuprophilicity

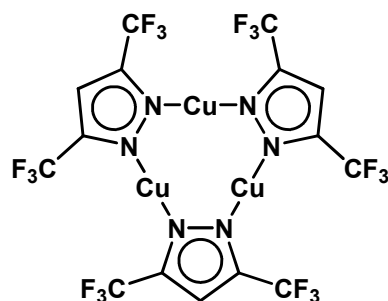
Polynuclear coinage-metal complexes are known to form fascinating supramolecular structures with unusual luminescence behavior.³²⁻³⁶ Many of their exciting properties originate from a pronounced tendency for formation of stacks through metallophilic

interactions.³⁷⁻³⁹ These attractive interactions that exist between d^{10} “closed-shell” elements of Group 11 have received extensive attention. Auophilic interactions, the attractive forces between closed-shell d^{10} metal ions of gold, have long been recognized. The term “auophilicity” has been introduced to describe the $Au^{1\cdots}Au^1$ bonding interactions that are apparent in many molecular and solid-state structures. They have been attributed to the ligand-induced⁴⁰ and relativistically-supported⁴¹ contraction of the 6s orbital which then favorably mix with 5d states to effectively reduce the population of the 5d valence shell. The question whether a similar metallophilicity exists for the other two coinage metals, copper and silver, is still a matter of controversy. Based on MP2 calculations Schwerdtfeger *et al.* determined that cuprophilic interactions between neutral pairs $[RCuL]_2$ should be attractive by up to -4 kcal mol^{-1} , and are therefore approximately three times weaker than auophilic interactions.⁴²⁻⁴⁴ Only a few examples of ligand-unsupported Cu^1 aggregates have been described in literature. For instance, Singh *et al.* reported pyrazolate substituted dimer of trimers $[Cu_3(2-(3(5)\text{-pz})py)_3]_2$ (16).⁴⁵ The structure of (16) reveals two virtually planar triangular copper units coupled via two $Cu\cdots Cu$ interactions ($Cu\cdots Cu = 2.905(3) \text{ \AA}$). The triangle of copper atoms is nearly equilateral; with $Cu\cdots Cu$ distances around $3.52(5) \text{ \AA}$. The authors claim that the deviation of the Cu atoms from the plane (Cu(1) 0.27 \AA , Cu(2) 0.08 \AA , Cu(3) 0.19 \AA) is clear evidence of the attractive nature of the $Cu\cdots Cu$ intertriangular interactions. Trimeric

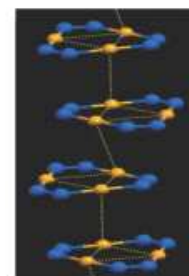
copper(I) pyrazolate (17) was reported by R. Dias and coworkers to show weak closed-shell cuprophilic interactions in the electronic ground state, which are enhanced in the emissive excited states contributing towards its bright luminescence bands.³⁶ The non-bonding intramolecular Cu \cdots Cu separations range from 3.221 to 3.242 Å. The shortest distance between copper atoms of neighboring trimers is 3.879 Å. These distances are however much longer than the sum of the van der Waals radii (2.80 Å). In comparison, the non-fluorinated analog {[3,5-(CH₃)₂Pz]Cu}₃ forms weakly linked pairs of trimers with much shorter Cu \cdots Cu contacts (average = 2.946 Å).



(16)



(17A)



(17B)

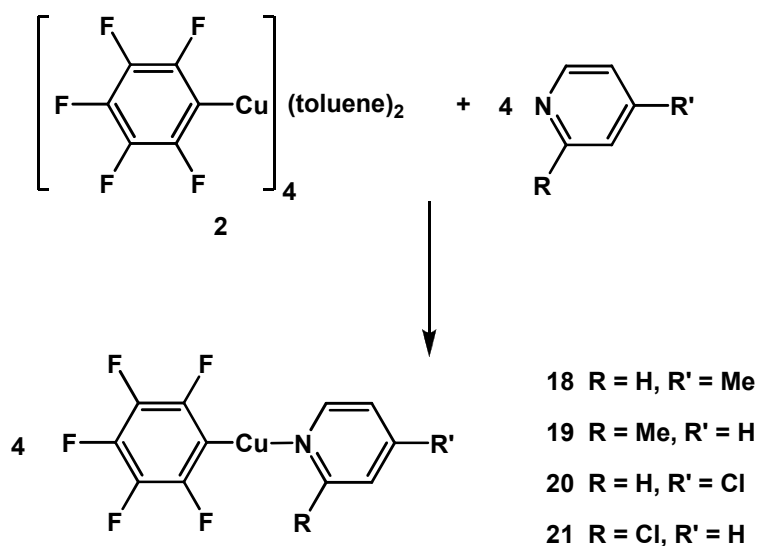
Chart 2.5 Examples of Trimeric Copper(I) Complexes; (16) Reprinted in part with permission from *J. Am. Chem. Soc.*, 1999, 119, 2942-2943, Copyright 1999 American Chemical Society; (17A and 17B) Reprinted in part with Permission from *J. Am. Chem. Soc.*, 2005, 127, 7847-7501, Copyright 2005 American Chemical Society.

2.5 Pentafluorophenylcopper(I) Pyridine Complexes

Previously we have shown that coordination of pyridine and 4,4'-bipyridine results in complete breakdown of the tetrameric structure of (8).²⁹ The cuprophilic and multiple perfluoroarene–arene interactions in turn lead to the formation of novel supramolecular structures. The monomeric copper(I) complex (12) shows intense blue luminescence in the solid state, the origin of which is still under investigation. The aim of this project was to incorporate electron donating and electron withdrawing substituents on various positions of the pyridine ring and investigate the effects of substitution on the structural and photophysical properties of the copper-pyridine complexes.

2.5.1 Synthesis

$[\text{C}_6\text{F}_5\text{Cu}]_4(\text{toluene})_2$ (9) was treated at ambient temperature in toluene or CH_2Cl_2 with an excess of the pyridine ligand under investigation (Scheme 2.3). Needle-like colorless to pale yellow crystals of the complexes $\text{C}_6\text{F}_5\text{Cu}(\text{Py}^*)$ were obtained by crystallization at $-35\text{ }^\circ\text{C}$ (18-21). The complexes are stable at low temperature ($-20\text{ }^\circ\text{C}$) under nitrogen atmosphere for extended periods of time, but they decompose with the formation of a green precipitate upon exposure to air. All the complexes are thermally stable upto $150\text{ }^\circ\text{C}$. The complexes are readily soluble in both polar and non-polar aprotic solvents.



Scheme 2.3 Preparation of Pentafluorophenylcopper(I) Pyridine Complexes.

2.5.2 Structures in Solution

Coordination of pyridine to copper in complexes (18-21) was confirmed by ^1H , ^{19}F and ^{13}C NMR spectroscopy, single crystal x-ray diffraction, and elemental analysis. As discussed in section 2.3.1, we have previously shown that coordination of nucleophiles to tetrameric pentafluorophenylcopper (8) leads to break-down of the aggregate to give a monomeric species which is, for example, reflected in a strong decrease in the chemical shift difference $\Delta\delta$ ($^{19}\text{F}_{m,p}$) in the ^{19}F NMR spectra.²⁹

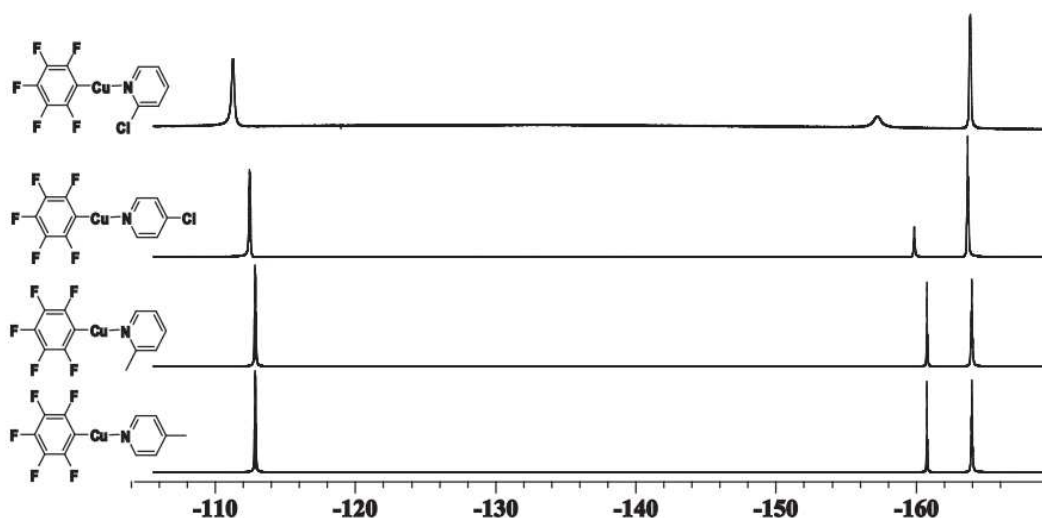


Figure 2.3 ^{19}F NMR spectra of compounds (18-21) in CDCl_3 at 25 $^\circ\text{C}$.

Complexes (18-20) show a strong decrease of $\Delta\delta$ ($^{19}\text{F}_{m,p}$) from 16.6 ppm to ~ 3.3 ppm (Figure 2.3), which is in agreement with breakdown of the tetrameric aggregate and formation of monomeric pyridine complexes (Table 2.1). However, the 2-chloro substituted pyridine complex (21) shows a distinctly larger $\Delta\delta$ ($^{19}\text{F}_{m,p}$) of 6.6 ppm, which indicates that, in solution, pyridine (partially) dissociates from the monomeric complex, possibly leading to higher aggregates. The latter is also evident from the chemical shift of the *ipso*-C atom of the C_6F_5 group ($\delta = 115$ ppm), which is between those of complexes (18-20) (δ in the range of 121.3 to 122.8) and that of the base-free tetramer (8) ($\delta = 98.7$). Further evidence comes from the relative small coupling constant 2J ($^{13}\text{C}_i$, ^{19}F) of 67 Hz. Strong broadening of the ^{19}F NMR signals for the compound (21) at room temperature

further indicates the presence of a dynamic equilibrium. However, this effect may also be due to hindered rotation due to the sterically demanding chlorine substituent. Nonetheless, a dissociation equilibrium is further supported by the observation of a concentration effect on the ^{19}F NMR spectra of (21), where $\Delta\delta (^{19}\text{F}_{m,p})$ increases with increasing concentration. Variable temperature ^{19}F NMR data for compound (21) were acquired at temperatures ranging from $-50\text{ }^{\circ}\text{C}$ to $+30\text{ }^{\circ}\text{C}$. Further broadening of the signals was observed at low temperature. In contrast, low temperature NMR spectroscopy of complexes (18-20) showed no evidence of a dynamic process down to $-50\text{ }^{\circ}\text{C}$.

Table 2.1 Comparison of ^{19}F and selected ^{13}C NMR data^a.

	$\Delta\delta (^{19}\text{F}_{m,p})$	$\delta(^{13}\text{C}_i)$	$^2J(^{13}\text{C}_i, ^{19}\text{F})$
$[\text{C}_6\text{F}_5\text{Cu}]_4(\text{tol})_2$ (9)	16.6	98.7	52
4-MePy-Cu C_6F_5 (18)	3.2	122.2	72
2-MePy-Cu C_6F_5 (19)	3.1	122.8	71
4-ClPy-Cu C_6F_5 (20)	3.8	121.3	75
2-ClPy-Cu C_6F_5 (21)	6.6	115.0	67

^aData were acquired in CDCl_3 at $25\text{ }^{\circ}\text{C}$ (ca. $1.8 \times 10^{-1}\text{ M}$).

2.5.3 Solid-State Structures of (18-21)

Single crystals of (19) and (21) were obtained via slow solvent evaporation from a mixture of toluene and hexanes, whereas needle-like crystals of (18) and (20) were obtained from the reaction mixture at low temperature. The solid state structures of complexes (18-21) have been investigated by x-ray diffraction analysis and plots are shown in Figure 2.4, 2.5, 2.6 and 2.7. The molecular structures of (18-21) confirm that mononuclear di-coordinated structures C_6F_5-Cu-L are present in the solid state with linear or nearly linear coordination geometry at copper (18: $177.88(8)^\circ$; 19: $174.66(8)^\circ$; 20: $176.34(7)^\circ$; 21: $176.19(11)^\circ/177.75(11)^\circ$).

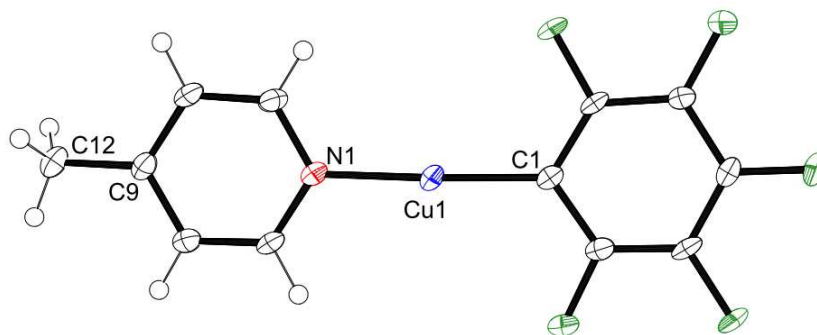


Figure 2.4 Molecular Structure of (18) (ORTEP, 50% probability). Selected Bond Lengths (Å) and Angles (deg): Cu1-C1 = 1.891(3), Cu1-N1 = 1.900(2), C9-C12 = 1.500(4), C1-Cu1-N1 = 177.9(1), (Py) // (Pf) = 2.89.

The Cu-C bonds of all complexes are within a narrow range from 1.887(2) to 1.901(3) Å, and thus considerably shorter than those found for the tetramer (8) (1.962(2) to 2.007(2) Å), which shows bridging rather than terminal aryl groups. These distances are similar to those of other dicoordinate organocopper-ligand complexes such as [(C₆H₂-2,4,6-*t*-Bu₃)Cu(Me₂S)]⁴⁶ with Cu-C = 1.886(3) Å, N-heterocyclic (carbene)copper (I) complexes (1.887(5) Å)⁴⁷, and a related dimeric complex containing a chelating oxazolinyl group (Cu-C = 1.899(5) Å).⁴⁸ The copper–nitrogen distances ((18): 1.900(2) Å; (19): 1.907(2) Å; (20): 1.897(2) Å, (21): 1.909(2) and 1.917(2) Å), are comparable to those in the oxazolinyl complex (Cu-N 1.902(4) Å)⁴⁸ and a related dimeric pyridylalkyl species [2-(SiMe₃)₂C(Cu)C₅H₄N]₂⁴⁹ with Cu-N = 1.910(3) Å. They are, however, slightly longer than that in the monomeric carbene copper(I) anilido complex, IPr-Cu-NHPh, (IPr = 1,3-Bis(2,6-diisopropylphenyl)imidazol-2-ylidene) with Cu1-N1 = 1.841(2) Å.⁵⁰

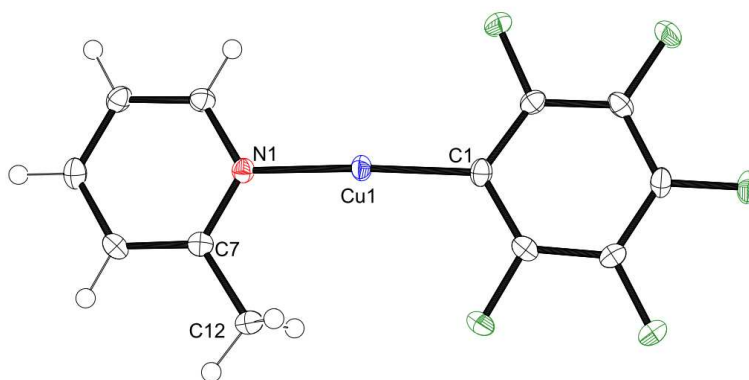


Figure 2.5 Molecular Structure of (19) (ORTEP, 50% probability). Selected Bond Lengths (Å) and Angles (deg): Cu1-C1 = 1.897(2), Cu1-N1 = 1.908(2), C7-C12 = 1.497(3), C1-Cu1-N1 = 174.65(8), (Py) // (Pf) = 5.32.

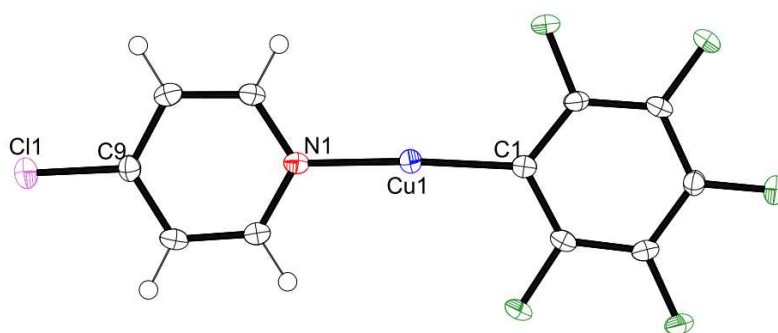


Figure 2.6 Molecular Structure of (20) (ORTEP, 50% probability). Selected Bond Lengths (Å) and Angles (deg): Cu1-C1 = 1.887(2), Cu1-N1 = 1.897(2), C9-C11 = 1.721(2), C1-Cu1-N1 = 176.33(7), (Py) // (Pf) = 2.34.

Interesting to note is also that the Cu-N bond lengths for the two independent molecules of (21) are slightly longer than those in the other complexes suggesting weaker coordination of the pyridine ligand to Cu. The latter is consistent with the conclusions drawn from the solution NMR studies on (21). The pentafluorophenyl groups and the pyridine rings are coplanar for $\text{C}_6\text{F}_5\text{Cu}(\text{Py})$ and nearly so for (18) (2.89°) and (20) (2.34°); however, large dihedral angles of 43.12° and 44.21° , respectively, were observed for the two independent molecules in complex (21). The latter is attributed to the high steric demand of the chloro substituent in 2-position of the pyridine ring. Interestingly, the methyl group in 2-position of (19) leads to only a slight twisting of the two aromatic rings of 5.32° .

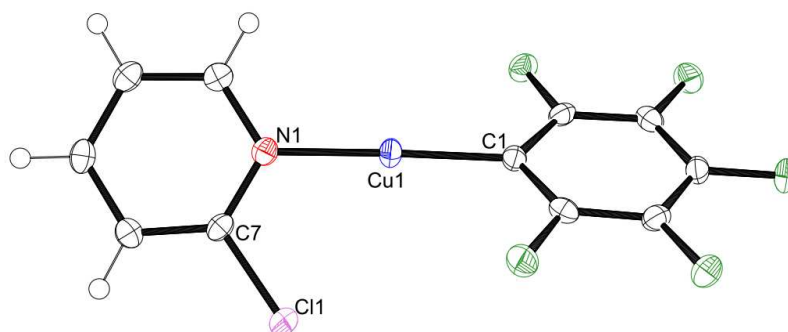


Figure 2.7 Molecular Structure of (21) (ORTEP, 50% probability). Selected Bond Lengths (\AA) and Angles (deg): $\text{Cu1-C1} = 1.902(3)$, $\text{Cu1-N1} = 1.917(2)$, $\text{C7-Cl1} = 1.726(3)$, $\text{C1-Cu1-N1} = 177.75(11)$, $(\text{Py}) // (\text{Pf}) = 44.21$.

Table 2.2 Comparison of Selected Bond Lengths [Å], Distances [Å], and Angles [°]^a.

	(12)	(18)	(19)	(20)	(21)	
					21-A	21-B
Cu1-C1	1.8913(17)	1.891(3)	1.8963(19)	1.8873(19)	1.901(3)	1.898(3)
Cu1-N1	1.9022(15)	1.900(2)	1.9072(16)	1.8972(16)	1.917(2)	1.909(2)
N1-C7	1.356(2)	1.352(3)	1.353(3)	1.354(2)	1.338(4)	1.340(4)
N1-C11	1.346(2)	1.345(3)	1.351(3)	1.345(2)	1.349(4)	1.349(4)
C-X (X=Cl, CH ₃)	---	1.501(4)	1.498(3)	1.7212(18)	1.727(3)	1.723(3)
C1-Cu1-N1	178.54(6)	177.88(8)	174.66(8)	176.34(7)	177.75(11)	176.19(11)
Py // Pf	0.0	2.89	5.32	2.34	44.21	43.12
Cu1...Cu1A	2.8924(3)	3.531(1)	3.245(0)	3.521(1)	3.480(1)	
Cu1A...Cu1B	2.8924(3)	3.698(1)	4.298(0)	3.784(1)	3.836(1)	
C1-Cu1...Cu1A	89.900(5)	95.89(7)	92.56(7)	98.83(5)	100.14(9) / 101.01(9)	
C1-Cu1...Cu1B	89.900(5)	83.27(7)	89.42(7)	77.94(5)	103.85(9) / 103.00(9)	
C1A-Cu1A...Cu1B	90.00	96.32(7)	91.44(7)	100.54(5)	90.40(9) / 92.45(8)	
N1-Cu1...Cu1A	90.097(5)	85.24(7)	92.69(5)	82.50(4)	80.31(7) / 75.55(7)	
N1-Cu1...Cu1B	90.097(5)	95.46(7)	85.23(5)	100.21(4)	75.59(7) / 80.53(7)	
N1A-Cu1A...Cu1B	90.00	84.88(7)	93.89(5)	81.07(7)	93.08(7) / 87.04(7)	
C7-N1-Cu1...Cu1B	90.00	65.79(20)	60.73(14)	115.12(14)	-109.82(20)	-109.98(20)
C11-N1-Cu1...Cu1B	90.00	112.49(19)	-119.27(15)	-62.23(14)	72.85(20)	70.33(20)
C2-C1-Cu1...Cu1B	90.00	-117.29(21)	122.00(18)	-119.67(16)	-116.40(23)	-113.80(22)
C6-C1-Cu1...Cu1B	90.00	65.26(20)	-58.19(16)	63.10(14)	63.35(23)	68.76(24)
Cu1A...Cu1...Cu1B	179.716(15)	175.16(1)	168.22(1)	170.54(1)	155.80(2)	

^aSymmetry operations used to generate equivalent Cu atoms for (18): (i) $-x + 1, -y + 1, -z$; (ii) $-x + 1, -y + 2, -z$; (iii) $x, 1 + y, z$. For (19): (i) $-x + 2, -y, -z + 1$; (ii) $-x + 2, -y + 1, -z + 1$; (iii) $x, 1 + y, z$. For (20): (i) $-x + 2, -y + 1, -z + 1$; (ii) $-x + 2, -y, -z + 1$; (iii) $x, y - 1, z$. For (21): (i) $x - 1, y, z$; (ii) $x - 1, y - 1, z$; (iii) $1 + x, 1 + y, z$; (iv) $1 + x, y, z$; (v) $x, y - 1, z$; (vi) $x, 1 + y, z$.

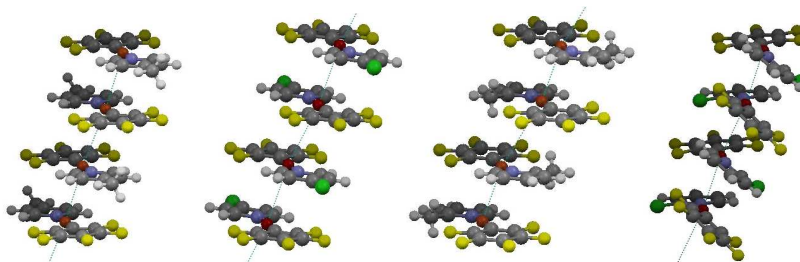
2.5.4 Supramolecular Structures

Further analysis of the extended structures shows that all complexes form chains of Cu atoms that progress throughout the entire crystal lattice. However, the stacking direction, and thus the orientation of the chains, as well as the Cu \cdots Cu separations vary considerably. The parent compound (12), which crystallizes in the P_{bcm} space group, shows a very unusual structure in that all atoms, including the hydrogen atoms reside on a crystallographic mirror plane.²⁹ Consequently, all copper atoms are equidistant and the stacking direction is perpendicular to the plane of the molecules.

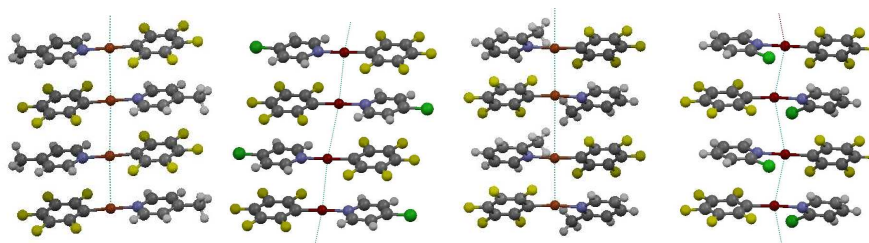
In sharp contrast, compounds (18-21) form stacks that progress along the crystallographic b -axis with the RCuL monomers aligned in such a way that the C₆F₅ groups undergo π -stacking interactions with the pyridyl moieties of the adjacent molecules and *vice versa* (Figure 2.8). In each stack, the successive molecules adopt an eclipsed rather than staggered arrangement and are offset so that the resulting stacks are tilted by an angle $\alpha = 23.9^\circ$ for (18), 26.8° for (19), 24.7° for (20) and 21.2° for (21), which results from lateral slippage of the aromatic groups, a phenomenon that is commonly encountered for stacks involving perfluoroarene-arene interactions.^{39, 51-54} The tilt angle was measured using the vector perpendicular to the plane containing pentafluorophenyl ring. The Cu \cdots Cu contacts between adjacent molecules alternate, thereby leading to formation of dimers with relatively short Cu \cdots Cu contacts of 3.245 to

3.531 Å that are in turn connected through longer Cu \cdots Cu contacts ranging from 3.698 to 4.297 Å to form the infinite Cu chains. The alternation is most pronounced for (19) with Cu \cdots Cu distances of 3.245 and 4.297 Å, respectively. Interesting is that relatively short contacts of 3.245 Å are observed for the 2-methyl substituted derivative, for which the individual molecules also show the largest deviation from linear coordination geometry at copper (C1-Cu1-N1 174.66(8)°).

(a) View sideways: (18-21)



(b) Along the crystallographic a-axis: 4-Me, 4-Cl, 2-Me; along the crystallographic c axis: 2-Cl:



(c) Space filling illustration of the tilting of the stacks:

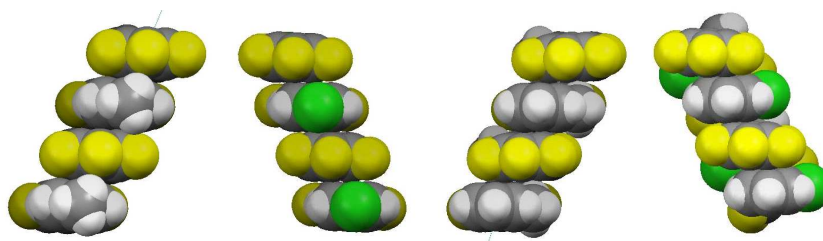


Figure 2.8 Plots of the Extended Structures of (18-21).

Formation of zigzag chains is evident for complexes (18-21), an effect that is most pronounced for (18) as apparent from a relatively small angle $\text{Cu1}\cdots\text{Cu1A}\cdots\text{Cu1B}$ of $155.79(2)^\circ$. The latter is likely related to the presence of the sterically demanding 2-chloro-substituent in (21), which also leads to tilting of the pyridyl and C_6F_5 groups with respect to each other. Unlike the parent pyridine complex, the substituted pyridine complexes show pentafluoroarene-arene π -stacking interactions, which seem to dominate over cuprophilic interactions and thus most likely ultimately determine the $\text{Cu}\cdots\text{Cu}$ separations³⁸, particularly in the case of (19), which shows “dimers” with relatively short $\text{Cu}\cdots\text{Cu}$ distances of 3.245 Å. For complexes (18-21) the supramolecular assembly is therefore certainly to a large extent governed by perfluoroarene-arene π -stacking interactions.

2.6 π -Complexes of Organocopper Compounds

An interesting motif of the polynuclear coinage metal complexes is that of binary structures, where they can act either as π -acids or π -bases toward arenes. For instance, stacking of trinuclear silver(I) pyrazolates $[[[3,5-(\text{CF}_3)_2\text{pz}]\text{Ag}]_3]$ (pz = pyrazolate) with electron rich arenes (benzene, mesitylene, and toluene) has been demonstrated (22).⁵⁵ These compounds represent rare silver(I) complexes featuring fluorinated pyrazolates and they tend to aggregate via intertrimer $\text{Ag}\cdots\text{Ag}$ contacts. The isolation of sandwich molecules with tight face-to-face contacts between toluene and $[[[3,5-(\text{CF}_3)_2\text{pz}]\text{Ag}]_3]$ points to the high π -acidic nature of the pyrazolate complex.⁵⁶ Recently Gabbai and coworkers reported that the trimeric organomercury species $[(\text{o-C}_6\text{F}_4)\text{Hg}]_3$ also forms one-dimensional stacks with arenes such as, biphenyl, triphenylene, naphthalene, acenaphthalene, anthracene and pyrene (23).^{57, 58} They found that these compounds form interesting supramolecular assemblies due to strong Hg-Hg interactions and secondary polyhapto- π interactions occurring between the electron-rich aromatic molecules and acidic mercury centers. These compounds also show intriguing photoluminescent properties in the solid state, which have been attributed to the occurrence of a mercury heavy atom effect. Fluorination of the ligand is a key feature that supports the π -acid properties of these metal complexes. The reverse situation is encountered with electron-rich trinuclear gold complexes such as $[(\text{p-tolN}=\text{COEt})\text{Au}]_3$, which act as π -basic

substrates toward electron-poor arenes.⁵⁹ For instance, this nucleophilic trinuclear Au(I) compound forms a 1:1 supramolecular stack with the organic Lewis acid octafluoronaphthalene ($C_{10}F_8$), in which the $Au_3(p\text{-tolN=COEt})_3$ molecules alternate with the octafluoronaphthalene (24). In addition, the adduct also shows bright phosphorescent emission in the solid state at room temperature and has potential application in molecular device materials. In yet another twist, cyclic Au_3 π -basic compounds $[Au(\mu\text{-}C^2, N^3\text{-bzim})]_3$ (bzim) 1-benzylimidazolate), and $[Au(\mu\text{-}C, N\text{-}C(OEt)=N\text{-}C_6H_4\text{-}CH_3)]_3$, have been shown to form alternating stacks with the trinuclear π -acid $[(o\text{-}C_6F_4)Hg]_3$.⁶⁰

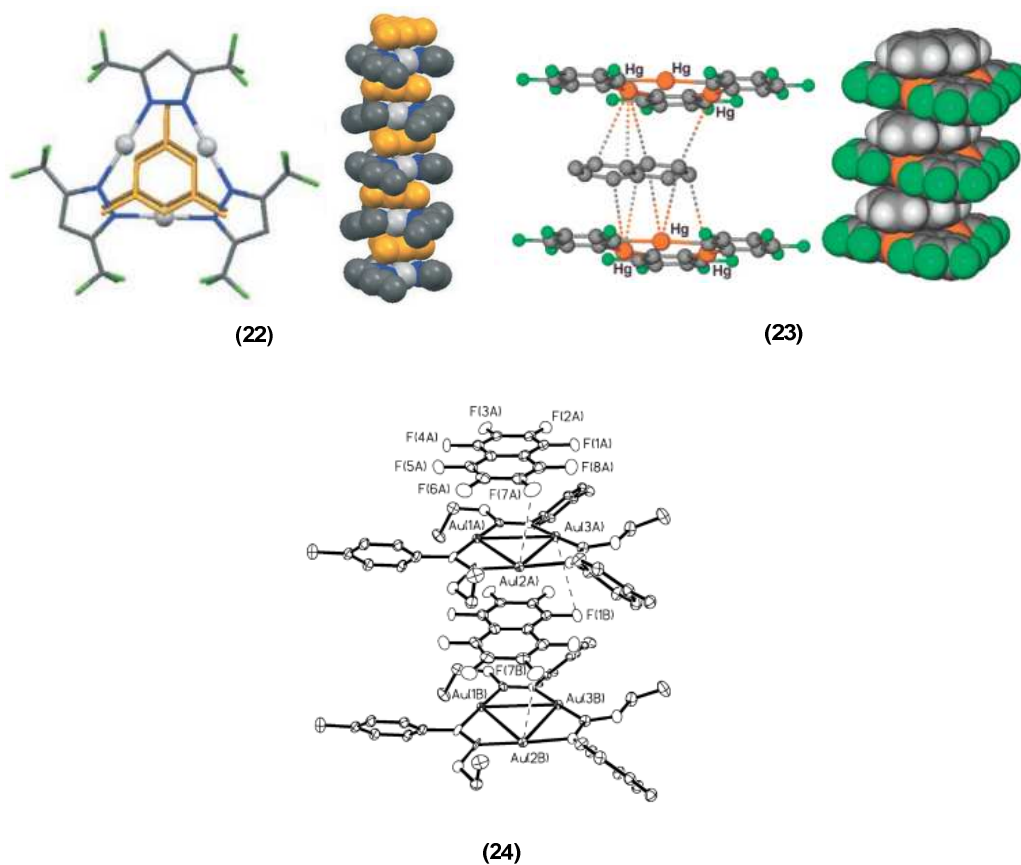
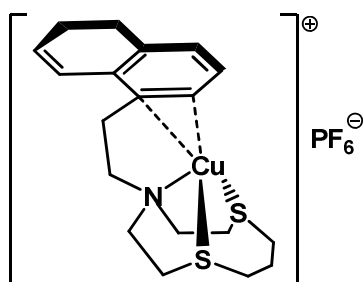


Chart 2.6 Examples of π -complexes; (22) Reprinted in part with permission from *Angew. Chem. Int. Ed.*, 2007, 46, 2192-2194, Copyright 2007 Wiley-VCH Verlag GmbH&Co. KGaA.; (23) Reprinted in part with permission from *Inorg. Chem.*, 2007, 46, 1388-1395, Copyright 2007 American Chemical Society; (24) *Dalton Trans.*, 2005, 2597-2602, Reproduced with permission of the Royal Society of Chemistry.

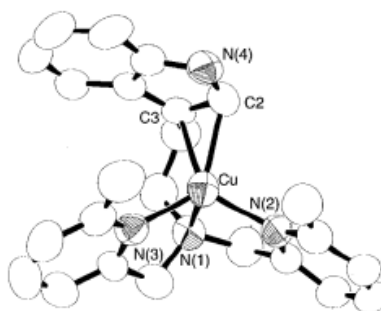
2.6.1 π -Complexes of Pentafluorophenylcopper

Copper(I) complexes with olefins and alkynes as ligands are very common. The 1:1 complex of pentafluorophenylcopper with dimethylacetylene and 2:1 complexes with butadiene and 1,5-cyclooctadiene were reported by Cairncross and Sheppard.¹⁷ However no structural studies were reported. π -Coordination of pentafluorophenylcopper to a diacetylene tweezer was reported by Lang *et al.*, who prepared the complex $\{[\text{Ti}](\text{CCSiMe}_3)_2\}\text{CuC}_6\text{F}_5$ ($[\text{Ti}] = (\eta^5\text{-C}_5\text{H}_4\text{SiMe}_3)_2\text{Ti}$) using a titanium thiolate precursor and pentafluorophenyl lithium.⁶¹ A variety of arene π -complexes of copper(I) salts such as $[\text{Cu}(\text{benzene})]\text{AlCl}_4$ ⁶² $[\text{Cu}(\text{benzene})_{0.5}]\text{triflate}$ ⁶³, $[\text{Cu}(\text{benzene})]_2\text{ZrCl}_6$ ⁶⁴, and paracyclophane complex $\{[\text{Cu}(p\text{-C}_6\text{H}_4\text{CH}_2\text{CH}_2\text{CH}_2)_2]\text{GaCl}_4\}_n$ ⁶⁵ have also been reported. All three complexes are polymeric in the solid state and exhibit an η^2 -binding mode of the benzene ring to copper(I). Moreover several cationic copper(I) complexes in which π -interaction between copper and an aromatic group is supported by chelation have been described.^{66, 67} For instance, Conry and coworkers synthesized and structurally characterized the copper-arene complex (25), which features an η^2 -bound naphthalene using a new NS_2 -macrocyclic ligand with a pendant naphthyl group.⁶⁸ Yamauchi and coworkers synthesized copper(I) complexes with an indole and pyridine based tridentate ligand N-(3-indolyethyl)-N,N-bis(6-methyl-2-pyridylmethyl)amine (Me_2IEP) (26).⁶⁹ The

Cu(I) complexes of indole-containing ligands have different structures that depend either on the side-chain length or the mobility of the indole ring.



(25)



(26)

Chart 2.7 Examples of Cu- π Complexes; (25) Reprinted in part with permission from *Organometallics*, 1998, 17, 3146-3148, Copyright 1998 American Chemical Society; (26) Reprinted in part with permission from *Angew. Chem. Int. Ed.*, 1999, 38, 2401-2403, Copyright 1999 Wiley-VCH Verlag GmbH&Co. KGaA.

2.6.2 Solid State Structure of $(\text{C}_6\text{F}_5\text{Cu})_4(\text{toluene})_2$ (9)

The solid state structure of (9) was characterized by x-ray crystallography and reported by Sundararaman *et al.*²⁴ As shown in Figure 2.9, both toluene molecules in $[\text{Cu}(\text{C}_6\text{F}_5)]_4(\eta^2\text{-toluene})_2$ are coordinated to opposite copper centers in an unsymmetrical η^2 -coordination mode. Unlike in (8), the four copper atoms in (9) do not lie in the same

plane but rather form an unusual butterfly structure with one short and one long diagonal Cu \cdots Cu distance of 2.5935(3) Å and 3.955(1) Å, respectively. The four Cu-Cu distances between adjacent copper atoms in (9) range from 2.4404(4) to 2.4729(4) Å and are only slightly longer than those in (8) with 2.4286(3)-2.4534(3) Å.

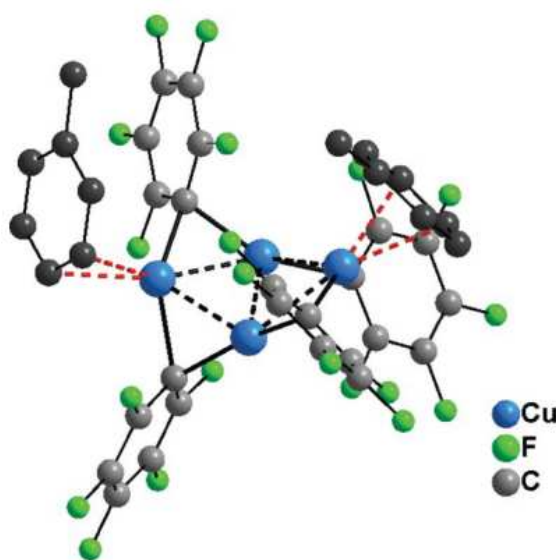


Figure 2.9 Molecular Structure of (9); *Dalton Trans.*, 2007, 2851-2858; Reproduced with Permission of the Royal Society of Chemistry.

2.7 Binary Stacks of Pentafluorophenylcopper with Arenes

We demonstrate here for the first time how multiple Cu \cdots π interactions can lead to luminescent supramolecular structures that feature an intact organocopper aggregate (8)

as the building block.⁷⁰ The ability of (8) to complex π -basic molecules such as naphthalene, bithiophene, anthracene and pyrene was investigated and it was shown that (8) and arenes form extended binary stacks in which the two components alternate.

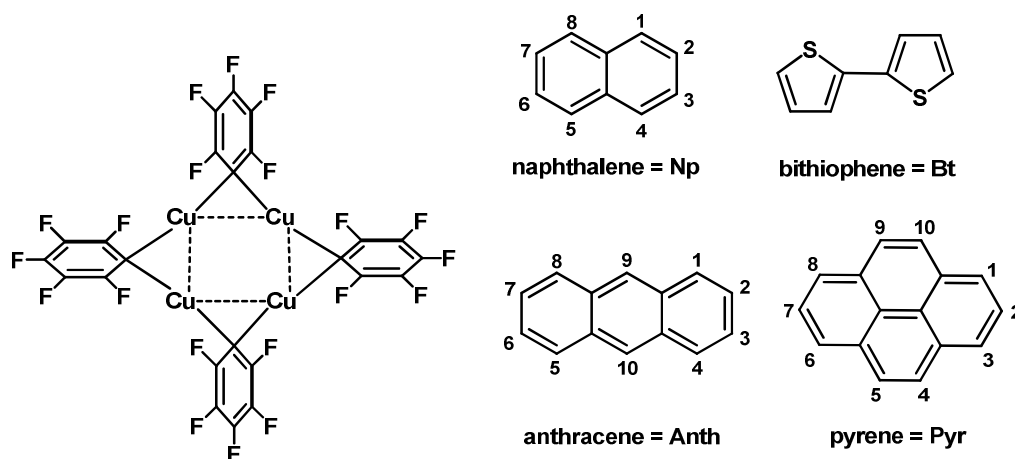
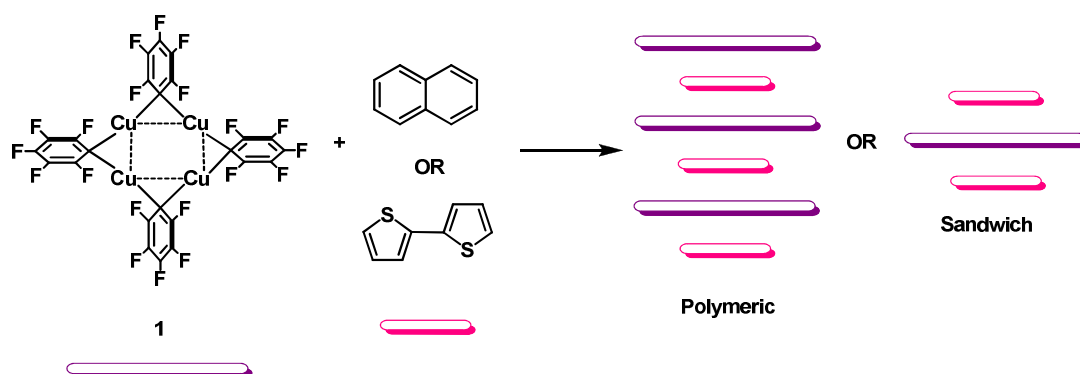


Chart 2.8 Pentafluorophenylcopper and Selected Arenes.

2.7.1 Synthesis of Complexes (27-33)

Treatment of (8) or (9) in CH_2Cl_2 with two equiv of naphthalene (Np) and 2,2'-bithiophene (Bt), respectively, and subsequent low temperature crystallization by careful layering with hexanes gave colorless crystals of the bis-adducts $8 \cdot (\text{arene})_2$ ((27), arene = Np; (28), arene = Bt) in high yields. The 1:1 complex $\{8 \cdot \text{arene}\}_n$ ((30), arene=Bt) was similarly obtained in 88% yield from a 1:1 mixture of (8) and Bt. However, the respective

complex with Np (29) could only be obtained in a mixture with the bis-adduct (27). Interestingly, treatment of (8) with either one or two equivalents of anthracene resulted in the same sandwich type complex $8\bullet(\text{Anth})_2$ (31) in 70% yield, formation of $\{8\bullet\text{Anth}\}_n$ was not observed. The 1:1 complex $\{8\bullet\text{arene}\}_n$ ((32), arene = Pyr) was obtained by the treatment of (8) with two equivalents of pyrene, while compound (33) with a stoichiometry of $(\text{C}_6\text{F}_5\text{Cu})_5\text{Pyr}_2$ was also obtained under similar conditions. However, we found that in these experiments the stoichiometry in the product did not necessarily correlate with the molar ratio of the starting materials. All compounds form colorless crystals, but the different adducts are easily distinguished since (27), (28) and (31) form needles, while (29), (30) and (33) gave plate-like crystals. Compound (32) was obtained as colorless blocks. Complexation was further confirmed by NMR spectroscopy, elemental analysis and x-ray diffraction studies. The ^1H and ^{19}F NMR spectra of the adducts in CDCl_3 show similar chemical shifts as the corresponding precursors, which not only confirms that both building blocks are incorporated into the products, but also suggests that dissociation takes place in solution.



Scheme 2.4 Schematic Representation of Different Types of π -Complexes.

2.7.2 Solid State Structures of Complexes (27-31)

Single crystal x-ray analyses were performed for all complexes and the structure plots are displayed in Figures 2.10, 2.11, 2.12 and 2.13. They reveal the formation of sandwich-like structures of the intact tetramer (8) and the corresponding arene in (27), (28) and (31) and the presence of one-dimensional binary stacks in (29) and (30). A different structure was found for (33), which will be discussed separately. For all structures, the four copper atoms of the $[\text{C}_6\text{F}_5\text{Cu}]_4$ building block form a rhombus-like geometry with one short (2.58-2.68 Å) and one long diagonal $\text{Cu}\cdots\text{Cu}$ distance (4.14-4.22 Å) (Table 2.3). This structural motif is similar to that found for other arylcopper donor complexes⁷¹ and contrasts the square planar arrangement typically observed for the respective base-free complexes, including that of (8). The Cu tetramer in (27), (28), (29) and (31) sits on a crystallographic inversion center, rendering the Cu atoms at opposite corners equivalent

and providing for a planar Cu₄ core. While the structure of (30) does not feature this inversion symmetry, the Cu₄ unit shows only a slight deviation from planarity with an interplanar angle of Cu1Cu2Cu4//Cu2Cu3Cu4 of 6.31° (cf. 37.53° for (9)). It is also interesting to note that the C-Cu-C angles for the arene-complexed Cu atoms are considerably wider than in (9) and the Cu atoms point toward the arene.

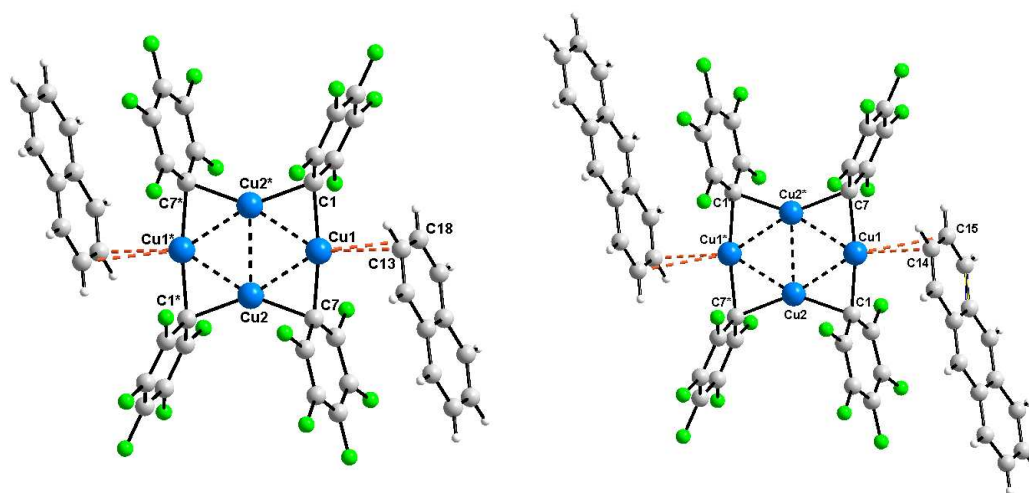


Figure 2.10 Plot of the Molecular Structure of (27) and (31). Symmetry operations used to generate equivalent atoms for (27): $-x + 2, -y + 1, -z + 1$. For (31): $-x + 1, -y, -z$ and $-x + 1, y - 0.5, -z + 0.5$.

Secondary Cu \cdots π interactions are observed for the sandwich-like structures, (27), (28) and (31). As for (9), the two copper atoms that are furthest apart from one another engage

in interactions with the arene molecules. The difference in the Cu \cdots C distances of 2.643(4) and 2.910(4) Å for (27) and 2.634(2) and 2.961(3) Å for (31) is reminiscent of the typical unsymmetric η^2 -binding of arenes to Cu(I). They are considerably longer than those observed for (9)²⁴ or other Np complexes of Cu(I) (2.129 to 2.414 Å).⁶⁷ They are, however, well within the sum of the van der Waal's radii for Cu ($r_{\text{vdw}} = 1.40$ Å) and C ($r_{\text{vdw}} = 1.70$ Å). Interestingly, the thiophene moiety in (28) is not bound through sulphur, but rather engages in π -interactions with slightly shorter Cu \cdots C distances in comparison to those observed for (27).^{67, 69, 72} The thiophene rings are slightly tilted with an interplanar angle of Th//Th = 8.32°.

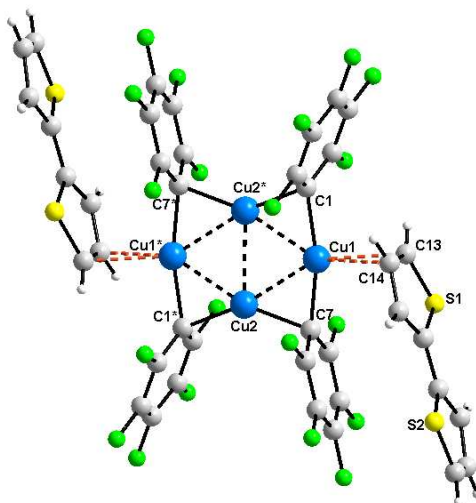


Figure 2.11 Plot of the Molecular Structure of (28). Symmetry operations used to generate equivalent atoms for (29): $-x + 1, -y + 1, -z$.

Table 2.3 Comparison of Selected Bond Lengths [Å], Distances [Å], and Angles [°]^a.

	8•(Tol) ₂	8•(Np) ₂	8•(Bt) ₂	8•(Anth) ₂	8•(Pyr) ₂	{8•Np} _n	{8•Bt} _n	{8•Pyr} _n
	(9)	(27)	(28)	(31)	(33)	(29)	(30)	(32)
Cu _{nb} ...Cu _{nb} ^d	2.594(1)	2.6343(11)	2.5866(6)	2.6159(7)	2.647(1)	2.6779(8)	2.6556(5)	2.656(2)
					2.696(1)			
Cu _b ...Cu _b ^d	3.955(0)	4.1796(11)	4.2220(6)	4.2069(5)	4.834(1)	4.1401(8)	4.1468(6)	3.979(1)
Cu _{nb} -C _{avg}	1.986	2.023	2.022	2.027	2.007	2.020	2.018	1.995
Cu _b -C _{avg}	2.092	1.998	1.995	1.990	2.044	1.990	2.010	2.083
C _{Pf} -Cu _{nb} -C _{Pf}	153.47(8)	140.8(2)	139.56(8)	140.63(9)	145.19(15)	142.66(11)	142.09(11)	159.52(10)
	155.94(8)				147.35(15)		143.55(10)	155.89(10)
					138.96(15)			
C _{Pf} -Cu _b -C _{Pf}	140.79(8)	167.7(2)	166.96(6)	167.38(10)	159.00(14)	169.48(11)	169.36(10)	141.09(9)
	140.98(8)				156.18(14)		159.61(11)	137.17(10)
Cu...C(π) ^c	2.271(3)	2.643(4)	2.507(2)	2.634(2)	2.379(4)	2.665(3)	2.5389(8) ^b	2.274(3)
	2.455(3)				2.389(4)			2.482(4)
	2.298(3)	2.910(4)	2.706(2)	2.961(3)	2.465(4)	2.815(3)	2.5356(7) ^b	2.323(3)
	2.339(3)							2.328(2)

^aCu_b / Cu_{nb}: bound / not bound to the arene; C_{Pf}: *ipso*-C of the C₆F₅ moiety. ^bCu...S distance; ^cCu...π: shortest Cu...C distance to arene; ^dSymmetry operations used to generate equivalent Cu atoms for (27): $-x + 2, -y + 1, -z + 1$; for (28): $-x + 1, -y + 1, z$; for (29) $-x + 1, -y + 2, -z + 2$; for (30): $-1 + x, y + 1, z$; for (31) $-x + 1, -y, -z$ and $-x + 1, y - 0.5, -z + 0.5$; for (32): (i) $-x + 1, -y, -z + 1$; (ii) $-x + 1, -y, -z$.

Intriguingly, the 1:1 complexes (29) and (30) form extended binary stacks in the solid state, where the intact tetramer (8) alternates with the arene. One of the aromatic rings of the Np and Bt moiety, respectively, interacts with the CuC_6F_5 group of one copper tetramer and the second ring shows short contacts to that of another tetramer (Figure 2.12, and 2.13), as a result these stacks are tilted with a tilt angle $\alpha = 36.9^\circ$ and 43.9° for (29) and (30), respectively.

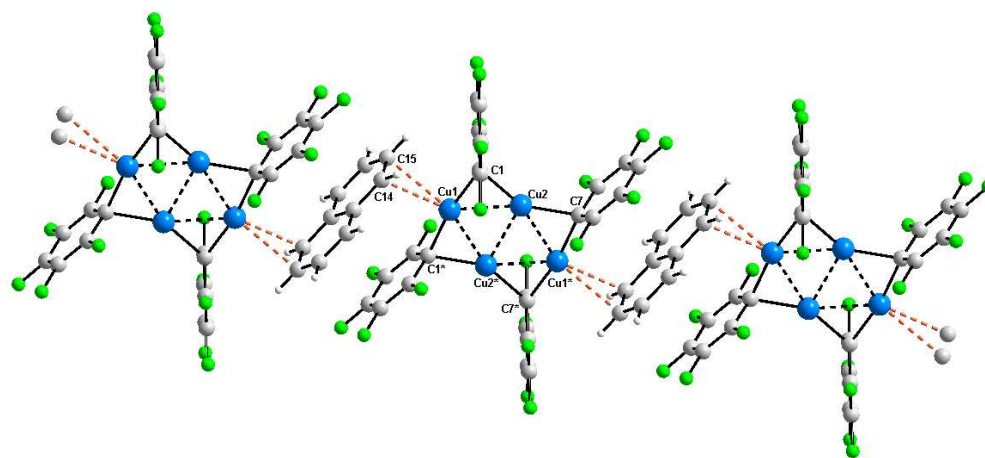


Figure 2.12 Plot of the Polymeric Structure of (29). Symmetry operations used to generate equivalent atoms for (29): $-x + 2, -y + 1, -z + 2$; $-x + 1, -y + 2, -z + 2$; $x - 1, y + 1, z$.

A comparison of the Cu $\cdots\pi$ interactions for (27) and (29) shows that the former binds through the 2,3-positions, while the latter forms short contacts to the 1,2-positions of naphthalene. Even more interestingly, Cu-S interactions lead to the extended structure of (30) in contrast to the Cu $\cdots\pi$ bonding motif of (28). The thiophene rings in (30) are non-equivalent and slightly twisted with respect to each other (Th//Th 7.76°). The sulfur atoms coordinate to copper with Cu-S distances of 2.5389(8) and 2.5356(7) Å, respectively, which are within the sum of the van der Waals radii for Cu ($r_{\text{vdw}} = 1.40$ Å) and S ($r_{\text{vdw}} = 1.80$ Å). The contacts are slightly longer than those reported in the literature for thioether adducts of organocopper tetramers (2.316 - 2.407 Å)^{9, 25, 73, 74}, which is to be expected based on the lower basicity of the thiophene S atom. In fact, there are very few known examples of thiophene coordinating to Cu(I) and the Cu \cdots S distances for (30) are the shortest reported to date.⁷⁵

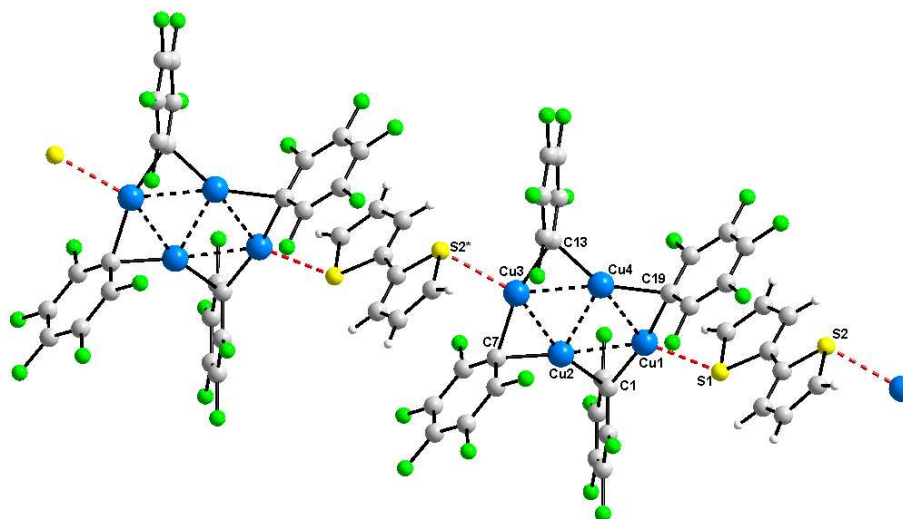


Figure 2.13 Plot of the Polymeric Structure of (30). Symmetry operations used to generate equivalent atoms for (30): $x - 1, y + 1, z$.

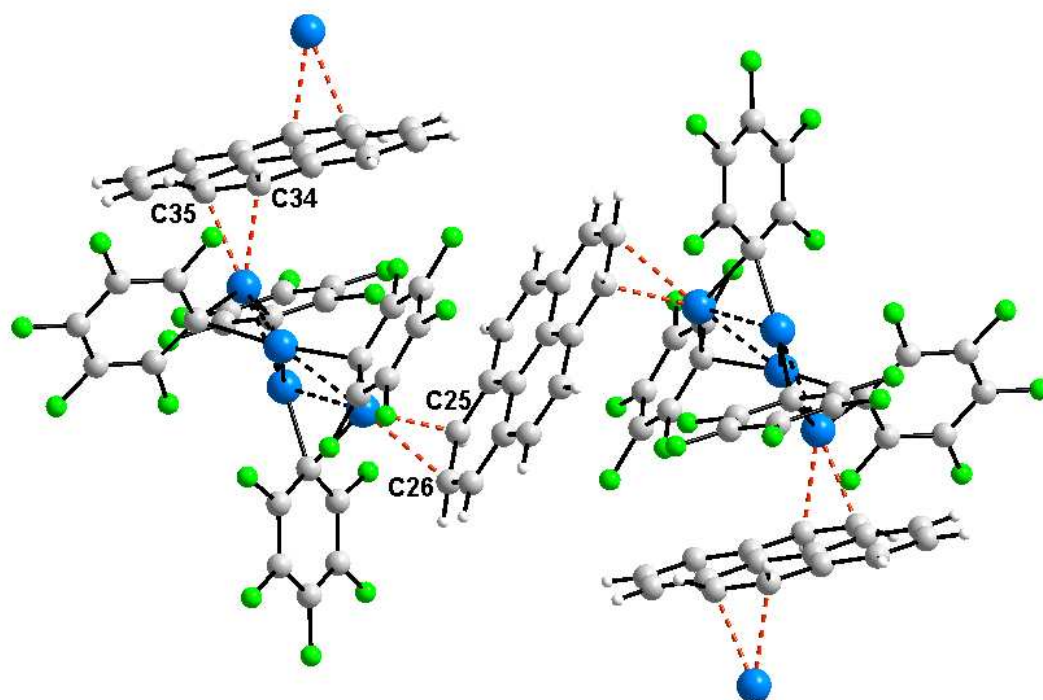
Arene binding in all cases is further supported by perfluoroarene-arene π -interactions^{39, 51-54, 76-79} with the shortest arene(centroid)···C contacts being 3.358, 3.270, 3.360, 3.332 and 3.378 Å to the Cu-bound *ipso*-carbon of the C₆F₅ groups for (27), (28), (29), (30) and (31) respectively. These distances are in the range typically associated with significant π -bonding interactions. Considerable ring slippage is evident from the longer centroid-centroid distances between the perfluorophenyl group and the naphthalene (3.732 Å in (27) and 3.599 Å in (29)), thiophene moiety (3.720 Å in (28) and 3.574/3.802 Å in (30)), and anthracene (3.829 Å in (31)) respectively.

2.7.3 Solid State Structures of (32) and (33)

In contrast to the extended stacks of (29) and (30), the 1:1 complex (32) forms a helical polymeric structure in the solid state, where the intact tetramer (8) alternates with pyrene. Unlike in (29) and (30) the Cu₄ core in (32) is highly puckered and forms a butterfly like structure with one short and one long diagonal Cu \cdots Cu distance of 2.656(2) Å and 3.979(1) Å, respectively, which is reminiscent of the toluene complex (9). The short Cu \cdots Cu distance in (32) is in a similar range as for (29) and (30) and is slightly longer than that in (9) (Cu \cdots Cu 2.5935(3) Å). On the other hand, the long diagonal Cu \cdots Cu distance of (32) is comparatively shorter than in (29) and (30). The angle between the (Cu1Cu2Cu3) and the (Cu1Cu4Cu3) planes of 34.89° is only slightly smaller than for the toluene complex (9) with 37.53° confirming a highly puckered Cu₄ core. Both pyrene molecules coordinate to the copper center in an unsymmetrical η^2 -fashion with short Cu \cdots C(π) distances. However, one of the pyrene coordinates through the 1,2-positions of the ring with Cu \cdots C distances of 2.274(3) and 2.482(4) Å, while another pyrene binds through the 9,10-positions of the ring with Cu \cdots C distances of 2.323(3) and 2.328(2) Å. These short Cu \cdots C(π) distances are similar to those for toluene complex (9), which is likely related to the butterfly arrangement of Cu₄ core. This can be traced back to very small angles at Cu (C_{Pf}-Cu_b-C_{Pf} = 137.17(10) and 141.09(9)° leading to more exposed Cu(I) centers. In complex (32), the Cu_b \cdots C_{avg} distances are slightly longer and Cu_{nb} \cdots C_{avg}

are slightly shorter than in complexes (27-31). However they are similar to the distances in (9), which again may be related to the highly puckered Cu_4C_4 core. In addition to the Cu- π interaction, pyrene binding is further supported by perfluoroarene-arene interaction with shortest pyrene(centroid)···C contacts of 3.310 Å. Related compounds with metal- π interactions have been reported by Petrukhina and coworkers, who showed that the highly Lewis acidic dirhodium tetrakis(trifluoroacetate) $\text{Rh}_2(\text{O}_2\text{CCF}_3)_4$ complex interacts with polycyclic aromatic hydrocarbons.⁸⁰ For instance, a pyrene-coordinated dirhodium complex exhibits a one-dimensional polymeric structure consisting of alternating metal complex and η^2 -coordinated pyrene.⁸¹ In contrast, in the heterobimetallic bismuth-rhodium tetracarboxylate complex $[\text{BiRh}(\text{O}_2\text{CCF}_3)_4 \bullet (\text{C}_{16}\text{H}_{10})]_\infty$ one pyrene shows η^6 -coordination to two bismuth center from two neighboring heterobimetallic units, while another pyrene binds in an η^2 -fashion to two different rhodium centers.⁸²

(a)



(b)

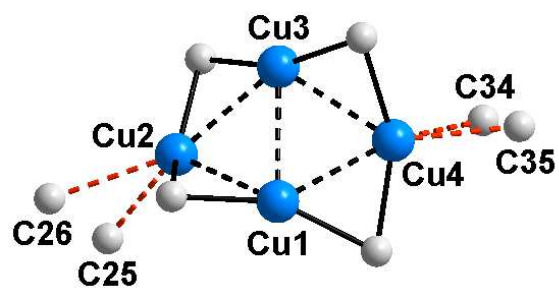
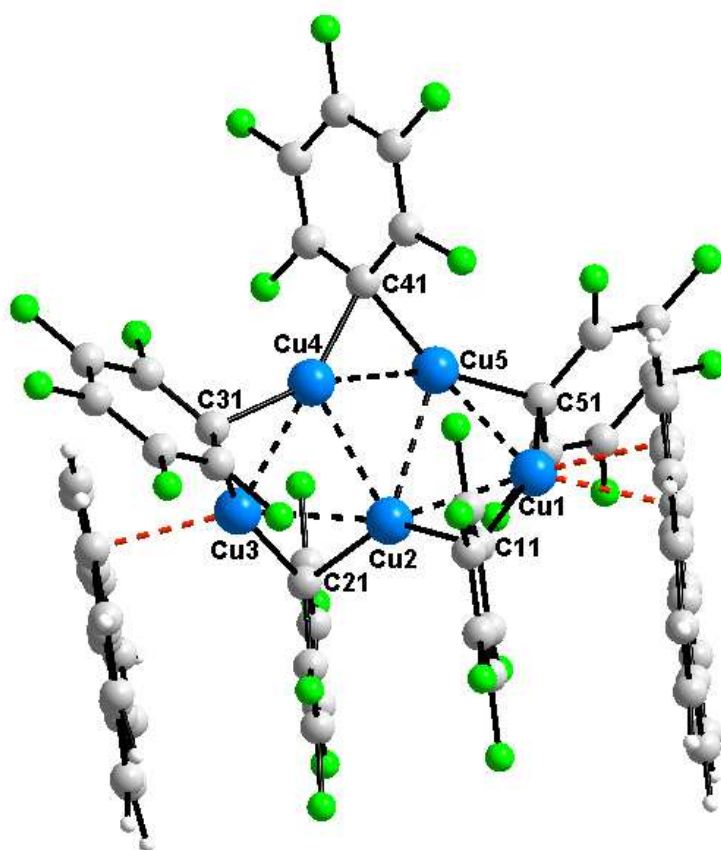


Figure 2.14 (a) Plot of the Polymeric Structure of (32). (b) View of the Puckered Cu_4C_4 Core. Symmetry operations used to generate equivalent atoms for (32): $-x + 1, -y, -z + 1$ and $-x + 1, -y, -z$.

Compound (33) crystallizes in the P2(1)/c space group with four molecules in the unit cell. Unlike the other arene complexes, this pyrene complex consists of five pentafluorophenylcopper moieties and two pyrene units that are coordinated to the copper centers. To the best of our knowledge, this is only the second example of a pentameric organocopper species, the only other pentameric structure known being $(\text{MesCu})_5$.⁸ However, in the pentameric structure of $(\text{MesCu})_5$ no short $\text{Cu}\cdots\text{Cu}$ contacts across the 10-membered Cu_5C_5 ring system were found. In contrast, (33) forms an unusual ribbon-like structure with two short $\text{Cu}\cdots\text{Cu}$ contacts across the ring system. The pentameric Cu_5 core is highly puckered with angles between the $(\text{Cu}_2\text{Cu}_3\text{Cu}_4)$ and $(\text{Cu}_2\text{Cu}_5\text{Cu}_4)$ planes of 39.94° and the $(\text{Cu}_2\text{Cu}_4\text{Cu}_5)$ and $(\text{Cu}_2\text{Cu}_1\text{Cu}_5)$ planes of 44.04° . Related multinuclear copper(I) carboxylate complexes were reported by Petrukhina and coworkers. For example, 2,6-bis-(trifluoromethylbenzoate)copper exhibits one-dimensional polymeric structures based on dicopper units that are further linked by intermolecular copper-oxygen interactions.⁸³ On the other hand, copper(I) 3,5-difluorobenzoate features a planar hexanuclear copper core composed of six copper atoms

bridged by six fluorinated benzoate ligands alternating above and below the plane. In this structure, relatively short Cu \cdots Cu contacts across the ring system of 2.7064(8) to 2.8259(8) Å were reported.⁸⁴ The two short diagonal Cu \cdots Cu distances in (33) are comparatively shorter and in the range of 2.647(1)-2.696(1) Å. They are similar to those in the respective tetrameric arene complexes. Cu- π interactions to the pyrene rings in (33) lead to short Cu \cdots C(π) distances. One pyrene shows an η^2 -coordination through the 9,10-positions to the copper center with Cu \cdots C distances of 2.389(4) and 2.379(4) Å, whereas, another pyrene binds in η^1 -fashion with 2.465(4) Å. They are considerably shorter than for complexes (27-31), but in a similar range as for the puckered structure of the toluene complex (9) and the pyrene complex (32). Again, arene binding is further supported in (33) by perfluoroarene-arene π -interactions with the shortest arene(centroid) \cdots C contacts being 3.325 and 3.233 Å to the Cu-bound *ipso*-carbon of the C₆F₅ groups.

(a)



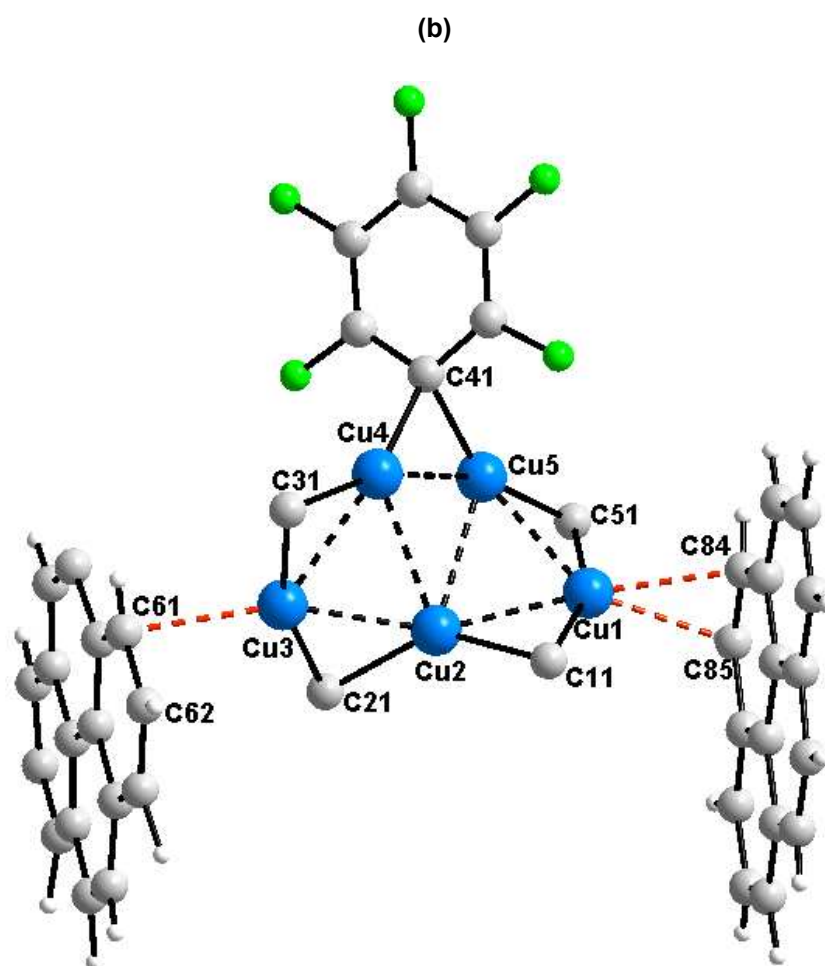


Figure 2.15 (a) Plot of the Molecular Structure of (33). (b) View of Cu_5C_5 Core.

2.8 Conclusions

In conclusion, we have synthesized and studied monomeric and oligomeric organocopper(I) complexes of pentafluorophenylcopper. Coordination of different

substituted pyridines results in complete breakdown of the tetrameric structure of (8) and perfluoroarene–arene interactions in turn support the extended supramolecular structures. Pentafluorophenylcopper (8) also serves as a building block for supramolecular materials. This supramolecular assembly of organocopper aggregates with different arenes was found to be supported through Cu- π , Cu-S and perfluoroarene-arene interactions. The stacked structures with $[\text{C}_6\text{F}_5\text{Cu}]_4$ and $[\text{C}_6\text{F}_5\text{Cu}]_5$ are highly unusual and have been observed for the first time in the case of organocopper aggregates.

2.9 Experimental Section

2.9.1 Materials and Instrumentation

4-Picoline, 2-picoline, 2-chloropyridine, 4-chloropyridine hydrochloride, naphthalene, anthracene and pyrene were purchased from Acros Organics. 4-picoline, 2-picoline, 2-chloropyridine, naphthalene, anthracene and pyrene were used as received. 4-chloropyridine hydrochloride was treated with 6M sodium hydroxide solution and extracted with ether. After removal of ether at 0 °C, 4-chloropyridine was dissolved in toluene, and the solution was degassed via several freeze-thaw cycles prior to use. $[\text{C}_6\text{F}_5\text{Cu}]_4$,²⁸ $[\text{C}_6\text{F}_5\text{Cu}]_4(\text{toluene})_2$,²⁴ and 2,2'-bithiophene⁸⁵ were prepared according to literature procedures. Deuterated chloroform (CDCl_3 >99.7%) was obtained from Cambridge Isotope Laboratories (CIL). All reactions and manipulations were carried out

in a similar manner to that described in Chapter 1A. Ether, hydrocarbon and chlorinated solvents were treated as described in Chapter 1A. Detailed description of NMR abbreviations and elemental analyses can be found in the experimental section of Chapter 1A. 470.2 MHz ^{19}F NMR spectra were obtained on a Varian INOVA NMR spectrometer equipped with a 5 mm dual broadband gradient probe (Nalorac, Varian Inc., Martinez, CA) and was referenced externally to α , α' , α'' -trifluorotoluene (0.05% in C_6D_6 ; $\delta = -63.73$ ppm). Melting points and decomposition temperatures were determined in sealed capillary tubes and are not corrected. X-ray diffraction intensities were collected on a Bruker SMART APEX CCD diffractometer at $T = 203(2)$ (28), $208(2)$ (33) and $100(2)$ K (18, 19, 20, 21, 27, 29, 30, 31, 32) using $\text{MoK}\alpha$ (0.71073 \AA) (18, 20, 28, 33) and $\text{CuK}\alpha$ (1.54178 \AA) (19, 21, 27, 29, 30, 31, 32) radiations. SADABS⁸⁶ or numerical absorption corrections were applied, the structures were solved using direct methods, completed by subsequent difference Fourier syntheses, and refined by full matrix least squares procedures on F^2 . All non-hydrogen atoms were refined with anisotropic displacement coefficients. The H atoms were placed at calculated positions and were refined as riding atoms. All software and source scattering factors are contained in the SHELXTL program package.⁸⁷

2.9.2 Reaction of Pentafluorophenylcopper with Substituted Pyridine

Synthesis of 4-MePy-CuC₆F₅ (18). Neat 4-picoline (0.067 g, 0.72 mmol) was added dropwise to a solution of (9) (0.16 g, 0.14 mmol) in toluene (5 mL) at room temperature. Upon addition of 4-picoline an intense yellow color developed. The reaction solution was kept at -35 °C for one day, and the pure product was isolated from the reaction solution as pale yellow crystals. The product obtained was washed with hexanes and dried under high vacuum. Yield: 0.13 g (72 %). For (18): T_m = 130-134 °C, T_{dec} = 148-155 °C; ¹H NMR (500 MHz, CDCl₃, 25 °C): δ = 8.52 (d, J = 6.0 Hz, 2H, Py-H2,6), 7.38 (d, J = 6.0 Hz, 2H, Py-H3,5), 2.50 (s, 3H, Me); ¹⁹F NMR (470.2 MHz, CDCl₃, 25 °C): δ = -112.9 (m, 2F, *ortho*-F), -160.8 (t, J (F, F) = 20 Hz, 1F, *para*-F), -164.0 (t, J = 19 Hz, 2F, *meta*-F); ¹³C NMR (125.7 MHz, CDCl₃, 25 °C): δ = 152.5 (Py-C4), 149.3 (dd, J (¹⁹F, C) = 224 Hz / 32 Hz, Pf-C2,6), 149.4 (Py-C2,6), 138.8 (dm, J (¹⁹F, C) = 245 Hz, Pf-C4), 136.5 (dm, J (¹⁹F, C) = 253 Hz, Pf-C3,5), 126.7 (Py-C3,5), 122.2 (t, J (¹⁹F, C) = 72 Hz, Pf-C1), 21.8 (Me); elemental analysis: calculated C 44.52, H 2.18, N 4.33%; found C 43.21, H 2.12, N 3.96%.

Synthesis of 2-MePy-CuC₆F₅ (19). Neat 2-picoline (0.05 g, 0.58 mmol) was added dropwise to a solution of (9) (0.13 g, 0.12 mmol) in toluene (5 mL) at room temperature. Upon addition of 2-picoline an intense yellow color developed. The crude product was obtained as colorless microcrystalline solid, which was washed with hexanes. Yield: 0.13

g (84 %). Slow evaporation of solvent at RT gave pale yellow single crystals of (19) suitable for x-ray diffraction analysis. For (19): $T_m = 141-144\text{ }^{\circ}\text{C}$, $T_{dec} = 147-150\text{ }^{\circ}\text{C}$; ^1H NMR (500 MHz, CDCl_3 , $25\text{ }^{\circ}\text{C}$): $\delta = 8.59$ (d, $J = 5.0\text{ Hz}$, 1H, Py-H6), 7.89 (pst, $J = 8.0\text{ Hz}$, 1H, Py-H4), 7.46 (d, $J = 8.0\text{ Hz}$, 1H, Py-H3), 7.38 (pst, $J = 7.0\text{ Hz}$ 1H, Py-H5), 2.93 (s, 3H, Me); ^{19}F NMR (470.2 MHz, CDCl_3 , $25\text{ }^{\circ}\text{C}$): $\delta = -113.1$ (m, 2F, *ortho*-F), -160.9 (t, $J(\text{F}, \text{F}) = 20\text{ Hz}$, 1F, *para*-F), -164.0 (m, 2F, *meta*-F); ^{13}C NMR (125.7 MHz, CDCl_3 , $25\text{ }^{\circ}\text{C}$): $\delta = 159.5$ (Py-C2), 149.7 (dd, $J(^{19}\text{F}, \text{C}) = 220\text{ Hz} / 33\text{ Hz}$, Pf-C2,6), 149.6 (Py-C6), 139.5 (Py-C4), 138.7 (dm, $J(^{19}\text{F}, \text{C}) = 244\text{ Hz}$, Pf-C4), 136.4 (dm, $J(^{19}\text{F}, \text{C}) = 253\text{ Hz}$, Pf-C3,5), 125.9 (Py-C3), 122.7 (Py-C5), 122.8 (t, $J(^{19}\text{F}, \text{C}) = 71\text{ Hz}$, Pf-C1), 26.0 (Me); elemental analysis: calculated C 44.52, H 2.18, N 4.33%; found C 44.38, H 2.17, N 4.17%.

Synthesis of 4-ClPy-CuC₆F₅ (20). A solution of 4-chloropyridine in toluene (5 mL) was added to a solution of (9) (0.13 g, 0.117 mmol) in toluene and the resulting dark yellow mixture was kept at $-35\text{ }^{\circ}\text{C}$ for one day. Crystallization from toluene gave pale yellow crystals of (20). Yield: 0.11 g, (68 %). Slow evaporation of solvent at RT gave pale yellow single crystals of (20) suitable for x-ray diffraction analysis. For (20): $T_m = 143-145\text{ }^{\circ}\text{C}$, $T_{dec} = 147-150\text{ }^{\circ}\text{C}$; ^1H NMR (500 MHz, CDCl_3 , $25\text{ }^{\circ}\text{C}$): $\delta = 8.59$ (d, $^2J = 6.5\text{ Hz}$, 2H, Py-H2,6), 7.60 (d, $^2J = 6.5\text{ Hz}$, 2H, Py-H3,5); ^{19}F NMR (470.2 MHz, CDCl_3 , $25\text{ }^{\circ}\text{C}$): $\delta = -112.6$ (m, 2F, *ortho*-F), -159.9 (t, $J(\text{F}, \text{F}) = 18\text{ Hz}$, 1F, *para*-F), -163.7 (m, 2F,

meta-F); ^{13}C NMR (125.7 MHz, CDCl_3 , 25 °C): δ = 150.7 (Py-C2,6), 149.9 (dd, J (^{19}F , C) = 222 Hz / 27 Hz, Pf-C2,6), 148.5 (Py-C4), 139.0 (dm, J (^{19}F , C) = 245, Pf-C4), 136.5 (dm, J (^{19}F , C) = 253 Hz, Pf-C3,5), 126.6 (Py-C3,5), 121.3 (t, J (^{19}F , C) = 75 Hz, Pf-C1); elemental analysis: calculated C 38.39, H 1.17, N 4.07%; found C 37.53, H 1.17, N 4.01 %.

Synthesis of 2-ClPy-CuC₆F₅ (21). Neat 2-Chloropyridine (0.023 g, 0.21 mmol) was added dropwise to a solution of (9) (0.057 g, 0.52 mmol) in toluene (5 mL) at room temperature. Upon addition of 2-chloropyridine an intense yellow color developed. The solution was kept at -35 °C for a day, which yielded light yellow crystals. Yield: 0.015 g (85 %). Slow evaporation of solvent at RT gave pale yellow single crystals of (21) suitable for x-ray diffraction analysis. For (21): T_m = 123-127 °C, T_{dec} = 130-133 °C; ^1H NMR (500 MHz, CDCl_3 , 25 °C): δ = 8.5 (d, J = 5.0 Hz, 1H, Py-H6), 7.90 (pst, J = 8.0 Hz, 1H, Py-H4), 7.55 (d, J = 8.5 Hz, 1H, Py-H3), 7.46 (pst, J = 6.0 Hz, 1H, Py-H5); ^{19}F NMR (470.2 MHz, CDCl_3 , 25 °C): δ = -110.5 (br, 2F, *ortho*-F), -156.3 (br, 1F, *para*-F), -162.9 (br, 2F, *meta*-F); ^{13}C NMR (125.7 MHz, CDCl_3 , 25 °C): δ = 151.7 (Py-C2), 150.9 (d, J (^{19}F , C) = 228 Hz / 28 Hz, Pf-C2,6), 150.4 (Py-C6), 140.8 (Py-C4), 140.4 (dm, J (^{19}F , C) = 249 Hz., Pf-C4), 136.5 (dm, J (^{19}F , C) = 254 Hz, Pf-C3,5), 125.9 (Py-C3), 123.6 (Py-C5), 115.0 (t, J (^{19}F , C) = 67 Hz, Pf-C1); elemental analysis: calculated C 38.39, H 1.17, N 4.07%; found C 38.25, H 1.07, N 4.02%.

2.9.3 Reaction of Pentafluorophenylcopper with Organic π -systems

Synthesis of (Naph)₂-CuC₆F₅ (27): Compound (9) (82.5 mg, 0.075 mmol) was mixed with naphthalene (19.1 mg, 0.15 mmol) in CH₂Cl₂ (5 mL) at room temperature. The mixture was stirred for 10 min and then layered with hexanes (2 mL). The solution was kept for crystallization at –35 °C for 3 d to give (27) as colorless needle-like crystals. Yield: 78 mg, 88%. T_m: 150-155 °C, T_{dec}: 170-175 °C; for C₄₄H₁₆Cu₄F₂₀ calcd C 44.83, H 1.37; found C 44.67, H 1.25.

Synthesis of (Bt)₂-CuC₆F₅ (28): Compound (9) (51.0 mg, 0.055 mmol) was mixed with 2,2'-bithiophene (18.4 mg, 0.11 mmol) in CH₂Cl₂ (5 mL) at room temperature. The mixture was stirred for 10 min and then layered with hexanes (2 mL). The solution was kept for crystallization at –35 °C for 3 d to give (28) as colorless needle-like crystals. Yield: 60 mg, 87%. T_m: 165-170 °C, T_{dec}: 128-135 °C; for C₄₀H₁₂Cu₄F₂₀S₄ calcd C 38.28, H 0.96; found C 38.23, H 0.89.

Synthesis of (Bt)-CuC₆F₅ (30): Compound (9) (75.2 mg, 0.068 mmol) was mixed with 2,2'-bithiophene (11.3 mg, 0.068 mmol) in CH₂Cl₂ (5 mL). The solution was kept at –35 °C for 2 d to give (30) as colorless plates. Yield: 65 mg, 88%. T_m: 175-180 °C, T_{dec}: 150-155 °C; for C₃₂H₆Cu₄F₂₀S₂ calcd C 35.30, H 0.56; found C 35.36, H 0.41.

Synthesis of (Anth)₂-CuC₆F₅ (31): Compound (9) (51.5 mg, 0.047 mmol) was mixed with anthracene (16.6 mg, 0.093 mmol) in CH₂Cl₂ (5 mL). The solution was kept at –35

°C for 3 d to give (31) as colorless plates. Yield: 42 mg, 70%. T_m : 260-270 °C, T_{dec} : 190-195 °C; for $C_{52}H_{20}Cu_4F_{20}$ calcd C 48.83, H 1.58; found C 48.61, H 1.49.

Synthesis of (Pyrene)-CuC₆F₅ (32): Compound (9) (85 mg, 0.077 mmol) was mixed with pyrene (31 mg, 0.15 mmol) in CH₂Cl₂ (5 mL). The solution was kept at –35 °C for 4 months to give (32) as colorless plates. Yield: 30 mg, 15%. T_m : 180-190 °C, T_{dec} : 145-150 °C.

Synthesis of (Pyrene)₂-CuC₆F₅ (33): Compound (9) (60 mg, 0.055 mmol) was mixed with pyrene (22 mg, 0.11 mmol) in CH₂Cl₂ (5 mL). The solution was kept at –35 °C for 4 d to give (32) as colorless plates. Yield: 35 mg, 40%.

2.10 References and Notes

1. Jastrzebski, J. T. B. H.; van Koten, G., Structures and Reactivities of Organocopper Compounds. In *Modern Organocopper Chemistry*, Krause, N., Ed. Wiley VCH GmbH: Weinheim, 2002; pp 1-44.
2. van Koten, G.; Noltes, J. G., Comprehensive Organometallic Chemistry. In Wilkinson, G.; Stone, F. G. A.; Abel, E. W., Eds. Pergamon Press: Oxford, 1981; Vol. 2, Chapter 14, p 709.
3. Krause, N., *Modern Organocopper Chemistry*. Wiley VCH GmbH: Weinheim, 2002.

4. Nakamura, E.; Mori, S. *Angew. Chem. Int. Ed.* **2000**, *39*, 3750-3771.
5. Nobel, D.; van Koten, G.; Spek, A. L. *Angew. Chem., Int. Ed. Engl.* **1989**, *28*, 208-210.
6. Janssen, M. D.; Corsten, M. A.; Spek, A. L.; Grove, D. M.; van Koten, G. *Organometallics* **1996**, *15*, 2810-2820.
7. Niemeyer, M. *Organometallics* **1998**, *17*, 4649-4656.
8. Meyer, E. M.; Gambarotta, S.; Floriani, C.; Chiesi-Villa, A.; Guastini, C. *Organometallics* **1989**, *8*, 1067-1079.
9. Gambarotta, S.; Floriani, C.; Chiesi-Villa, A.; Guastini, C. *J. Chem. Soc., Chem. Commun.* **1983**, 1156-1158.
10. Eriksson, H.; Håkansson, M. *Organometallics* **1997**, *16*, 4243-4244.
11. Eriksson, H.; Ortendahl, M.; Håkansson, M. *Organometallics* **1996**, *15*, 4823-4831.
12. Eriksson, H.; Håkansson, M.; Jagner, S. *Inorg. Chim. Acta* **1998**, *277*, 233-236.
13. Håkansson, M.; Eriksson, H.; Berglund Åhman, A.; Jagner, S. *J. Organomet. Chem.* **2000**, *595*, 102-108.
14. Håkansson, M.; Eriksson, H.; Jagner, S. *Inorg. Chim. Acta.* **2006**, *359*, 2519-2524.
15. Boéré, R. T.; Masuda, J. D.; Tran, P. *J. Organomet. Chem.* **2006**, *691*, 5585-5591.

16. Cairncross, A.; Sheppard, W. A. *J. Am. Chem. Soc.* **1968**, *90*, 2186-2187.
17. Cairncross, A.; Omura, H.; Sheppard, W. A. *J. Am. Chem. Soc.* **1971**, *93*, 248-249.
18. DePasquale, R. J.; Tamborski, C. *J. Org. Chem.* **1969**, *34*, 1736-1740.
19. Jukes, A. E.; Dua, S. S.; Gilman, H. *J. Organomet. Chem.* **1970**, *24*, 791-796.
20. MacNeil, K. J.; Burton, D. J. *J. Org. Chem.* **1993**, *58*, 4411-4417.
21. MacNeil, K. J.; Burton, D. J. *J. Org. Chem.* **1995**, *60*, 4085-4089.
22. Burton, D. J.; Heinze, P. L. *J. Fluorine Chem.* **1985**, *29*, 359-361.
23. Burton, D. J.; Yang, Z. Y.; MacNeil, K. J. *J. Fluorine Chem.* **1991**, *52*, 251-255.
24. Sundararaman, A.; Lalancette, R. A.; Zakharov, L. N.; Rheingold, A. L.; Jäkle, F. *Organometallics* **2003**, *22*, 3526-3532.
25. Olmstead, M. M.; Power, P. P. *J. Am. Chem. Soc.* **1990**, *112*, 8008-8014.
26. Gambarotta, S.; Strologo, S.; Floriani, C.; Chiesi-Villa, A.; Guastini, C. *Organometallics* **1984**, *3*, 1444-1445.
27. He, X.; Olmstead, M. M.; Power, P. P. *J. Am. Chem. Soc.* **1992**, *114*, 9668-9670.
28. Cairncross, A.; Sheppard, W. A.; Wonchoba, E.; Guildford, W. J.; House, C. B.; Coates, R. M. *Org. Synth.* **1980**, *59*, 122-131.
29. Sundararaman, A.; Zakharov, L. N.; Rheingold, A. L.; Jäkle, F. *Chem. Commun.* **2005**, 1708-1710.

30. Mountford, A. J.; Lancaster, S. J.; Coles, S. J.; Horton, P. N.; Hughes, D. L.; Hursthouse, M. B.; Light, M. E. *Organometallics* **2006**, 25, 3837-3847.
31. Wieland, T.; Mathias, S. W. Z. *Anorg. Allg. Chem.* **2002**, 628, 1841-1847.
32. Lee, Y.-A.; Eisenberg, R. *J. Am. Chem. Soc.* **2003**, 125, 7778-7779.
33. Yang, G.; Raptis, R. G. *Inorg. Chem.* **2003**, 42, 261-263.
34. White-Morris, R. L.; Olmstead, M. M.; Attar, S.; Balch, A. L. *Inorg. Chem.* **2005**, 44, 5021-5029.
35. Kishimura, A.; Yamashita, T.; Aida, T. *J. Am. Chem. Soc.* 2005, 127, 179-183.
36. Dias, H. V. R.; Diyabalanage, H. V. K.; Eldabaja, M. G.; Elbjeirami, O.; Rawashdeh-Omary, M. A.; Omary, M. A. *J. Am. Chem. Soc.* **2005**, 127, 7489-7501.
37. Siemeling, U.; Vorfeld, U.; Neumann, B.; Stammer, H.-G. *Chem. Commun.* **1997**, 1723-1724.
38. Zhang, X.-M.; Tong, M.-L.; Gong, M.-L.; Lee, H.-K.; Luo, L.; Li, K.-F.; Tong, Y.-X.; Chen, X.-M. *Chem. Eur. J.* **2002**, 8, 3187- 3194.
39. Zhang, J.-P.; Wang, Y.-B.; Huang, X.-C.; Lin, Y.-Y.; Chen, X.-M. *Chem. Eur. J.* **2005**, 11, 552-561.
40. Haeberlen, O. D.; Schmidbaur, H.; RoÈsch, N. *J. Am. Chem. Soc.* **1994**, 116, 8241-8248.

41. Pyykkö, P. *Chem. Rev.* **1988**, 88, 563-594.
42. Borovik, A. S.; Barron, A. R. *J. Am. Chem. Soc.* **2002**, 124, 3743-3748.
43. Sauteret, C. H., J.-P.; Frey, R.; Pradere, F.; Ducuing, J.; Baughman, R. H.; Chance, R. R. *Phys. Rev. Lett.* **1976**, 36, 956-958.
44. Hargittai, M.; Schwerdtfeger, P.; Reffy, B.; Brown, R. *Chem. Eur. J.* **2003**, 9, 327-333.
45. Singh, K.; Long, J. R.; Stavropoulos, P. *J. Am. Chem. Soc.* **1997**, 119, 2942-2943.
46. Goj, L. A.; Blue, E. D.; Delp, S. A.; Gunnoe, T. B.; Cundari, T. R.; Petersen, J. L. *Organometallics* **2006**, 25, 4097-4104.
47. Mankad, N. P.; Gray, T. G.; Laitar, D. S.; Sadighi, J. P. *Organometallics* **2004**, 23, 1191-1193.
48. Wehman, E.; van Koten, G.; Jastrzebski, J. T. B. H.; Rotteveel, M. A.; Stam, C. H. *Organometallics* **1988**, 7, 1477-1485.
49. Papasergio, R. I.; Raston, C. L.; White, A. H. *J. Chem. Soc., Chem. Commun.* **1983**, 1419-1420.
50. Goj, L. A.; Blue, E. D.; Munro-Leighton, C.; Gunnoe, T. B.; Petersen, J. L. *Inorg. Chem.* **2005**, 44, 8647-8649.
51. Collings, J. C.; Roscoe, K. P.; Thomas, R. L.; Batsanov, A. S.; Stimson, L. M.; Howard, J. A. K.; Marder, T. B. *New J. Chem.* **2001**, 25, 1410-1417.

52. Hori, A.; Shinohe, A.; Yamasaki, M.; Nishibori, E.; Aoyagi, S.; Sakata, M. *Angew. Chem. Int. Ed.* **2007**, *46*, 7617-7620.
53. Bacchi, S.; Benaglia, M.; Cozzi, F.; Demartin, F.; Filippini, G.; A. Gavezzotti. *Chem. Eur. J.* **2006**, *12*, 3538–3546.
54. Reichenbacher, K.; Süß, H. I.; Hulliger, J. *Chem. Soc. Rev.* **2005**, *34*, 22-30.
55. Dias, H. V. R.; Gamage, C. S. P. *Angew. Chem. Int. Ed.* **2007**, *46*, 2192-2194.
56. Dias, H. V. R.; Gamage, C. S. P.; Keltner, J.; Diyabalanage, H. V. K.; Omari, I.; Eyobo, Y.; Dias, N. R.; Roehr, N.; McKinney, L.; Poth, T. *Inorg. Chem.* **2007**, *46*, 2979-2987.
57. Haneline, M. R.; Tsunoda, M.; Gabbai, F. P. *J. Am. Chem. Soc.* **2002**, *124*, 3737-3742.
58. Burrell, C. N.; Bodine, M. I.; Elbjeirami, O.; Reibenspies, J. H.; Omary, M. A.; Gabbai, F. P. *Inorg. Chem.* **2007**, *46*, 1388-1395.
59. Mohamed, A. A.; Rawashdeh-Omary, M. A.; Omary, M. A.; Fackler, J. P., Jr. *Dalton Trans.* **2005**, 2597-2602.
60. Burini, A.; Fackler, J. P., Jr.; Galassi, R.; Macchioni, A.; Omary, M. A.; Rawashdeh-Omary, M. A.; Pietroni, B. R.; Sabatini, S.; Zuccaccia, C. *J. Am. Chem. Soc.* **2002**, *124*, 4570-4571.

61. Lang, H.; Köhler, K.; Rheinwald, G.; Zsolnai, L.; Büchner, M.; Driess, A.; Huttner, G.; Strähle, J. *Organometallics* **1999**, *18*, 598-605.
62. Turner, R. W.; Amma, E. L. *J. Am. Chem. Soc.* **1966**, *88*, 1877-1882.
63. Dines, M. B.; Bird, P. *J. Chem. Soc., Chem. Comm.* **1973**, 12-12.
64. Dattelbaum, A. M.; Martin, J. D. *Inorg. Chem.* **1999**, *38*, 6200-6205.
65. Schmidbaur, H.; Bublak, W.; Huber, B.; Reber, G.; Müller, G. *Angew. Chem. Int. Ed. Engl.* **1986**, *25*, 1089-1090.
66. Striejewske, W. S.; Conry, R. R. *Chem. Commun.* **1998**, 555-556.
67. Conry, R. R.; Striejewske, W. S.; Tipton, A. A. *Inorg. Chem.* **1999**, *38*, 2833-2843.
68. Conry, R. R.; Striejewske, W. S. *Organometallics* **1998**, *17*, 3146-3148.
69. Shimazaki, Y.; Yokoyama, H.; Yamauchi, O. *Angew. Chem. Int. Ed.* **1999**, *38*, 2401-2403.
70. Doshi, A.; Venkatasubbaiah, K.; Rheingold, A. L.; Jäkle, F. *Chem. Commun.* **2008**, 4264-4266.
71. Wehman, E.; van Koten, G.; Knotter, M.; Spelten, H.; Heijdenrijk, D.; Mak, A. N. S.; Stam, C. H. *J. Organomet. Chem.* **1987**, *325*, 293-309.
72. Gudat, D.; Nieger, M.; Schmitz, K.; Szarvas, L. *Chem. Commun.* **2002**, 1820-1821.

73. Knotter, D. M.; Smeets, W. J. J.; Spek, A. L.; van Koten, G. *J. Am. Chem. Soc.* **1990**, *112*, 5895-5896.
74. Lenders, B.; Grove, D. M.; Smeets, W. J. J.; van der Sluis, P.; Spek, A. L.; van Koten, G. *Organometallics* **1991**, *10*, 786-791.
75. Hanton, L. R.; Richardson, C.; Robinsonb, W. T.; Turnbulla, J. M. *Chem. Commun.* **2000**, 2465-2466, and references therein.
76. Patrick, C. R.; Prosser, G. S. *Nature* **1960**, *187*, 1021-1021.
77. Batsanov, A. S.; Collings, J. C.; Howard, J. A. K.; Marder, T. B.; Perepichka, D. F. *Acta Crystallogr. Sect. C: Cryst. Struct. Commun.* **2001**, *C57*, 1306-1307.
78. Smith, C. E.; Smith, P. S.; Thomas, R. L.; Robins, E. G.; Collings, J. C.; Dai, C.; Scott, A. J.; Borwick, S.; Batsanov, A. S.; Watt, S. W.; Clark, S. J.; Viney, C.; Howard, J. A. K.; Clegg, W.; Marder, T. B. *J. Mater. Chem.* **2004**, *14*, 413-420.
79. Watt, S. W.; Dai, C.; Scott, A. J.; Burke, J. M.; Thomas, R. L.; Collings, J. C.; Viney, C.; Clegg, W.; Marder, T. B. *Angew. Chem. Int. Ed.* **2004**, *43*, 3061-3063.
80. Petrukhina, M. A. *Coord. Chem. Rev.* **2007**, *251*, 1690-1698.
81. Cotton, F. A.; Dikarev, E. V.; Petrukhina, M. A. *J. Am. Chem. Soc.* **2001**, *123*, 11655-11663.
82. Dikarev, E. V.; Li, B.; Rogachev, A. Y.; Zhang, H.; Petrukhina, M. A. *Organometallics* **2008**, *27*, 3728-3735.

83. Sevryugina, Y.; Vaughn, D. D., II; Petrukhina, M. A. *Inorg. Chim. Acta* **2007**, 360, 3103-3107.
84. Sevryugina, Y.; Rogachev, A. Y.; Petrukhina, M. A. *Inorg. Chem.* **2007**, 46, 7870-7879.
85. Nelson, T. D.; Crouch, R. D. *Organic Reactions (Hoboken, NJ, United States)*, Publisher: (John Wiley&Sons, Inc.) 2004, 63.
86. Sheldrick, G. M. *SADABS, Version 2. Multi-Scan Absorption Correction Program, University of Göttingen, Germany*, **2001**.
87. Sheldrick, G. M. *SHELXTL, Version 6.14, Bruker AXS Inc., Madison, WI*, **2004**.

Appendix

Appendix 1

Appendix 1.1 The following tables are supplementary material for the x-ray crystal structures of compound **MB(MesNMe₂)₂** (43). Bond lengths and bond angles are listed for **MB(MesNMe₂)₂** (43).

Crystal Data and Structure Refinement Details of MB(MesNMe₂)₂.

	MB(MesNM₂)₂ (43)
empirical Formula	C ₃₀ H ₄₁ BN ₂
formula Weight	440.46
<i>T</i> , K	100(2)
Wavelength, Å	1.54178
crystal system	Orthorhombic
space group	Pna2(1)
<i>a</i> , Å	a = 11.0009(3)
<i>b</i> , Å	19.9855(5) Å
<i>c</i> , Å	12.1466(3) Å
<i>α</i> , deg	90
<i>β</i> , deg	90

γ , deg	90
V , Å ³	2670.53(12)
<i>Section 1.01</i> Z	4
ρ_{calcd} , g cm ⁻³	1.096
μ , mm ⁻¹	0.466
F(000)	960
crystal size, mm	0.20 x 0.16 x 0.05
Limiting indices	-12 ≤ h ≤ 13, -23 ≤ k ≤ 23, -14 ≤ l ≤ 14
θ range, deg	4.26 – 67.30
reflns collected	20289
independent reflns	4645
absorption correction	Semi-empirical from equivalents
refinement method	Full-matrix least-squares on F^2
data/restraints/parameters	4645 / 1 / 309
Goodness-of-fit on F^2	1.039
Final R indices	$R_1 = 0.0429$
$[I > 2\sigma(I)]^{[a]}$	$wR_2 = 0.1095$
R indices (all data) ^[a]	$R_1 = 0.0472$
	$wR_2 = 0.1129$
Peak/hole (e Å ⁻³)	0.259 / -0.181

$$[a] R1 = \Sigma ||F_o| - |F_c|| / \Sigma |F_o|; wR2 = \{ \Sigma [w(F_o^2 - F_c^2)^2] / \Sigma [w(F_o^2)^2] \}^{1/2}.$$

Bond Lengths (Å) and Bond Angles (deg) of MB(MesNMe₂)₂ (43)

B(1)-C(8)	1.569(3)	B(1)-C(8)	1.569(3)
B(1)-C(14)	1.573(3)	B(1)-C(14)	1.573(3)
B(1)-C(3)	1.576(3)	B(1)-C(3)	1.576(3)
N(1)-C(1)	1.404(3)	N(1)-C(1)	1.404(3)
N(1)-C(26)	1.433(3)	N(1)-C(26)	1.433(3)
N(1)-C(27)	1.434(3)	N(1)-C(27)	1.434(3)
N(2)-C(4)	1.396(3)	N(2)-C(4)	1.396(3)
N(2)-C(30)	1.436(4)	N(2)-C(30)	1.436(4)
N(2)-C(28)	1.451(4)	N(2)-C(28)	1.451(4)
C(1)-C(10)	1.391(3)	C(1)-C(10)	1.391(3)
C(1)-C(7)	1.397(3)	C(1)-C(7)	1.397(3)
C(2)-C(16)	1.379(3)	C(2)-C(16)	1.379(3)
C(2)-C(8)	1.407(3)	C(2)-C(8)	1.407(3)
C(3)-C(5)	1.403(3)	C(3)-C(5)	1.403(3)

C(3)-C(13)	1.413(3)	C(3)-C(13)	1.413(3)
C(4)-C(18)	1.392(3)	C(4)-C(18)	1.392(3)
C(4)-C(11)	1.398(3)	C(4)-C(11)	1.398(3)
C(5)-C(7)	1.396(3)	C(5)-C(7)	1.396(3)
C(8)-B(1)-C(14)	121.82(18)	C(8)-B(1)-C(14)	121.82(18)
C(8)-B(1)-C(3)	115.02(17)	C(8)-B(1)-C(3)	115.02(17)
C(14)-B(1)-C(3)	123.16(17)	C(14)-B(1)-C(3)	123.16(17)
C(1)-N(1)-C(26)	118.96(19)	C(1)-N(1)-C(26)	118.96(19)
C(1)-N(1)-C(27)	117.91(19)	C(1)-N(1)-C(27)	117.91(19)
C(26)-N(1)-C(27)	115.8(2)	C(26)-N(1)-C(27)	115.8(2)
C(4)-N(2)-C(30)	119.8(2)	C(4)-N(2)-C(30)	119.8(2)
C(4)-N(2)-C(28)	118.5(3)	C(4)-N(2)-C(28)	118.5(3)
C(30)-N(2)-C(28)	117.9(2)	C(30)-N(2)-C(28)	117.9(2)
C(10)-C(1)-C(7)	117.54(18)	C(10)-C(1)-C(7)	117.54(18)
C(10)-C(1)-N(1)	119.92(19)	C(10)-C(1)-N(1)	119.92(19)
C(7)-C(1)-N(1)	122.5(2)	C(7)-C(1)-N(1)	122.5(2)
C(16)-C(2)-C(8)	122.0(2)	C(16)-C(2)-C(8)	122.0(2)

C(5)-C(3)-C(13)	117.09(18)	C(5)-C(3)-C(13)	117.09(18)
C(5)-C(3)-B(1)	120.74(17)	C(5)-C(3)-B(1)	120.74(17)
C(13)-C(3)-B(1)	121.89(17)	C(13)-C(3)-B(1)	121.89(17)
C(18)-C(4)-N(2)	121.2(2)	C(18)-C(4)-N(2)	121.2(2)
C(18)-C(4)-C(11)	117.0(2)	C(18)-C(4)-C(11)	117.0(2)
N(2)-C(4)-C(11)	121.9(2)	N(2)-C(4)-C(11)	121.9(2)
C(7)-C(5)-C(3)	120.98(18)	C(7)-C(5)-C(3)	120.98(18)
C(7)-C(5)-C(17)	118.19(18)	C(7)-C(5)-C(17)	118.19(18)
C(3)-C(5)-C(17)	120.75(18)	C(3)-C(5)-C(17)	120.75(18)
C(20)-C(6)-C(12)	121.5(2)	C(20)-C(6)-C(12)	121.5(2)
C(5)-C(7)-C(1)	121.55(19)	C(5)-C(7)-C(1)	121.55(19)
C(20)-C(8)-C(2)	116.06(18)	C(20)-C(8)-C(2)	116.06(18)
C(20)-C(8)-B(1)	122.89(17)	C(20)-C(8)-B(1)	122.89(17)

Appendix 2

Appendix 2.1 The following tables are supplementary material for the X-ray crystal structures of compounds **(Styryl)₂BTip** (29) and **(Styryl)₂BHQ** (30). Bond lengths and bond angles are listed for (29-30).

Crystal Data and Structure Refinement Details of (Styryl)₂BTip and (Styryl)₂BHQ

	(Styryl) ₂ BTip (29)	(Styryl) ₂ BQ (30)
empirical Formula	C ₃₄ H ₄₄ B	C ₂₅ H ₂₀ BNO
formula Weight	463.50	361.23
<i>T</i> , K	100(2)	100(2)
Wavelength, Å	1.54178	1.54178
crystal system	Monoclinic	Monoclinic
space group	P2(1)/c	P2(1)/c
<i>a</i> , Å	18.3275(2)	14.0629(3)
<i>b</i> , Å	9.93390(10)	14.0772(3)
<i>c</i> , Å	16.5112(2)	9.7274(2)
α , deg	90	90
β , deg	104.0860(10)	98.3180(10)
γ , deg	90	90
<i>V</i> , Å ³	2915.70(6)	1900.56(7)

<i>Section 1.02</i>	<i>Z</i>	4	4
ρ_{calcd} , g cm ⁻³		1.056	1.262
μ , mm ⁻¹		0.429 (CuK α)	0.585 (CuK α)
F(000)		1012	760
crystal size, mm		0.25 x 0.17 x 0.11	0.34 x 0.21 x 0.21
Limiting indices		-21<=h<=21	-16<=h<=16
		-9<=k<=9	-16<=k<=15
		-18<=l<=19	-11<=l<=11
θ range, deg		4.98 – 67.27	3.18 – 67.07
reflns collected		22780	14033
independent reflns		5007	3299
absorption correction		Semi-empirical equivalents	from Semi-empirical equivalents
refinement method		Full-matrix on F^2	least-squares Full-matrix on F^2
data/restraints/parameters		5007 / 0 / 324	3299 / 0 / 253
Goodness-of-fit on F^2		1.041	1.027
Final R indices		R1 = 0.0366	R1 = 0.0367
$[I > 2\sigma(I)]^{[a]}$		wR2 = 0.0925	wR2 = 0.0989
R indices (all data) ^[a]		R1 = 0.0408	R1 = 0.0401
		wR2 = 0.0956	wR2 = 0.1022
Peak/hole (e Å ⁻³)		0.237 / -0.153	0.237 / -0.194

[a] $R1 = \Sigma||F_o| - |F_c|| / \Sigma|F_o|$; $wR2 = \{ \Sigma[w(F_o^2 - F_c^2)^2] / \Sigma[w(F_o^2)^2] \}^{1/2}$.

Bond Lengths (Å) and Bond Angles (deg) of (Styryl)₂BTip (29)

B(1)-C(7)	1.5627(17)	C(16)-C(30)	1.4741(17)
B(1)-C(13)	1.5631(17)	C(8)-C(7)	1.4048(16)
B(1)-C(1)	1.5823(16)	C(22)-C(4)	1.5183(15)
C(12)-C(11)	1.3819(17)	C(22)-C(24)	1.5261(16)
C(12)-C(7)	1.4054(16)	C(22)-C(23)	1.5304(16)
C(9)-C(8)	1.3828(16)	C(3)-C(2)	1.3884(16)
C(9)-C(10)	1.3955(17)	C(3)-C(4)	1.3954(15)
C(5)-C(4)	1.3909(16)	C(1)-C(2)	1.4113(15)
C(5)-C(6)	1.3977(16)	C(2)-C(19)	1.5230(15)
C(10)-C(11)	1.3958(17)	C(26)-C(25)	1.5257(16)
C(10)-C(28)	1.4717(17)	C(28)-C(29)	1.3196(19)
C(6)-C(1)	1.4070(15)	C(19)-C(21)	1.5277(17)
C(6)-C(25)	1.5245(15)	C(19)-C(20)	1.5290(17)
C(14)-C(15)	1.3788(16)	C(25)-C(27)	1.5258(17)
C(14)-C(13)	1.4077(16)	C(30)-C(31)	1.3150(19)
C(18)-C(17)	1.3840(17)	C(32)-C(33)	1.520(2)

C(18)-C(13)	1.4044(16)	C(32)-C(32)#1	1.521(3)
C(16)-C(17)	1.3957(17)	C(33)-C(34)	1.512(2)
C(16)-C(15)	1.4002(17)		
C(7)-B(1)-C(13)	121.24(10)	C(18)-C(13)-C(14)	116.14(10)
C(7)-B(1)-C(1)	120.65(10)	C(18)-C(13)-B(1)	120.40(10)
C(13)-B(1)-C(1)	118.10(10)	C(14)-C(13)-B(1)	123.42(10)
C(11)-C(12)-C(7)	121.47(11)	C(2)-C(3)-C(4)	121.75(10)
C(8)-C(9)-C(10)	120.76(11)	C(5)-C(4)-C(3)	117.88(10)
C(4)-C(5)-C(6)	121.84(10)	C(5)-C(4)-C(22)	121.38(10)
C(9)-C(10)-C(11)	117.71(10)	C(3)-C(4)-C(22)	120.72(10)
C(9)-C(10)-C(28)	123.37(11)	C(18)-C(17)-C(16)	121.01(11)
C(11)-C(10)-C(28)	118.92(11)	C(6)-C(1)-C(2)	118.53(10)
C(5)-C(6)-C(1)	119.83(10)	C(6)-C(1)-B(1)	121.86(10)
C(5)-C(6)-C(25)	119.56(10)	C(2)-C(1)-B(1)	119.58(9)
C(1)-C(6)-C(25)	120.60(10)	C(3)-C(2)-C(1)	120.16(10)
C(15)-C(14)-C(13)	122.17(11)	C(3)-C(2)-C(19)	119.37(10)
C(17)-C(18)-C(13)	121.98(11)	C(1)-C(2)-C(19)	120.39(10)

C(17)-C(16)-C(15)	117.79(11)	C(14)-C(15)-C(16)	120.89(11)
C(17)-C(16)-C(30)	119.53(11)	C(29)-C(28)-C(10)	127.59(13)
C(15)-C(16)-C(30)	122.65(11)	C(2)-C(19)-C(21)	112.14(10)
C(9)-C(8)-C(7)	122.19(11)	C(2)-C(19)-C(20)	110.66(10)
C(4)-C(22)-C(24)	111.79(9)	C(21)-C(19)-C(20)	111.38(10)
C(4)-C(22)-C(23)	111.01(9)	C(6)-C(25)-C(26)	112.47(9)
C(24)-C(22)-C(23)	110.51(10)	C(6)-C(25)-C(27)	111.34(10)
C(8)-C(7)-C(12)	116.37(10)	C(26)-C(25)-C(27)	110.54(10)
C(8)-C(7)-B(1)	120.54(10)	C(31)-C(30)-C(16)	126.48(12)
C(12)-C(7)-B(1)	123.08(10)	C(33)-C(32)-C(32)#1	113.94(14)
C(12)-C(11)-C(10)	121.49(11)	C(34)-C(33)-C(32)	113.57(12)

Bond Lengths (Å) and Bond Angles (deg) of (Styryl)₂BQ (30)

B(1)-O(1)	1.5233(15)	C(12)-C(13)	1.4056(17)
B(1)-C(9)	1.6054(17)	C(12)-C(15)	1.4708(17)
B(1)-C(1)	1.6093(17)	C(13)-C(14)	1.3829(17)
B(1)-N(1)	1.6365(16)	C(15)-C(16)	1.3193(18)

C(1)-C(2)	1.3952(16)	C(17)-N(1)	1.3298(16)
C(1)-C(6)	1.4028(17)	C(17)-C(18)	1.4037(17)
C(2)-C(3)	1.3912(17)	C(18)-C(19)	1.3745(18)
C(3)-C(4)	1.3954(17)	C(19)-C(25)	1.4151(19)
C(4)-C(5)	1.4010(17)	C(20)-C(21)	1.3777(19)
C(4)-C(7)	1.4738(17)	C(20)-C(25)	1.4184(18)
C(5)-C(6)	1.3811(17)	C(21)-C(22)	1.4135(18)
C(7)-C(8)	1.3199(19)	C(22)-C(23)	1.3743(17)
C(9)-C(10)	1.3968(16)	C(23)-O(1)	1.3356(14)
C(9)-C(14)	1.4028(16)	C(23)-C(24)	1.4104(17)
C(10)-C(11)	1.3888(17)	C(24)-N(1)	1.3597(15)
C(11)-C(12)	1.3931(17)	C(24)-C(25)	1.3963(17)
O(1)-B(1)-C(9)	110.52(9)	C(13)-C(12)-C(15)	122.96(11)
O(1)-B(1)-C(1)	111.06(9)	C(14)-C(13)-C(12)	120.54(10)
C(9)-B(1)-C(1)	116.29(10)	C(13)-C(14)-C(9)	122.44(11)
O(1)-B(1)-N(1)	98.95(9)	C(16)-C(15)-C(12)	127.50(12)
C(9)-B(1)-N(1)	110.56(9)	N(1)-C(17)-C(18)	120.00(11)

C(1)-B(1)-N(1)	108.06(9)	C(19)-C(18)-C(17)	121.27(11)
C(2)-C(1)-C(6)	116.41(11)	C(18)-C(19)-C(25)	119.47(11)
C(2)-C(1)-B(1)	122.50(10)	C(21)-C(20)-C(25)	119.35(12)
C(6)-C(1)-B(1)	121.00(10)	C(20)-C(21)-C(22)	123.59(12)
C(3)-C(2)-C(1)	121.95(11)	C(23)-C(22)-C(21)	118.14(12)
C(2)-C(3)-C(4)	120.99(11)	O(1)-C(23)-C(22)	129.32(11)
C(3)-C(4)-C(5)	117.52(11)	O(1)-C(23)-C(24)	112.52(10)
C(3)-C(4)-C(7)	120.38(11)	C(22)-C(23)-C(24)	118.16(11)
C(5)-C(4)-C(7)	122.09(11)	N(1)-C(24)-C(25)	124.54(11)
C(6)-C(5)-C(4)	120.94(11)	N(1)-C(24)-C(23)	110.71(11)
C(5)-C(6)-C(1)	122.14(11)	C(25)-C(24)-C(23)	124.75(11)
C(8)-C(7)-C(4)	126.79(12)	C(24)-C(25)-C(19)	115.55(11)
C(10)-C(9)-C(14)	116.38(11)	C(24)-C(25)-C(20)	116.01(12)
C(10)-C(9)-B(1)	123.93(10)	C(19)-C(25)-C(20)	128.44(12)
C(14)-C(9)-B(1)	119.58(10)	C(17)-N(1)-C(24)	119.16(10)
C(11)-C(10)-C(9)	121.73(11)	C(17)-N(1)-B(1)	133.68(10)
C(10)-C(11)-C(12)	121.42(11)	C(24)-N(1)-B(1)	107.15(9)

C(11)-C(12)-C(13)	117.49(11)	C(23)-O(1)-B(1)	110.66(9)
C(11)-C(12)-C(15)	119.53(11)		

Appendix 3

Appendix 3.1 The following tables are supplementary material for the x-ray crystal structures of compounds **4-MePy-CuC₆F₅** (18), **2-MePy-CuC₆F₅** (19), **4-ClPy-CuC₆F₅** (20) and **2-ClPy-CuC₆F₅** (21). Bond lengths and bond angles are listed for (18-21).

Crystal Data and Structure Refinement Details of 4-MePy-CuC₆F₅ and 2-MePy-CuC₆F₅

	4-MePy-CuC₆F₅ (18)	2-MePy-CuC₆F₅ (19)
empirical Formula	C ₁₂ H ₇ CuF ₅ N	C ₁₂ H ₇ CuF ₅ N
formula Weight	323.73	323.73
<i>T</i> , K	100(2)	100(2)
Wavelength, Å	0.71073	1.54178
crystal system	Triclinic	Monoclinic
space group	P-1	P2(1)/c
<i>a</i> , Å	5.9779(4)	6.10850(10)

b , Å	7.2228(6)	7.5034(2)
c , Å	13.4698(10)	25.0325(5)
α , deg	91.634(2)	90
β , deg	90.298(2)	95.5830(10)
γ , deg	95.320(2)	90
V , Å ³	578.83(8)	1141.91(4)
<i>Section 1.03</i> Z	2	4
ρ_{calcd} , g cm ⁻³	1.857	1.883
μ , mm ⁻¹	1.935 (MoK α)	3.228 (CuK α)
F(000)	320	640
crystal size, mm	0.30 x 0.30 x 0.20	0.25 x 0.21 x 0.17
Limiting indices	$-7 \leq h \leq 7$ $-9 \leq k \leq 9$ $-17 \leq l \leq 17$	$-7 \leq h \leq 7$ $-7 \leq k \leq 8$ $-29 \leq l \leq 29$
θ range, deg	1.51 – 27.49	3.55 – 65.01
reflns collected	4730	8938
independent reflns	2463	1914
absorption correction	Semi-empirical equivalents	from Semi-empirical equivalents
refinement method	Full-matrix on F^2	least-squares Full-matrix on F^2
data/restraints/parameters	2463 / 0 / 172	1914 / 0 / 173
Goodness-of-fit on F^2	1.064	1.186

Final <i>R</i> indices	<i>R</i> 1 = 0.0422	<i>R</i> 1 = 0.0260
$[I > 2\sigma(I)]^{[a]}$	<i>wR</i> 2 = 0.1168	<i>wR</i> 2 = 0.0696
<i>R</i> indices (all data) ^[a]	<i>R</i> 1 = 0.0464	<i>R</i> 1 = 0.0263
	<i>wR</i> 2 = 0.1207	<i>wR</i> 2 = 0.0699
Peak/hole (e Å ⁻³)	1.379 / -0.721	0.246 / -0.472

[a] $R1 = \Sigma||F_o| - |F_c|| / \Sigma|F_o|$; $wR2 = \{ \Sigma[w(F_o^2 - F_c^2)^2] / \Sigma[w(F_o^2)^2] \}^{1/2}$.

Bond Lengths (Å) and Bond Angles (deg) of 4-MePy-CuC₆F₅ (18)

Cu(1)-C(1)	1.891(3)	C(2)-C(1)	1.393(3)
Cu(1)-N(1)	1.900(2)	C(6)-C(1)	1.380(4)
F(5)-C(5)	1.347(3)	C(6)-C(5)	1.382(4)
F(4)-C(4)	1.348(3)	C(12)-C(9)	1.501(4)
F(2)-C(2)	1.359(3)	C(7)-C(8)	1.380(4)
F(6)-C(6)	1.363(3)	C(5)-C(4)	1.383(4)
F(3)-C(3)	1.357(3)	C(11)-C(10)	1.384(4)
N(1)-C(11)	1.345(3)	C(9)-C(10)	1.393(4)
N(1)-C(7)	1.352(3)	C(9)-C(8)	1.393(4)
C(2)-C(3)	1.376(4)	C(4)-C(3)	1.378(4)

C(1)-Cu(1)-N(1)	177.88(8)	C(10)-C(9)-C(8)	117.1(2)
C(11)-N(1)-C(7)	118.0(2)	C(10)-C(9)-C(12)	121.6(2)
C(11)-N(1)-Cu(1)	121.36(18)	C(8)-C(9)-C(12)	121.3(2)
C(7)-N(1)-Cu(1)	120.64(18)	F(4)-C(4)-C(3)	120.5(2)
F(2)-C(2)-C(3)	116.8(2)	F(4)-C(4)-C(5)	120.0(2)
F(2)-C(2)-C(1)	119.5(2)	C(3)-C(4)-C(5)	119.5(2)
C(3)-C(2)-C(1)	123.7(2)	C(11)-C(10)-C(9)	120.1(2)
F(6)-C(6)-C(1)	119.6(2)	C(6)-C(1)-C(2)	114.1(2)
F(6)-C(6)-C(5)	115.8(2)	C(6)-C(1)-Cu(1)	121.36(19)
C(1)-C(6)-C(5)	124.7(2)	C(2)-C(1)-Cu(1)	124.5(2)
N(1)-C(7)-C(8)	122.4(2)	C(7)-C(8)-C(9)	120.1(2)
F(5)-C(5)-C(4)	119.6(2)	F(3)-C(3)-C(2)	121.4(2)
		F(3)-C(3)-C(4)	119.0(2)
		C(2)-C(3)-C(4)	119.5(2)

Bond Lengths (Å) and Bond Angles (deg) of 2-MePy-CuC₆F₅ (19)

Cu(1)-C(1)	1.897(2)	C(6)-F(6)	1.367(2)
Cu(1)-N(1)	1.9078(16)	C(7)-C(8)	1.392(3)

N(1)-C(11)	1.349(3)	C(7)-C(12)	1.497(3)
N(1)-C(7)	1.354(3)	C(8)-C(9)	1.384(3)
C(1)-C(2)	1.383(3)	C(8)-H(8)	0.9500
C(1)-C(6)	1.384(3)	C(9)-C(10)	1.388(3)
C(2)-F(2)	1.363(2)	C(9)-H(9)	0.9500
C(2)-C(3)	1.381(3)	C(10)-C(11)	1.379(3)
C(3)-F(3)	1.351(2)	C(10)-H(10)	0.9500
C(3)-C(4)	1.378(3)	C(11)-H(11)	0.9500
C(4)-F(4)	1.346(2)	C(12)-H(12A)	0.9800
C(4)-C(5)	1.378(3)	C(12)-H(12B)	0.9800
C(5)-F(5)	1.349(2)	C(12)-H(12C)	0.9800
C(5)-C(6)	1.378(3)		
C(1)-Cu(1)-N(1)	174.66(8)	C(5)-C(6)-C(1)	124.77(18)
C(11)-N(1)-C(7)	119.09(17)	N(1)-C(7)-C(8)	120.63(18)
C(11)-N(1)-Cu(1)	120.77(13)	N(1)-C(7)-C(12)	116.98(17)
C(7)-N(1)-Cu(1)	120.15(13)	C(8)-C(7)-C(12)	122.39(18)
C(2)-C(1)-C(6)	113.73(18)	C(9)-C(8)-C(7)	119.92(18)

C(2)-C(1)-Cu(1)	124.12(15)	C(9)-C(8)-H(8)	120
C(6)-C(1)-Cu(1)	122.15(15)	C(7)-C(8)-H(8)	120
F(2)-C(2)-C(3)	116.11(16)	C(8)-C(9)-C(10)	119.15(19)
F(2)-C(2)-C(1)	119.68(17)	C(8)-C(9)-H(9)	120.4
C(3)-C(2)-C(1)	124.20(18)	C(10)-C(9)-H(9)	120.4
F(3)-C(3)-C(4)	119.22(17)	C(11)-C(10)-C(9)	118.42(18)
F(3)-C(3)-C(2)	121.73(17)	C(11)-C(10)-H(10)	120.8
C(4)-C(3)-C(2)	119.04(18)	C(9)-C(10)-H(10)	120.8
F(4)-C(4)-C(3)	120.22(18)	N(1)-C(11)-C(10)	122.80(18)
F(4)-C(4)-C(5)	120.11(18)	N(1)-C(11)-H(11)	118.6
C(3)-C(4)-C(5)	119.67(18)	C(10)-C(11)-H(11)	118.6
F(5)-C(5)-C(6)	121.83(17)	C(7)-C(12)-H(12A)	109.5
F(5)-C(5)-C(4)	119.58(18)	C(7)-C(12)-H(12B)	109.5
C(6)-C(5)-C(4)	118.59(18)	H(12A)-C(12)-H(12B)	109.5
F(6)-C(6)-C(5)	115.79(17)	C(7)-C(12)-H(12C)	109.5
F(6)-C(6)-C(1)	119.44(18)	H(12A)-C(12)-H(12C)	109.5
		H(12B)-C(12)-H(12C)	109.5

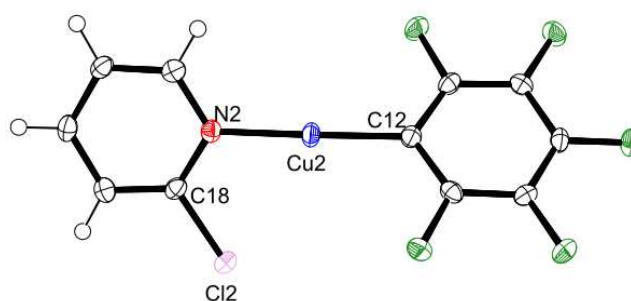
Crystal Data and Structure Refinement Details of 4-ClPy-CuC₆F₅ (20) and 2-ClPy-CuC₆F₅ (21)

	4-ClPy-CuC₆F₅ (20)	2-ClPy-CuC₆F₅ (21)
empirical Formula	C ₁₁ H ₄ ClCuF ₅ N	C ₁₁ H ₄ ClCuF ₅ N
formula Weight	344.15	344.15
<i>T</i> , K	100(2)	100(2)
Wavelength, Å	0.71073	1.54178
crystal system	Triclinic	Monoclinic
space group	P-1	P2(1)/c
<i>a</i> , Å	5.9903(9)	12.5523(2)
<i>b</i> , Å	7.2800(10)	7.1538(2)
<i>c</i> , Å	13.0816(19)	24.8910(5)
<i>α</i> , deg	88.434(2)	90
<i>β</i> , deg	86.879(2)	98.5210(10)
<i>γ</i> , deg	83.596(2)	90
<i>V</i> , Å ³	565.95(14)	2210.46(8)
<i>Section 1.04</i> <i>Z</i>	2	8
<i>ρ</i> _{calcd} , Mg m ⁻³	2.019	2.068
<i>μ</i> , mm ⁻¹	2.214 (MoK _α)	5.561 (CuK _α)
F(000)	336	1344
crystal size, mm	0.20 x 0.20 x 0.10	0.18 x 0.16 x 0.10

Limiting indices	$-7 \leq h \leq 7$	$-14 \leq h \leq 14$
	$-9 \leq k \leq 9$	$-8 \leq k \leq 8$
	$-16 \leq l \leq 16$	$-29 \leq l \leq 28$
θ range, deg	2.82 – 27.53	5.42 – 64.44
reflns collected	4782	13162
independent reflns	2449	3535
absorption correction	Semi-empirical equivalents	from Semi-empirical equivalents
refinement method	Full-matrix least-squares on F^2	Full-matrix least-squares on F^2
data/restraints/parameters	2449 / 0 / 172	3535 / 0 / 343
Goodness-of-fit on F^2	1.074	1.161
Final R indices	$R1 = 0.0275$	$R1 = 0.0335$
$[I > 2\sigma(I)]^{[a]}$	$wR2 = 0.0750$	$wR2 = 0.0882$
R indices (all data) ^[a]	$R1 = 0.0296$	$R1 = 0.0365$
	$wR2 = 0.0767$	$wR2 = 0.0906$
Peak/hole ($e \text{ \AA}^{-3}$)	0.769 / -0.298	0.566 / -0.348

[a] $R1 = \Sigma||F_o| - |F_c|| / \Sigma|F_o|$; $wR2 = \{ \Sigma[w(F_o^2 - F_c^2)^2] / \Sigma[w(F_o^2)^2] \}^{1/2}$.

Appendix 3.2 The following is ORTEP plot of the second molecule of **2-ClPy-CuC₆F₅** (21) (50% probability).



Selected Bond Lengths (Å) and Angles (deg): Cu2-C12 = 1.899(3), Cu2-N2 = 1.909(2) ,
C18-Cl2 = 1.723(3), C12-Cu2-N2 = 176.19(10), (Py) // (Pf) = 43.13.

Bond Lengths (Å) and Bond Angles (deg) of 4-ClPy-CuC₆F₅ (20)

Cu(1)-C(1)	1.8873(19)	C(2)-C(3)	1.377(3)
Cu(1)-N(1)	1.8972(16)	C(3)-C(4)	1.388(2)
Cl(1)-C(9)	1.7212(18)	C(4)-C(5)	1.384(2)
N(1)-C(11)	1.345(2)	C(5)-C(6)	1.371(3)
N(1)-C(7)	1.354(2)	C(7)-C(8)	1.381(3)
F(2)-C(2)	1.3649(19)	C(7)-H(7A)	0.95
F(3)-C(3)	1.3487(19)	C(8)-C(9)	1.384(3)
F(4)-C(4)	1.342(2)	C(8)-H(8A)	0.95
F(5)-C(5)	1.347(2)	C(9)-C(10)	1.388(2)

F(6)-C(6)	1.3676(19)	C(10)-C(11)	1.379(3)
C(1)-C(2)	1.386(2)	C(10)-H(10A)	0.95
C(1)-C(6)	1.389(2)	C(11)-H(11A)	0.95
C(1)-Cu(1)-N(1)	176.34(7)	C(6)-C(5)-C(4)	119.03(16)
C(11)-N(1)-C(7)	117.74(16)	F(6)-C(6)-C(5)	116.19(15)
C(11)-N(1)-Cu(1)	120.47(12)	F(6)-C(6)-C(1)	118.86(16)
C(7)-N(1)-Cu(1)	121.74(13)	C(5)-C(6)-C(1)	124.96(16)
C(2)-C(1)-C(6)	113.29(16)	N(1)-C(7)-C(8)	122.79(17)
C(2)-C(1)-Cu(1)	126.00(14)	N(1)-C(7)-H(7A)	118.6
C(6)-C(1)-Cu(1)	120.65(13)	C(8)-C(7)-H(7A)	118.6
F(2)-C(2)-C(3)	116.08(15)	C(7)-C(8)-C(9)	118.13(17)
F(2)-C(2)-C(1)	119.28(16)	C(7)-C(8)-H(8A)	120.9
C(3)-C(2)-C(1)	124.63(16)	C(9)-C(8)-H(8A)	120.9
F(3)-C(3)-C(2)	121.80(15)	C(8)-C(9)-C(10)	120.16(17)
F(3)-C(3)-C(4)	119.10(16)	C(8)-C(9)-Cl(1)	120.78(14)
C(2)-C(3)-C(4)	119.10(16)	C(10)-C(9)-Cl(1)	119.07(14)
F(4)-C(4)-C(5)	120.81(16)	C(11)-C(10)-C(9)	117.93(16)

F(4)-C(4)-C(3)	120.20(16)	C(11)-C(10)-H(10A)	121
C(5)-C(4)-C(3)	118.98(16)	C(9)-C(10)-H(10A)	121
F(5)-C(5)-C(6)	121.58(16)	N(1)-C(11)-C(10)	123.24(16)
F(5)-C(5)-C(4)	119.38(16)	N(1)-C(11)-H(11A)	118.4
		C(10)-C(11)-H(11A)	118.4

Bond Lengths (Å) and Bond Angles (deg) of 2-ClPy-CuC₆F₅ (21)

Cu(2)-C(12)	1.899(3)	C(11)-C(10)	1.378(4)
Cu(2)-N(2)	1.908(2)	C(11)-H(11)	0.9500
Cu(1)-C(1)	1.901(3)	C(9)-C(8)	1.377(4)
Cu(1)-N(1)	1.917(2)	C(9)-C(10)	1.395(4)
Cl(1)-C(7)	1.726(3)	C(9)-H(9)	0.9500
Cl(2)-C(18)	1.723(3)	C(19)-H(19)	0.9500
C(13)-F(13)	1.359(3)	C(22)-N(2)	1.349(4)
C(13)-C(12)	1.381(4)	C(22)-C(21)	1.377(4)
C(13)-C(14)	1.387(4)	C(22)-H(22)	0.9500
C(18)-N(2)	1.339(4)	C(7)-N(1)	1.338(4)

C(18)-C(19)	1.379(4)	C(7)-C(8)	1.380(4)
C(2)-F(2)	1.356(3)	C(14)-F(14)	1.347(3)
C(2)-C(3)	1.384(4)	C(14)-C(15)	1.381(4)
C(2)-C(1)	1.387(4)	C(10)-H(10)	0.9500
C(17)-F(17)	1.360(3)	C(4)-F(4)	1.352(3)
C(17)-C(12)	1.384(4)	C(4)-C(3)	1.375(4)
C(17)-C(16)	1.386(4)	C(4)-C(5)	1.375(4)
C(20)-C(19)	1.384(4)	C(21)-H(21)	0.9500
C(20)-C(21)	1.389(4)	C(3)-F(3)	1.351(3)
C(20)-H(20)	0.9500	C(8)-H(8)	0.9500
C(6)-F(6)	1.356(3)	C(16)-F(16)	1.353(3)
C(6)-C(1)	1.383(4)	C(16)-C(15)	1.373(4)
C(6)-C(5)	1.385(4)	C(5)-F(5)	1.353(3)
C(11)-N(1)	1.350(4)	C(15)-F(15)	1.347(3)
C(12)-Cu(2)-N(2)	176.19(10)	C(8)-C(7)-Cl(1)	120.6(2)
C(1)-Cu(1)-N(1)	177.75(11)	C(6)-C(1)-C(2)	114.2(2)

F(13)-C(13)-C(12)	120.0(2)	C(6)-C(1)-Cu(1)	120.9(2)
F(13)-C(13)-C(14)	115.9(2)	C(2)-C(1)-Cu(1)	124.8(2)
C(12)-C(13)-C(14)	124.1(3)	F(14)-C(14)-C(15)	119.7(2)
N(2)-C(18)-C(19)	124.1(3)	F(14)-C(14)-C(13)	121.5(2)
N(2)-C(18)-Cl(2)	115.43(19)	C(15)-C(14)-C(13)	118.9(3)
C(19)-C(18)-Cl(2)	120.5(2)	C(11)-C(10)-C(9)	118.7(3)
F(2)-C(2)-C(3)	116.0(2)	C(11)-C(10)-H(10)	120.7
F(2)-C(2)-C(1)	120.1(2)	C(9)-C(10)-H(10)	120.7
C(3)-C(2)-C(1)	123.8(3)	F(4)-C(4)-C(3)	120.1(2)
F(17)-C(17)-C(12)	120.1(2)	F(4)-C(4)-C(5)	120.1(3)
F(17)-C(17)-C(16)	116.0(2)	C(3)-C(4)-C(5)	119.8(2)
C(12)-C(17)-C(16)	123.8(3)	C(22)-C(21)-C(20)	118.7(3)
C(19)-C(20)-C(21)	119.7(2)	C(22)-C(21)-H(21)	120.7
C(19)-C(20)-H(20)	120.2	C(20)-C(21)-H(21)	120.7
C(21)-C(20)-H(20)	120.2	F(3)-C(3)-C(4)	119.6(2)
F(6)-C(6)-C(1)	119.7(2)	F(3)-C(3)-C(2)	121.3(3)
F(6)-C(6)-C(5)	116.2(2)	C(4)-C(3)-C(2)	119.1(2)

C(1)-C(6)-C(5)	124.1(3)	C(9)-C(8)-C(7)	118.1(3)
N(1)-C(11)-C(10)	122.5(3)	C(9)-C(8)-H(8)	121
N(1)-C(11)-H(11)	118.7	C(7)-C(8)-H(8)	121
C(10)-C(11)-H(11)	118.7	F(16)-C(16)-C(15)	119.3(2)
C(8)-C(9)-C(10)	119.3(3)	F(16)-C(16)-C(17)	121.5(2)
C(8)-C(9)-H(9)	120.3	C(15)-C(16)-C(17)	119.2(2)
C(10)-C(9)-H(9)	120.4	F(5)-C(5)-C(4)	119.6(2)
C(18)-C(19)-C(20)	117.5(3)	F(5)-C(5)-C(6)	121.4(2)
C(18)-C(19)-H(19)	121.2	C(4)-C(5)-C(6)	118.9(3)
C(20)-C(19)-H(19)	121.2	F(15)-C(15)-C(16)	120.2(2)
N(2)-C(22)-C(21)	122.6(3)	F(15)-C(15)-C(14)	120.2(2)
N(2)-C(22)-H(22)	118.7	C(16)-C(15)-C(14)	119.6(2)
C(21)-C(22)-H(22)	118.7	C(7)-N(1)-C(11)	117.5(2)
C(13)-C(12)-C(17)	114.4(2)	C(7)-N(1)-Cu(1)	119.80(19)
C(13)-C(12)-Cu(2)	123.9(2)	C(11)-N(1)-Cu(1)	122.62(18)
C(17)-C(12)-Cu(2)	121.6(2)	C(18)-N(2)-C(22)	117.5(2)
N(1)-C(7)-C(8)	123.8(3)	C(18)-N(2)-Cu(2)	120.46(19)

N(1)-C(7)-Cl(1)	115.58(19)	C(22)-N(2)-Cu(2)	122.07(18)
-----------------	------------	------------------	------------

Appendix 3.3 The following tables are supplementary material for the x-ray crystal structures of compounds **8-Np₂** (27), **8-Bt₂** (28), **{8-Np}_n** (29), **{8-Bt}_n** (30), **8-Anth₂** (31), **{8-Pyr}_n** (32), and **8-Pyrene₂** (33). Bond lengths and bond angles are listed for (27-33).

Crystal Data and Structure Refinement Details of 1-Np₂, 1-Bt₂ and 1-Anth₂

	8-Np₂ (27)	8-Bt₂ (28)	8-Anth₂ (31)
empirical Formula	C ₄₄ H ₁₆ Cu ₄ F ₂₀	C ₄₀ H ₁₂ Cu ₄ F ₂₀ S ₄	C ₅₂ H ₂₀ Cu ₄ F ₂₀
formula Weight	1178.73	1254.90	1278.84
<i>T</i> , K	100(2)	203(2) K	100(2)
Wavelength, Å	1.54178	0.71073	1.54178
crystal system	monoclinic	Monoclinic	Monoclinic
space group	P(2)1/c	P2(1)/c	P2(1)/c
<i>a</i> , Å	11.7660(5)	11.8629(15)	11.9453(3)
<i>b</i> , Å	6.4260(3)	6.3870(8)	6.3138(2)
<i>c</i> , Å	26.2579(10)	26.727(3)	28.3348(9)
<i>α</i> , deg	90	90	90

β , deg	102.9340(10)	97.690(2)	94.131(2)
Γ , deg	90	90	90
V , Å ³	1934.94(14)	2006.8(4)	2131.47(11)
<i>Section 1.05</i> Z	2	2	2
ρ_{calcd} , Mg m ⁻³	2.023	2.077	1.993
μ , mm ⁻¹	3.701	2.426	3.427
F(000)	1152	1224	1256
crystal size, mm	0.24 x 0.18 x 0.12	0.37 x 0.10 x 0.07	0.44 x 0.09 x 0.08
Limiting indices	-13<= h <=14	-15<= h <=15	-14<= h <=14
	-7<= k <=6	-8<= k <=3	-7<= k <=7
	-31<= l <=30	-33<= l <=35	-31<= l <=26
θ range, deg	3.85 – 68.08	1.54 – 28.26	3.13 – 64.98
reflns collected	12142	13608	9822
independent reflns	3440	4762	3336
absorption correction	Numerical	Multi-scan	Semi-empirical from equivalents
refinement method	Full-matrix least-squares on F^2	Full-matrix least-squares on F^2	Full-matrix least-squares on F^2
data/restraints/parameters	3440 / 0 / 308	4762 / 0 / 312	3336 / 0 / 344
Goodness-of-fit on F^2	1.236	1.076	1.054
Final R indices	R1 = 0.0356	R1 = 0.0305	R1 = 0.0312

$[I > 2\sigma(I)]^{[a]}$	wR2 = 0.0889	wR2 = 0.0849	wR2 = 0.0823
R indices (all data) ^[a]	R1 = 0.0424	R1 = 0.0352	R1 = 0.0336
	wR2 = 0.1277	wR2 = 0.0880	wR2 = 0.0847
Peak/hole (e Å ⁻³)	0.696 / -0.905	0.589 / -0.452	0.695 and -0.363
[a] $R1 = \Sigma F_o - F_c /\Sigma F_o $; $wR2 = \{\Sigma[w(F_o^2-F_c^2)^2]/\Sigma[w(F_o^2)^2]\}^{1/2}$.			

Bond Lengths (Å) and Bond Angles (deg) of 8-Np₂ (27)

C(1)-C(6)	1.392(6)	C(10)-F(8)	1.330(4)
C(1)-C(2)	1.395(6)	C(10)-C(11)	1.384(6)
C(1)-Cu(1)	2.008(4)	C(11)-F(9)	1.338(5)
C(1)-Cu(2)#1	2.018(4)	C(11)-C(12)	1.374(6)
C(2)-F(1)	1.337(5)	C(12)-F(10)	1.349(5)
C(2)-C(3)	1.404(6)	C(13)-C(14)	1.366(6)
C(3)-F(2)	1.331(5)	C(13)-C(18)	1.417(6)
C(3)-C(4)	1.379(7)	C(14)-C(15)	1.405(6)
C(4)-F(3)	1.348(5)	C(15)-C(16)	1.427(6)
C(4)-C(5)	1.378(7)	C(15)-C(19)	1.428(5)
C(5)-F(4)	1.345(5)	C(16)-C(22)	1.410(6)

C(5)-C(6)	1.351(6)	C(16)-C(17)	1.420(6)
C(6)-F(5)	1.365(5)	C(17)-C(18)	1.376(6)
C(7)-C(8)	1.378(6)	C(19)-C(20)	1.356(6)
C(7)-C(12)	1.395(6)	C(20)-C(21)	1.414(6)
C(7)-Cu(1)	1.987(4)	C(21)-C(22)	1.366(6)
C(7)-Cu(2)	2.028(4)	C(1)-C(2)#1	2.4408(7)
C(8)-F(6)	1.348(4)	C(1)-C(2)	2.4993(8)
C(8)-C(9)	1.400(5)	C(2)-C(1)#1	2.018(4)
C(9)-F(7)	1.336(5)	C(2)-C(1)#1	2.4408(7)
C(9)-C(10)	1.378(6)	C(2)-C(2)#1	2.6343(11)
C(6)-C(1)-C(2)	114.3(4)	F(9)-C(11)-C(10)	118.9(4)
C(6)-C(1)-Cu(1)	115.6(3)	C(12)-C(11)-C(10)	119.3(4)
C(2)-C(1)-Cu(1)	120.7(3)	C(9)-C(10)-C(11)	120.4(3)
C(6)-C(1)-Cu(2)#1	110.9(3)	F(10)-C(12)-C(11)	118.4(4)
C(2)-C(1)-Cu(2)#1	114.2(3)	F(10)-C(12)-C(7)	118.9(3)
Cu(1)-C(1)-Cu(2)#1	74.63(13)	C(11)-C(12)-C(7)	122.7(4)
F(1)-C(2)-C(1)	120.8(4)	C(14)-C(13)-C(18)	120.3(4)

F(1)-C(2)-C(3)	116.2(4)	C(13)-C(14)-C(15)	120.8(4)
C(1)-C(2)-C(3)	123.0(4)	C(14)-C(15)-C(16)	119.7(4)
F(2)-C(3)-C(4)	120.7(4)	C(14)-C(15)-C(19)	122.3(4)
F(2)-C(3)-C(2)	121.5(4)	C(16)-C(15)-C(19)	118.1(4)
C(4)-C(3)-C(2)	117.7(4)	C(22)-C(16)-C(17)	122.2(4)
F(3)-C(4)-C(5)	120.4(4)	C(22)-C(16)-C(15)	119.5(4)
F(3)-C(4)-C(3)	118.1(4)	C(17)-C(16)-C(15)	118.3(4)
C(5)-C(4)-C(3)	121.5(4)	C(18)-C(17)-C(16)	120.8(4)
F(4)-C(5)-C(6)	122.3(4)	C(17)-C(18)-C(13)	120.1(4)
F(4)-C(5)-C(4)	119.7(4)	C(20)-C(19)-C(15)	120.7(4)
C(6)-C(5)-C(4)	118.0(4)	C(19)-C(20)-C(21)	121.1(4)
C(5)-C(6)-F(5)	116.9(4)	C(22)-C(21)-C(20)	119.7(4)
C(5)-C(6)-C(1)	125.4(4)	C(21)-C(22)-C(16)	120.9(4)
F(5)-C(6)-C(1)	117.6(3)	C(7)-Cu(1)-C(1)	167.72(16)
C(8)-C(7)-C(12)	116.2(3)	C(7)-Cu(1)-Cu(2)#1	116.66(11)
C(8)-C(7)-Cu(1)	117.6(3)	C(1)-Cu(1)-Cu(2)#1	52.88(10)
C(12)-C(7)-Cu(1)	122.1(3)	C(7)-Cu(1)-Cu(2)	52.23(10)

C(8)-C(7)-Cu(2)	108.1(3)	C(1)-Cu(1)-Cu(2)	116.78(11)
C(12)-C(7)-Cu(2)	105.2(3)	Cu(2)#1-Cu(1)-Cu(2)	64.44(3)
Cu(1)-C(7)-Cu(2)	77.00(13)	C(1)#1-Cu(2)-C(7)	140.79(16)
F(6)-C(8)-C(7)	120.0(3)	C(1)#1-Cu(2)-Cu(1)#1	52.49(10)
F(6)-C(8)-C(9)	117.2(3)	C(7)-Cu(2)-Cu(1)#1	166.28(12)
C(7)-C(8)-C(9)	122.8(4)	C(1)#1-Cu(2)-Cu(1)	165.93(11)
F(7)-C(9)-C(10)	120.8(3)	C(7)-Cu(2)-Cu(1)	50.76(11)
F(7)-C(9)-C(8)	120.7(4)	Cu(1)#1-Cu(2)-Cu(1)	115.56(3)
C(10)-C(9)-C(8)	118.5(4)	C(1)#1-Cu(2)-Cu(2)#1	110.86(11)
F(8)-C(10)-C(9)	119.5(4)	C(7)-Cu(2)-Cu(2)#1	107.46(12)
F(8)-C(10)-C(11)	120.1(4)	Cu(1)#1-Cu(2)-Cu(2)#1	58.86(2)
F(9)-C(11)-C(12)	121.8(4)	Cu(1)-Cu(2)-Cu(2)#1	56.71(2)

Bond Lengths (Å) and Bond Angles (deg) of 8-Bt₂ (28)

Cu(1)-C(7)	1.975(2)	F(12)-C(12)	1.350(3)
Cu(1)-C(1)	2.014(2)	C(1)-C(6)	1.377(3)
Cu(1)-Cu(2)#1	2.4500(4)	C(1)-C(2)	1.387(3)

Cu(1)-Cu(2)	2.5013(4)	C(1)-Cu(2)#1	2.023(2)
Cu(1)-C(13)	2.507(2)	C(2)-C(3)	1.377(3)
Cu(2)-C(7)	2.021(2)	C(3)-C(4)	1.375(4)
Cu(2)-C(1)#1	2.023(2)	C(4)-C(5)	1.367(4)
Cu(2)-Cu(1)#1	2.4501(4)	C(5)-C(6)	1.380(3)
Cu(2)-Cu(2)#1	2.5866(6)	C(7)-C(8)	1.381(3)
S(1)-C(13)	1.705(3)	C(7)-C(12)	1.390(3)
S(1)-C(16)	1.712(2)	C(8)-C(9)	1.381(3)
S(2)-C(20)	1.666(4)	C(9)-C(10)	1.369(4)
S(2)-C(17)	1.702(3)	C(10)-C(11)	1.377(4)
F(2)-C(2)	1.355(3)	C(11)-C(12)	1.378(3)
F(3)-C(3)	1.344(3)	C(13)-C(14)	1.363(4)
F(4)-C(4)	1.335(3)	C(14)-C(15)	1.432(3)
F(5)-C(5)	1.344(3)	C(15)-C(16)	1.416(3)
F(6)-C(6)	1.348(3)	C(16)-C(17)	1.454(3)
F(8)-C(8)	1.352(3)	C(17)-C(18)	1.523(3)
F(9)-C(9)	1.340(3)	C(18)-C(19)	1.484(4)

F(10)-C(10)	1.340(3)	C(19)-C(20)	1.330(5)
F(11)-C(11)	1.337(3)		
C(7)-Cu(1)-C(1)	166.96(9)	F(6)-C(6)-C(1)	120.28(19)
C(7)-Cu(1)-Cu(2)#1	115.01(6)	F(6)-C(6)-C(5)	116.3(2)
C(1)-Cu(1)-Cu(2)#1	52.81(6)	C(1)-C(6)-C(5)	123.4(2)
C(7)-Cu(1)-Cu(2)	52.08(6)	C(8)-C(7)-C(12)	114.76(19)
C(1)-Cu(1)-Cu(2)	115.36(6)	C(8)-C(7)-Cu(1)	118.47(16)
Cu(2)#1-Cu(1)-Cu(2)	62.979(14)	C(12)-C(7)-Cu(1)	122.33(17)
C(7)-Cu(1)-C(13)	100.14(8)	C(8)-C(7)-Cu(2)	109.38(15)
C(1)-Cu(1)-C(13)	92.70(8)	C(12)-C(7)-Cu(2)	104.54(15)
Cu(2)#1-Cu(1)-C(13)	143.64(6)	Cu(1)-C(7)-Cu(2)	77.50(7)
Cu(2)-Cu(1)-C(13)	151.58(6)	F(8)-C(8)-C(7)	119.59(19)
C(7)-Cu(2)-C(1)#1	139.56(8)	F(8)-C(8)-C(9)	116.6(2)
C(7)-Cu(2)-Cu(1)#1	167.22(6)	C(7)-C(8)-C(9)	123.8(2)
C(1)#1-Cu(2)-Cu(1)#1	52.45(6)	F(9)-C(9)-C(10)	120.2(2)
C(7)-Cu(2)-Cu(1)	50.42(6)	F(9)-C(9)-C(8)	121.4(2)
C(1)#1-Cu(2)-Cu(1)	167.52(6)	C(10)-C(9)-C(8)	118.5(2)

Cu(1)#1-Cu(2)-Cu(1)	117.022(14)	F(10)-C(10)-C(9)	119.7(2)
C(7)-Cu(2)-Cu(2)#1	107.91(6)	F(10)-C(10)-C(11)	119.4(2)
C(1)#1-Cu(2)-Cu(2)#1	111.53(6)	C(9)-C(10)-C(11)	120.8(2)
Cu(1)#1-Cu(2)-Cu(2)#1	59.480(11)	F(11)-C(11)-C(10)	119.8(2)
Cu(1)-Cu(2)-Cu(2)#1	57.542(13)	F(11)-C(11)-C(12)	121.7(2)
C(13)-S(1)-C(16)	92.15(12)	C(10)-C(11)-C(12)	118.4(2)
C(20)-S(2)-C(17)	92.54(16)	F(12)-C(12)-C(11)	117.5(2)
C(6)-C(1)-C(2)	114.8(2)	F(12)-C(12)-C(7)	118.87(19)
C(6)-C(1)-Cu(1)	121.44(16)	C(11)-C(12)-C(7)	123.6(2)
C(2)-C(1)-Cu(1)	114.27(17)	C(14)-C(13)-S(1)	112.01(19)
C(6)-C(1)-Cu(2)#1	113.97(16)	C(14)-C(13)-Cu(1)	83.10(15)
C(2)-C(1)-Cu(2)#1	110.84(16)	S(1)-C(13)-Cu(1)	108.52(11)
Cu(1)-C(1)-Cu(2)#1	74.73(7)	C(13)-C(14)-C(15)	114.1(2)
F(2)-C(2)-C(3)	117.1(2)	C(16)-C(15)-C(14)	109.4(2)
F(2)-C(2)-C(1)	119.0(2)	C(15)-C(16)-C(17)	127.0(2)
C(3)-C(2)-C(1)	123.9(2)	C(15)-C(16)-S(1)	112.25(16)
F(3)-C(3)-C(4)	120.5(2)	C(17)-C(16)-S(1)	120.73(18)

F(3)-C(3)-C(2)	121.1(3)	C(16)-C(17)-C(18)	125.0(2)
C(4)-C(3)-C(2)	118.3(2)	C(16)-C(17)-S(2)	121.14(18)
F(4)-C(4)-C(5)	119.8(3)	C(18)-C(17)-S(2)	113.79(16)
F(4)-C(4)-C(3)	119.7(3)	C(19)-C(18)-C(17)	101.8(2)
C(5)-C(4)-C(3)	120.4(2)	C(20)-C(19)-C(18)	117.6(3)
F(5)-C(5)-C(4)	119.5(2)	C(19)-C(20)-S(2)	114.0(2)
F(5)-C(5)-C(6)	121.4(2)		
C(4)-C(5)-C(6)	119.1(2)		

Bond Lengths (Å) and Bond Angles (deg) of 8-Anth₂ (31)

Cu(1)-C(1)	1.975(2)	C(4)-F(3)	1.338(3)
Cu(1)-C(7)	2.006(2)	C(4)-C(3)	1.379(4)
Cu(1)-Cu(2)#1	2.4441(5)	C(3)-F(2)	1.342(3)
Cu(1)-Cu(2)	2.5093(5)	C(11)-F(9)	1.344(3)
Cu(2)-C(1)	2.023(2)	C(11)-C(10)	1.385(4)
Cu(2)-C(7)#1	2.030(2)	C(10)-F(8)	1.334(3)
Cu(2)-Cu(1)#1	2.4441(5)	C(10)-C(9)	1.375(4)

Cu(2)-Cu(2)#1	2.6159(7)	C(9)-F(7)	1.341(3)
C(12)-F(10)	1.357(3)	C(20)-C(21)	1.361(4)
C(12)-C(11)	1.377(4)	C(20)-C(19)	1.430(4)
C(12)-C(7)	1.390(4)	C(24)-C(25)	1.397(4)
C(6)-F(5)	1.355(3)	C(24)-C(23)	1.426(4)
C(6)-C(5)	1.377(4)	C(24)-C(19)	1.434(4)
C(6)-C(1)	1.388(3)	C(21)-C(22)	1.417(4)
C(8)-F(6)	1.344(3)	C(18)-C(19)	1.391(4)
C(8)-C(9)	1.382(4)	C(18)-C(17)	1.402(3)
C(8)-C(7)	1.395(4)	C(15)-C(16)	1.366(4)
C(1)-C(2)	1.392(4)	C(15)-C(14)	1.432(4)
C(7)-Cu(2)#1	2.030(2)	C(25)-C(26)	1.399(3)
C(5)-F(4)	1.337(3)	C(13)-C(14)	1.364(4)
C(5)-C(4)	1.389(4)	C(13)-C(26)	1.429(3)
C(2)-F(1)	1.351(3)	C(17)-C(16)	1.425(3)
C(2)-C(3)	1.381(4)	C(17)-C(26)	1.438(4)
		C(23)-C(22)	1.359(4)

C(1)-Cu(1)-C(7)	167.38(10)	F(1)-C(2)-C(3)	117.1(2)
C(1)-Cu(1)-Cu(2)#1	115.70(7)	F(1)-C(2)-C(1)	119.3(2)
C(7)-Cu(1)-Cu(2)#1	53.19(7)	C(3)-C(2)-C(1)	123.6(2)
C(1)-Cu(1)-Cu(2)	52.00(7)	F(3)-C(4)-C(3)	120.0(2)
C(7)-Cu(1)-Cu(2)	116.35(7)	F(3)-C(4)-C(5)	119.7(2)
	63.738(15)	C(3)-C(4)-C(5)	120.3(2)
Cu(2)#1-Cu(1)-Cu(2)			
C(1)-Cu(2)-C(7)#1	140.63(9)	F(2)-C(3)-C(4)	119.8(2)
C(1)-Cu(2)-Cu(1)#1	166.38(7)	F(2)-C(3)-C(2)	121.4(2)
C(7)#1-Cu(2)-Cu(1)#1	52.27(7)	C(4)-C(3)-C(2)	118.8(2)
C(1)-Cu(2)-Cu(1)	50.26(7)	F(9)-C(11)-C(12)	121.4(2)
C(7)#1-Cu(2)-Cu(1)	166.20(7)	F(9)-C(11)-C(10)	120.3(2)
Cu(1)#1-Cu(2)-Cu(1)	116.262(15)	C(12)-C(11)-C(10)	118.3(2)
C(1)-Cu(2)-Cu(2)#1	107.15(7)	F(8)-C(10)-C(9)	119.8(3)
C(7)#1-Cu(2)-Cu(2)#1	111.09(7)	F(8)-C(10)-C(11)	119.9(3)
Cu(1)#1-Cu(2)-Cu(2)#1	59.343(15)	C(9)-C(10)-C(11)	120.3(2)
Cu(1)-Cu(2)-Cu(2)#1	56.919(14)	F(7)-C(9)-C(10)	119.4(2)

F(10)-C(12)-C(11)	116.9(2)	F(7)-C(9)-C(8)	121.4(2)
F(10)-C(12)-C(7)	118.7(2)	C(10)-C(9)-C(8)	119.2(2)
C(11)-C(12)-C(7)	124.4(2)	C(21)-C(20)-C(19)	120.8(2)
F(5)-C(6)-C(5)	117.4(2)	C(25)-C(24)-C(23)	121.7(2)
F(5)-C(6)-C(1)	118.7(2)	C(25)-C(24)-C(19)	119.4(2)
C(5)-C(6)-C(1)	123.9(2)	C(23)-C(24)-C(19)	118.9(2)
F(6)-C(8)-C(9)	116.9(2)	C(20)-C(21)-C(22)	120.7(2)
F(6)-C(8)-C(7)	119.8(2)	C(19)-C(18)-C(17)	121.3(2)
C(9)-C(8)-C(7)	123.3(2)	C(16)-C(15)-C(14)	120.2(2)
C(6)-C(1)-C(2)	114.8(2)	C(24)-C(25)-C(26)	121.3(2)
C(6)-C(1)-Cu(1)	122.09(18)	C(14)-C(13)-C(26)	121.0(2)
C(2)-C(1)-Cu(1)	119.24(18)	C(18)-C(17)-C(16)	122.0(2)
C(6)-C(1)-Cu(2)	104.37(17)	C(18)-C(17)-C(26)	119.3(2)
C(2)-C(1)-Cu(2)	107.85(17)	C(16)-C(17)-C(26)	118.7(2)
Cu(1)-C(1)-Cu(2)	77.74(8)	C(18)-C(19)-C(20)	122.2(2)
C(12)-C(7)-C(8)	114.4(2)	C(18)-C(19)-C(24)	119.5(2)
C(12)-C(7)-Cu(1)	114.57(18)	C(20)-C(19)-C(24)	118.2(2)

C(8)-C(7)-Cu(1)	122.24(18)	C(13)-C(14)-C(15)	120.3(2)
C(12)-C(7)-Cu(2)#1	110.17(17)	C(22)-C(23)-C(24)	120.9(2)
C(8)-C(7)-Cu(2)#1	113.92(17)	C(15)-C(16)-C(17)	121.2(2)
Cu(1)-C(7)-Cu(2)#1	74.54(8)	C(23)-C(22)-C(21)	120.4(2)
F(4)-C(5)-C(6)	122.4(2)	C(25)-C(26)-C(13)	122.2(2)
F(4)-C(5)-C(4)	119.1(2)	C(25)-C(26)-C(17)	119.2(2)
C(6)-C(5)-C(4)	118.5(2)	C(13)-C(26)-C(17)	118.7(2)

Crystal Data and Structure Refinement Details of {8-Np}_n, {8-Bt}_n and {8-Pyr}_n

	{8-Np} _n (29)	{8-Bt} _n (30)	{8-Pyr} _n (32)
empirical Formula	C ₃₄ H ₈ Cu ₄ F ₂₀	C ₃₂ H ₆ Cu ₄ F ₂₀ S ₂	C ₈₄ H ₂₈ Cu ₈ F ₄₀ Cl ₈
formula Weight	1050.56	1088.65	2588.98
<i>T</i> , K	100(2)	100(2)	100(2)
Wavelength, Å	1.54178	1.54178	1.54178
crystal system	Triclinic	Triclinic	Triclinic
space group	P-1	P-1	P-1
<i>a</i> , Å	9.2770(11)	11.0271(7)	10.6450(2)
<i>b</i> , Å	9.2816(10)	11.5270(7)	12.0190(2)
<i>c</i> , Å	10.6576(11)	14.6181(10)	17.1415(3)

α , deg	69.563(3)	86.590(3)	76.7070(10)
β , deg	72.278(2)	82.263(3)	78.8590(10)
γ , deg	74.354(3)	61.462(2)	80.0390(10)
V , Å ³	805.27(15)	1617.46(18)	2075.08(6)
<i>Section 1.06</i> Z	1	2	1
ρ_{calcd} , Mg m ⁻³	2.166	2.235	2.072
μ , mm ⁻¹	4.334	5.522	5.839
F(000)	508	1052	1260
crystal size, mm	0.39 x 0.35 x 0.29	0.34 x 0.30 x 0.13	0.60 x 0.52 x 0.52
Limiting indices	-10 ≤ h ≤ 10	-13 ≤ h ≤ 13	-12 ≤ h ≤ 12
	-10 ≤ k ≤ 10	-13 ≤ k ≤ 13	-14 ≤ k ≤ 14
	-12 ≤ l ≤ 12	-17 ≤ l ≤ 11	-20 ≤ l ≤ 19
θ range, deg	4.55 – 64.87	4.37 – 67.78	3.81 – 71.23
reflns collected	5335	13129	20200
independent reflns	2452	5277	6873
absorption correction	Semi-empirical from equivalents	Numerical	Numerical
refinement method	Full-matrix least-squares on F^2	Full-matrix least-squares on F^2	Full-matrix least-squares on F^2
data/restraints/parameters	2452 / 0 / 263	5277 / 0 / 523	6873 / 0 / 631
Goodness-of-fit on F^2	1.175	1.207	1.180
Final R indices	$R_1 = 0.0276$	$R_1 = 0.0283$	$R_1 = 0.0294$

$[I > 2\sigma(I)]^{[a]}$	wR2 = 0.0724	wR2 = 0.0717	wR2 = 0.0727
R indices (all data) ^[a]	R1 = 0.0276	R1 = 0.0286	R1 = 0.0295
	wR2 = 0.0724	wR2 = 0.0719	wR2 = 0.0728
Peak/hole (e Å ⁻³)	0.315 / -0.282	0.395 / -0.366	0.619 / -0.485
[a] $R1 = \Sigma F_o - F_c / \Sigma F_o $; $wR2 = \{ \Sigma[w(F_o^2 - F_c^2)^2] / \Sigma[w(F_o^2)^2] \}^{1/2}$.			

Bond Lengths (Å) and Bond Angles (deg) of {8-Np}_n (29)

Cu(1)-C(1)	1.978(3)	C(1)-Cu(2)#1	2.025(3)
Cu(1)-C(7)	2.001(3)	C(12)-F(10)	1.344(3)
Cu(1)-Cu(2)	2.4611(5)	C(12)-C(11)	1.375(4)
Cu(1)-Cu(2)#1	2.4695(6)	C(11)-F(9)	1.339(3)
Cu(2)-C(7)	2.015(3)	C(9)-F(7)	1.341(3)
Cu(2)-C(1)#1	2.025(3)	C(3)-F(2)	1.345(3)
Cu(2)-Cu(1)#1	2.4695(5)	C(3)-C(4)	1.378(4)
Cu(2)-Cu(2)#1	2.6779(8)	C(5)-F(4)	1.336(3)
F(6)-C(8)	1.355(3)	C(5)-C(6)	1.378(4)
F(3)-C(4)	1.334(3)	C(5)-C(4)	1.383(4)
C(2)-F(1)	1.354(3)	C(14)-C(15)	1.378(4)

C(2)-C(3)	1.369(4)	C(14)-C(13)	1.417(4)
C(2)-C(1)	1.397(4)	C(14)-H(14)	0.95
F(5)-C(6)	1.351(3)	C(16)-C(17)	1.361(4)
C(10)-F(8)	1.334(3)	C(16)-C(15)	1.408(4)
C(10)-C(11)	1.382(4)	C(16)-H(16)	0.95
C(10)-C(9)	1.386(4)	C(13)-C(17)#2	1.416(4)
C(7)-C(8)	1.395(4)	C(13)-C(13)#2	1.431(5)
C(7)-C(12)	1.400(4)	C(15)-H(15)	0.95
C(8)-C(9)	1.377(4)	C(17)-C(13)#2	1.416(4)
C(1)-C(6)	1.392(4)	C(17)-H(17)	0.95
C(1)-Cu(1)-C(7)	169.48(11)	Cu(1)-C(1)-Cu(2)#1	76.17(9)
C(1)-Cu(1)-Cu(2)	118.55(7)	F(10)-C(12)-C(11)	116.8(2)
C(7)-Cu(1)-Cu(2)	52.46(7)	F(10)-C(12)-C(7)	119.5(2)
C(1)-Cu(1)-Cu(2)#1	52.76(7)	C(11)-C(12)-C(7)	123.7(2)
C(7)-Cu(1)-Cu(2)#1	117.95(8)	F(9)-C(11)-C(12)	121.8(2)
Cu(2)-Cu(1)-Cu(2)#1	65.791(18)	F(9)-C(11)-C(10)	119.0(2)
C(7)-Cu(2)-C(1)#1	142.66(11)	C(12)-C(11)-C(10)	119.2(3)

C(7)-Cu(2)-Cu(1)	51.96(7)	F(7)-C(9)-C(8)	121.4(2)
C(1)#1-Cu(2)-Cu(1)	165.28(8)	F(7)-C(9)-C(10)	119.7(2)
C(7)-Cu(2)-Cu(1)#1	165.12(7)	C(8)-C(9)-C(10)	118.9(2)
C(1)#1-Cu(2)-Cu(1)#1	51.07(7)	F(2)-C(3)-C(2)	121.5(3)
Cu(1)-Cu(2)-Cu(1)#1	114.209(18)	F(2)-C(3)-C(4)	119.6(2)
C(7)-Cu(2)-Cu(2)#1	108.96(7)	C(2)-C(3)-C(4)	119.0(3)
C(1)#1-Cu(2)-Cu(2)#1	108.02(8)	F(4)-C(5)-C(6)	121.5(2)
Cu(1)-Cu(2)-Cu(2)#1	57.255(16)	F(4)-C(5)-C(4)	119.7(2)
Cu(1)#1-Cu(2)-Cu(2)#1	56.954(17)	C(6)-C(5)-C(4)	118.7(3)
F(1)-C(2)-C(3)	117.3(2)	F(3)-C(4)-C(3)	120.0(3)
F(1)-C(2)-C(1)	118.9(2)	F(3)-C(4)-C(5)	119.7(3)
C(3)-C(2)-C(1)	123.7(3)	C(3)-C(4)-C(5)	120.3(2)
F(8)-C(10)-C(11)	120.1(3)	F(5)-C(6)-C(5)	117.1(2)
F(8)-C(10)-C(9)	119.9(2)	F(5)-C(6)-C(1)	119.3(2)
C(11)-C(10)-C(9)	119.9(2)	C(5)-C(6)-C(1)	123.6(3)
C(8)-C(7)-C(12)	114.3(2)	C(15)-C(14)-C(13)	120.8(3)
C(8)-C(7)-Cu(1)	117.75(19)	C(15)-C(14)-H(14)	119.6

C(12)-C(7)-Cu(1)	117.62(19)	C(13)-C(14)-H(14)	119.6
C(8)-C(7)-Cu(2)	117.14(19)	C(17)-C(16)-C(15)	120.3(3)
C(12)-C(7)-Cu(2)	108.34(18)	C(17)-C(16)-H(16)	119.8
Cu(1)-C(7)-Cu(2)	75.58(9)	C(15)-C(16)-H(16)	119.8
F(6)-C(8)-C(9)	116.9(2)	C(17)#2-C(13)-C(14)	122.5(3)
F(6)-C(8)-C(7)	119.2(2)	C(17)#2-C(13)-C(13)#2	119.4(3)
C(9)-C(8)-C(7)	123.9(3)	C(14)-C(13)-C(13)#2	118.2(3)
C(6)-C(1)-C(2)	114.7(2)	C(14)-C(15)-C(16)	120.5(3)
C(6)-C(1)-Cu(1)	117.52(19)	C(14)-C(15)-H(15)	119.8
C(2)-C(1)-Cu(1)	121.50(19)	C(16)-C(15)-H(15)	119.8
C(6)-C(1)-Cu(2)#1	109.51(18)	C(16)-C(17)-C(13)#2	120.9(3)
C(2)-C(1)-Cu(2)#1	109.29(19)	C(16)-C(17)-H(17)	119.5
		C(13)#2-C(17)-H(17)	119.5

Bond Lengths (Å) and Bond Angles (deg) of {8-Bt}_n (30)

C(1)-C(6)	1.385(4)	C(17)-F(14)	1.337(3)
C(1)-C(2)	1.401(4)	C(17)-C(18)	1.382(4)

C(1)-Cu(1)	2.002(3)	C(18)-F(15)	1.352(3)
C(1)-Cu(2)	2.018(3)	C(19)-C(20)	1.389(4)
C(2)-F(1)	1.344(3)	C(19)-C(24)	1.394(4)
C(2)-C(3)	1.378(4)	C(19)-Cu(1)	1.996(3)
C(3)-F(2)	1.349(3)	C(19)-Cu(4)	2.020(3)
C(3)-C(4)	1.373(4)	C(20)-F(16)	1.353(3)
C(4)-F(3)	1.338(3)	C(20)-C(21)	1.383(4)
C(4)-C(5)	1.385(4)	C(21)-F(17)	1.341(3)
C(5)-F(4)	1.334(3)	C(21)-C(22)	1.376(4)
C(5)-C(6)	1.385(4)	C(22)-F(18)	1.334(3)
C(6)-F(5)	1.354(3)	C(22)-C(23)	1.382(4)
C(7)-C(12)	1.392(4)	C(23)-F(19)	1.344(3)
C(7)-C(8)	1.395(4)	C(23)-C(24)	1.380(4)
C(7)-Cu(3)	2.010(3)	C(24)-F(20)	1.345(3)
C(7)-Cu(2)	2.011(3)	C(25)-C(26)	1.351(5)
C(8)-F(6)	1.348(3)	C(25)-S(1)	1.726(3)
C(8)-C(9)	1.383(4)	C(26)-C(27)	1.429(4)

C(9)-F(7)	1.349(3)	C(27)-C(28)	1.361(4)
C(9)-C(10)	1.368(4)	C(28)-C(29)	1.447(4)
C(10)-F(8)	1.344(3)	C(28)-S(1)	1.742(3)
C(10)-C(11)	1.378(4)	C(29)-C(30)	1.371(4)
C(11)-F(9)	1.339(3)	C(29)-S(2)	1.745(3)
C(11)-C(12)	1.387(4)	C(30)-C(31)	1.416(4)
C(12)-F(10)	1.349(3)	C(31)-C(32)	1.351(4)
C(13)-C(18)	1.386(4)	C(32)-S(2)	1.732(3)
C(13)-C(14)	1.398(4)	Cu(1)-Cu(2)	2.4549(5)
C(13)-Cu(4)	2.023(3)	Cu(1)-Cu(4)	2.4884(5)
C(13)-Cu(3)	2.032(3)	Cu(1)-S(1)	2.5389(8)
C(14)-F(11)	1.343(3)	Cu(2)-Cu(3)	2.4549(5)
C(14)-C(15)	1.382(4)	Cu(2)-Cu(4)	2.6556(5)
C(15)-F(12)	1.349(3)	Cu(3)-Cu(4)	2.4611(5)
C(15)-C(16)	1.369(4)	Cu(3)-S(2)#1	2.5356(7)
C(16)-F(13)	1.340(3)	S(2)-Cu(3)#2	2.5356(7)
C(16)-C(17)	1.387(4)		

C(6)-C(1)-C(2)	114.9(2)	C(21)-C(20)-C(19)	123.7(3)
C(6)-C(1)-Cu(1)	117.94(19)	F(17)-C(21)-C(22)	120.2(2)
C(2)-C(1)-Cu(1)	119.8(2)	F(17)-C(21)-C(20)	120.9(2)
C(6)-C(1)-Cu(2)	112.38(18)	C(22)-C(21)-C(20)	118.8(3)
C(2)-C(1)-Cu(2)	108.93(19)	F(18)-C(22)-C(21)	120.2(3)
Cu(1)-C(1)-Cu(2)	75.26(9)	F(18)-C(22)-C(23)	119.7(2)
F(1)-C(2)-C(3)	118.1(2)	C(21)-C(22)-C(23)	120.0(2)
F(1)-C(2)-C(1)	119.0(2)	F(19)-C(23)-C(24)	121.2(3)
C(3)-C(2)-C(1)	122.9(3)	F(19)-C(23)-C(22)	119.3(2)
F(2)-C(3)-C(4)	119.2(2)	C(24)-C(23)-C(22)	119.4(3)
F(2)-C(3)-C(2)	121.2(3)	F(20)-C(24)-C(23)	117.4(2)
C(4)-C(3)-C(2)	119.6(3)	F(20)-C(24)-C(19)	119.7(2)
F(3)-C(4)-C(3)	120.2(2)	C(23)-C(24)-C(19)	122.9(3)
F(3)-C(4)-C(5)	119.4(3)	C(26)-C(25)-S(1)	111.4(2)
C(3)-C(4)-C(5)	120.4(3)	C(25)-C(26)-C(27)	113.0(3)
F(4)-C(5)-C(6)	122.5(2)	C(28)-C(27)-C(26)	113.2(3)
F(4)-C(5)-C(4)	119.3(2)	C(27)-C(28)-C(29)	130.1(2)

C(6)-C(5)-C(4)	118.2(3)	C(27)-C(28)-S(1)	110.4(2)
F(5)-C(6)-C(1)	118.8(2)	C(29)-C(28)-S(1)	119.6(2)
F(5)-C(6)-C(5)	117.1(3)	C(30)-C(29)-C(28)	129.1(3)
C(1)-C(6)-C(5)	124.1(3)	C(30)-C(29)-S(2)	109.8(2)
C(12)-C(7)-C(8)	114.4(2)	C(28)-C(29)-S(2)	121.0(2)
C(12)-C(7)-Cu(3)	114.16(19)	C(29)-C(30)-C(31)	113.6(3)
C(8)-C(7)-Cu(3)	123.4(2)	C(32)-C(31)-C(30)	113.4(3)
C(12)-C(7)-Cu(2)	109.06(18)	C(31)-C(32)-S(2)	111.2(2)
C(8)-C(7)-Cu(2)	113.3(2)	C(19)-Cu(1)-C(1)	169.36(10)
Cu(3)-C(7)-Cu(2)	75.25(9)	C(19)-Cu(1)-Cu(2)	116.75(7)
F(6)-C(8)-C(9)	116.6(2)	C(1)-Cu(1)-Cu(2)	52.67(7)
F(6)-C(8)-C(7)	120.1(2)	C(19)-Cu(1)-Cu(4)	52.16(7)
C(9)-C(8)-C(7)	123.4(3)	C(1)-Cu(1)-Cu(4)	117.21(7)
F(7)-C(9)-C(10)	120.1(2)	Cu(2)-Cu(1)-Cu(4)	64.985(15)
F(7)-C(9)-C(8)	120.4(3)	C(19)-Cu(1)-S(1)	98.87(8)
C(10)-C(9)-C(8)	119.5(3)	C(1)-Cu(1)-S(1)	91.74(7)
F(8)-C(10)-C(9)	120.0(3)	Cu(2)-Cu(1)-S(1)	144.34(2)

F(8)-C(10)-C(11)	119.8(3)	Cu(4)-Cu(1)-S(1)	150.52(2)
C(9)-C(10)-C(11)	120.2(3)	C(7)-Cu(2)-C(1)	143.55(10)
F(9)-C(11)-C(10)	120.0(3)	C(7)-Cu(2)-Cu(1)	159.18(8)
F(9)-C(11)-C(12)	121.3(3)	C(1)-Cu(2)-Cu(1)	52.07(7)
C(10)-C(11)-C(12)	118.7(3)	C(7)-Cu(2)-Cu(3)	52.35(7)
F(10)-C(12)-C(11)	117.1(3)	C(1)-Cu(2)-Cu(3)	162.75(8)
F(10)-C(12)-C(7)	119.1(2)	Cu(1)-Cu(2)-Cu(3)	115.257(19)
C(11)-C(12)-C(7)	123.8(3)	C(7)-Cu(2)-Cu(4)	105.81(8)
C(18)-C(13)-C(14)	114.5(2)	C(1)-Cu(2)-Cu(4)	109.80(7)
C(18)-C(13)-Cu(4)	118.25(19)	Cu(1)-Cu(2)-Cu(4)	58.116(15)
C(14)-C(13)-Cu(4)	109.06(19)	Cu(3)-Cu(2)-Cu(4)	57.416(14)
C(18)-C(13)-Cu(3)	111.74(19)	C(7)-Cu(3)-C(13)	159.61(11)
C(14)-C(13)-Cu(3)	122.8(2)	C(7)-Cu(3)-Cu(2)	52.39(7)
Cu(4)-C(13)-Cu(3)	74.73(9)	C(13)-Cu(3)-Cu(2)	117.70(7)
F(11)-C(14)-C(15)	117.3(2)	C(7)-Cu(3)-Cu(4)	113.28(7)
F(11)-C(14)-C(13)	119.8(2)	C(13)-Cu(3)-Cu(4)	52.47(7)
C(15)-C(14)-C(13)	122.9(3)	Cu(2)-Cu(3)-Cu(4)	65.395(15)

F(12)-C(15)-C(16)	119.6(2)	C(7)-Cu(3)-S(2)#1	102.70(7)
F(12)-C(15)-C(14)	120.5(3)	C(13)-Cu(3)-S(2)#1	92.09(7)
C(16)-C(15)-C(14)	119.9(3)	Cu(2)-Cu(3)-S(2)#1	147.90(2)
F(13)-C(16)-C(15)	120.8(3)	Cu(4)-Cu(3)-S(2)#1	143.92(2)
F(13)-C(16)-C(17)	119.3(3)	C(19)-Cu(4)-C(13)	142.09(11)
C(15)-C(16)-C(17)	119.9(2)	C(19)-Cu(4)-Cu(3)	165.02(8)
F(14)-C(17)-C(18)	121.9(3)	C(13)-Cu(4)-Cu(3)	52.80(7)
F(14)-C(17)-C(16)	119.7(2)	C(19)-Cu(4)-Cu(1)	51.27(7)
C(18)-C(17)-C(16)	118.4(3)	C(13)-Cu(4)-Cu(1)	163.79(8)
F(15)-C(18)-C(17)	116.2(3)	Cu(3)-Cu(4)-Cu(1)	113.820(19)
F(15)-C(18)-C(13)	119.4(2)	C(19)-Cu(4)-Cu(2)	107.83(8)
C(17)-C(18)-C(13)	124.3(3)	C(13)-Cu(4)-Cu(2)	109.84(7)
C(20)-C(19)-C(24)	115.1(2)	Cu(3)-Cu(4)-Cu(2)	57.189(15)
C(20)-C(19)-Cu(1)	118.84(19)	Cu(1)-Cu(4)-Cu(2)	56.898(14)
C(24)-C(19)-Cu(1)	116.7(2)	C(25)-S(1)-C(28)	91.95(14)
C(20)-C(19)-Cu(4)	111.97(19)	C(25)-S(1)-Cu(1)	98.31(10)
C(24)-C(19)-Cu(4)	111.18(19)	C(28)-S(1)-Cu(1)	113.61(9)

Cu(1)-C(19)-Cu(4)	76.57(9)	C(32)-S(2)-C(29)	91.98(14)
F(16)-C(20)-C(21)	116.9(2)	C(32)-S(2)-Cu(3)#2	82.87(9)
F(16)-C(20)-C(19)	119.4(2)	C(29)-S(2)-Cu(3)#2	112.69(9)

Bond Lengths (Å) and Bond Angles (deg) of {8-Pyr}_n (32)

Cu(1)-C(1)	1.970(2)	C(18)-C(13)	1.390(4)
Cu(1)-C(19)	2.015(2)	C(13)-C(14)	1.397(4)
Cu(1)-Cu(4)	2.4588(5)	C(14)-F(14)	1.352(3)
Cu(1)-Cu(2)	2.5042(5)	C(14)-C(15)	1.377(4)
Cu(1)-Cu(3)	2.6563(5)	C(17)-F(17)	1.346(3)
Cu(3)-C(13)	1.986(3)	C(17)-C(16)	1.377(4)
Cu(3)-C(7)	2.008(3)	C(16)-F(16)	1.336(3)
Cu(3)-Cu(2)	2.4490(5)	C(16)-C(15)	1.375(4)
Cu(3)-Cu(4)	2.4782(5)	C(15)-F(15)	1.347(3)
Cu(2)-C(7)	2.053(3)	C(22)-F(22)	1.339(3)
Cu(2)-C(1)	2.126(3)	C(22)-C(23)	1.377(4)
Cu(2)-C(25)	2.274(3)	C(22)-C(21)	1.378(4)
Cu(2)-C(26)	2.482(3)	C(24)-F(24)	1.353(3)

Cu(4)-C(19)	2.055(2)	C(24)-C(23)	1.384(4)
Cu(4)-C(13)	2.098(2)	C(24)-C(19)	1.395(4)
Cu(4)-C(35)	2.323(2)	C(20)-F(20)	1.359(3)
Cu(4)-C(34)	2.328(3)	C(20)-C(21)	1.374(4)
Cl(1)-C(41)	1.773(4)	C(20)-C(19)	1.385(4)
Cl(2)-C(41)	1.745(4)	C(21)-F(21)	1.346(3)
Cl(3)-C(42)	1.757(3)	C(23)-F(23)	1.340(3)
F(12)-C(12)	1.350(3)	C(31)-C(30)	1.346(4)
C(12)-C(11)	1.379(4)	C(31)-C(32)	1.428(4)
C(12)-C(7)	1.386(4)	C(29)-C(32)#1	1.420(4)
C(1)-C(2)	1.389(4)	C(29)-C(28)	1.422(4)
C(1)-C(6)	1.390(4)	C(29)-C(29)#1	1.426(5)
C(7)-C(8)	1.387(4)	C(27)-C(26)	1.392(4)
C(6)-F(6)	1.353(3)	C(27)-C(28)	1.395(4)
C(6)-C(5)	1.384(4)	C(30)-C(28)	1.441(4)
C(5)-F(5)	1.343(3)	C(32)-C(25)#1	1.416(4)
C(5)-C(4)	1.374(4)	C(32)-C(29)#1	1.420(4)

C(9)-F(9)	1.347(3)	C(26)-C(25)	1.391(4)
C(9)-C(10)	1.371(4)	C(25)-C(32)#1	1.416(4)
C(9)-C(8)	1.382(4)	C(34)-C(35)	1.357(4)
C(2)-F(2)	1.356(3)	C(34)-C(33)	1.445(4)
C(2)-C(3)	1.374(4)	C(37)-C(36)	1.421(4)
C(8)-F(8)	1.346(3)	C(37)-C(33)#2	1.423(4)
C(3)-F(3)	1.345(3)	C(37)-C(37)#2	1.424(5)
C(3)-C(4)	1.381(4)	C(36)-C(38)	1.393(4)
C(11)-F(11)	1.341(3)	C(36)-C(35)	1.447(4)
C(11)-C(10)	1.376(4)	C(39)-C(40)	1.380(4)
C(10)-F(10)	1.342(3)	C(39)-C(38)	1.387(4)
C(4)-F(4)	1.337(3)	C(33)-C(40)#2	1.395(4)
C(18)-F(18)	1.354(3)	C(33)-C(37)#2	1.423(4)
C(18)-C(17)	1.380(4)	C(40)-C(33)#2	1.395(4)
		Cl(4)-C(42)	1.768(4)
C(1)-Cu(1)-C(19)	155.88(10)	F(10)-C(10)-C(9)	119.8(3)
C(1)-Cu(1)-Cu(4)	150.54(8)	F(10)-C(10)-C(11)	120.2(3)

C(19)-Cu(1)-Cu(4)	53.58(7)	C(9)-C(10)-C(11)	120.0(3)
C(1)-Cu(1)-Cu(2)	55.20(7)	F(4)-C(4)-C(5)	120.6(3)
C(19)-Cu(1)-Cu(2)	133.90(8)	F(4)-C(4)-C(3)	119.6(3)
Cu(4)-Cu(1)-Cu(2)	106.601(18)	C(5)-C(4)-C(3)	119.8(2)
C(1)-Cu(1)-Cu(3)	93.79(8)	F(18)-C(18)-C(17)	115.8(2)
C(19)-Cu(1)-Cu(3)	109.49(7)	F(18)-C(18)-C(13)	120.3(2)
Cu(4)-Cu(1)-Cu(3)	57.803(14)	C(17)-C(18)-C(13)	123.9(2)
Cu(2)-Cu(1)-Cu(3)	56.570(14)	C(18)-C(13)-C(14)	113.8(2)
C(13)-Cu(3)-C(7)	159.51(10)	C(18)-C(13)-Cu(3)	119.11(19)
C(13)-Cu(3)-Cu(2)	146.14(8)	C(14)-C(13)-Cu(3)	114.05(18)
C(7)-Cu(3)-Cu(2)	53.74(7)	C(18)-C(13)-Cu(4)	110.38(18)
C(13)-Cu(3)-Cu(4)	54.73(7)	C(14)-C(13)-Cu(4)	119.50(18)
C(7)-Cu(3)-Cu(4)	136.35(7)	Cu(3)-C(13)-Cu(4)	74.65(9)
Cu(2)-Cu(3)-Cu(4)	107.725(18)	F(14)-C(14)-C(15)	116.6(2)
C(13)-Cu(3)-Cu(1)	89.55(8)	F(14)-C(14)-C(13)	119.2(2)
C(7)-Cu(3)-Cu(1)	110.93(7)	C(15)-C(14)-C(13)	124.2(2)
Cu(2)-Cu(3)-Cu(1)	58.578(14)	F(17)-C(17)-C(16)	119.5(2)

Cu(4)-Cu(3)-Cu(1)	57.096(13)	F(17)-C(17)-C(18)	121.3(2)
C(7)-Cu(2)-C(1)	141.01(10)	C(16)-C(17)-C(18)	119.2(2)
C(7)-Cu(2)-C(25)	114.31(10)	F(16)-C(16)-C(15)	120.3(2)
C(1)-Cu(2)-C(25)	102.81(10)	F(16)-C(16)-C(17)	119.9(2)
C(7)-Cu(2)-Cu(3)	52.08(7)	C(15)-C(16)-C(17)	119.8(2)
C(1)-Cu(2)-Cu(3)	96.12(7)	F(15)-C(15)-C(16)	119.6(2)
C(25)-Cu(2)-Cu(3)	156.52(8)	F(15)-C(15)-C(14)	121.3(2)
C(7)-Cu(2)-C(26)	110.03(10)	C(16)-C(15)-C(14)	119.1(2)
C(1)-Cu(2)-C(26)	94.03(10)	F(22)-C(22)-C(23)	119.8(3)
C(25)-Cu(2)-C(26)	33.66(10)	F(22)-C(22)-C(21)	119.9(3)
Cu(3)-Cu(2)-C(26)	158.55(7)	C(23)-C(22)-C(21)	120.3(2)
C(7)-Cu(2)-Cu(1)	115.45(7)	F(24)-C(24)-C(23)	116.6(2)
C(1)-Cu(2)-Cu(1)	49.54(7)	F(24)-C(24)-C(19)	119.6(2)
C(25)-Cu(2)-Cu(1)	118.59(7)	C(23)-C(24)-C(19)	123.8(2)
Cu(3)-Cu(2)-Cu(1)	64.851(15)	F(20)-C(20)-C(21)	116.6(2)
C(26)-Cu(2)-Cu(1)	134.51(7)	F(20)-C(20)-C(19)	119.4(2)
C(19)-Cu(4)-C(13)	137.18(10)	C(21)-C(20)-C(19)	124.0(3)

C(19)-Cu(4)-C(35)	106.65(9)	C(20)-C(19)-C(24)	114.4(2)
C(13)-Cu(4)-C(35)	104.23(9)	C(20)-C(19)-Cu(1)	117.40(18)
C(19)-Cu(4)-C(34)	112.93(9)	C(24)-C(19)-Cu(1)	110.17(18)
C(13)-Cu(4)-C(34)	109.31(10)	C(20)-C(19)-Cu(4)	113.21(18)
C(35)-Cu(4)-C(34)	33.92(10)	C(24)-C(19)-Cu(4)	121.45(19)
C(19)-Cu(4)-Cu(1)	52.08(7)	Cu(1)-C(19)-Cu(4)	74.34(8)
C(13)-Cu(4)-Cu(1)	92.62(7)	F(21)-C(21)-C(20)	121.5(3)
C(35)-Cu(4)-Cu(1)	158.35(7)	F(21)-C(21)-C(22)	119.4(2)
C(34)-Cu(4)-Cu(1)	149.63(7)	C(20)-C(21)-C(22)	119.0(3)
C(19)-Cu(4)-Cu(3)	115.11(7)	F(23)-C(23)-C(22)	119.9(2)
C(13)-Cu(4)-Cu(3)	50.62(7)	F(23)-C(23)-C(24)	121.6(3)
C(35)-Cu(4)-Cu(3)	136.43(7)	C(22)-C(23)-C(24)	118.5(2)
C(34)-Cu(4)-Cu(3)	112.93(7)	C(30)-C(31)-C(32)	121.4(3)
Cu(1)-Cu(4)-Cu(3)	65.101(15)	C(32)#1-C(29)-C(28)	120.3(2)
F(12)-C(12)-C(11)	116.8(2)	C(32)#1-C(29)-(29)#1	119.6(3)
F(12)-C(12)-C(7)	119.3(2)	C(28)-C(29)-C(29)#1	120.0(3)
C(11)-C(12)-C(7)	123.9(3)	C(26)-C(27)-C(28)	120.1(3)

C(2)-C(1)-C(6)	114.5(2)	C(31)-C(30)-C(28)	121.3(3)
C(2)-C(1)-Cu(1)	114.62(19)	C(27)-C(28)-C(29)	119.6(3)
C(6)-C(1)-Cu(1)	124.4(2)	C(27)-C(28)-C(30)	121.9(3)
C(2)-C(1)-Cu(2)	116.94(18)	C(29)-C(28)-C(30)	118.5(2)
C(6)-C(1)-Cu(2)	103.82(17)	C(25)#1-C(32)-(29)#1	118.4(3)
Cu(1)-C(1)-Cu(2)	75.26(9)	C(25)#1-C(32)-C(31)	122.5(3)
C(12)-C(7)-C(8)	114.4(2)	C(29)#1-C(32)-C(31)	119.1(2)
C(12)-C(7)-Cu(3)	112.09(18)	C(25)-C(26)-C(27)	121.2(3)
C(8)-C(7)-Cu(3)	116.14(19)	C(25)-C(26)-Cu(2)	64.93(15)
C(12)-C(7)-Cu(2)	121.91(19)	C(27)-C(26)-Cu(2)	108.88(19)
C(8)-C(7)-Cu(2)	112.14(19)	C(26)-C(25)-C(32)#1	120.3(3)
Cu(3)-C(7)-Cu(2)	74.18(9)	C(26)-C(25)-Cu(2)	81.41(17)
F(6)-C(6)-C(5)	116.4(2)	C(32)#1-C(25)-Cu(2)	101.76(17)
F(6)-C(6)-C(1)	120.2(2)	C(35)-C(34)-C(33)	121.4(2)
C(5)-C(6)-C(1)	123.4(3)	C(35)-C(34)-Cu(4)	72.85(15)
F(5)-C(5)-C(4)	119.5(3)	C(33)-C(34)-Cu(4)	109.06(16)
F(5)-C(5)-C(6)	121.2(3)	C(36)-C(37)-C(33)#2	119.3(2)

C(4)-C(5)-C(6)	119.2(3)	C(36)-C(37)-C(37)#2	120.2(3)
F(9)-C(9)-C(10)	119.9(3)	C(33)#2-C(37)-(37)#2	120.5(3)
F(9)-C(9)-C(8)	121.0(3)	C(38)-C(36)-C(37)	119.2(2)
C(10)-C(9)-C(8)	119.1(3)	C(38)-C(36)-C(35)	122.4(2)
F(2)-C(2)-C(3)	116.5(2)	C(37)-C(36)-C(35)	118.4(2)
F(2)-C(2)-C(1)	119.5(2)	C(40)-C(39)-C(38)	120.6(3)
C(3)-C(2)-C(1)	124.1(3)	C(34)-C(35)-C(36)	121.3(2)
F(8)-C(8)-C(9)	116.5(2)	C(34)-C(35)-Cu(4)	73.23(15)
F(8)-C(8)-C(7)	119.9(2)	C(36)-C(35)-Cu(4)	109.00(16)
C(9)-C(8)-C(7)	123.6(3)	C(39)-C(38)-C(36)	120.9(3)
F(3)-C(3)-C(2)	121.2(3)	C(40)#2-C(33)-(37)#2	119.5(2)
F(3)-C(3)-C(4)	119.9(2)	C(40)#2-C(33)-C(34)	122.4(2)
C(2)-C(3)-C(4)	118.9(3)	C(37)#2-C(33)-C(34)	118.2(2)
F(11)-C(11)-C(10)	119.2(3)	C(39)-C(40)-C(33)#2	120.6(3)
F(11)-C(11)-C(12)	121.9(3)	Cl(3)-C(42)-Cl(4)	111.90(17)
C(10)-C(11)-C(12)	118.9(3)	Cl(2)-C(41)-Cl(1)	112.32(19)

Crystal Data and Structure Refinement Details of 8-Pyrene₂

	8-Pyrene ₂ (33)
empirical Formula	C ₆₂ H ₂₀ Cu ₅ F ₂₅
formula Weight	1557.48
<i>T</i> , K	208(2)
Wavelength, Å	0.71073
crystal system	Monoclinic
space group	P2(1)/c
<i>a</i> , Å	20.198(2)
<i>b</i> , Å	12.9529(14)
<i>c</i> , Å	20.522(2)
<i>α</i> , deg	90
<i>β</i> , deg	98.0300(10)
<i>γ</i> , deg	90
<i>V</i> , Å ³	5316.2(10)
<i>Section 1.07</i> <i>Z</i>	4
ρ_{calcd} , Mg m ⁻³	1.946
μ , mm ⁻¹	2.100
F(000)	3048
crystal size, mm	0.40 x 0.40 x 0.08
Limiting indices	-24 ≤ <i>h</i> ≤ 24

	$-15 \leq k \leq 15$		
	$-21 \leq l \leq 25$		
θ range, deg	1.86 – 26.00		
reflns collected	53143		
independent reflns	10143		
absorption correction	Absorption correction	Multi-scan	
refinement method	Refinement method	Full-matrix	least-squares on F^2
data/restraints/parameters	10143 / 0 / 909		
Goodness-of-fit on F^2	1.036		
Final R indices	$R1 = 0.0367$		
$[I > 2\sigma(I)]^{[a]}$	$wR2 = 0.0893$		
R indices (all data) ^[a]	$R1 = 0.0550$		
	$wR2 = 0.1029$		
Peak/hole (e Å ⁻³)	0.703 and –0.555		

Bond Lengths (Å) and Bond Angles (deg) of 8-Pyrene₂ (33)

Cu(1)-C(11)	2.018(4)	C(25)-C(26)	1.374(5)
Cu(1)-C(51)	2.110(3)	C(31)-C(32)	1.393(5)
Cu(1)-C(85)	2.379(4)	C(31)-C(36)	1.393(5)

Cu(1)-C(84)	2.389(4)	C(32)-C(33)	1.373(5)
Cu(1)-Cu(5)	2.4487(6)	C(33)-C(34)	1.373(6)
Cu(1)-Cu(2)	2.4654(6)	C(34)-C(35)	1.367(6)
Cu(2)-C(11)	2.020(3)	C(35)-C(36)	1.377(5)
Cu(2)-C(21)	2.034(3)	C(41)-C(42)	1.387(5)
Cu(2)-Cu(3)	2.4612(6)	C(41)-C(46)	1.395(5)
Cu(2)-Cu(4)	2.6475(6)	C(42)-C(43)	1.366(5)
Cu(2)-Cu(5)	2.6958(7)	C(43)-C(44)	1.374(5)
Cu(3)-C(21)	2.000(3)	C(44)-C(45)	1.376(5)
Cu(3)-C(31)	2.049(3)	C(45)-C(46)	1.371(5)
Cu(3)-Cu(4)	2.4551(6)	C(51)-C(52)	1.383(5)
Cu(3)-C(61)	2.465(4)	C(51)-C(56)	1.394(5)
Cu(4)-C(41)	1.997(4)	C(52)-C(53)	1.378(5)
Cu(4)-C(31)	2.018(3)	C(53)-C(54)	1.379(6)
Cu(4)-Cu(5)	2.5024(6)	C(54)-C(55)	1.367(6)
Cu(5)-C(41)	1.983(3)	C(55)-C(56)	1.372(5)
Cu(5)-C(51)	1.994(3)	C(61)-C(62)	1.391(9)

F(12)-C(12)	1.333(5)	C(61)-C(71)	1.391(8)
F(13)-C(13)	1.344(5)	C(62)-C(63)	1.385(9)
F(14)-C(14)	1.351(5)	C(63)-C(72)	1.380(6)
F(15)-C(15)	1.335(5)	C(64)-C(65)	1.331(7)
F(16)-C(16)	1.358(4)	C(64)-C(72)	1.433(6)
F(22)-C(22)	1.353(4)	C(65)-C(73)	1.385(7)
F(23)-C(23)	1.344(5)	C(66)-C(67)	1.349(9)
F(24)-C(24)	1.346(4)	C(66)-C(73)	1.412(7)
F(25)-C(25)	1.346(4)	C(67)-C(68)	1.353(9)
F(26)-C(26)	1.354(4)	C(68)-C(74)	1.439(8)
F(32)-C(32)	1.348(5)	C(69)-C(70)	1.334(8)
F(33)-C(33)	1.339(5)	C(69)-C(74)	1.384(7)
F(34)-C(34)	1.340(4)	C(70)-C(71)	1.495(8)
F(35)-C(35)	1.345(5)	C(71)-C(75)	1.415(5)
F(36)-C(36)	1.350(4)	C(72)-C(75)	1.419(6)
F(42)-C(42)	1.358(4)	C(73)-C(76)	1.417(6)
F(43)-C(43)	1.349(4)	C(74)-C(76)	1.407(7)

F(44)-C(44)	1.341(4)	C(75)-C(76)	1.428(6)
F(45)-C(45)	1.346(4)	C(81)-C(82)	1.370(7)
F(46)-C(46)	1.346(4)	C(81)-C(91)	1.390(6)
F(52)-C(52)	1.357(4)	C(82)-C(83)	1.376(7)
F(53)-C(53)	1.337(4)	C(83)-C(92)	1.405(5)
F(54)-C(54)	1.343(4)	C(84)-C(85)	1.340(6)
F(55)-C(55)	1.343(5)	C(84)-C(92)	1.439(5)
F(56)-C(56)	1.351(4)	C(85)-C(93)	1.437(6)
C(11)-C(16)	1.379(5)	C(86)-C(87)	1.376(7)
C(11)-C(12)	1.416(5)	C(86)-C(93)	1.386(5)
C(12)-C(13)	1.370(6)	C(87)-C(88)	1.373(8)
C(13)-C(14)	1.333(7)	C(88)-C(94)	1.391(6)
C(14)-C(15)	1.380(7)	C(89)-C(90)	1.336(8)
C(15)-C(16)	1.404(6)	C(89)-C(94)	1.444(7)
C(21)-C(22)	1.385(5)	C(90)-C(91)	1.427(7)
C(21)-C(26)	1.396(5)	C(91)-C(95)	1.424(5)
C(22)-C(23)	1.382(5)	C(92)-C(95)	1.415(5)

C(23)-C(24)	1.363(6)	C(93)-C(96)	1.426(5)
C(24)-C(25)	1.371(6)	C(94)-C(96)	1.420(6)
		C(95)-C(96)	1.420(5)
		C(32)-C(33)-C(34)	118.7(4)
C(11)-Cu(1)-C(51)	156.18(13)	F(34)-C(34)-C(35)	119.9(4)
C(11)-Cu(1)-C(85)	107.01(14)	F(34)-C(34)-C(33)	119.7(4)
C(51)-Cu(1)-C(85)	94.63(13)	C(35)-C(34)-C(33)	120.3(3)
C(11)-Cu(1)-C(84)	106.47(13)	F(35)-C(35)-C(34)	119.4(4)
C(51)-Cu(1)-C(84)	97.10(13)	F(35)-C(35)-C(36)	121.2(4)
C(85)-Cu(1)-C(84)	32.65(13)	C(34)-C(35)-C(36)	119.3(4)
C(11)-Cu(1)-Cu(5)	109.89(10)	F(36)-C(36)-C(35)	117.2(4)
C(51)-Cu(1)-Cu(5)	51.23(9)	F(36)-C(36)-C(31)	119.3(3)
C(85)-Cu(1)-Cu(5)	142.18(10)	C(35)-C(36)-C(31)	123.4(4)
C(84)-Cu(1)-Cu(5)	124.61(11)	C(42)-C(41)-C(46)	114.5(3)
C(11)-Cu(1)-Cu(2)	52.42(9)	C(42)-C(41)-Cu(5)	119.7(2)
C(51)-Cu(1)-Cu(2)	103.77(9)	C(46)-C(41)-Cu(5)	111.8(2)
C(85)-Cu(1)-Cu(2)	148.46(11)	C(42)-C(41)-Cu(4)	110.4(2)

C(84)-Cu(1)-Cu(2)	158.03(9)	C(46)-C(41)-Cu(4)	117.8(3)
Cu(5)-Cu(1)-Cu(2)	66.538(19)	Cu(5)-C(41)-Cu(4)	77.91(13)
C(11)-Cu(2)-C(21)	138.96(15)	F(42)-C(42)-C(43)	116.9(3)
C(11)-Cu(2)-Cu(3)	134.19(10)	F(42)-C(42)-C(41)	119.1(3)
C(21)-Cu(2)-Cu(3)	51.77(9)	C(43)-C(42)-C(41)	124.0(3)
C(11)-Cu(2)-Cu(1)	52.33(10)	F(43)-C(43)-C(42)	121.7(3)
C(21)-Cu(2)-Cu(1)	142.52(9)	F(43)-C(43)-C(44)	119.4(3)
Cu(3)-Cu(2)-Cu(1)	157.71(3)	C(42)-C(43)-C(44)	118.8(3)
C(11)-Cu(2)-Cu(4)	110.31(11)	F(44)-C(44)-C(43)	120.1(3)
C(21)-Cu(2)-Cu(4)	103.02(10)	F(44)-C(44)-C(45)	119.7(3)
Cu(3)-Cu(2)-Cu(4)	57.307(16)	C(43)-C(44)-C(45)	120.2(3)
Cu(1)-Cu(2)-Cu(4)	100.68(2)	F(45)-C(45)-C(46)	121.9(3)
C(11)-Cu(2)-Cu(5)	101.02(11)	F(45)-C(45)-C(44)	119.0(3)
C(21)-Cu(2)-Cu(5)	117.54(11)	C(46)-C(45)-C(44)	119.1(3)
Cu(3)-Cu(2)-Cu(5)	103.34(2)	F(46)-C(46)-C(45)	116.9(3)
Cu(1)-Cu(2)-Cu(5)	56.436(16)	F(46)-C(46)-C(41)	119.7(3)
Cu(4)-Cu(2)-Cu(5)	55.843(16)	C(45)-C(46)-C(41)	123.3(3)

C(21)-Cu(3)-C(31)	159.02(13)	C(52)-C(51)-C(56)	114.0(3)
C(21)-Cu(3)-Cu(4)	111.17(10)	C(52)-C(51)-Cu(5)	124.1(3)
C(31)-Cu(3)-Cu(4)	52.28(10)	C(56)-C(51)-Cu(5)	111.8(2)
C(21)-Cu(3)-Cu(2)	53.04(9)	C(52)-C(51)-Cu(1)	109.1(3)
C(31)-Cu(3)-Cu(2)	106.01(10)	C(56)-C(51)-Cu(1)	118.7(3)
Cu(4)-Cu(3)-Cu(2)	65.163(18)	Cu(5)-C(51)-Cu(1)	73.20(11)
C(21)-Cu(3)-C(61)	106.71(15)	F(52)-C(52)-C(53)	116.3(3)
C(31)-Cu(3)-C(61)	93.99(15)	F(52)-C(52)-C(51)	119.4(3)
Cu(4)-Cu(3)-C(61)	134.83(16)	C(53)-C(52)-C(51)	124.2(4)
Cu(2)-Cu(3)-C(61)	159.04(13)	F(53)-C(53)-C(54)	119.8(3)
C(41)-Cu(4)-C(31)	145.18(15)	F(53)-C(53)-C(52)	121.8(4)
C(41)-Cu(4)-Cu(3)	144.98(10)	C(54)-C(53)-C(52)	118.4(4)
C(31)-Cu(4)-Cu(3)	53.44(10)	F(54)-C(54)-C(55)	120.2(4)
C(41)-Cu(4)-Cu(5)	50.80(9)	F(54)-C(54)-C(53)	119.5(4)
C(31)-Cu(4)-Cu(5)	162.43(10)	C(55)-C(54)-C(53)	120.3(3)
Cu(3)-Cu(4)-Cu(5)	109.48(2)	F(55)-C(55)-C(54)	119.4(4)
C(41)-Cu(4)-Cu(2)	113.84(9)	F(55)-C(55)-C(56)	121.5(4)

C(31)-Cu(4)-Cu(2)	100.56(11)	C(54)-C(55)-C(56)	119.1(4)
Cu(3)-Cu(4)-Cu(2)	57.530(17)	F(56)-C(56)-C(55)	117.2(3)
Cu(5)-Cu(4)-Cu(2)	63.055(17)	F(56)-C(56)-C(51)	118.9(3)
C(41)-Cu(5)-C(51)	147.36(15)	C(55)-C(56)-C(51)	123.8(4)
C(41)-Cu(5)-Cu(1)	138.89(10)	C(62)-C(61)-C(71)	121.6(5)
C(51)-Cu(5)-Cu(1)	55.57(10)	C(62)-C(61)-Cu(3)	88.6(3)
C(41)-Cu(5)-Cu(4)	51.29(10)	C(71)-C(61)-Cu(3)	99.2(3)
C(51)-Cu(5)-Cu(4)	159.65(11)	C(63)-C(62)-C(61)	121.2(5)
Cu(1)-Cu(5)-Cu(4)	105.37(2)	C(72)-C(63)-C(62)	119.2(6)
C(41)-Cu(5)-Cu(2)	112.38(10)	C(65)-C(64)-C(72)	122.1(5)
C(51)-Cu(5)-Cu(2)	99.42(11)	C(64)-C(65)-C(73)	121.9(5)
Cu(1)-Cu(5)-Cu(2)	57.026(17)	C(67)-C(66)-C(73)	120.6(6)
Cu(4)-Cu(5)-Cu(2)	61.101(17)	C(66)-C(67)-C(68)	121.6(7)
C(16)-C(11)-C(12)	114.0(4)	C(67)-C(68)-C(74)	120.4(6)
C(16)-C(11)-Cu(1)	122.7(3)	C(70)-C(69)-C(74)	123.8(6)
C(12)-C(11)-Cu(1)	115.0(3)	C(69)-C(70)-C(71)	120.5(5)
C(16)-C(11)-Cu(2)	107.6(3)	C(61)-C(71)-C(75)	116.9(5)

C(12)-C(11)-Cu(2)	115.8(3)	C(61)-C(71)-C(70)	126.8(5)
Cu(1)-C(11)-Cu(2)	75.25(12)	C(75)-C(71)-C(70)	116.2(5)
F(12)-C(12)-C(13)	117.2(4)	C(63)-C(72)-C(75)	119.8(4)
F(12)-C(12)-C(11)	119.4(3)	C(63)-C(72)-C(64)	122.3(5)
C(13)-C(12)-C(11)	123.4(4)	C(75)-C(72)-C(64)	117.9(4)
C(14)-C(13)-F(13)	118.9(4)	C(65)-C(73)-C(66)	121.3(5)
C(14)-C(13)-C(12)	119.5(4)	C(65)-C(73)-C(76)	118.8(4)
F(13)-C(13)-C(12)	121.6(5)	C(66)-C(73)-C(76)	119.8(5)
C(13)-C(14)-F(14)	121.5(5)	C(69)-C(74)-C(76)	118.1(5)
C(13)-C(14)-C(15)	121.9(4)	C(69)-C(74)-C(68)	122.9(6)
F(14)-C(14)-C(15)	116.6(5)	C(76)-C(74)-C(68)	119.0(5)
F(15)-C(15)-C(14)	123.0(4)	C(71)-C(75)-C(72)	121.2(4)
F(15)-C(15)-C(16)	119.5(5)	C(71)-C(75)-C(76)	120.1(4)
C(14)-C(15)-C(16)	117.5(4)	C(72)-C(75)-C(76)	118.6(4)
F(16)-C(16)-C(11)	118.2(3)	C(74)-C(76)-C(73)	118.4(4)
F(16)-C(16)-C(15)	118.1(4)	C(74)-C(76)-C(75)	121.2(4)
C(11)-C(16)-C(15)	123.7(4)	C(73)-C(76)-C(75)	120.4(4)

C(22)-C(21)-C(26)	113.9(3)	C(82)-C(81)-C(91)	121.8(4)
C(22)-C(21)-Cu(3)	118.6(2)	C(81)-C(82)-C(83)	120.6(5)
C(26)-C(21)-Cu(3)	119.3(3)	C(82)-C(83)-C(92)	120.5(5)
C(22)-C(21)-Cu(2)	108.6(2)	C(85)-C(84)-C(92)	121.5(4)
C(26)-C(21)-Cu(2)	114.4(3)	C(85)-C(84)-Cu(1)	73.3(2)
Cu(3)-C(21)-Cu(2)	75.19(11)	C(92)-C(84)-Cu(1)	108.9(2)
F(22)-C(22)-C(23)	117.1(3)	C(84)-C(85)-C(93)	122.2(4)
F(22)-C(22)-C(21)	118.9(3)	C(84)-C(85)-Cu(1)	74.1(2)
C(23)-C(22)-C(21)	124.0(3)	C(93)-C(85)-Cu(1)	108.3(2)
F(23)-C(23)-C(24)	120.7(4)	C(87)-C(86)-C(93)	121.0(5)
F(23)-C(23)-C(22)	120.4(4)	C(88)-C(87)-C(86)	120.8(5)
C(24)-C(23)-C(22)	118.9(4)	C(87)-C(88)-C(94)	120.8(5)
F(24)-C(24)-C(23)	119.5(4)	C(90)-C(89)-C(94)	121.6(5)
F(24)-C(24)-C(25)	120.1(4)	C(89)-C(90)-C(91)	122.3(5)
C(23)-C(24)-C(25)	120.4(4)	C(81)-C(91)-C(95)	118.5(4)
F(25)-C(25)-C(24)	119.8(4)	C(81)-C(91)-C(90)	123.7(4)
F(25)-C(25)-C(26)	121.1(4)	C(95)-C(91)-C(90)	117.8(4)

C(24)-C(25)-C(26)	119.1(4)	C(83)-C(92)-C(95)	119.2(4)
F(26)-C(26)-C(25)	117.3(3)	C(83)-C(92)-C(84)	122.7(4)
F(26)-C(26)-C(21)	119.0(3)	C(95)-C(92)-C(84)	118.2(3)
C(25)-C(26)-C(21)	123.7(4)	C(86)-C(93)-C(96)	119.1(4)
C(32)-C(31)-C(36)	114.0(3)	C(86)-C(93)-C(85)	123.5(4)
C(32)-C(31)-Cu(4)	109.1(3)	C(96)-C(93)-C(85)	117.4(3)
C(36)-C(31)-Cu(4)	122.9(3)	C(88)-C(94)-C(96)	119.2(4)
C(32)-C(31)-Cu(3)	119.3(3)	C(88)-C(94)-C(89)	123.2(5)
C(36)-C(31)-Cu(3)	112.1(3)	C(96)-C(94)-C(89)	117.6(4)
Cu(4)-C(31)-Cu(3)	74.27(12)	C(92)-C(95)-C(96)	120.3(3)
F(32)-C(32)-C(33)	116.7(4)	C(92)-C(95)-C(91)	119.6(3)
F(32)-C(32)-C(31)	119.1(3)	C(96)-C(95)-C(91)	120.1(3)
C(33)-C(32)-C(31)	124.1(4)	C(95)-C(96)-C(94)	120.5(3)
F(33)-C(33)-C(32)	121.3(4)	C(95)-C(96)-C(93)	120.5(3)
F(33)-C(33)-C(34)	119.9(4)	C(94)-C(96)-C(93)	119.1(3)

List of Publications

1. "Resolution of Planar-Chiral Ferrocenylborane Lewis Acids: The Impact of Steric Effects on the Stereoselective Binding of Ephedrine Derivative." R. Boshra; K. Venkatasubbaiah; **A. Doshi**; F. Jäkle, *Organometallics*, **2009**, 28, 4141–4149.
2. "Binary Stacks of $[\text{CuC}_6\text{F}_5]_4$ with Arenes." **A. Doshi**; K. Venkatasubbaiah; A. L. Rheingold; F. Jäkle, *Chem. Commun.* **2008**, 4264-4266.
3. "Fluoride-Promoted Intramolecular Aryl and Allyl Migration from Boron to Tin." R. Boshra; **A. Doshi**; F. Jäkle, *Organometallics* **2008**, 27, 1534-1541.
4. "Allylation of Ketones with Ferrocene-Based Planar Chiral Lewis Acid." R. Boshra; **A. Doshi**; F. Jäkle, *Angew. Chem. Int. Ed.* **2008**, 47, 1134-1137.
5. "Examination of the Mixed Valence State of the Doubly Boron-Bridged Diferrocene Cation $[(\text{FeCp}_2 - (\mu\text{-C}_{10}\text{H}_6(\text{BPh})_2)]^{+}$." K. Venkatasubbaiah; **A. Doshi**; I. Nowik; R. H. Herber; A. L. Rheingold; F. Jäkle, *Chem. Eur. J.* **2008**, 14, 444-458.
6. "Simultaneous Fluoride Binding to Ferrocene-Based Heteronuclear Bidentate Lewis Acids." R. Boshra; K. Venkatasubbaiah; **A. Doshi**; R. A. Lalancette; L. Kakalis; F. Jäkle, *Inorg. Chem.* **2007**, 46, 10174-10186.

7. "Polystyrene Supported Borane Complexes PS-BH₂·D." **A. Doshi** and F.

Jäkle, *Main Group Chem.* **2006**, 5, 309-318.

VITA

Ami P. Doshi

Date of Birth August 23rd, 1979

Birth Place Mumbai, India

Education

1990-1994 G. P. P. High School, Mumbai, India

1994-1999 Chauhan Institute of Science, Mumbai, India.

Degree achieved: B.Sc. in Chemistry.

1999-2001 M. V. L. U. College, University of Mumbai, India.

Degree achieved: M.Sc. in Chemistry.

2004-Present Department of Chemistry, Rutgers University-
Newark, Newark, NJ.

Degree sought: Ph.D. in Chemistry. Advisor:

Frieder Jäkle.

Awards

- Graduate Student Excellence Award, Graduate Student Governing Association (GSGA), Fall 2008.
- Student Travel Award-ACS Division of Inorganic Chemistry, 232nd ACS National Meeting, September 10-14, 2006, San Francisco, CA.